



Copyright Undertaking

This thesis is protected by copyright, with all rights reserved.

By reading and using the thesis, the reader understands and agrees to the following terms:

1. The reader will abide by the rules and legal ordinances governing copyright regarding the use of the thesis.
2. The reader will use the thesis for the purpose of research or private study only and not for distribution or further reproduction or any other purpose.
3. The reader agrees to indemnify and hold the University harmless from and against any loss, damage, cost, liability or expenses arising from copyright infringement or unauthorized usage.

IMPORTANT

If you have reasons to believe that any materials in this thesis are deemed not suitable to be distributed in this form, or a copyright owner having difficulty with the material being included in our database, please contact lbsys@polyu.edu.hk providing details. The Library will look into your claim and consider taking remedial action upon receipt of the written requests.

**THEORY AND APPLICATION OF SECOND-
ORDER DIRECT ANALYSIS IN STATIC
AND DYNAMIC DESIGN OF FRAME
STRUCTURES**

DU ZUOLEI

PhD

The Hong Kong Polytechnic University

2019

**The Hong Kong Polytechnic University
Department of Civil and Environmental Engineering**

**THEORY AND APPLICATION OF SECOND-
ORDER DIRECT ANALYSIS IN STATIC
AND DYNAMIC DESIGN OF FRAME
STRUCTURES**

DU Zuolei

**A thesis submitted in
partial fulfillment of the requirements for
the degree of Doctor of Philosophy**

May 2018

CERTIFICATE OF ORIGINALITY

I hereby declare that this thesis is my own work and that, to the best of my knowledge and belief, it reproduces no material previously published or written, nor material that has been accepted for the award of any other degree or diploma, except where due acknowledgment has been made in the text.

_____ (Signed)

DU Zuo-Lei _____ (Name of student)

To my wife & parents

for their love and encouragements

ABSTRACT

The modern design codes such as Eurocode3 (2005), AISC360 (2016), CoPHK (2011) and GB50017 (2017) recommend the use of direct analysis method (DAM) instead of traditional effective length method for daily design. However, the research and applications of DAM mainly focus on frame structures subjected to static loads. Performance-based seismic design (PBSD) is a new trend in structural engineering and appears in most of the modern design codes or specifications such as Eurocode-8 (2005) and FEMA356 (2000). The philosophy inherent to the approach is to accurately capture the structural behavior under earthquake actions which is substantially in line with DAM, and the demanded performance according to the occupied functions is estimated. It is found that little work has been carried out on the extension of DAM to PBSD. The pushover analysis and time history analysis should be used with effective length method for PBSD in current practice as the member imperfections have not been taken into account. The DAM requires explicit consideration of member initial imperfections to suppress the use of effective length factor while PBSD needs to simulate progressive yielding along the section depth and member length. Thus, an advanced and high-performance beam-column element with member imperfection is urgently required for static and dynamic design.

In the past decades, the stiffness and flexibility methods have been extensively used to derive beam-column elements. As the flexibility-based type elements can meet the compatibility and equilibrium conditions at the element level, they are more competent in direct analysis considering both geometrical and material nonlinearities. In this research project, an advanced flexibility-based beam-column element with member

initial imperfections, finite joint stiffness, rigid zone and end offsets, and distributed material nonlinearity is proposed for the second-order direct analysis of frame structures under static and dynamic actions. Considerable care has been taken to verify the accuracy and efficiency of this new element.

To account for material nonlinearity, the stiffness-based elements with the plastic hinge method and the flexibility-based elements with the plastic zone method are well adopted in the second-order inelastic analysis. The former emphasizes the computational efficiency with relatively less-accurate structural responses, while the latter aims to precisely simulate the structural behavior but needs typically more computer time. One proposed element is generally sufficient to model a practical member in engineering structure without the assumption of effective length. The limitations of stiffness-based elements and conventional flexibility-based elements are removed in the new element.

To further improve the computational efficiency of the proposed element, an alternative approach following the concept of the plastic hinge method is proposed by considering the elastoplastic behavior of steel members through the integration points using the stress resultant plasticity model rather than the fiber section. This method yields high accuracy comparable to the plastic zone method but requires much less computer time and resources, without the need of a fiber mesh along the section.

To consider the effect of finite joint stiffness, two zero-length springs representing moment-rotation relationships are attached at the ends of the proposed beam-column element. The contribution of axial force on the bending moments are first discussed. The proposed hybrid beam-column element can well capture the behavior of a joint under monotonic or cyclic loading.

The current AISC360 (2016) specified a new effective stress-strain method for design of noncompact and slender concrete-filled steel tube (CFT) members. However, there is still lack of a practical tool for second-order direct analysis of this kind of members experiencing complicated behaviors such as local plate buckling, concrete confinement and yielding of steel tube. The stiffness change of the CFT members under combined axial force and bending moments should be considered during the incremental-iterative procedure of direct analysis. The proposed beam-column element with fiber section technique provides a new solution for the design of noncompact and slender CFT members using the effective stress-strain relationships. This method complies with the provisions in AISC360 (2016) and several recommendations are introduced for improvement of design codes.

Special concentrically braced frames (SCBFs) are widely used in high seismic regions due to their structural efficiency and high ductility for energy dissipation. SCBFs are allowed for large inelastic deformation through tensile yielding, buckling and post-buckling behaviors of braces. The accurate modeling of braces with acceptable computational costs is vital to capture the real structural behavior of SCBFs subjected to earthquakes. A hybrid beam-column element with consideration of gusset plate connection is proposed for modeling of SCBFs. It shows significant improvement in the time history analysis of SCBFs.

In summary, this research project proposes a comprehensive method for second-order static and dynamic analysis of frame structures with consideration of member initial imperfections, material yielding and semi-rigid connections. It will significantly improve the current design practice and help the engineers to produce a safer and more economic design.

Keywords: Flexibility-based; beam-column element; direct analysis; second-order; initial imperfection; residual stress; distributed nonlinearity; noncompact and slender CFT members; special concentrically braced frames;

PUBLICATIONS

Journal paper:

- (1) Du, Zuo-Lei, Yao-Peng Liu, and Siu-Lai Chan. "A second-order flexibility-based beam-column element with member imperfection." *Engineering Structures* 143 (2017): 410-426.
- (2) Du, Zuo-Lei, Yao-Peng Liu, and Siu-Lai Chan. "A practical analytical model for special concentrically braced frames." *Journal of Constructional Steel Research*. (Under Review)
- (3) Du, Zuo-Lei, Yao-Peng Liu, and Siu-Lai Chan. "A force-based element for direct analysis using stress-resultant plasticity model." *Steel and Composite Structures*. (Under Review)
- (4) Du, Zuo-Lei, Yao-Peng Liu, and Siu-Lai Chan. "Direct analysis method for noncompact and slender CFT members." *Thin-Walled Structures*. (Under Review)
- (5) Du, Zuo-Lei, Yao-Peng Liu, and Siu-Lai Chan. "A consistent analytical model for tapered steel members with symmetric or asymmetric variations." *International Journal of Structural Stability and Dynamics*. (to be submitted)

Conference paper:

- (1) Du, Zuo-Lei, Yao-Peng Liu, Siu-Lai Chan, and Wei-Qi Tan. "A flexibility-based element for second-order inelastic analysis using plastic hinge method." *8th European Conference on Steel and Composite Structures* 1.2-3 (2017): 1056-1065.

- (2) Du, Zuo-Lei, Yao-Peng Liu, Siu-Lai Chan, and Wei-Qi Tan. "Consideration of imperfections in special concentrically braced frames." *The 8th International Conference on Steel and Aluminium Structures* (2016).
- (3) Yao-Peng Liu, Du, Zuo-Lei, Siu-Lai Chan. " Distributed plastic hinge analysis by a new flexibility-based beam-column element." 第九屆海峽兩岸及香港鋼、組合及金屬結構技術研討會 (2017).
- (4) Liu, Yao-Peng, Siu-Lai Chan, Zuo-Lei Du, and Jian-Wei He. "Second-order direct analysis of long-span roof structures." *8th European Conference on Steel and Composite Structures* 1.2-3 (2017): 3930-3939.
- (5) Liu, Yao-Peng, Siu-Lai Chan, Zuo-Lei Du. "Second order plastic hinge analysis for seismic and static design of building structures." *11th International Conference on Advances in Steel and Concrete Composite Structures* (2015)

ACKNOWLEDGMENTS

I would like to express my appreciation to Professor Siu-Lai Chan, my research advisor, for his informative guidance, valuable support during my doctoral program. I also wish to thank Dr. Yao-Peng Liu for the knowledge and foresight transmitted about the academic research and programming technology. This long relationship with such friendly and enthusiastic supervisors brought happiness to me and will keep encouraging me in my future life.

I also would like to thank the financial support of the research project “Development of an energy absorbing device for flexible rock-fall barriers (ITS/059/16FP)” funded by the Research Grant Council grant from the Hong Kong SAR Government, and Hong Kong Polytechnic University for providing resources in the completion of my doctoral program.

I wish to express my deepest gratitude to my wife, Hong Liu, for her love, support, encouragement, and sacrifice during my doctoral studies. I will never be able to thank her enough for accompanying me to accomplish this arduous task. I am thankful for the boundless love from my parents Xin-Shi Du and Ru-Xin Xiong. I am appreciated for their effort in raising and cultivating my brother and me, and being patient in waiting for me to complete my doctoral study.

Finally, I wish to thank the NIDA team members, who include but are not limited to Dr. Z. H. Zhou, Dr. S. W. Liu, Dr. S. H. Cho, Dr. H. Yu, Mr. Sam Chan, Mr. Y. Q. Tang, Mr. R. Bai, Mr. W. F. Chen, Miss W. Q. Tan, Mr. J. W. He, Mr. L. Chen, Mr.

Jake Chan, Mr. W. Du, Mr. P. S. Zheng and Mr. S. B. Ji for their great help during my studies.

CONTENTS

CERTIFICATE OF ORIGINALITY.....	3
ABSTRACT	5
PUBLICATIONS	9
ACKNOWLEDGMENTS	11
CONTENTS.....	I
LIST OF FIGURES	IV
LIST OF TABLES	VIII
LIST OF SYMBOLS	IX
CHAPTER 1. INTRODUCTION.....	12
1.1 Background	12
1.2 Objectives.....	14
1.3 Organization.....	16
CHAPTER 2. LITERATURE REVIEW.....	19
2.1 Beam-column elements for second-order analysis	19
2.2 Plasticity models for material nonlinearity	25
2.3 Modeling of member initial imperfections	30
2.4 Modeling of semi-rigid connections	32
2.5 Design method for CFT members with noncompact and slender sections	33
2.6 Design method of special concentrically braced frames.....	35
CHAPTER 3. FLEXIBILITY-BASED BEAM-COLUMN ELEMENT CONSIDERING MEMBER IMPERFECTION	41

3.1	Introduction	41
3.2	Element formulations	44
3.3	Member imperfection.....	60
3.4	Numerical examples.....	64
3.5	Concluding remarks	72
3.6	Appendix – Analytical Solutions of Single Imperfect Column under Axial Load	74
CHAPTER 4.TWO PLASTICITY MODELS FOR MATERIAL NONLINEARITY		
89		
4.1	Introduction	89
4.2	Distributed plasticity analysis	91
4.3	Stress-resultant plasticity model	92
4.4	Integration of rate equations and section tangent stiffness	95
4.5	Verification examples	99
4.6	Concluding remarks	104
CHAPTER 5. SEMI-RIGID CONNECTIONS UNDER MONOTONIC AND CYCLIC LOADS		
118		
5.1	Introduction	118
5.2	Modeling of connection behavior under monotonic loading	119
5.3	Modeling of connection behavior under cyclic loading.....	126
5.4	Flexibility-based beam-column element accounting for semi-rigid joints	130
5.5	Numerical examples.....	133
5.6	Concluding remarks	140

CHAPTER 6. DIRECT ANALYSIS OF NONCOMPACT AND SLENDER CFT MEMBERS	167
6.1 Introduction	167
6.2 Design methods for CFT members with noncompact or slender sections in AISC360.....	171
6.3 Direct analysis method	176
6.4 Validation examples	181
6.5 Concluding remarks	186
 CHAPTER 7. DIRECT ANALYSIS OF SPECIAL CONCENTRICALLY BRACED FRAMES	 201
7.1 Introduction	201
7.2 Semi-rigid connection and rigid end zone for gusset plate connections ..	206
7.3 Material representation and residual stress	208
7.4 Analytical model for SCBF system.....	211
7.5 Numerical examples.....	216
7.6 Concluding remarks	220
 CHAPTER 8. SUMMARY AND FUTURE WORK	 236
8.1 Summary	236
8.2 Future work	239
 REFERENCES	 241

LIST OF FIGURES

Fig. 2.1 Section discretization	39
Fig. 2.2 Commonly used configurations of SCBFs	40
Fig. 2.3 Structural behavior of brace and failure locations	40
Fig. 3.1 Basic forces versus displacements relations	75
Fig. 3.2 Layout of columns	75
Fig. 3.3 Load vs. deflection curves for “pinned-pinned”: (a) $\lambda = 50$, (b) $\lambda = 100$,	77
Fig. 3.4 Load vs. deflection curves for “pinned-fixed”: (a) $\lambda = 50$, (b) $\lambda = 100$,	78
Fig. 3.5 Load vs. deflection curves for “fixed-fixed”: (a) $\lambda = 50$, (b) $\lambda = 100$,	80
Fig. 3.6 A single fixed-ended beam under a member point load	80
Fig. 3.7 Load-displacement curves of point B	81
Fig. 3.8 Deformation of integration points along the member.....	82
Fig. 3.9 Layout and load pattern of the planar frame by Ziemian and McGuire (2002)	83
Fig. 3.10 Imperfection pattern of the planar frame by Ziemian and McGuire (2002)	83
Fig. 3.11 Response curves of the frame by Ziemian and McGuire (2002).....	84
Fig. 3.12 Bending moment, axial force and percentage of the cross-section yielded	84
Fig. 3.13 Layout and load pattern of Harrison’s space frame	85
Fig. 3.14 Horizontal displacement of the top point.....	85
Fig. 4.1 Distributed plasticity by fiber section approach	106

Fig. 4.2 Fiber discretization for wide-flange section	106
Fig. 4.3 Yield function and limit function for section state	107
Fig. 4.4 Backward-Euler return procedure.....	107
Fig. 4.5. Full surface under interaction of force resultants	108
Fig. 4.6 Layout of cantilever column and loading patterns	108
Fig. 4.7 Bending moment-plastic rotation about y-axis for case 1	109
Fig. 4.8 Bending moment-plastic rotation about y-axis for case 2	109
Fig. 4.9 Layout and loading pattern of the Vogel's six-story frame	110
Fig. 4.10 Horizontal displacement of the Vogel's six-story frame	110
Fig. 4.11 Layout and loading pattern of the high strength steel frame (Unit: mm)	111
Fig. 4.12 Loading protocol for the top displacement.....	111
Fig. 4.13 Base shear versus overall drift ratio.....	112
Fig. 4.14 Layout of four-story 3D steel frame	112
Fig. 4.15 Displacement under four earthquakes.....	114
Fig. 4.16 Base Shear under four earthquakes.....	116
Fig. 4.17 Consuming time of time history analysis under four earthquakes....	117
Fig. 5.1 Finite element model of the end-plate connection using solid elements	141
Fig. 5.2 Finite element model of the end-plate connection using shell elements	141
Fig. 5.3 Modeling of a semi-rigid jointed member	142
Fig. 5.4 Layouts and load patterns of the frames	143
Fig. 5.5 Loading-deflection curves of models with various connection types.	143
Fig. 5.6 Layouts of sway and non-sway frames.....	144

Fig. 5.7 Applied force vs. horizontal displacement	145
Fig. 5.8 Layouts and load patterns of three-story sway frames	147
Fig. 5.9 Loading-deflection curves for models of three-story sway frames	148
Fig. 5.10 Layouts and load patterns for William’s toggle frame	150
Fig. 5.11 Loading-deflection curves of William’s toggle frame.....	153
Fig. 5.12 Vertical load history.....	154
Fig. 5.13 Layouts and dynamic loadings for William’s toggle frame	155
Fig. 5.14 The transient response of William’s toggle frame.....	156
Fig. 5.15 Layout of one-story frame	157
Fig. 5.16 Frequency against joint stiffness.....	158
Fig. 5.17 Layout and load pattern of one-story frame.....	158
Fig. 5.18 The transient response of the frame	160
Fig. 5.19 Layout and load pattern of a column	160
Fig. 5.20 Cyclic load history	161
Fig. 5.21 Load-deformation response of the Pinch type model	161
Fig. 5.22 The load-displacement histories of various pinch type models	164
Fig. 6.1. Typical fiber mesh of CFT member	189
Fig. 6.2. Effective stress-strain relationships for steel tube	190
Fig. 6.3. Effective stress-strain relationships for concrete infill	191
Fig. 6.4. Dimensions and material properties of KOM2001.....	191
Fig. 6.5. Load-deflection curves of KOM2001.....	192
Fig. 6.6. Dimensions and material properties for two rectangular CFT members	193
Fig. 6.7. Layout and loading scheme for two rectangular CFT tests	193
Fig. 6.8. Load-deflection curves for S-150-2.0 and BRA4-2-5-02.....	194

Fig. 6.9. Dimensions and material properties of CC4-D-4-1	195
Fig. 6.10. Load-deflection curves for CC4-D-4-1.....	195
Fig. 6.11. Dimensions and material properties for two circular CFT members	196
Fig. 6.12. Layout and loading scheme for two circular CFT tests	197
Fig. 6.13. Load-deflection curves for TB002 and EC4-D-4-0.....	198
Fig. 7.1 Configuration and modelling of gusset plate connection	222
Fig. 7.2 Moment-rotation function of gusset plate connection	222
Fig. 7.3 Fracture model of steel material	223
Fig. 7.4 Residual stress patterns.....	224
Fig. 7.5 Comparison of analytical models for SCBFs	225
Fig. 7.6 Configuration of a single HSS brace	225
Fig. 7.7 Symmetrical loading protocol.....	226
Fig. 7.8 Brace hysteretic curves for different models: (a) M1, (b) M2, (c) M3 and (d) M4	228
Fig. 7.9 Finite element model of SCBF	229
Fig. 7.10 Seismic performance of SCBF with different number of elements..	229
Fig. 7.11 Test specimen of single-story frame.....	230
Fig. 7.12 Analytical model.....	230
Fig. 7.13 Asymmetrical loading protocol	231
Fig. 7.14 Response of single-story frame	231
Fig. 7.15 Test specimen of three-story one-bay frame.....	232
Fig. 7.16 Analytical model.....	233
Fig. 7.17 Symmetrical loading protocol.....	233
Fig. 7.18 Response of three-story one-bay frame	234

LIST OF TABLES

Table 3-1 Numerical integration methods for flexibility-based beam-column element	86
Table 3-2 Numerical integration methods for flexibility-based beam-column element	86
Table 3-3 Theory results of a fixed-ended beam under different point loads	87
Table 3-4 Models (M1~M7) for the planar frame by Ziemian and McGuire (2002)	87
Table 5-1 Comparison of the critical load values for a non-sway frame	165
Table 5-2 Comparison of the critical load values for a sway frame	165
Table 5-3 Comparison of the critical load values for multistory sway frame..	166
Table 6-1 Classification of steel elements in composite members	199
Table 6-2. Definitions of cp and cm	200
Table 7-1 Four models for simulation of the single HSS brace	235

LIST OF SYMBOLS

N	Shape function
B	Strain-displacement transformation matrix
P	Element forces in basic axis system
D	Element displacements in basic axis system
u	Displacement field
ϵ	Strain field
σ	Stress field
Ψ	Transformation matrix
d	Section displacements
Π_{HR}	Total work potential term
$\Pi_{ext}(\mathbf{u})$	External work potential term
Ω	Volume of element
S	Stress resultants of cross-sections
A	Area of cross-sections
b	Matrix of displacement-dependent force interpolation functions
v, w	Lateral displacement
v_0, w_0	Initial imperfection
b*	Matrix of end forces-section forces interpolation functions
\mathbf{k}_S	Section tangent stiffness matrix
\mathbf{E}_t	Material tangent stiffness at an arbitrary point
\mathbf{f}_S	Section tangent flexibility matrix
l_{ij}^*	j th integrated Lagrangian polynomial at integration point ξ_i

\mathbf{K}_e	Element stiffness matrix in basic axis system
\mathbf{F}_e	Element flexibility matrix in basic axis system
\mathbf{K}_T	Element stiffness matrix in global axis system
T	Transformation matrix from basic to local system
δ_0	Amplitude of the half-sine function
W_{el}	Elastic section modulus
W_{pl}	Plastic section modulus
f_y	Characteristic yield strength of the material
N_{cr}	Elastic critical axial load
α	Imperfection factor corresponding to the buckling curve (a_0 , a , b , c or d)
τ_b	Additional reduction factor
f	Yield function
F	Limit function
\mathbf{k}_{se}	Elastic section tangent stiffness matrix
S	Connection stiffness
c_{sr}	Relative strength ratio
λ	Slenderness ratio
P_c	Allowable compressive strength
P_{no}	Nominal compressive strength of zero length, doubly symmetric axially loaded composite member
P_e	Elastic critical buckling load
K	Effective length factor
R_e	Rotational stiffness in elastic stage

e	Distance of the rigid zone
E	Eccentricity transform matrix

CHAPTER 1. INTRODUCTION

1.1 Background

The modern design codes such as Eurocode-3 (2005), AISC360 (2016), CoPHK (2011) and GB50017 (2017) recommend the use of direct analysis method (DAM) instead of traditional effective length method for daily design. However, the research and applications of DAM mainly focus on frame structures subjected to static loads. Performance-based seismic design (PBSD) is a new trend in structural engineering and appears in most of the modern design codes or specifications such as Eurocode-8 (2005) and FEMA356 (2000). The philosophy inherent to the approach is to accurately capture the structural behavior under earthquake actions which is essentially in line with DAM, and the demanded performance according to the occupied functions is estimated.

Compared to current seismic analysis approaches such as the lateral force (LF) and the response spectrum (RS) analysis methods based on linear and elastic assumptions, the analysis method for performance-based design requires consideration of the material and geometrical nonlinearities. The nonlinear static and dynamic analysis, which are also commonly called “push-over” and “time-history” analysis respectively, are two well-accepted methods for performance-based seismic design.

AISC360 (2016) provides detailed requirements in direct analysis, which should include: (1) deformation of members, connections and other components; (2) $P-\Delta$ and $P-\delta$ effects; (3) initial geometric imperfections; (4) material inelasticity and

residual stresses; and (5) uncertainty of strength and stiffness in the system, members and connection. Similar requirements are also presented in CoPHK (2011) and Eurocode-3 (2005). It can be seen that the above requirements should be also considered in the seismic analysis so that the actual structural behavior can be predicted for PBSB.

It is found that little work has been carried out on the extension of DAM to PBSB. The pushover analysis and time history analysis should be used with effective length method for PBSB in current practice as the member imperfections have not been taken into account. The DAM requires explicit consideration of member initial imperfections to suppress the use of effective length factor while PBSB needs to simulate progressive yielding along the section depth and member length. Thus, an advanced and high-performance beam-column element with member imperfection is urgently required for the static and dynamic design.

In the past decades, the stiffness and flexibility methods have been extensively used to derive beam-column elements. The stiffness-based elements have achieved great successes in handling large elastic deflection problems while the conventional flexibility-based elements have played a dominant role in second-order inelastic analysis. The accuracy of the former can be improved by enforcing equilibrium along mid-span or “stations” along the member length to achieve equilibrium which is not guaranteed along an element. However, as the actual location of plastic hinge can be anywhere along the element, the shape function becomes inadequate to describe the sharp angle due to formation of plastic hinge such that several stiffness-based elements should be used to represent the material yielding, which will significantly increase computer time and even cause difficulties in modeling of member imperfections. In contrast, the equilibrium along a flexibility-based element can always be guaranteed.

However, the conventional flexibility-based elements cannot meet the codified requirements of direct analysis because they did not take member initial imperfections into account. Being aware of the above, it motivates the author to develop a new element for direct analysis of static and dynamic problems by safety and economic design principles.

For the practical design of frame structures using direct analysis method (DAM), the beam-column element adopted should have the merits of the above two types of elements. As the flexibility-based type elements can meet the compatibility and equilibrium conditions at the element level, they are more competent in direct analysis considering both geometrical and material nonlinearities.

Thus, an advanced flexibility-based beam-column element with member initial imperfections, finite joint stiffness, rigid zone and end offsets, and distributed material nonlinearity is proposed for second-order direct analysis of frame structures under static and dynamic actions in this research project. Considerable care has been taken to verify the accuracy and efficiency of this new element. Further, the proposed element is applied to conduct direct analysis of two widely used structural forms, i.e. structures with concrete-filled steel tube (CFT) members and special concentrically braced frames (SCBFs).

1.2 Objectives

The main objective of this research project is to propose an advanced and high-performance beam-column element explicitly considering member initial imperfections and distributed plasticity so that the direct analysis method (DAM) can be smoothly extended to performance-based seismic design (PBSD) without the need

of effective length method. The proposed element should have high accuracy even using one element per member and consequently, the computational efficiency in nonlinear dynamic analysis can be significantly enhanced. Furthermore, the requirements of direct analysis method need to be satisfied by incorporating the features into the proposed element.

Currently, the direct analysis method (DAM) is mainly implemented via the stiffness-based beam-column elements. Though being efficient in second-order elastic analysis, they face difficulties in second-order inelastic analysis which is required in PBS. In contrast, the flexibility-based beam-columns show excellent performance in handling elastoplastic problems because they strictly satisfy the equilibrium of bending moments and axial force along the element. For this reason, the flexibility-based type element is selected as the candidate for PBS under the framework of direct analysis. First, a new flexibility-based beam-column element considering member initial geometrical imperfection is derived. Several typical imperfection mode shapes such as sine function and polynomial function are allowed in this element. Second, the residual stress can be explicitly modeled by the proposed element via the fiber section technology through which the influence of residual stress on the structural response can be assessed. To save computer time and resource, an alternative method to form the sectional stiffness is proposed. The effects such as joint flexibility, rigid zone and end offsets, are also considered and finally an advanced hybrid beam-column element is developed to meet the general requirements of direct analysis. In summary, the goals of this research project are listed as:

- To develop an advanced flexibility-based beam-column element with initial member imperfections to minimize the degrees of freedom and improve the convergence of nonlinear analysis;
- To consider residual stress in the proposed element with fiber section

- technology to improve accuracy;
- To propose a distributed plastic hinge method to improve computational efficiency in second-order inelastic analysis;
 - To program and incorporate the proposed element and plastic methods into the existing computer program for practical use;
 - To consider joint flexibility in the proposed element;
 - To consider end rigid zone and end offsets in the proposed element;
 - To apply the proposed method in direct analysis of frame structures with noncompact and slender CFT members;
 - To apply the proposed method in the performance-based seismic design of special concentrically braced frames (SCBFs).

1.3 Organization

The outline of this thesis is presented as follows:

Chapter 1 introduces the background, objectives, and organization of this thesis.

Chapter 2 presents a literature survey. First, the beam-column elements for direct analysis are discussed. Plasticity models adopted in the beam-column elements for material nonlinearity are commented. Further, the modeling approaches of member initial imperfections and semi-rigid connection are reviewed. Finally, the design methods for CFT members with noncompact and slender sections, and special concentrically braced frames are outlined.

Chapter 3 describes a new flexibility-based beam-column element with member imperfection. First, the equilibrium and compatibility equations are derived on the basis of Hellinger-Reissner variational functional. Second, the element flexibility matrix is formed by the integration of the section flexibility matrix along the member. Meanwhile, the curvature-based displacement interpolation (CBDI) for second-order flexibility-based elements is introduced. Further, the transformation from the basic

coordinate system to the global coordinate system and the process of element state determination are presented. The advantage of the proposed element for consideration of member imperfection is highlighted. Finally, several numerical examples are used to verify the accuracy and validation of the proposed element.

Chapter 4 describes two plasticity models used in beam-column elements for the consideration of material nonlinearity. First, a conventional method, a distributed plasticity model with fiber sections technology, is illustrated. Second, a new stress-resultant plasticity model is incorporated into the proposed flexibility-based element to enhance numerical efficiency. The critical steps of forming section tangent stiffness, i.e., the integration algorithm and return mapping algorithm, are presented to allow for hysteretic behavior. The proposed method is evaluated with the conventional method via several benchmarking examples.

In Chapter 5, the joint flexibility, as an essential factor affecting structural behavior, is considered by improving the proposed element described in Chapter 3. First, several semi-rigid connection models for the joints subjected to monotonic or cyclic loading are introduced. Then, the proposed flexibility-based beam-column element is modified to account for semi-rigid behavior. Finally, several static and dynamic examples are adopted to verify the performance of the hybrid element to model frame structures with semi-rigid connections under static or dynamic loads.

In Chapter 6, the proposed method is applied to design of frame structures with CFT members made of noncompact and slender sections. First, the design methods suggested by AISC360 (2016) are introduced and discussed. Second, the direct analysis method is extended to analyze CFT members with noncompact and slender sections. Finally, four experiments from literature, including rectangular and circular CFT members, are adopted to verify the proposed method.

In Chapter 7, the proposed method is applied to design of special concentrically braced frames (SCBFs). First, the special features of SCBFs are discussed. The proposed element is improved to incorporate the effect of rigid end zones, material nonlinearity, and residual stress. Then, a practical analytical model for SCBF systems is proposed. Finally, a considerable number of benchmark examples are used to illustrate the accuracy and efficiency of the proposed model.

In Chapter 8, the conclusions drawn from this study are illustrated. Some suggestions for future work are also presented.

CHAPTER 2. LITERATURE REVIEW

This chapter presents a review on the development of beam-column elements and its related problems in regarding practical application. It mainly includes the review on the several existing beam-column elements, geometrical imperfection, approaches to model material nonlinearity, joint flexibility, modeling of concrete filled steel tube (CFT) members and the design of special concentrically braced frame.

2.1 Beam-column elements for second-order analysis

Finite element method was invented to solve complex elasticity and structural analysis problems in civil and aeronautical engineering in the early 1940s. Beam-column, as an effective kind of finite element to model beams and columns, attracted a considerable amount of research. Several kinds of beam-column elements with unique features were developed. Numerous scholars had made substantial efforts on nonlinear engineering problems. Generally, these elements can be divided into three categories: displacement, flexibility and mixed element. Extensive researches have been conducted on the structural analysis of frame structures with consideration of geometrical and material nonlinearities. Meanwhile, some reliable numerical methods were developed to solve the nonlinear problems. For instance, Chan (1988) proposed an approach, called minimizing the residual displacements, to solve geometric and material nonlinear problems. Chan and Zhou (1994) proposed a pointwise-equilibrating-polynomial (PEP) element which can model one member with one element and show excellent performance on solving nonlinear geometrical problems. Chen and Chan (1995) proposed an element with plastic hinges at the mid-span and

two ends which can be used to model material nonlinearity. Izzuddin and Smith (1996) proposed a new formulation to consider elastoplastic material behavior using distributed plasticity. Izzuddin (1996) introduced geometrical imperfection in a local Eulerian system to beam-columns. Spacone (1996) proposed a mixed beam-column element, which has a high accuracy in the nonlinear analysis of structural members. Neuenhofer and Filippou (1998) proposed a flexibility-based beam-column element for geometrically nonlinear analysis of frame structures. Pi *et al.* (2006) employed an accurate rotation matrix to derive nonlinear strain, and proposed a beam-column element to model steel and concrete composite members based on total Lagrangian framework.

In this section, these three kinds of beam-column elements have been reviewed and their features are discussed.

2.1.1 Displacement-based beam-column element

The displacement-based beam-column element is most widely used element and is embedded in most commercial software packages. This kind of element assumes a shape function to discrete and interpolate the displacement fields along the element. The general derivation process of stiffness matrix will be stated concisely. Conceptionally, the displacement field of the element can be described by shape function and the nodal displacements at two ends as,

$$\mathbf{u}(x) = \mathbf{N}(x)\mathbf{D} \tag{2.1}$$

in which, \mathbf{N} is the shape function and \mathbf{D} is the nodal displacements. As the shape function is generally defined by limited order of polynomial function, it will lead to an approximate displacement field and further may give an inaccurate stiffness matrix. Taking the cubic beam-column element for example, its shape functions for transverse

displacements are,

$$N_1 = \frac{1}{8}(1 - \xi)(1 - \xi^2) \quad (2.2)$$

$$N_2 = -\frac{1}{8}(1 + \xi)(1 - \xi^2) \quad (2.3)$$

$$\xi = 2x/L \quad (2.4)$$

in which, x is the distance from the first end, L is the member length. In Equations (2.2) to (2.4), the shape function only has an algebraic accuracy of three degrees. The deformation fields can be deduced as,

$$\mathbf{d}(x) = \mathbf{B}(x)\mathbf{D} \quad (2.5)$$

in which, \mathbf{B} is the strain-displacement transformation matrix in related to shape functions; \mathbf{d} is an approximate strain field.

The simple element is a cubic element, in which cubic and linear functions are assumed. Rewriting Equation (2.5) in differential form, we can get the increment of stress field as,

$$d\mathbf{S}(x) = \mathbf{k}(x)d\mathbf{d}(x) = \mathbf{k}(x)\mathbf{B}(x)d\mathbf{D} \quad (2.6)$$

in which, $\mathbf{k}(x)$ is the section stiffness matrix. Integrating stress resultants $\mathbf{S}(x)$ along the element, the equilibrium condition can be obtained,

$$\mathbf{P} = \int_0^L \mathbf{B}^T(x)\mathbf{S}(x) dx \quad (2.7)$$

Finally, the tangent stiffness matrix can be obtained as,

$$\mathbf{K} = \frac{\partial \mathbf{P}}{\partial \mathbf{D}} = \int_0^L \mathbf{B}^T(x)\mathbf{k}(x)\mathbf{B}(x) dx \quad (2.8)$$

The discretization error limits the accuracy of the cubic element. Results predicted by

the Hermite element are precise if the deflection of the element is small, whereas if the deflection or the axial force is sufficiently large, the results could be erroneous due to the cubic deflection function is incapable of capturing the deformation (Chan and Gu, 2000). Accordingly, modeling a single member commonly requires two or more elements to improve the accuracy. Research indicated that Hermite element overestimated 21.6% of the buckling load for a simple-supported strut when a member was modeled by only one single element (So and Chan, 1991). Additionally, this element usually ignores the member initial curvature. Hence, this kind of element is unable to directly apply in the second-order direct analysis. The common solution to overcome this problem is adopted refined the finite element mesh. This will bring additional workload to engineers and increase the computer time. This conventional displacement-based beam-column does not satisfy the requirement of the practical design.

Chan and Zhou (1994) initially proposed a Pointwise-Equilibrating-Polynomial (PEP) element which has been promoted in varied kinds of second-order analysis over the last decades. The element is particularly effective and workable for second-order nonlinear analysis and allows for a single element per member. There are four compatibility conditions and two equilibrium conditions in the PEP element. The shape function of the element is a fifth-order polynomial.

Apart from increasing the order of the shape function, Liu *et al.* (2014) introduced internal degrees of freedom to form a curved arbitrarily-located plastic (ALH) element. Before the elemental stiffness matrix is assembled into the global stiffness matrix, the internal degrees of freedom need to be condensed, which can reduce the dimension of the global stiffness matrix and improve the computational efficiency. By imposing an internal node to the element, the ALH element can model the arbitrarily-located plastic

hinge along the member. Its capability of material nonlinearity will be discussed in the following section.

Through the increasing order of the shape function or adding internal nodes, the accuracy of the displacement-based element is improved. However, these approaches also lead to the complexity of formula derivation. Miguel Ferreria *et al.* (2017) proposed an improved displacement-based element (IDBE) by adding the corrective fields to alleviate error of the shape functions. The corrective nonlinear strain fields $\mathbf{d}_{NL,0,s}$ are defined as

$$\int_0^L \mathbf{B}(x) \mathbf{d}_{NL,0,s}(x) dx = 0 \quad (2.9)$$

Compared with the conventional displacement-based element, its accuracy can be easily improved by increasing integration points. But internal iteration steps are needed to determine the element status, and additional parameters associated with element state are needed to be stored.

2.1.2 Flexibility-based beam-column element

Compared with the displacement-based elements using displacement interpolation shape functions, the flexibility-based beam-column element is deduced from exact force interpolation functions. The typical form of this element will be introduced. The governing equation is defined as below,

$$\mathbf{S}(x) = \mathbf{b}(x)\mathbf{P} \quad (2.10)$$

where \mathbf{b} is the force shape functions. This equation satisfies the equilibrium condition and do not make any approximation. Using special shape function, the element is able to consider second-order effect. Rewriting Equation (2.10) in

differential form, we can get the increment of deformation field,

$$\mathbf{d}\mathbf{d}(x) = \mathbf{f}(x)d\mathbf{S}(x) = \mathbf{f}(x)\mathbf{b}(x)d\mathbf{P} \quad (2.11)$$

where \mathbf{f} is the section flexibility matrix. The compatibility condition can be expressed as,

$$\mathbf{D} = \int_0^L \mathbf{b}^T(x)\mathbf{d}(x) dx \quad (2.12)$$

Finally, the flexibility matrix of the beam-column element can be obtained as,

$$\mathbf{K} = \frac{\partial \mathbf{D}}{\partial \mathbf{P}} = \int_0^L \mathbf{b}^T(x)\mathbf{f}(x)\mathbf{b}(x) dx \quad (2.13)$$

Because of the exact force interpolation function, flexibility-based elements can provide more accurate numerical results comparing with displacement-base elements. Its numerical error is only involved with integration along the element, which can be relieved by increasing the number of integration points. Many scholars devote to the research of exquisite element, such as King *et al.* (1992), Pi and Trahair (1994), Neuenhofer and Filippou (1998), Barsan and Chiorean (1999), El-Tawil and Deierlein (2001), Nukala and White (2004a), Scott and Fenves (2006), Saritas and Soydas (2012). Although these elements are utilized to numerous frame analyses, they do not consider the influence of member initial imperfection. It means they are unsuitable for second-order direct analysis, especially when the structure is complex in such case the effective length method is not applicable. Chiorea (2017) accounted for initial geometrical imperfections by applying a uniform member load and solving the second-order differential equation. This method is not convenient to satisfy different patterns of the initial geometrical imperfection in design codes.

Some scholars also developed a beam-column element based on the equilibrium

equation, called stability function element, such as Chan and Gu (2000). The tangent stiffness can be deduced from the equilibrium equation as below,

$$EI \frac{d^2 v_1}{dx^2} = -Pv + \frac{M_1 + M_2}{L} x - M_1 \quad (2.14)$$

in which, EI is the flexural stiffness; M_1 and M_2 are the end moments; P is the axial force. With the boundary conditions, the relationship between the forces and the deformations can be derived as follows,

$$M_1 = \frac{EI}{L} [c_1 \theta_1 + c_2 \theta_2] \quad (2.15)$$

$$M_2 = \frac{EI}{L} [c_2 \theta_1 + c_1 \theta_2] \quad (2.16)$$

$$P = EA \left[\frac{u}{L} - b_1 (\theta_1 + \theta_2)^2 - b_{21} (\theta_1 - \theta_2)^2 \right] \quad (2.17)$$

where c_1 and c_2 are the stability function, b_1 and b_2 are the curvature function owing to axial loads. Noted that these parameters are depended on the various loading conditions. It needs three sets of stiffness matrixes for the cases $P > 0$, $P = 0$ and $P < 0$. Thus, there exists a potential risk in the numerical instability during the process of the analysis.

2.2 Plasticity models for material nonlinearity

Performance-based design method is adopted in most design codes, which requires structural analysis with material and geometrical nonlinearities. The inelastic deformation should be accurately predicted during the analysis process. To achieve this aim, scholars developed beam-column elements considering material nonlinearity by three methods, i.e., concentrated plasticity, distributed plasticity and distributed plastic hinge.

2.2.1 Concentrated plasticity

As we known, time history analysis, due to small time increment and some iterations during the incremental-iterative process, is time-consuming. Concentrated plasticity method, also well-known as plastic hinge method, is a good compromise between the accuracy and the computational efficiency and therefore is widely used to consider material nonlinearity. Plastic hinge method assumes that ideally plastic behavior occurs at the end of members, and the length of plastic hinge is considered as zero. Noted that the plastic hinge is lumped only at the end of beam-column elements, while the rest of the element remains elastic during the analysis. Through defining different plastic hinge models, the beam-column element with plastic hinge can have various performance. Several plasticity models will be discussed in the following subsections.

2.2.1.1 Perfectly elastic-plastic hinge model

This model assumes that two ends of the beam-column element remain elastic before their internal forces reach the cross-section plastic strength. When the internal force violates the yield criteria surface, the section will be assumed to fully yield and a fully plastic hinge happens. This model is simple and adopted by many design codes, such as AISC-LRFD (2011), but it does not consider the gradually yielding process from elastic to plastic state.

2.2.1.2 Elastic-plastic hinge model

Unlike perfectly elastic-plastic hinge model, the elastic-plastic hinge model can reflect the degradation of frame section stiffness, which is closer to the actual situation. There are three types of elastic-plastic hinge models: column tangent modulus model,

stiffness degradation model and refined-plastic hinge model. The column tangent modulus model reduces the elastic modulus as the axial force increases, and the relationship between tangent modulus and axial force can be defined by designers. The design codes, such as AISC-LRFD (2011), also give the reduction factors of the tangent modulus. Liew *et al.* (1993) also improved the equations of reduction factors as showed in Equation (2.18) and (2.19).

$$\frac{E_t}{E} = 1.0 \quad \text{for } P \leq 0.39 P_y \quad (2.18)$$

$$\frac{E_t}{E} = -2.7243 \frac{P}{P_y} \quad \text{for } P > 0.39 P_y \quad (2.19)$$

Clearly, this method considers the influence of axial force, and is efficient to the plastic strength for columns under heavy axial force. However, it cannot be able to model the plastic strength change of beams which are usually dominated by bending moments. The stiffness degradation model adjusts stiffness based on the force situation to simulate gradual yielding. It means the element stiffness varies from elastic to perfectly plastic. Liew *et al.* (1993) proposed a coefficient matrix to change elemental stiffness as,

$$\begin{pmatrix} \Delta M_A \\ \Delta M_B \end{pmatrix} = \frac{E_t I}{L} \begin{bmatrix} \phi_A [S_1 - \frac{S_2^2}{S_1} (1 - \phi_B)] & \phi_A \phi_B S_2 \\ \phi_A \phi_B S_2 & \phi_B [S_1 - \frac{S_2^2}{S_1} (1 - \phi_A)] \end{bmatrix} \begin{pmatrix} \Delta \theta_A \\ \Delta \theta_B \end{pmatrix} \quad (2.20)$$

ϕ is a scalar parameter and determined by axial force and moment. Thus, it considers the interaction between the axial force and the bending moment and also allows gradual degradation of element stiffness from elastic to fully plastic.

Iu *et al.* (2009) developed a refined plastic hinge model for steel frames which allows for gradual yielding, having the same features as distributed plasticity. When the cross-section becomes fully plastic, this model also can consider strain hardening. Combined

with a fourth-order beam-column element, it achieves high accuracy and fewer iterations when solving material nonlinearity problems. In this model, partial plasticity is modeled by initial yield and full yield functions, and accordingly the axial stiffness and bending stiffness varies from infinity to zero. For seismic design, Dides and De la Llera (2005) conducted a dynamic analysis of building structures by the lumped plasticity models.

The concentrated plasticity model is used not only in modeling steel structures but also in modeling RC structures. Zhao *et al.* (2012) adopted the lumped plasticity model to model RC flexural members and evaluated the plastic-hinge length by comparing with distributed plasticity model. Babazdeh *et al.* (2016) also investigated the plastic-hinge length of RC bridge columns. They found that the plastic hinge model developed for shorter columns produces a conservative prediction of long RC bridge columns. Compared with steel structures, the behavior of RC or composite structures is largely affected by the reinforcement ratio. Generally, the plastic hinge models for RC or composite structures are section-dependent, and therefore it is inconvenient for practical use.

2.2.1.3 Stress resultant model

The stress resultant model is also able to model the gradual yielding of frame sections. This kind of model is derived from the classical material constitutive model. The latter one is presented in stress space, while the former is described in stress-resultant space. This model has been used to simulate material nonlinearity of shell sections and frame sections. Stress resultant model is studied by many scholars, such as Orbison (1982), Hajjar (1998), Ma (2004), Alemdar (2005). El-Tawil (1998) proposed a bounding surface plasticity model, which can obtain a better result when using Mroz's kinematic

rule in stress-resultant space. Generalized plasticity firstly was used to model metal behaviors. This model has only two parameters with clear physical meaning and can describe the process from elastic to plastic. Auricchio and Taylor (1999, 1995 and 1993) also developed a return map algorithm to determine the stress state, which was proved to be very efficient. Some scholars extended generalized plasticity concept to describe stress resultants of frame sections. Kostic (2013, 2016) proposed a generalized plasticity model to represent the gradual yielding of frame sections. This model has two surfaces: loading surface and limited surface. The interaction between the axial force and bending moments has been taken into account. Long and Hung (2008) introduced the effective strain and the plastic modulus to model gradual yielding. However, these two parameters are difficult to determine, which lead inconvenience to practical use.

2.2.2 Distributed plasticity

Though the aforementioned concentrated plasticity models are effective in elastic-plastic analysis, they are unable to reflect the distribution of plasticity along the members due to its zero-length assumption. The distributed plasticity models are developed to overcome the disadvantages of the concentrated plasticity models. Generally, the distributed plasticity is achieved by fiber section approach. This method is section-independent, and any frame sections can be discretized to several finite regions to get more accuracy inelastic response, as seen in Fig. 2.1. The uniaxial material is imposed to each fiber. It means that the state of each fiber can be determined by axial strain and curvature of the frame section. The constitutive relationship of uniaxial material can be defined by users. The models such as elastic-perfectly plastic with zero tensile strength for concrete and Giuffre-Menegotto-Pinto

model for steel have been widely used. Filippou (1983) and Botez *et al.* (2014) compared concentrated plastic hinge and distributed plasticity by conducting progressive collapse analysis. They found that though distributed plasticity costs more run-time than the plastic hinge method, it can provide more trustful results and make better progressive collapse verdict. Astroza *et al.* (2014) adopted distributed plasticity using fiber sections to identify damage by a nonlinear stochastic filtering technique. The accuracy of distributed plasticity is affected by the integration scheme and number of integration points. Scott and Fenves (2006) evaluated several integration schemes and reported their precision with different number of integration points. He *et al.* (2016) tried to resolve this disadvantage by studying the relationship between the optimal element size and the number of integration points. Though evaluating the possible plastic-hinge length, the optimal element size can be used to mesh members. In practice, this method can be used to model frame structures with any sections, such as steel, RC or composite sections. Based on the distributed plasticity models, Kucukler *et al.* (2014) used the stiffness reduction method to capture the effects of residual stress and geometrical imperfections. Pan *et al.* (2016) investigated the effect of reinforcement anchorage slip in the footing by efficient fiber beam-column elements. In general, the distributed plasticity model performs well in computational accuracy with wider application range. The main obstacle of this model lies in the less computational efficiency.

2.3 Modeling of member initial imperfections

As mentioned above, the Pointwise-Equilibrating-Polynomial (PEP) element can consider member initial imperfection and allow large deflection via only a single element per member. The PEP element was used for the second-order inelastic

analysis of steel frameworks was proposed by Zhou and Chan (2004). An arbitrary elastic-perfectly plastic hinge can be formed along the element length. The PEP element was employed to the second-order analysis of single angle trusses and further validated by experiment results (Chan and Cho, 2008; Cho and Chan, 2008; Fong *et al.*, 2009). The PEP element was extended to the nonlinear analysis of composite steel and concrete members and frameworks and verified by a range of experiments (Fong *et al.*, 2009, 2011). Liu *et al.* (2010) adopted this element to conduct the pushover analysis for performance-based seismic design. An imperfection truss element is proposed by Zhou *et al.* (2014) to consider geometrically nonlinear buckling and seismic performance of suspend-dome. However, their work did not consider material nonlinearity. The ALH element (Liu *et al.*, 2014a, 2014b) can not only model member P- δ effect directly but also material nonlinearities using the plastic hinge method. Bar-spring models were developed by Meimand *et al.* (2013) to simulate geometrical imperfections and nonlinear material behavior. A set of slope-deflection equations or closed-form equations (Smith-Pardo and Aristizábal-Ochoa, 1999; Chan and Gu 2000; Aristizabal-Ochoa 2010) based on the classical stability functions were used to capture the imperfections by the corresponding beam-column elements. The geometrical-nonlinear axial factor (Aristizabal-Ochoa, 2000) can include transverse forces caused by initial imperfections, but these formulas are limited to elastic members. The stability functions were further refined by Goto and Chen (1987) through a power series without truncations. Following this research, the power series was formulated, and a full set of stiffness equations for nonlinear analysis was proposed by Goto and Chen (1987). Ekhande *et al.* (1989) recommended a new expression of the stability functions for the sake of the analysis of three-dimensional frames. Chan and Gu (2000) developed the stability function including the member initial imperfection for second-

order elastic analysis allowing for one element per member. A stability function accounting for lateral-torsional buckling was proposed by Kim *et al.* (2006) with sufficient accuracy for engineering practice.

In summary, there is lack of study on the flexibility-based beam-column elements incorporating member initial imperfection at the elemental level for second-order inelastic analysis. Although the studies of stiffness-based beam-column elements considering initial imperfection are sufficient, this kind of elements does not show good performance on second-order inelastic analysis.

2.4 Modeling of semi-rigid connections

The connection behavior may significantly affect the system behavior. In such case, the joint flexibility should be carefully considered in the process of second-order direct analysis. It is hard to propose a generalized model for connection systems due to their variety and especially the different geometry of the connected members. Therefore, experimental tests are commonly used to explore the joint behavior and then some empirical formulas are developed according to experimental data. A rather considerable amount of research works on monotonic loading tests and cyclic loading tests for different connection systems have been conducted in the past few decades, for example, Prabha *et al.* (2010). Valuable data about joint behavior have been collected to form various mathematical functions representing the different nonlinear behavior of diverse connection types. The details about modeling of connection will be described in Chapter 5.

After obtaining the formulation of connection models, different semi-rigid connection modeling approaches are proposed. Asgarian *et al.* (2015) developed a three-dimensional joint flexibility element to represent the local behavior of a tubular joint.

This element has two nodes with one located at the intersection of diagonal braces and chord and horizontal braces and chord, and the other one located at the intersection of the brace centerline with wall of chord. Hence, local joint deformation can be taken into account during the analysis, and relatively accurate predictions can be produced by this element. Yu and Zhu (2016) introduced an independent zero-length element to simulate the connections in the nonlinear dynamic collapse analysis with finite particle method (FPM). The zero-length element with the hysteretic relationship of moment and rotation can absorb energy and therefore improve the anti-collapse capacity of the whole structure. On the contrary, fully rigid or ideally pinned connections do not make any contribution to the energy absorbing. More importantly, this effect also is in conjunction with axial forces, which has been ignored by many researchers.

2.5 Design method for CFT members with noncompact and slender sections

The concrete-filled steel tube (CFT) members have been studied by many researchers based on experimental tests or numerical simulation. Various loading conditions such as axial compression, flexural, and their combination were set up to test the complex behaviors of CFT members. Several parameters, such as yield stress F_y of the steel tube, the compressive strength of the concrete infill, width-to-thickness ratios of the steel tube, column length to depth ratio and so on, were investigated through numerous tests. However, most experiments force on compact CFT members, such as Nishiyama *et al.* (2002), Kim (2005), Gourley *et al.* (2008) and Hajjar (2013). In contrast, there is few tests on the noncompact and slender CFT members, which brings about few researches on the development of design method for these kinds of CFT members.

In the field of numerical simulation, the complex behaviors of CFT such as steel tube yielding, local buckling, concrete confinement, crack, and slippage between the steel tube and the concrete infill, make them difficult to be directly modeled by numerical methods for practical use. Generally, there are two categories of modeling methods to predict the behavior of CFT members: detailed 3D finite element models and simple beam-column element models. The first method can explicitly account for the effects of local buckling and hoop stresses in the steel tube, and the effects of confinement on the concrete infill. Due to the accurate and relative detailing modeling of CFT members, this method often is used to conduct parameter studies with true experiments or calibrate other numerical modeling methods by researchers. Lai *et al.* (2014) built detailed 3D finite element models to model noncompact or slender rectangular CFT members to address gaps in the experimental database. Lai and Varma (2015) conducted various of parametric studies of noncompact and slender circular CFT members to by 3D finite element modes. Lam *et al.* (2012) adopted three-dimensional 8-node solid elements to model the stub concrete-filled steel tubular column with tapered members. Liew and Xiong (2009) used continuum solid and shell elements to study the behavior of CFT members with initial preload. Du *et al.* (2017) adopted 8-node reduced integration brick elements to study the behaviors of high-strength steel in CFT members.

The second method adopts beam-column elements to consider the complex behaviors of CFT members explicitly or implicitly. The explicit one adds extra degrees-of-freedom to the end nodes of beam-column elements. Tort and Hajjar (2010) extended the conventional 12 DOF beam element into 18 DOF beam element to consider the slip deformation between the steel tube and the concrete infill of rectangular CFT members. Lee and Filippou (2015) proposed a composite frame element to capture the

bond-slip behavior at the interface between the steel tube and concrete infill based on an extension of the Hu-Washizu variational principle. Its highlight is the exact interpolation of the total section forces. These kinds of beam-column elements, solving problems, need to introduce additional DOF although they can be condensed in elemental level. The implicit approach commonly adopts fiber-based beam-column elements with effective stress-strain relationship to reflect complex behaviors of CFT members phenomenally. Regarding CFT members with compact sections, there are several effective stress-strain relationships available to be utilized by fiber-based beam-column elements, such as Tort and Hajja (2010), Sakino *et al.* (2004), Han *et al.* (2005) and Liang (2009). As for noncompact and slender CFT members, available effective stress-strain relationships are few. Lai and Varma (2016) proposed effective stress-strain relationships for noncompact and slender circular or rectangular CFT members. They also were implemented in a nonlinear fiber analysis macro model to verify its conservatism. But NFA was only capable of analyzing the problems of P-M. As for the problems with P-M-M or torsional force, this method was not suitable. Meanwhile, NFA divided one single CFT member into several components, which would lead to heavier computer time.

2.6 Design method of special concentrically braced frames

During the last decades, several strong earthquakes happened around the world. These earthquakes caused huge loss of property and human life. Special concentrically braced frames (SCBFs) are widely used in high seismic regions due to structural efficiency and particularly high ductility for energy dissipation. SCBFs are allowed for large inelastic deformation through tensile yielding, buckling and post-buckling behaviors of braces. This structural system can provide reasonable lateral stiffness and

strength in elastic range, and have advantages on energy dissipation and ductility in plastic range to achieve operational performance targets. Recently, the performance-based seismic design (PBSD) is recommended by many modern codes to achieve an economic design. This design method requires more accurate numerical analysis. For this reason, the accurate modeling of braces with acceptable computational costs is vital to capture the real structural behavior of SCBFs subjected to earthquakes.

Lots of scholars proposed modeling methods to capture the complex behaviors of SCBFs, such as buckling capacity, tensile yielding, post-buckling, the fracture and post-fracture behavior. Previous researches (Hsiao *et al.* 2012, 2013; Karamanci and Lignos 2014; Krishnan 2010; Uriz 2005) show that the initial curvature of steel braces should be taken into account so that the buckling and post-buckling behavior of steel braces can be triggered in numerical analysis. Several elements per member are recommended to capture the complex behavior of braces and accurate prediction compared to the test results is reported (Hsiao 2012, 2013; Karamanci 2014; Uriz, 2005). This treatment will significantly increase the computational time. Krishnan (2010) proposes a modified elastoplastic fiber element, which consists of three fiber segments demarcated by two external nodes and four internal nodes, to simulate the inelastic behavior of slender columns and braces. However, the element formulation is too complicated with lower numerical efficiency. Hsiao (2012) modeled the beams, columns, and braces by fully nonlinear beam-column elements which fail to consider local second-order effect or $P-\delta$ effect. Meanwhile, this study indicated that a special node located at the middle of braces must be assigned to model the initial member imperfection. This is one reason for that multi-elements are needed to model a single brace. Uriz (2008) suggested that the brace member should be subdivided into two inelastic beam-column elements for an accurate representation of its complex behavior.

Though an extensive set of experimental data of braces with different cross sections and slenderness ratios were matched with his proposed model, all these specimens are single brace components.

Extensive works have been conducted on the modeling of braces as well as their joints connected to beams and columns and aim to accurately predict the cyclic deterioration in strength and stiffness of structural components. The typical behavior and the potential failure locations of a single brace are shown in Fig. 2.3. Uriz (2005) points out the limitation of the traditional phenomenological model in predicting peak responses of steel braces and proposes a brace component model which can well simulate the post-buckling behavior and fracture of steel braces subjected to cyclic loading. Yoo *et al.* (2008) use continuum finite element (FE) model to study the behavior of gusset plate connection and the interaction between the connection and framing elements. They also point out that proper detailing of gusset plate connection will improve the performance of SCBFs. Uriz and Mahin (2008) propose a force-based fiber element to simulate the behavior of gusset plate connection while Hsiao *et al.* (2012) introduce rotational hinges attached to ends of the beam-column element to model the connections. Lehman *et al.* (2008) conduct an experimental test to improve the economy and performance of gusset plate connections. Fell *et al.* (2009) experimentally investigate the inelastic buckling and fracture behavior of steel braces including square hollow section, pipe and wide-flange H-shape section. Generally, the geometry and properties of the gusset plate determine the stiffness of zero-length end spring.

To improve the design practice for the braced frames, a practical analytical model is proposed. The accuracy of the proposed model is verified using a series of experimental specimens, single-brace component and full-scale multistory frames.

The computation cost of the proposed model was also compared with other fiber-type finite element model, which uses several elements to model one brace.

FIGURES

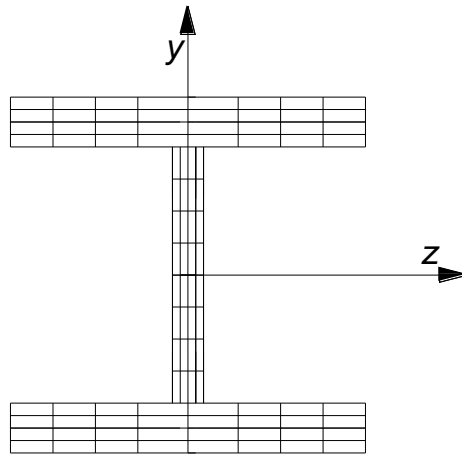
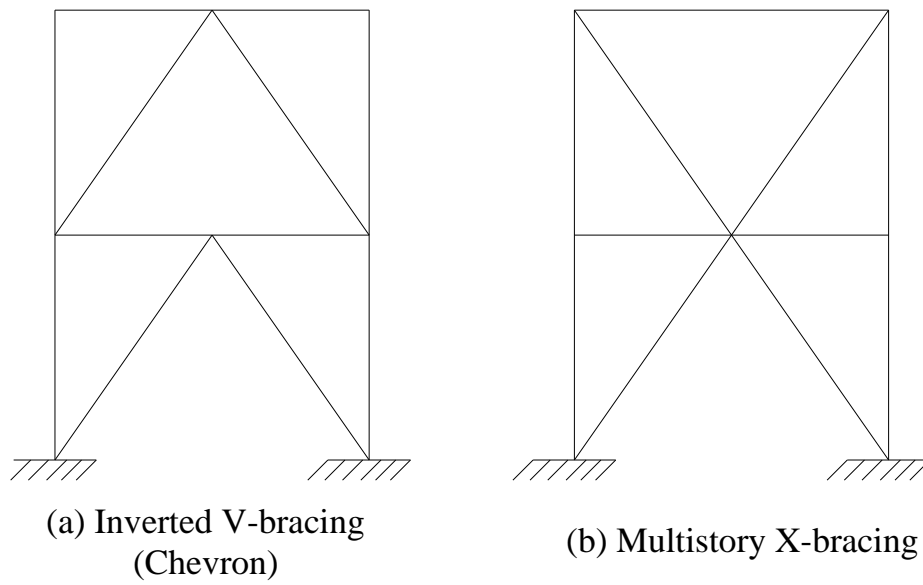


Fig. 2.1 Section discretization



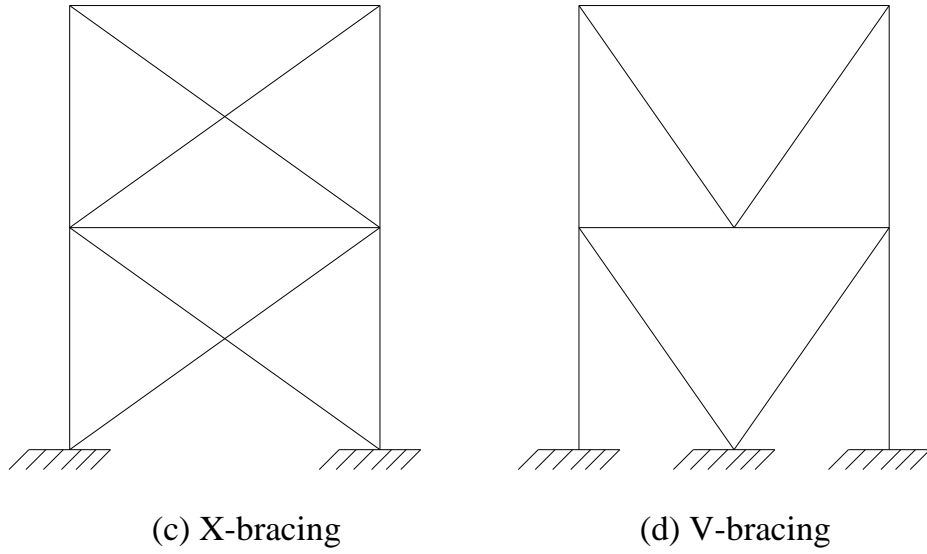


Fig. 2.2 Commonly used configurations of SCBFs

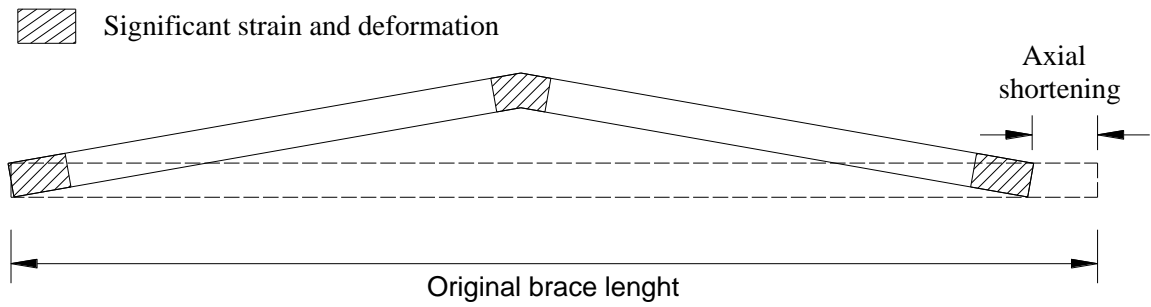


Fig. 2.3 Structural behavior of brace and failure locations

CHAPTER 3. FLEXIBILITY-BASED BEAM-COLUMN ELEMENT CONSIDERING MEMBER IMPERFECTION

3.1 Introduction

The modern design codes such as AISC360 (2016) and Eurocode-3 (2005) specify a rational approach, i.e., second-order direct analysis method (DAM), for stability analysis and design. “Direct Analysis” is also well-known as “Second-order Analysis” or “Advanced Analysis”. This method has several advantages compared with the conventional effective length method (ELM). Firstly, it has a wider range of application as it can be applied to all types of structural systems. Secondly, more accurate internal forces and moments of members can be captured by direct analysis. Thirdly, accurate consideration of column restraints brings a rotational design of beams and connections. Lastly, accessing the member and system stability in an integrated way makes the whole design procedure simpler without the need of effective length factor.

General speaking, the factors such as initial imperfection, material yielding, second-order effects and joint flexibility may affect the deflection and instability of the structural system. Regarding initial imperfection, it consists of geometrical imperfections and residual stress. In comparison of DAM, “Indirect Analysis” means that the analysis ignores one or several key factors above. The second-order effects, the member initial bowing and their coupling effects make a big contribution to the geometrical nonlinearity of individual members and the structural system. Therefore,

it is necessary to develop a practical second-order beam-column element to consider the member initial bowing for global analysis. The first global buckling mode is commonly adopted to determine the frame imperfection as well as the member initial imperfections in accordance with design codes. The practical design requires a simple modeling method, using as fewer elements as possible, to model initial out-of-straightness because more elements will lead to significant increase of modeling efforts and computer time.

There are several researches focusing on the development of beam-columns elements. As for displacement-based elements, Chan and Zhou (1995) directly incorporated member initial bowing in the elemental formulation. And this element has high accuracy. Liu *et al.* (2014a, 2014b) also developed a beam-column, using condense degrees of freedom (DOFs) technology, for second-order direct analysis. Based on the stability function, Chan and Gu (2000) developed a nonlinear beam-column element which performs well on modeling highly slender members under axial compressional force. Furthermore, the refined plastic hinge technique is introduced to the beam-column element to consider material nonlinearity of steel and composite structures (Liu *et al.* 2010, 2012). The element stiffness matrices of the beam-column elements developed by Chan (1995, 2000) and Liu *et al.* (2014a, 2014b) were formed by exact integration method which is better than the numerical integration method regarding numerical efficiency. Excellent performance and fast convergence are reported in their works. Ziemian and McGuire (2002) proposed a modified tangent modulus approach considering residual stress and plastic hinge for second-order inelastic analysis. Their method is simple and can be easily incorporated into the conventional displacement-based beam-column elements, but the geometric imperfections are not included at the element level.

For the flexibility-based beam-column elements, extensive works have been done to improve their performance (Alemdar, 2005; De-Souza, 2000; Jafari, 2010; Neuenhofer, 1997, 1998; Rezaiee-Pajand 2015; Spacone 1996). Neuenhofer and Filippou extended the elastic flexibility-based beam-column to consider material nonlinearity (1997) and second-order effect (1998). Neuenhofer and Filippou (1998) introduced Newton-Raphson method to determine elemental state and form element stiffness matrix. Nukala and White (2004a) summarized four algorithms to determine element state for nonlinear beam-column elements based on Hellinger-Reissner (HR) variational principle. This principle was adopted by De Souza (2000) to derive the weak form of equilibrium and compatibility equations for a new flexibility-based element. With the corotational technology, this new element was capable of large displacement inelastic analysis of 3-dimensional frame. Though flexibility-based beam-column elements have been improved largely, they still cannot explicitly model initial member geometric imperfections which is a vital factor emphasized by Eurocode-3 (2005) and CoPHK (2011) in the practical design.

From above, displacement-based elements and flexibility-based elements show unique superiority for computational efficiency and wide application range. The former can solve problems of geometric nonlinearity with a simple procedure and quick convergence to get reasonably accurate results, which save much computer time. On the other hand, the latter shows powerful capacity on geometric and material nonlinearity. Strict satisfaction of force equilibrium enables it to erase fitting errors of shape function. Although increasing the number of modeling elements can increase the accuracy by displacement-based elements, it will bring extra works for modeling the member initial imperfection and post-processing. Elastic-plasticity problems can be handled by the displacement-based elements equipped with refined plastic hinge

technique by Liew (1993). Recently, the plastic hinges can be formed in arbitrary location along the member in some elements proposed by Liu *et al.* (2014a, 2014b). But they may give inadequate results for the more complicated plastic behavior of member under complex loading scenarios.

In this study, a second-order flexibility-based beam-column element is proposed for direct analysis. The equilibrium and compatibility equations are derived by Hellinger-Reissner (HR) functional. The original work by Neuenhofer (1998) is improved here by incorporating member initial geometric imperfection at the elemental level to satisfy the requirements of the practical design. As for geometric nonlinearity, the effect of $P - \delta$ and $P - \delta_0$ can be directly accounted for. In terms of material nonlinearity, the distributed plasticity approach is used in the proposed element. The stiffness matrix of cross-sections at integration points can be assembled by fiber section technology or be directly calculated by stress-resultant plasticity model, which will be introduced in Chapter 4.

3.2 Element formulations

The flexibility-based beam-column element proposed by Neuenhofer and Filippou (1998) will be improved by incorporating initial member geometric imperfection at the elemental level for direct analysis.

The following assumptions have been adopted in the proposed element:

1. The effect of warping and shear deformation is ignored;
2. Euler-Bernoulli beam theory is adopted by the proposed element.

For simplicity, the proposed element is derived in the elemental basic coordinate system excluding the rigid body movement. The description of the proposed element will be arranged as:

1. The kinematic hypothesis is presented for the proposed element.
2. The equilibrium and compatibility equations are introduced by the Hellinger-Reissner (HR) functional.
3. The section flexibility matrix is formed by the integration along the cross-section to assemble the elemental flexibility matrix.
4. The curvature-based displacement interpolation (CBDI) technique proposed by Neuenhofer and Filippou (1998) will be briefly introduced to calculate the displacements of integration points.
5. The transformation from basic coordination system to global coordination system will be carried out by a corotational approach.

3.2.1 Basic coordinate system

In the global coordinate system, there are six degrees of freedom for each node, i.e., three translational and three rotational DOFs, as shown in Fig. 3.1. Excluding the rigid body modes, the proposed beam-column element can be simply expressed in the elemental basic coordinate system. In the basic coordinate system, the total degrees of freedom (DOF) are six, with \mathbf{P} for element forces and \mathbf{D} for the corresponding end displacements. They are given below,

$$\mathbf{P} = \{P_1 P_2 P_3 P_4 P_5 P_6\}^T = \{N M_{Iz} M_{Jz} M_{Iy} M_{Jy} T\}^T \quad (3.1)$$

$$\mathbf{D} = \{D_1 D_2 D_3 D_4 D_5 D_6\}^T = \{u \theta_{Iz} \theta_{Jz} \theta_{Iy} \theta_{Jy} \psi\}^T \quad (3.2)$$

3.2.2 Kinematic hypothesis

Ignoring the effect of warping, the displacement field of the three-dimensional beam-column element based on Bernoulli-Euler beam theory can be given as,

$$\mathbf{u}(x, y, z) = \begin{Bmatrix} u_x(x, y, z) \\ u_y(x, y, z) \\ u_z(x, y, z) \end{Bmatrix} = \begin{Bmatrix} u(x) - y \cdot v'(x) - z \cdot w'(x) \\ v(x) - z \cdot \psi(x) \\ w(x) + y \cdot \psi(x) \end{Bmatrix} \quad (3.3)$$

where $u(x)$, $v(x)$ and $w(x)$ are displacement along the x direction, y direction and z direction respectively; $\psi(x)$ is torsional angle about x direction.

The Green-Lagrange strain tensor can be simplified and written regarding the displacement components as,

$$\begin{cases} E_{xx} \cong \frac{\partial u_x}{\partial x} + \frac{1}{2} \left(\frac{\partial u_y}{\partial x} \right)^2 + \frac{1}{2} \left(\frac{\partial u_z}{\partial x} \right)^2 \\ E_{xy} \cong \frac{1}{2} \left(\frac{\partial u_x}{\partial y} + \frac{\partial u_y}{\partial x} \right) \\ E_{xz} \cong \frac{1}{2} \left(\frac{\partial u_x}{\partial z} + \frac{\partial u_z}{\partial x} \right) \end{cases} \quad (3.4)$$

Ignoring the contribution of torsional deformation on the axial strains, the strain field at the arbitrary location (x, y, z) of the cross section can be derived by the substituting Equation (3.3) into Equation (3.4). It can be expressed as

$$\boldsymbol{\varepsilon}(x, y, z) = \boldsymbol{\Psi}(y, z) \mathbf{d}(x) \quad (3.5)$$

where $\boldsymbol{\Psi}(y, z)$ is a 3x4 transformation matrix as shown in Equation (3.7); $\varepsilon_0(x)$ is the strain along neutral axis; $\kappa_y(x)$ and $\kappa_z(x)$ are curvatures of cross-sections about y and z axes respectively; $\varphi(x)$ is the torsional angle about x axis.

$$\mathbf{d}(x) = \begin{Bmatrix} \varepsilon_0(x) \\ \kappa_z(x) \\ \kappa_y(x) \\ \varphi(x) \end{Bmatrix}$$

$$\begin{aligned}
 &= \left\{ \begin{array}{c} u'(x) + \frac{1}{2} \left((v(x) + v_0(x))' \right)^2 + \frac{1}{2} \left((w(x) + w_0(x))' \right)^2 - \frac{1}{2} (v_0'(x))^2 - \frac{1}{2} (w_0'(x))^2 \\ (v(x) + v_0(x))'' - v_0''(x) \\ - \left((w(x) + w_0(x))'' - w_0''(x) \right) \\ \psi'(x) \end{array} \right\} \\
 &= \left\{ \begin{array}{c} u'(x) + \frac{1}{2} (v'(x))^2 + \frac{1}{2} (w'(x))^2 + v'(x) v_0'(x) + w'(x) w_0'(x) \\ v''(x) \\ -w''(x) \\ \psi'(x) \end{array} \right\}
 \end{aligned} \tag{3.6}$$

$$\mathbf{\Psi}(y, z) = \begin{bmatrix} 1 & -y & z & 0 \\ 0 & 0 & 0 & -z \\ 0 & 0 & 0 & y \end{bmatrix} \tag{3.7}$$

In Equation (3.6), $v_0(x)$ and $w_0(x)$ are lateral initial geometrical imperfections with respect to y and z axes respectively. They will be explained and will be detailed in section 4 of this thesis. It is worth to point that the effect of member initial geometric imperfection is directly incorporated which is not mentioned in previous researches (De-Souza, 2000; Neuenhofer, 1997; Rezaiee-Pajand, 2015).

3.2.3 Hellinger-Reissner variational formulation

Regarding displacement-based elements, equilibrium and compatibility equations are generally induced by the principle of minimum potential energy. The proposed element is derived by the Hellinger-Reissner (HR) variational principle. This principle has two variables: displacement field \mathbf{u} and stress field $\boldsymbol{\sigma}$ as given in Equation (3.8).

$$\Pi_{HR}(\boldsymbol{\sigma}, \mathbf{u}) = \int_{\Omega} \{ \boldsymbol{\varepsilon}(x, y, z) \boldsymbol{\sigma} - \chi(\boldsymbol{\sigma}) \} d\Omega + \mathbf{\Pi}_{ext}(\mathbf{u}) \tag{3.8}$$

in which, $\Pi_{ext}(\mathbf{u})$ is the external work potential term due to the external loads and given in Equation (3.9); Ω is the volume of elements in the undeformed pattern; σ is the stress field of cross-sections as given in matrix form in Equation (3.11).

$$\Pi_{ext}(\mathbf{u}) = \overline{\mathbf{P}}^T \mathbf{D} \quad (3.9)$$

$$\boldsymbol{\sigma} = \begin{Bmatrix} \sigma_x \\ \tau_{xy} \\ \tau_{xz} \end{Bmatrix} \quad (3.10)$$

where σ_x is the normal stress; τ_{xy} and τ_{xz} are the shear stress along z and y respectively.

After getting the stress of cross-sections, the stress resultants $\mathbf{S}(x)$ at the integration points can be integrated over the cross-section areas,

$$\mathbf{S}(x) = \begin{Bmatrix} N(x) \\ M_z(x) \\ M_y(x) \\ T(x) \end{Bmatrix} = \int_A \boldsymbol{\Psi}(y, z)^T \boldsymbol{\sigma} dA \quad (3.11)$$

Substituting Equation (3.11) into Equation (3.8), we can rewrite the variational formulation as

$$\Pi_{HR}(\mathbf{S}, \mathbf{u}) = \int_L \left\{ \mathbf{S}^T \begin{Bmatrix} u' + \frac{1}{2}v'^2 + \frac{1}{2}w'^2 + v'v'_0 + w'w'_0 \\ v'' \\ -w'' \\ \psi' \end{Bmatrix} - \chi(\mathbf{S}) \right\} dx + \overline{\mathbf{P}}^T \mathbf{D} \quad (3.12)$$

In the basic coordinate system, the boundary conditions can be presented as

$$u(0) = v(0) = w(0) = v(L) = w(L) = \psi(0) = 0 \quad (3.13)$$

$$\delta u(0) = \delta v(0) = \delta w(0) = \delta v(L) = \delta w(L) = \delta \psi(0) = 0 \quad (3.14)$$

$$\begin{cases} u(L) = D_1 & v'(0) = D_2 & v'(L) = D_3 \\ w'(0) = D_4 & w'(L) = D_5 & \psi(L) = D_6 \end{cases} \quad (3.15)$$

$$\delta v_0(x) = \delta w_0(x) = \delta v_0'(x) = \delta w_0'(x) = 0 \quad (3.16)$$

The stationary of the Hellinger-Reissner potential can be obtained by taking the first variation about the independent fields: the displacement field and the stress resultant field. After setting the stationary equal to zero, the equation can be written as

$$\delta \Pi_{HR}(\mathbf{S}, \mathbf{u}) = \delta_{\mathbf{S}} \Pi_{HR} + \delta_{\mathbf{u}} \Pi_{HR} = 0 \quad (3.17)$$

When Equation (3.17) always holds, it can produce the equilibrium and compatibility equations simultaneously. They are given in Equation (3.18) and (3.19) respectively as,

$$\delta_{\mathbf{u}} \Pi_{HR} = 0 \quad (3.18)$$

$$\delta_{\mathbf{S}} \Pi_{HR} = 0 \quad (3.19)$$

3.2.4 Equilibrium equations

Substituting Equation (3.6) and Equation (3.16) into Equation (3.18), the equilibrium equations can be rewritten in expanded form as

$$\delta_{\mathbf{u}} \Pi_{HR} = \int_L \mathbf{S}^T \left\{ \begin{array}{c} \delta u' + v' \delta v' + w' \delta w' + v'_0 \delta v' + w'_0 \delta w' \\ \delta v'' \\ -\delta w'' \\ \delta \psi' \end{array} \right\} dx - \bar{\mathbf{P}}^T \delta \mathbf{D} = 0 \quad (3.20)$$

Making use of Equation(3.11) and Equation (3.2), Equation (3.20) can be rewritten as

$$\begin{aligned} & \int_L [N(\delta u' + v' \delta v' + w' \delta w' + v'_0 \delta v' + w'_0 \delta w') + M_z \delta v'' + M_y \delta w'' \\ & \quad + T \delta \psi'] dx \\ & - \sum_{i=1}^6 P_i \delta D_i = 0 \end{aligned} \quad (3.21)$$

Introducing the boundary conditions defined in Equation (3.14) into Equation (3.21), integration by parts can be conducted as

$$\begin{aligned}
 & \int_L \{N' \delta u + [(Nv')' + (Nv_0')' - M_z''] \delta v + [(Nw')' + (Nw_0')' + M_y''] \delta w \\
 & \quad + T' \delta \psi\} dx + [-N(L) + P_1] \delta D_1 + [M_z(0) + P_2] \delta D_2 \\
 & \quad + [-M_z(L) + P_3] \delta D_3 + [M_y(0) + P_4] \delta D_4 + [-M_y(L) + P_5] \delta D_5 \\
 & \quad + [-T(L) + P_6] \delta D_6 = 0
 \end{aligned} \tag{3.22}$$

To keep Equation (3.22) always holding, the following equations of equilibrium are obtained as

$$\left. \begin{aligned}
 & -\frac{d^2 M_z(x)}{dx^2} + \frac{d}{dx} \left[N(x) \frac{dv(x)}{dx} \right] + \frac{d}{dx} \left[N(x) \frac{dv_0(x)}{dx} \right] = 0 \\
 & \frac{d^2 M_y(x)}{dx^2} + \frac{d}{dx} \left[N(x) \frac{dw(x)}{dx} \right] + \frac{d}{dx} \left[N(x) \frac{dw_0(x)}{dx} \right] = 0 \\
 & \frac{dN(x)}{dx} = 0 \\
 & \frac{dT(x)}{dx} = 0
 \end{aligned} \right\} x \in [0, L] \tag{3.23}$$

with the natural boundary conditions as

$$\begin{aligned}
 N(L) = P_1 \quad M_z(0) = -P_2 \quad M_z(L) = P_3 \\
 M_y(0) = -P_4 \quad M_y(L) = P_5 \quad T(L) = P_6
 \end{aligned} \tag{3.24}$$

Using Equations (3.23) and (3.24), the following stress resultant fields $\mathbf{S}(x)$ are obtained as

$$\mathbf{S}(x) = \begin{Bmatrix} N(x) \\ M_z(x) \\ M_y(x) \\ T(x) \end{Bmatrix} = \mathbf{b}(x) \mathbf{P} \tag{3.25}$$

where

$$\mathbf{b}(x) = \begin{bmatrix} 1 & 0 & 0 & 0 & 0 & 0 \\ v(\xi) + v_0(\xi) & \xi - 1 & \xi & 0 & 0 & 0 \\ -w(\xi) - w_0(\xi) & 0 & 0 & \xi - 1 & \xi & 0 \\ 0 & 0 & 0 & 0 & 0 & 1 \end{bmatrix}, \xi = \frac{x}{L} \tag{3.26}$$

in which, $\mathbf{b}(x)$ is the matrix of displacement-dependent force interpolation functions; x is the basic coordinate along x-direction. It should be noted that $v(\xi)$ and $w(\xi)$,

being included in Equation (3.25), are denoted the P - δ effect due to external loads. Meanwhile, $v_0(\xi)$ and $w_0(\xi)$ represent the initial imperfections.

3.2.5 Compatibility equations

The compatibility equations are introduced weakly using Equation (3.19), which can be further expressed as

$$\delta_{\mathbf{S}} \Pi_{HR} = \int_L \delta \mathbf{S}^T \left[\begin{array}{c} u' + \frac{1}{2} v'^2 + \frac{1}{2} w'^2 + v'v_0' + w'w_0' \\ v'' \\ -w'' \\ \psi' \end{array} \right] - \frac{\partial \chi(\mathbf{S})}{\partial \mathbf{S}} dx = 0 \quad (3.27)$$

Based on the definition of the complementary energy density, the deformation of cross-sections can be given as

$$\frac{\partial \chi(\mathbf{S})}{\partial \mathbf{S}} = \mathbf{d}(x) = \begin{Bmatrix} \varepsilon_0(x) \\ \kappa_z(x) \\ \kappa_y(x) \\ \varphi(x) \end{Bmatrix} \quad (3.28)$$

Then, substituting Equation (3.28) into Equation (3.27), we have

$$\int_L [\delta N \left(u' + \frac{1}{2} v'^2 + \frac{1}{2} w'^2 + v'v_0' + w'w_0' - \varepsilon_0 \right) + \delta M_z (v'' - \kappa_z) + \delta M_y (-w'' - \kappa_y) + \delta T (\psi' - \varphi)] dx = 0 \quad (3.29)$$

Considering the boundary conditions in Equation (3.15), Equation (3.29) can be integrated by parts as

$$\begin{aligned} & \int_L \left\{ \delta N' u + \left[\frac{1}{2} (\delta N v')' + (\delta N v_0')' - \delta M_z'' \right] v + \left[\frac{1}{2} (\delta N w')' + (\delta N w_0')' + \delta M_y'' \right] w \right. \\ & \left. + \delta N \varepsilon_0 + \delta M_z \kappa_z + \delta M_y \kappa_y + \delta T \varphi \right\} dx \\ & - \delta N(L) D_1 + \delta M_z(0) D_2 - \delta M_z(L) D_3 + \delta M_y(0) D_4 - \delta M_y(L) D_5 - \delta T(L) D_6 = 0 \end{aligned}$$

(3.30)

To keep Equation (3.30) always holding, the following differential equations are obtained as

$$\left. \begin{aligned} \frac{d\delta N(x)}{dx} &= 0 \\ -\frac{d^2\delta M_z(x)}{dx^2} + \frac{1}{2}\frac{d}{dx}\left[\delta N(x)\frac{dv(x)}{dx}\right] + \frac{d}{dx}\left[\delta N(x)\frac{dv_0(x)}{dx}\right] &= 0 \\ \frac{d^2\delta M_y(x)}{dx^2} + \frac{1}{2}\frac{d}{dx}\left[\delta N(x)\frac{dw(x)}{dx}\right] + \frac{d}{dx}\left[\delta N(x)\frac{dw_0(x)}{dx}\right] &= 0 \\ \frac{d\delta T(x)}{dx} &= 0 \end{aligned} \right\} x \in [0, L]$$

(3.31)

Considering the similarity between Equation (3.23) and Equation (3.31), the following virtual fields (section forces $\delta\mathbf{S}(x)$) and end forces $\delta\mathbf{P}$ can be obtained as

$$\delta\mathbf{S}(x) = \begin{pmatrix} \delta N(x) \\ \delta M_z(x) \\ \delta M_y(x) \\ \delta T(x) \end{pmatrix} = \mathbf{b}^*(x)\delta\mathbf{P} \quad (3.32)$$

where

$$\mathbf{b}^*(x) = \begin{bmatrix} 1 & 0 & 0 & 0 & 0 & 0 \\ \frac{1}{2}v(\xi) + v_0(\xi) & \xi - 1 & \xi & 0 & 0 & 0 \\ -\frac{1}{2}w(\xi) - w_0(\xi) & 0 & 0 & \xi - 1 & \xi & 0 \\ 0 & 0 & 0 & 0 & 0 & 1 \end{bmatrix}, \xi = \frac{x}{L} \quad (3.33)$$

Substituting Equation (3.32) into Equation (3.30), the equation between virtual internal forces and virtual end forces is shown below.

$$\int_L \delta\mathbf{S}(x)^T \mathbf{d}(x) dx = \delta\mathbf{P}^T \mathbf{D} \quad (3.34)$$

Rewriting Equation (3.34) with the relation between virtual section forces $\delta\mathbf{S}(x)$ and virtual end forces $\delta\mathbf{P}$, the end displacements \mathbf{D} can be given as

$$\mathbf{D} = \int_L \mathbf{b}^*(x)^T \mathbf{d}(x) dx \quad (3.35)$$

3.2.6 Section flexibility matrix

For linear analysis cases, section stress resultant, in Equation(3.11), can be directly calculated by formulation. However, section stress resultant need to be obtained by integration over the cross-section. The nonlinear section constitutive relation between section forces and deformations is given as

$$\begin{aligned} \mathbf{S}(x) &= \mathbf{C}[\mathbf{d}(x)] = \int_A \boldsymbol{\Psi}(y, z)^T \boldsymbol{\sigma}(\boldsymbol{\varepsilon}(x, y, z)) dA \\ &= \int_A \boldsymbol{\Psi}(y, z)^T \boldsymbol{\sigma}(\boldsymbol{\Psi}(y, z)\mathbf{d}(x)) dA \end{aligned} \quad (3.36)$$

The section tangent stiffness matrix $\mathbf{k}_s(x)$ can be obtained by taking the partial derivatives of Equation (3.36) as

$$\begin{aligned} \mathbf{k}_s(x) &= \frac{\partial \mathbf{S}(x)}{\partial \mathbf{d}(x)} = \int_A \boldsymbol{\Psi}(y, z)^T \frac{\partial \boldsymbol{\sigma}(x, y, z)}{\partial \boldsymbol{\varepsilon}(x, y, z)} \frac{\partial \boldsymbol{\varepsilon}(x, y, z)}{\partial \mathbf{d}(x)} dA \\ &= \int_A \boldsymbol{\Psi}(y, z)^T \mathbf{E}_t(x, y, z) \boldsymbol{\Psi}(y, z) dA \end{aligned} \quad (3.37)$$

in which, where $\mathbf{E}_t(x, y, z)$ is the material tangent stiffness at an arbitrary point (x, y, z) of the beam-column element.

Then, the section tangent flexibility matrix can be obtained by inverting the section tangent stiffness matrix $\mathbf{k}_s(x)$ in (3.37) as shown below.

$$\mathbf{f}_s(x) = \mathbf{k}_s(x)^{-1} \quad (3.38)$$

3.2.7 Element flexibility matrix

The elemental flexibility matrix considering the \mathbf{P} - δ effect can be obtained by taking derivative of the end nodal displacements \mathbf{D} in Equation (3.35) with respect to end nodal forces \mathbf{P} as

$$\begin{aligned}
\mathbf{F}_e &= \frac{\partial \mathbf{D}}{\partial \mathbf{P}} = \int_L \left(\frac{\partial \mathbf{b}^*(x)^T}{\partial \mathbf{P}} \mathbf{d}(x) + \mathbf{b}^*(x)^T \frac{\partial \mathbf{d}(x)}{\partial \mathbf{P}} \right) dx \\
&= \int_L \left(\frac{\partial \mathbf{b}^*(x)^T}{\partial v(x)} \mathbf{d}(x) \frac{\partial v(x)^T}{\partial \mathbf{P}} + \frac{\partial \mathbf{b}^*(x)^T}{\partial w(x)} \mathbf{d}(x) \frac{\partial w(x)^T}{\partial \mathbf{P}} + \mathbf{b}^*(x)^T \frac{\partial \mathbf{d}(x)}{\partial \mathbf{S}(x)} \frac{\partial \mathbf{S}(x)}{\partial \mathbf{P}} \right) dx \\
&= \int_L \left(\frac{\partial \mathbf{b}^*(x)^T}{\partial v(x)} \mathbf{d}(x) \frac{\partial v(x)^T}{\partial \mathbf{P}} + \frac{\partial \mathbf{b}^*(x)^T}{\partial w(x)} \mathbf{d}(x) \frac{\partial w(x)^T}{\partial \mathbf{P}} \right. \\
&\quad \left. + \mathbf{b}^*(x)^T \mathbf{f}_s(x) [\mathbf{b}(x) + \frac{\partial \mathbf{b}(x)}{\partial v(x)} \mathbf{P} \frac{\partial v(x)^T}{\partial \mathbf{P}} + \frac{\partial \mathbf{b}(x)}{\partial w(x)} \mathbf{P} \frac{\partial w(x)^T}{\partial \mathbf{P}}] \right) dx \\
&= \int_L \{ \mathbf{b}^*(x)^T \mathbf{f}_s(x) [\mathbf{b}(x) + \mathbf{h}(x)] + \mathbf{g}(x) \} dx
\end{aligned} \tag{3.39}$$

where $\mathbf{b}^*(x)$ and $\mathbf{b}(x)$ expressed in Equations (3.33) and (3.26) respectively are dependent on lateral displacements, initial imperfections and location x along the element, $\mathbf{f}_s(x)$ is the section flexibility matrix given in Equation (3.37), and $\mathbf{h}(x)$ and $\mathbf{g}(x)$ are given by,

$$\mathbf{h}(x) = \frac{\partial \mathbf{b}(x)}{\partial v(x)} \mathbf{P} \frac{\partial v(x)^T}{\partial \mathbf{P}} + \frac{\partial \mathbf{b}(x)}{\partial w(x)} \mathbf{P} \frac{\partial w(x)^T}{\partial \mathbf{P}} = P_1 \begin{bmatrix} \mathbf{0} \\ \mathbf{V}(x) \\ -\mathbf{W}(x) \\ \mathbf{0} \end{bmatrix} \tag{3.40}$$

$$\mathbf{g}(x) = \frac{\partial \mathbf{b}^*(x)^T}{\partial v(x)} \mathbf{d}(x) \frac{\partial v(x)^T}{\partial \mathbf{P}} + \frac{\partial \mathbf{b}^*(x)^T}{\partial w(x)} \mathbf{d}(x) \frac{\partial w(x)^T}{\partial \mathbf{P}} \tag{3.41}$$

$$= \frac{1}{2} \kappa_z \begin{bmatrix} \mathbf{V}(x) \\ \mathbf{0} \\ \mathbf{0} \\ \mathbf{0} \\ \mathbf{0} \end{bmatrix} - \frac{1}{2} \kappa_y \begin{bmatrix} \mathbf{W}(x) \\ \mathbf{0} \\ \mathbf{0} \\ \mathbf{0} \\ \mathbf{0} \end{bmatrix}$$

with

$$V(x) = \frac{\partial v(x)}{\partial \mathbf{P}} = \left[\frac{\partial v(x)}{\partial P_1} \quad \frac{\partial v(x)}{\partial P_2} \quad \frac{\partial v(x)}{\partial P_3} \quad \frac{\partial v(x)}{\partial P_4} \quad \frac{\partial v(x)}{\partial P_5} \quad \frac{\partial v(x)}{\partial P_6} \right] \quad (3.42)$$

$$W(x) = \frac{\partial w(x)}{\partial \mathbf{P}} = \left[\frac{\partial w(x)}{\partial P_1} \quad \frac{\partial w(x)}{\partial P_2} \quad \frac{\partial w(x)}{\partial P_3} \quad \frac{\partial w(x)}{\partial P_4} \quad \frac{\partial w(x)}{\partial P_5} \quad \frac{\partial w(x)}{\partial P_6} \right] \quad (3.43)$$

3.2.8 Curvature-based displacement interpolation (CBDI)

Regarding the displacement $v(x)$ and $w(x)$, they are directly given by the shape functions of displacement-based elements. However, only curvatures are obtained by the flexibility-based elements explicitly. Therefore, $v(x)$ and $w(x)$ need to be calculated by curvatures as so to get the flexibility matrix. Neuenhofer and Filippou (1998) proposed a method to an interpolation function to get displacements by curvatures, called CBDI. The displacements, v_i and w_i , at every integration point ξ_i (for $i= 1, \dots, n$) are represented by integration of all curvatures k_{zj} and k_{yj} (for $j= 1, \dots, n$). The interpolation function is given as

$$v_i = \sum_{j=1}^n l_{ij}^* k_{zj} \quad w_i = \sum_{j=1}^n l_{ij}^* k_{yj} \quad (3.44)$$

where n represents the number of integration points along the element; l_{ij}^* is the j th integrated Lagrangian polynomial at the integration point ξ_i . As obtaining displacements v_i and w_i , $V(x)$ and $W(x)$ in Equations (3.42) and (3.43) can be expressed as follows

$$\frac{\partial \mathbf{v}}{\partial \mathbf{P}} = \begin{bmatrix} \frac{\partial v_1}{\partial P_1} & \frac{\partial v_1}{\partial P_2} & \frac{\partial v_1}{\partial P_3} & \frac{\partial v_1}{\partial P_4} & \frac{\partial v_1}{\partial P_5} & \frac{\partial v_1}{\partial P_6} \\ \vdots & \vdots & \vdots & \vdots & \vdots & \vdots \\ \frac{\partial v_n}{\partial P_1} & \frac{\partial v_n}{\partial P_2} & \frac{\partial v_n}{\partial P_3} & \frac{\partial v_n}{\partial P_4} & \frac{\partial v_n}{\partial P_5} & \frac{\partial v_n}{\partial P_6} \end{bmatrix} \quad (3.45)$$

$$\frac{\partial \mathbf{w}}{\partial \mathbf{P}} = \begin{bmatrix} \frac{\partial w_1}{\partial P_1} & \frac{\partial w_1}{\partial P_2} & \frac{\partial w_1}{\partial P_3} & \frac{\partial w_1}{\partial P_4} & \frac{\partial w_1}{\partial P_5} & \frac{\partial w_1}{\partial P_6} \\ \vdots & \vdots & \vdots & \vdots & \vdots & \vdots \\ \frac{\partial w_n}{\partial P_1} & \frac{\partial w_n}{\partial P_2} & \frac{\partial w_n}{\partial P_3} & \frac{\partial w_n}{\partial P_4} & \frac{\partial w_n}{\partial P_5} & \frac{\partial w_n}{\partial P_6} \end{bmatrix} \quad (3.46)$$

For simplicity, the above two equations can also be given in matrix form as

$$\begin{bmatrix} \frac{\partial \mathbf{v}}{\partial \mathbf{P}} \\ \frac{\partial \mathbf{w}}{\partial \mathbf{P}} \end{bmatrix} = \begin{bmatrix} \mathbf{A}_z & \mathbf{B} \\ \mathbf{B} & \mathbf{A}_y \end{bmatrix}^{-1} \begin{bmatrix} \mathbf{I}^* \mathbf{a}_z \\ -\mathbf{I}^* \mathbf{a}_y \end{bmatrix} \quad (3.47)$$

in which, influence matrix \mathbf{I}^* is given as

$$\mathbf{I}^* = L^2 \begin{bmatrix} \frac{1}{2}(\xi_1^2 - \xi_1) & \frac{1}{2}(\xi_1^3 - \xi_1) & \cdots & \frac{1}{n(n+1)}(\xi_1^{n+1} - \xi_1) \\ \vdots & \vdots & \ddots & \vdots \\ \frac{1}{2}(\xi_n^2 - \xi_n) & \frac{1}{6}(\xi_n^3 - \xi_n) & \cdots & \frac{1}{n(n+1)}(\xi_n^{n+1} - \xi_n) \end{bmatrix} \mathbf{G}^{-1} \quad (3.48)$$

and

$$\mathbf{G} = \begin{bmatrix} 1 & \xi_1 & \xi_1^2 & \cdots & \xi_1^{n-1} \\ \vdots & \vdots & \vdots & \ddots & \vdots \\ 1 & \xi_n & \xi_n^2 & \cdots & \xi_n^{n-1} \end{bmatrix} \quad (3.49)$$

\mathbf{A}_z , \mathbf{A}_y and \mathbf{B} are the $2n \times 2n$ matrixes and the corresponding elements are given below

$$\begin{cases} A_{zij} = \delta_{ij} - l_{ij}^* f_{22}(\xi_j) P_1 \\ A_{yij} = \delta_{ij} - l_{ij}^* f_{33}(\xi_j) P_1 \\ B_{ij} = l_{ij}^* f_{23}(\xi_j) P_1 \end{cases} \quad (3.50)$$

Where

$$\delta_{ij} = \begin{cases} 1, & \text{for } i = j \\ 0, & \text{for } i \neq j \end{cases} \quad (3.51)$$

and $f_{2l}(\xi_j)$ and $f_{3l}(\xi_j)$ are the section flexibility matrixes at the integration point ξ_i as

$$\begin{cases} f_{2l}(\xi_j) = \left. \frac{\partial k_z(\xi)}{\partial S_l(\xi)} \right|_{\xi=\xi_j} \\ f_{3l}(\xi_j) = \left. \frac{\partial k_y(\xi)}{\partial S_l(\xi)} \right|_{\xi=\xi_j} \end{cases} \quad (l = 2, 3) \quad (3.52)$$

\mathbf{a}_z and \mathbf{a}_y are the $2n \times 6$ matrixes and the corresponding elements are given below

$$\begin{cases} a_{zjk} = \sum_{l=1}^4 f_{2l}(\xi_j) b_{lk}(\xi_j) \\ a_{yjk} = \sum_{l=1}^4 f_{3l}(\xi_j) b_{lk}(\xi_j) \end{cases} \quad (k = 1, 2, \dots, 6) \quad (3.53)$$

in which $b_{lk}(\xi_j)$ is given in Equation (25).

Theoretically, when a plastic hinge (fully plastic state) forms in a section (an integration point), the curvature k_{zj} or k_{yj} will be infinity mathematically, which will lead to numerical difficulty. In practical design, the rotation of plastic hinge should meet the requirements of design codes and cannot be infinite. During the analysis, the element will be removed from the structural system once its internal curvatures exceed the design limit. However, the proposed element has advantages on modelling member imperfection. To archive this, the conventional flexibility-based elements need at least two elements per member, which not only bring heavy computer time but also may cause the numerical problem when several plastic hinges are formed. The problem can be overcome by the proposed element allowing for “one element per member”.

3.2.9 Transformation from basic to global system

The conventional solvers in software like NIDA (2018) are generally based on stiffness matrix. It is also noted that the shell elements for shear walls and concrete slabs were commonly developed on the basis of stiffness method. Thus, the flexibility

matrix in Equation (3.39) needs to be inverted to get the element stiffness matrix \mathbf{K}_e as

$$\mathbf{K}_e = \mathbf{F}_e^{-1} \quad (3.54)$$

It should be pointed out that the above derivation is formulated in the basic system without rigid body modes. Hence, a transformation between the basic system and the global system is required to include the rigid body modes. In this thesis, the transformation following the co-rotational method by Chan and Zhou (1994) is adopted and therefore the elemental tangent stiffness matrix \mathbf{K}_T can be expressed as

$$\mathbf{K}_T = \mathbf{L}(\mathbf{T}^T \mathbf{K}_e \mathbf{T} + \mathbf{N}) \mathbf{L}^T \quad (3.55)$$

where, \mathbf{T} and \mathbf{L} are the matrices to transfer the stiffness matrix from basic to local system and from local to global system respectively; \mathbf{N} is the matrix to consider the work contributed by the initial force and the translational displacements. More details about these matrices can be found in the paper of Chan and Zhou (1994).

3.2.10 Element state determination

According to the classic procedure in finite element programs, the nodal displacements can be obtained by solving the global equations about the global stiffness matrix and external forces. Then the status of beam-columns is updated by the nodal displacement. The process of updating is easy for displacement-based beam-column elements whose shape functions can determine the internal forces and deformations directly. But this way is not applicable for flexibility-based beam-column elements because the nodal force is still unknown, and their shape function cannot be used directly. Therefore, an additional step of element state determination should be conducted before carrying out the standard procedure. Using nodal displacements to get nodal forces involves a trial-and-error process. The process can be executed in global level or local level.

In the global level, the nodal forces are corrected in every incremental-iterative numerical iteration, such as Newton-Raphson method and Arc-length method. Global equations are needed to be solved in the global iteration, which will cause huge computer time to achieve global and local convergence. If elements can be convergent in the local iteration, it can save much compute time especially when there are some plastic hinges formed in some members. The iteration in local level involves two sub-levels: elemental level and section level. Four types of iterations are discussed by Nukala and White (2004b) for flexibility-based beam-columns elements to deal with combination problems of geometric and material nonlinearity. They suggested that the N-L algorithm (“N” stands for nonlinear iteration at element level and “L” for a linear solution at section level) can reduce the number of global iterations. Therefore, the proposed element adopts the N-L algorithm to determine the status when conducting elemental update.

For the N-L algorithm, the status of sections is only updated as the iteration of elements. The details of the N-L algorithm are given in blow. In the following, the subscript i stands for the iteration index of global iteration. The subscript j represents the iteration index of elemental iteration.

Step 1: Extract incremental end displacements $\Delta \mathbf{D}_{i+1}$ from global analysis, and accumulate total end displacements as $\mathbf{D}_{i+1} = \mathbf{D}_i + \Delta \mathbf{D}_{i+1}$;

Step 2: Compute incremental end forces by $\Delta \mathbf{P} = \mathbf{K}_{e_i} \Delta \mathbf{D}_{i+1}$;

Step 3: Initial parameters before iteration at the element level:

3.1) Total end forces based on last load step: $\mathbf{P}_{i+1}^1 = \mathbf{P}_i$;

3.2) Incremental end forces of current load step: $\Delta \mathbf{P}_{i+1}^1 = \Delta \mathbf{P}$;

3.3) Section forces based on last load step: $\mathbf{S}_{i+1}^1 = \mathbf{S}_i$;

3.4) Section flexibility matrix based on last load step: $\mathbf{f}_{s_{i+1}}^1 = \mathbf{f}_{s_i}$;

Step 4: Start iteration j from 1 to N at the element level:

4.1) Total end forces: $\mathbf{P}_{i+1}^{j+1} = \mathbf{P}_{i+1}^j + \Delta \mathbf{P}_{i+1}^j$;

4.2) Increment of section forces: $\Delta \mathbf{S}_{i+1}^j = \mathbf{b}_{i+1}^j \mathbf{P}_{i+1}^{j+1} - \mathbf{S}_{i+1}^j$;

4.3) Trial section deformations: $\Delta \mathbf{d}_{i+1}^j = \mathbf{f}_{s_{i+1}}^j \Delta \mathbf{S}_{i+1}^j$, $\mathbf{d}_{i+1}^{j+1} = \mathbf{d}_{i+1}^j + \Delta \mathbf{d}_{i+1}^j$;

4.4) Update v_{i+1}^{j+1} and w_{i+1}^{j+1} through Eq. (43);

4.5) Update \mathbf{b}_{i+1}^{j+1} and \mathbf{b}_{i+1}^{*j+1} using Eqs. (25) and (32) respectively;

4.6) Trial section forces: $\mathbf{S}_{i+1}^{j+1} = \mathbf{b}_{i+1}^{j+1} \mathbf{P}_{i+1}^{j+1}$;

4.7) Trial end displacements: $\Delta \mathbf{D}_{i+1}^{j+1} = \mathbf{D}_{i+1} - \mathbf{D}_{i+1}^j$;

4.8) Update element flexibility matrix $\mathbf{F}_{e_{i+1}}^{j+1}$ through Eq. (38);

4.9) Determine unbalanced end forces: $\mathbf{F}_{e_{i+1}}^{j+1} \Delta \mathbf{P}_{i+1}^{j+1} = \Delta \mathbf{D}_{i+1}^{j+1}$, get $\Delta \mathbf{P}_{i+1}^{j+1}$;

4.10) If ($\|\Delta \mathbf{D}_{i+1}^{j+1}\| < \text{tolerance}$), exit loop; otherwise, j+1 and go to step (4.1).

Step 5: Determine elemental stiffness for next load step: $\mathbf{K}_{e_{i+1}} = \mathbf{F}_{e_{i+1}}^{-1}$

3.3 Member imperfections

There are several provisions for global imperfections and local imperfections when conducting direct analysis in AISC360 (2016) and Eurocode-3 (2005). Global

imperfections generally refer to structural sway and local imperfections are member bowing. They are caused by practical construction tolerance and manufacturing process of the steel members. In the numerical simulation, it is easy to deal with the global imperfections by adjusting nodal coordinates or introducing notional horizontal load. As a consequence, the details of the global imperfections will not be discussed in this thesis. The application of member initial imperfection on numerical modeling for direct analysis will be explained herein. Generally, there are two methods, i.e., equivalent geometrical imperfection method and modified modulus approach, for considering local imperfection. They will be briefly discussed here.

3.3.1 Equivalent geometrical imperfection method

In steel structures, there unavoidably exist member initial imperfections, including the geometrical imperfections and the mechanical imperfections (residual stresses). These imperfections cannot be ignored during the analysis procedure as they will affect the structural behavior. The traditional design approach, indirect analysis, uses column buckling curves to consider these unfavorable factors. Column buckling curves are determined by section types and production process, which is based on individual members. In the global analysis, this method ignores the coupling effect between structural components and structural system, which may lead to an unrealistic prediction of structural behavior.

Equivalent geometrical imperfection approach is suggested by Eurocode-3 (2005) to consider these imperfections in a uniform form, i.e., the equivalent geometrical imperfection. The concept of this method was proposed by Ayrton and Perry (1886). It assumes that the imperfection shape of members is a half-sine function. The amplitude of the half-sine function is represented by δ_0 which varies upon section

types. For the proposed element, the initial geometrical imperfection function in Equation (3.6) can be represented as,

$$v_0(x) = \delta_{0,y} \sin \frac{x}{L} \quad w_0(x) = \delta_{0,z} \sin \frac{x}{L} \quad (3.56)$$

where x is the coordinate along the x-axis in the local coordinate system; $\delta_{0,y}$ and $\delta_{0,z}$ are the maximum amplitudes of initial geometrical imperfections, located at the mid-span of members, about y- and z-axis respectively. Calibrating from column buckling curves, Table 5.1 of Eurocode-3 (2005) is based on the following formula to determine $\delta_{0,y}$ and $\delta_{0,z}$ as

$$\delta_0 = \begin{cases} \alpha(\bar{\lambda} - 0.2) \frac{W_{el}}{A}, & \text{for Elastic Analysis} \\ \alpha(\bar{\lambda} - 0.2) \frac{W_{pl}}{A}, & \text{for Plastic Analysis} \end{cases} \quad (3.57)$$

$$\bar{\lambda} = \sqrt{Af_y/N_{cr}} \quad (3.58)$$

in which, A , W_{el} and W_{pl} are the area, elastic section modulus and plastic section modulus of the cross section respectively; f_y is the characteristic yield strength of the material; N_{cr} is the elastic critical axial load; α is the imperfection factor corresponding to the buckling curve (a_0 , a , b , c or d) and section shape, as listed in Table 6.1 of Eurocode-3 (2005).

It should be noted that the magnitude of imperfection δ_0 calculated by Equation (3.57) will be different for same sectional and material properties in the elastic and plastic analysis. Therefore, the plastic analysis will make more conservatives prediction of structural than elastic analysis when all members remain elastic due to the larger magnitude of imperfection δ_0 being pre-set at the beginning of the analysis.

Generally, the traditional approach, column buckling curves method, is altered by the equivalent geometrical imperfection method. It considers the coupling effect of several unfavorable factors which include the slenderness ratio, geometrical

imperfections, residual stress as well as loading eccentricity in the global analysis. The equivalent geometrical imperfection method can be used in practical design for considering these unfavorable factors in some modern design codes, such as Eurocode-3 (2005) and CoPHK (2011). To satisfy the requirements of design codes, the proposed element can incorporate the initial geometrical member imperfection directly. Besides, the residual stresses can also be considered explicitly by the fiber section technology.

3.3.2 Modified modulus approach

Surovek-Maleck and White (2004) and Ziemian and McGuire (2002) proposed an approach, called the modified modulus method, to model the two kinds of imperfections mentioned above. This method has been included in AISC360 (2016). It does not consider the initial bowing imperfection explicitly during the procedure of analysis. The flexural check at the design stage considers the effect of the local member imperfection. Regarding the material residual stress, AISC360 (2016) reduces the stiffness of members to reflect its influence explicitly. An overall stiffness reduction factor, 0.8 is suggested by AISC360 (2016) to reduce the stiffness of structural systems. The properties of cross sections with considering the reduction factor is shown as,

$$EA_e = 0.8EA \quad EI_{e,y} = 0.8\tau_b EI_y \quad EI_{e,z} = 0.8\tau_b EI_z \quad (3.59)$$

$$\tau_b = \begin{cases} 1, & \text{for } \frac{P}{P_y} \leq 0.5 \\ 4 \frac{P}{P_y} \left(1 - \frac{P}{P_y}\right), & \text{for } \frac{P}{P_y} > 0.5 \end{cases} \quad (3.60)$$

where τ_b is determined by applied axial force P and the axial yield strength P_y . The calculation of the flexural stiffness needs to consider this additional reduction factor τ_b .

Maleck and White (2004) believed that τ_b reflects the influence of residual stress and the factor 0.8 considers the coupling effect between axial force and flexural moments. Taking I-shape section, for example, the Lehigh residual stress pattern proposed by Galambos and Ketter (1959) will lead to different reduction factor τ_b for major-axis and minor-axis if equation (3.58) is applied.

3.4 Numerical examples

To verify the accuracy, efficiency and versatility of the proposed, four examples, involving geometrical nonlinearity, or material nonlinearity, or both, are studied. The first three examples are planar problems and the last one is a space problem.

Displacement-based beam-column elements generally adopt cubic shape function or other higher-order shape functions to fit the member deflection. While the flexibility-based beam-column elements use the numerical integration. The proposed element, one of the flexibility-based beam-column elements, also adopts numerical integration approach along the member to form the elemental stiffness. The section stiffness at integration points should reflect the stiffness of the weight length. Thus, the integration scheme plays an important role in the prediction of the behavior of the proposed element. In the inelastic analysis, the integration points are better to be located as near as possible to the place of plastic hinges formed. Table 3-1 shows the features of common approaches which has been studied by Scott (2006). All these integration methods have high accuracy when using more than five integration points. The difference between the methods is the location of integrations. For example, Gauss-Lobatto has integration points at two ends of the element, while none of Gauss-Legendre's integration points locates at the ends though it has the highest accuracy.

Therefore, the Gauss-Legendre method is suggested to be applied to the elastic analysis. In the inelastic analysis, it is better to use the Gauss-Lobatto method because plastic hinges of practical structures often form at the locations of its integration points. Newton-Cotes integration method with uniform integration points along the element is applicable for simple cases. In the following examples, suitable integration scheme will be adopted.

3.4.1 Single initially-curved column under different boundary conditions

Fig. 3.2 shows the column with three boundary conditions: pinned-pinned, pinned-fixed and fixed-fixed. The column is subjected to an axial force. This example is usually employed for buckling check. Various amplitudes of the initial member imperfection of columns are studied to check the performance of the proposed element for direct analysis. The analytical result of this example can be obtained by solving differential equilibrium equations, also given in Appendix I, to verify the accuracy of the proposed element.

In the numerical models, the material is assumed to be elastic so that the capability of geometrical nonlinearity of the proposed element can be directly verified. The material and section properties are unitless for simplicity. The Young's modulus E is 10^7 ; the area of cross section A is 1.0; the moment of inertia I is 0.833. Therefore, the integration procedure across the section in equation (3.37) is not needed. Gauss-Legendre integration scheme, with five integration points, is adopted to accumulate the elemental stiffness along the column.

In practice, the slenderness ratio of columns affects the critical buckling loading in related to column instability. In this example, the column with same end condition is assumed to have three slenderness ratios, i.e., 50, 100 and 150. The slenderness ratio

$\lambda = L/\sqrt{I/A}$ is changed by setting different member lengths, which can verify the practicability of the proposed element to model columns ranging from short to long. Besides, the amplitude of the local member imperfection, δ_0 , is also studied by taking as $L/1000$, $L/500$ and $L/200$, which covers most situations in practical structures.

Figs. 3.3 to 3.5 show the results of the column subjected to axial compression with three slenderness ratios under three typical boundary conditions. Both numerical results and analytical results are plotted with three kinds of the amplitude of member imperfection. From these figures, all results under different conditions produced by the proposed element agree well with the analytical results obtained by equations in Appendix I. This example illustrates the high accuracy of the proposed element.

Ignoring the influence of member imperfection, the critical loads of three typical boundary conditions: “pinned-pinned”, “pinned-fixed” and “fixed-fixed” are 1.0, 2.0408 and 4.0 respectively with multiplying by $\pi^2 EI/L$. The ultimate loads shown in figures is less than the Euler buckling critical loads. The difference comes from the consideration of member imperfection in the proposed method. Therefore, the ignorance of member imperfection will overestimate the column capacity and lead to unsafe design.

3.4.2 Distributed plasticity analysis of a fixed-ended beam

Fig. 3.6 shows the layout of a single beam with member length L of 6 m. The beam is subjected to a concentrated point load. This example is also used to verify the ability dealing with member load of the proposed element. Several plastic hinges will be formed in this example. The cross-section is W30x99, with cross-sectional area A of $1.87e^{-2} \text{ m}^2$, and second-moment area I of $1.661e^{-3} \text{ m}^4$. The section plastic modulus is $5.113e^{-4} \text{ m}^3$. The steel grade is S275, with Young’s modulus E of 205 GPa and yield

stress f_y of 275 MPa. The local member imperfection is ignored in this example for easy comparison with analytical results.

Chen and Sohal (1995) also studied this example and provided the analytical results using the plastic hinge method. They also indicated the number and forming sequence the plastic hinges. In the numerical model, the web of the cross-section is meshed into 16×4 fibers, and flanges at top and bottom of the cross-section are divided into 4×16 fibers. The constitutive relationship of each fiber is assumed to be elastic-perfectly plastic. The beam is modeled by one or two proposed elements. To explore the influence of different integration scheme on the analysis, three models are built as shown Table 3-2. For the models using two element, a node is inserted at the point B. Table 3-3 gives the analytical result of details about hinge sequence, applied load and deflection by Chen and Sohal (1995). The load vs. deflection curves of the present study with the analytical solution are plotted in Fig. 3.7. From the figure, the results of Model 1, Model 2 and Model 3, calculated by the proposed element, agree well with the analytical solutions. The ultimate load capacities obtained by these models are almost same. Apparently, the curve obtained by plastic hinge method is less smooth than the proposed method.

From the figure, Model 2 has similar load-deflection curves with Model 3. Therefore, two elements with 5 Newton-Cotes' integration points make a same accurate prediction as that of 2 elements with 7 Newton-Cotes' integration points. Both Model 2 and Model 3 have integration points accurately located at where the plastic hinges appear. Therefore, they can make an accurate prediction of deformation and internal forces of members. However, though Model 1 has ten integration points along the member, integration points do not accurately locate at same places. Fig. 3.8 shows the detailed deflection of the beam when the load factor is 8.0. The deflection values of

integration points are also shown in the figure. Both Model 1 and Model 2 have integration points located at point B and two ends of the beam. Therefore, their ultimate capacities are similar though the deflection curves are slightly different.

The proposed element is verified by the example that exhibits highly nonlinearity of material with three plastic hinges. Meanwhile, the member loads can also be properly considered at the element level if the proper integration scheme is used. For practical design, the two ends and the middle point of members have relatively larger moment than other locations in such case the plastic hinges often form at these points. Gauss-Lobatto integration scheme with 5 or 7 integration points covers these locations, which can produce acceptable results. Generally, increasing the number of elements per member or increasing the number of integration points are two approaches to improve the accuracy of plastic analysis. Though the first approach can largely improve the accuracy, it increases the number of global degree of freedom (DOF) and then increases the number of equilibrium equations which leads to more computer time. Besides, it also leads to numerical problems when some elements located at the inside of the member fail. In contrast, the increase of integration points will only lead to more computer time at the elemental level which does not increase the dimension of system stiffness matrix. Therefore, the integration scheme can be selected according to applied loads and end conditions of members, which can be automatically carried out by the program, such as NIDA (2018). Thus, the proposed element is practical in the second-order inelastic analysis.

3.4.3 Second-order direct analysis of a two-story 2D steel frame

This benchmark example is firstly studied by Ziemian *et al.* (1992). This example exhibits highly geometrical and material nonlinearities and is suitable to verify the

performance of beam-column elements. Fig. 3.9 shows the layout and load patterns of this example. Several frame sections are applied, and all sections have same material properties, with young modulus 199810 MPa and yielding stress 248 MPa. The bottom of all columns is assumed to be pinned. The connections between beams and columns are rigid in numerical models. The load combination is 1.2 DL + 1.6 LL. Displacement of the top point of the right column on the second floor is monitored during analysis. In this example, the effects and the modeling approaches of global imperfection, member imperfection, and residual stress will be studied. Table 3-4 shows details of seven models with different settings. The global and member imperfection patterns are determined by the first eigen-buckling mode, as given in Fig. 3.10. The proposed element is used in models M1 ~ M3. All members are modeled using one-member-one-element strategy. All cross sections use the same mesh strategy with the web divided into 32 x 8 fibers, and the flange divided into 8 x 32 fibers. Gauss-Lobatto integration method is adopted, and seven integration points are located along the member including two ends and middle point to capture the plastic behavior of members.

Plastic hinge method, embedded in the educational program MASTAN2 (2002), is used in models M4 and M5. Model M6 and M7 use program FE++2015 (2001) provided by MASTAN2 (2002). M4 ~ M7 do not consider imperfection directly. The material of all models uses the elastic-perfectly plastic model. Fig. 3.11 shows load factor vs. lateral displacement (Δ_t) curves from results of all models. Ultimate load factors from M1, M4, and M7 are similar with less than 1.04. These three models do not consider the imperfection. For M4, its load factor is more than 1.04, which uses plastic hinge method. For the plastic zone method, model 1 and model 6 make an identical prediction of frame behavior. The reason is that fiber sections provide a

smoother transition of the stiffness from elastic to fully plastic than that provided by the plastic hinge method. Under the combined effect of both geometrical and material nonlinearities, the plastic hinge leads to a less accurate simulation due to its assumption of discontinuous transition.

In direct analysis, it is inevitable to consider initial member imperfection, eccentricity of applied load and residual stress of cross-sections. As for the local member imperfection, several different methods are adopted by model 2, 5 and 7. In Model 2, only local imperfections are modeled with an amplitude of $L/300$, and the global imperfection is ignored. Model 5 uses the modified modulus method to consider the local member imperfection. Residual stress is considered by Model 7. Model 2 and Model 5 make the similar prediction when the load factor is less than 0.75. Then, their results are diverse. Model 2 has a larger ultimate load factor than Model 5. Comparing the results of Model 6 and Model 7, residual stress slightly reduces the ultimate capacity of the frame.

The results of Model 3 show that imperfections in local and global level largely decrease the ultimate capacity of the frame. The stiffness of the structural system is more flexible than other models when the load factor is less than 0.7. Fig. 3.12 shows the status of yielding about the cross-section and internal forces of members when the load factor is 1.0. The percentage of section area yielded in some locations is bigger than 90%. Meanwhile, some fibers of beam sections, located at the middle of members, become plastic.

In this example, results obtained by several methods are adopted to verify the accuracy and ability of the proposed element. This element can be a powerful tool for practical design.

3.4.4 Second-order direct analysis of Harrison's space frame

Fig. 3.13 shows a spatial frame tested by Harrison (1965). This test will be used to verify the accuracy and practicability of the proposed element. The layout and load patterns of this test are demonstrated in Fig. 3.13. Young modulus of the material used in this test is 198432 MPa. Shear modulus is 79373 MPa. The yield stress of beams and columns are 214.3 MPa and 210.8 MPa respectively. The shape of the section is CHS, with diameter 42.72 mm and thickness 4.47 mm. All beams and columns use the same section. The length of all members is same as 1.2192 m. The boundaries of columns on base are fixed. The connections between columns are supposed to be rigid. The fiber section technology is also adopted in this example, with discretizing the section into 20 fibers along the circular direction and four fibers along the diametrical direction, as illustrated in Fig. 3.13. Each one of members is modeled one proposed element respectively. To capture the plastic hinge located at two ends and middle point, Gauss-Lobatto integration scheme with seven integration points is adopted. Material property of each fiber is modeled by elastic-perfectly-plastic model. Member imperfection is introduced according to first buckling mode with the magnitudes δ_0 being $L/500$, which satisfied the requirements of CoPHK (2011).

Fig. 3.14 shows results from several scholars, about horizontal drift Δ_x (as illustrated in Fig. 3.13 vs. applied loading factors. The experimental results by Harrison (1965) are also plotted. These results are perfectly predicted by the proposed element with initial imperfection. Form Fig. 3.14, all numerical results appear more stiffness, while the experimental results are relatively flexible. This deviation may be caused by: 1. lack-of-fit problem during the test process; 2. the assumption of rigid connection in numerical models. Though displacement-based element is used by both Teh and Clarke (1999) and Liu *et al.* (2014), their results diversified when loading factor is

achieving 0.85. All members remain elastic when loading factor is less than 0.85. And there is no plastic hinge forming in the structural system. When plastic hinge appears, plastic zone method and plastic hinge method work and reveal different features. Both of their results exhibit slightly stiffer than the experimental results, which may be caused by ignorance of initial geometrical imperfections in their numerical models. This phenomenon also can be seen in results predicted the proposed element without setting member imperfections.

This experimental test shows that the proposed element is capable of satisfying the requirements of SODA. It can predict relatively high results and applies to space frames.

3.5 Concluding remarks

In this chapter, a new flexibility-based beam-column element is proposed. This element inherits advantages of flexibility-based elements, having high accuracy. The highlight of the proposed element is that it is capable to incorporate member imperfection explicitly. Meanwhile the distributed plasticity method is adopted to capture the plastic behavior. The fiber section approach also makes it possible to consider residual stress. These features of the proposed element will be a powerful tool for practical design to satisfy requirements of second-order direct analysis (SODA).

The capacity about both geometrical and material nonlinearities of the proposed element is confirmed by several benchmarked examples. The first two examples provide closed-form solutions to check its accuracy. The last two examples demonstrate its application. The results obtained by the proposed element are also

verified by that produced by other scholars using other methods. Some meaningful conclusions are obtained as,

- (1) Member imperfection can be explicitly modeled by the proposed element at the elemental level without introducing internal forces, which is convenient and practical.
- (2) Fiber section technology is adopted by the proposed element, which can capture the process of gradually yielding and makes it easy to incorporate residual stress effect.
- (3) Because distributed plasticity analysis method uses limited integration points to monitor the plastic status of the member, appropriate integration method should be employed to capture the accurate location of plastic hinges.
- (4) The proposed element, having acceptable accuracy for practical design when one member being modeled by one proposed element, can save much computer time. Besides, it could not produce numerical problem due to member failure.
- (5) To make full use of flexibility-based element and displacement-based element, the first one can be used to model these members being controlled by material nonlinearity, and the second one is efficient to simulate the other that remain elastic or are dominated by geometrical nonlinearity. This strategy can maintain accuracy and also save much computer time.
- (6) Without considering geometrical imperfection in structural systems or individual members will overestimate the ultimate resistance of structural systems. Though design codes provide the other method to model geometrical imperfection, like through applying notional force. But they are practical to limited structural types, like regular structures. The proposed eradicate these shortages and can model initial imperfection explicitly.

3.6 Appendix – Analytical Solutions of Single Imperfect Column under Axial Load

The axial shortening of a single imperfect column subjected to axial load only can be obtained by directly solving the differential equilibrium equation as,

$$u_2 = \frac{PL}{EA} + Lb_1(\theta_1 + \theta_2)^2 + Lb_2(\theta_1 - \theta_2)^2 + \delta_0 b_{vs}(\theta_1 - \theta_2) - \frac{b_{vv}\delta_0^2}{L}$$

in which, P is applied axial load; L is member length; EA is axial rigidity; δ_0 is the amplitude of imperfection at mid-span; and

$$c_1 = \frac{\varphi \cdot (\sin\varphi - \varphi \cdot \cos\varphi)}{2(1 - \cos\varphi) - \varphi \cdot \sin\varphi}$$

$$c_2 = \frac{\varphi \cdot (\varphi - \sin\varphi)}{2(1 - \cos\varphi) - \varphi \cdot \sin\varphi}$$

$$c_0 = \frac{\pi q \cdot \varphi \cdot \sin\varphi}{(1 - q)(1 - \cos\varphi)}$$

$$b_1 = \frac{\varphi \cdot (\sin\varphi - \varphi \cdot \cos\varphi)}{2(1 - \cos\varphi) - \varphi \cdot \sin\varphi}$$

$$b_2 = \frac{\varphi - \sin\varphi}{8\varphi \cdot (1 - \cos\varphi)}$$

$$b_{vs} = \frac{\varphi \cdot [(2\sin\varphi - (1 - q)(\varphi - \sin\varphi)]}{2\pi(1 - q)^2(1 - \cos\varphi)}$$

$$b_{vv} = \frac{q \cdot \varphi \cdot [(1 - q)(\varphi - \sin\varphi) - 4\sin\varphi]}{2(1 - q)^2(1 - \cos\varphi)} + \frac{\pi^2 q(2 - q)}{4(1 - q)^2}$$

$$\varphi = \sqrt{\frac{PL^2}{EI}}$$

$$q = \frac{PL^2}{\pi^2 EI}$$

For “pinned-pinned” case:

$$\theta_1 = \frac{c_0 \delta_0}{(c_2 - c_1)L} \quad \theta_2 = \frac{c_0 \delta_0}{(c_1 - c_2)L}$$

For “pinned-fixed” case:

$$\theta_1 = 0 \quad \theta_2 = \frac{c_0 \delta_0}{c_1 L}$$

For “fixed-fixed” case:

$$\theta_1 = 0 \quad \theta_2 = 0$$

FIGURES

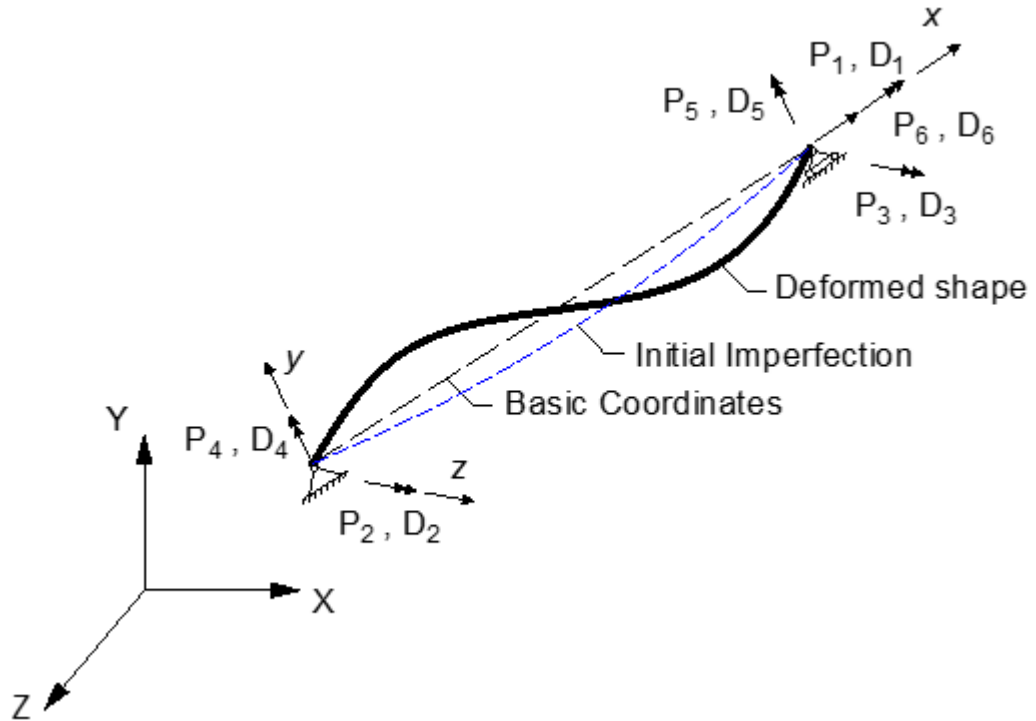


Fig. 3.1 Basic forces versus displacements relations

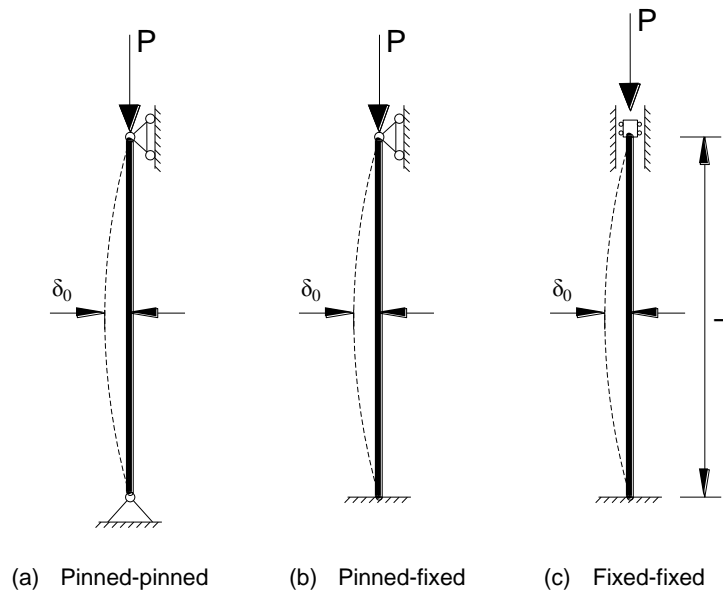
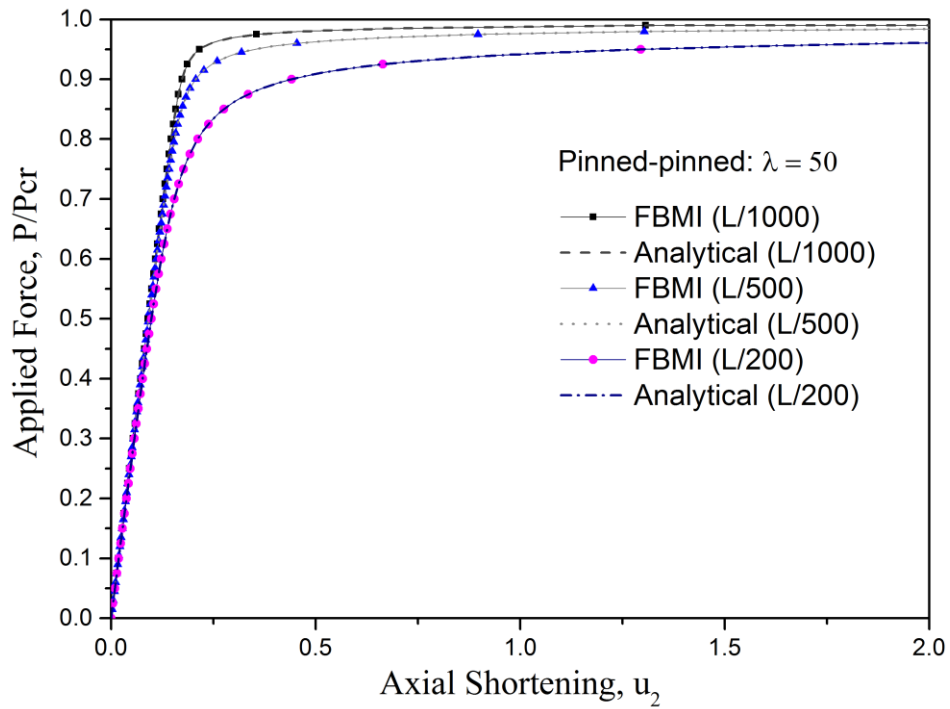
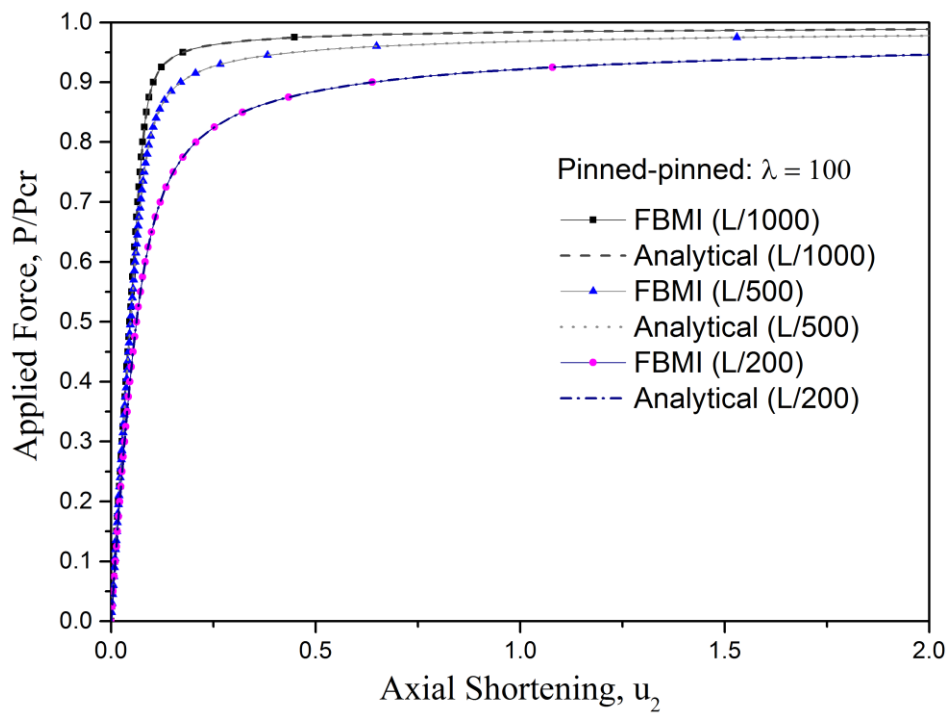


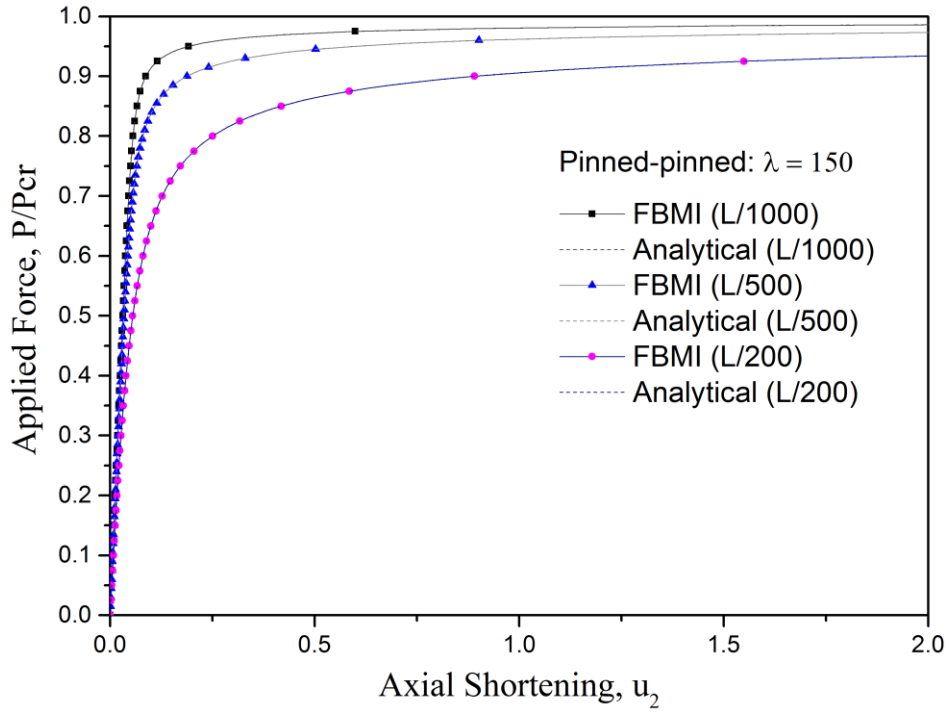
Fig. 3.2 Layout of columns (δ_0 is amplitude of the geometrical imperfection)



(a)



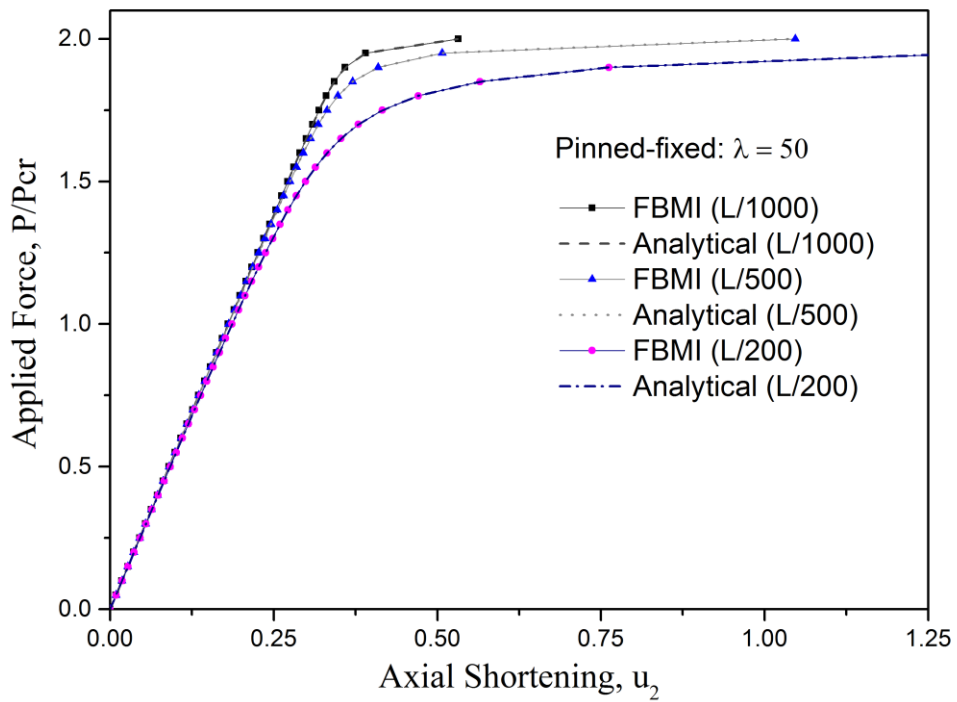
(b)



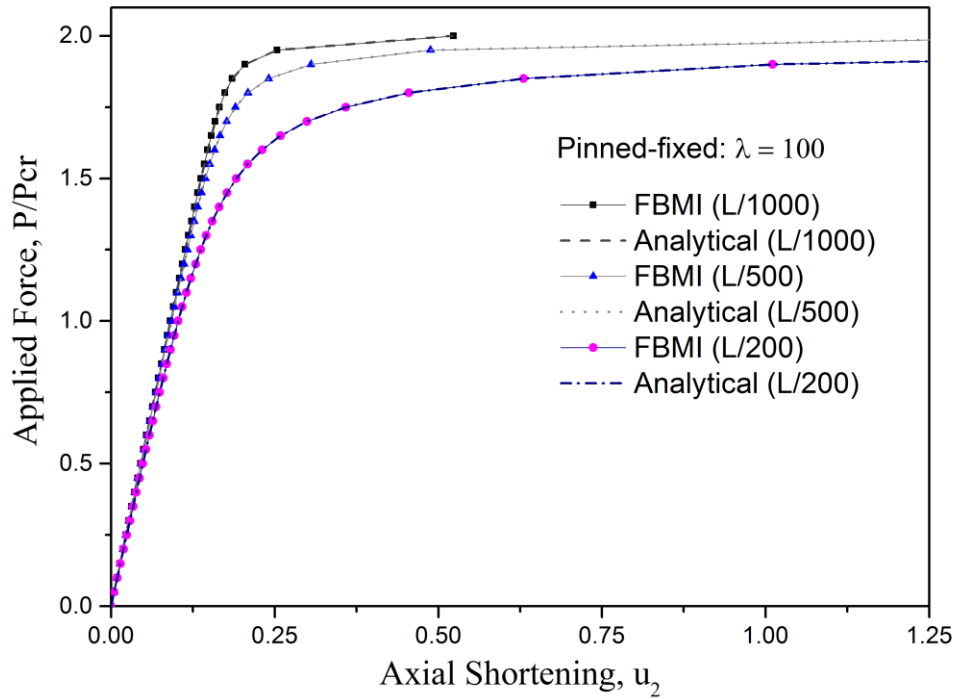
(c)

Fig. 3.3 Load vs. deflection curves for “pinned-pinned”: (a) $\lambda = 50$, (b) $\lambda = 100$,

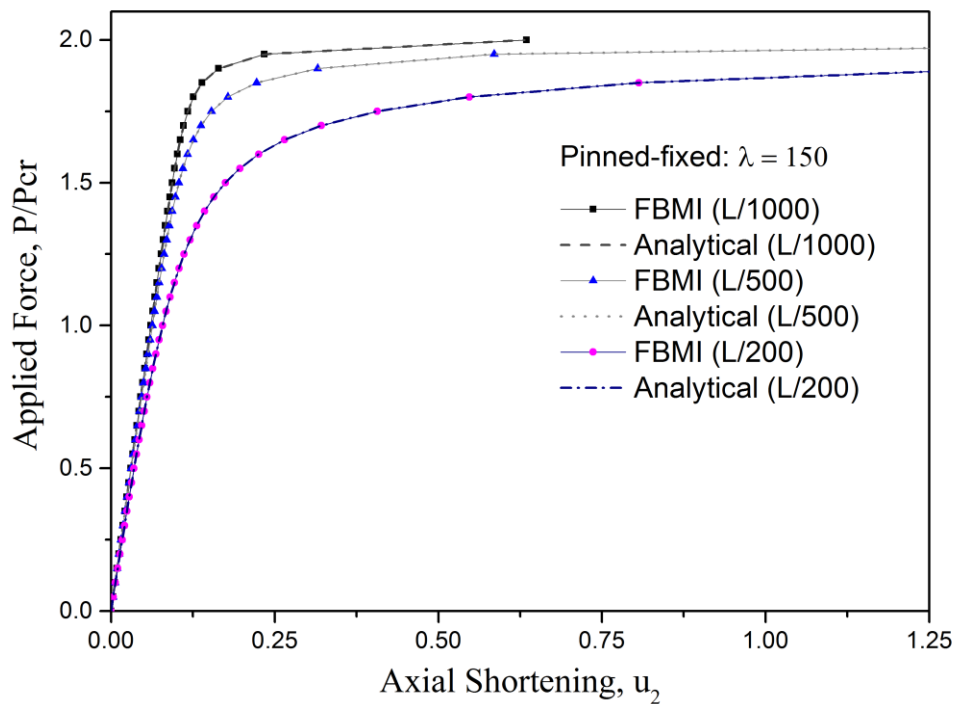
(c) $\lambda = 150$



(a)

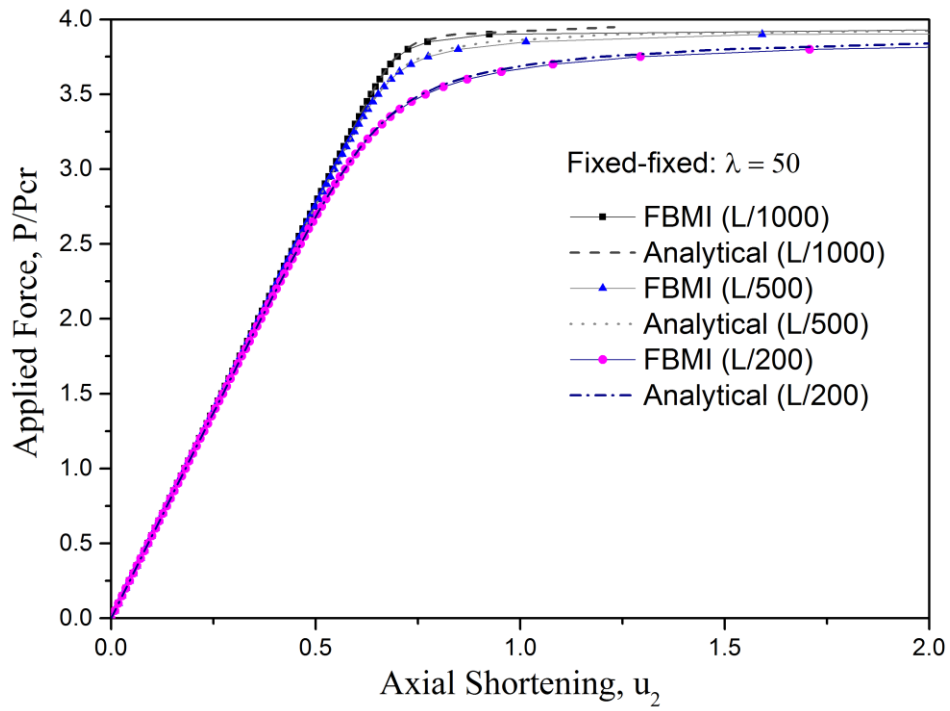


(b)

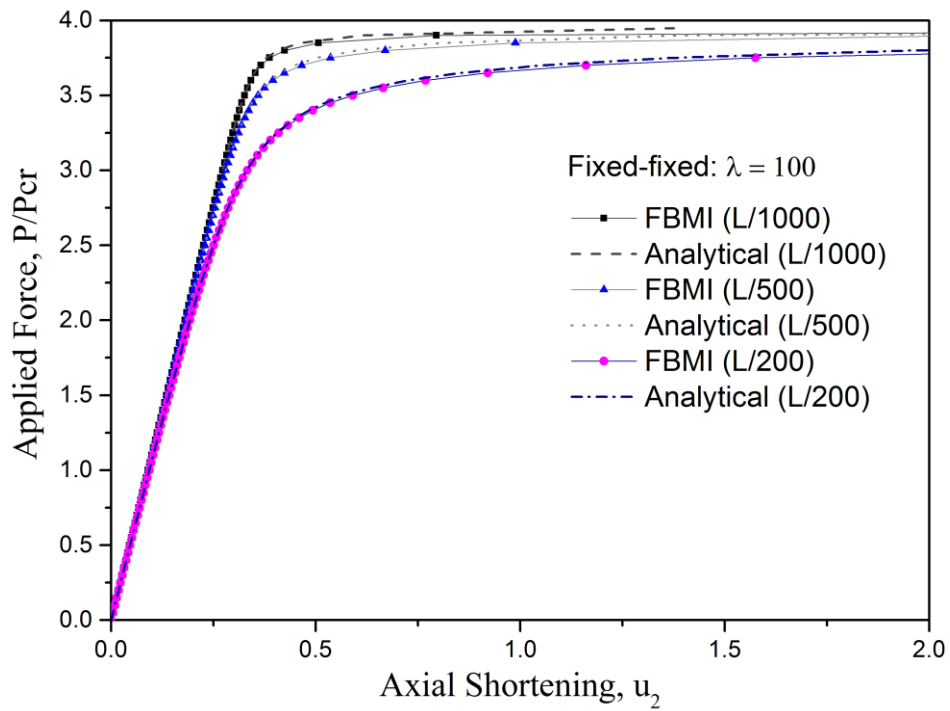


(c)

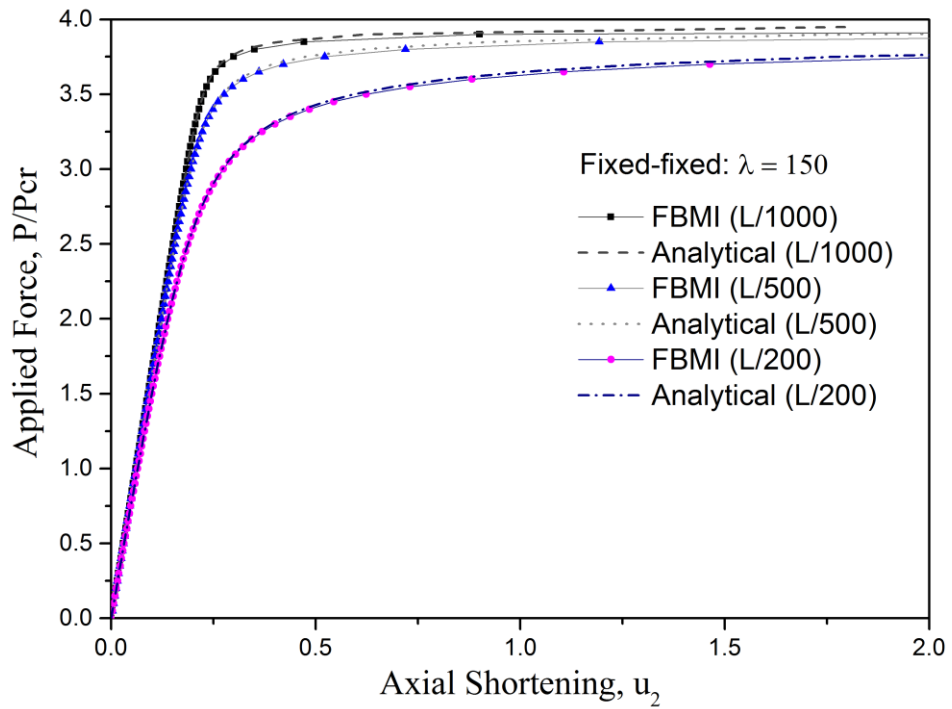
Fig. 3.4 Load vs. deflection curves for “pinned-fixed”: (a) $\lambda = 50$, (b) $\lambda = 100$,(c) $\lambda = 150$



(a)



(b)



(c)

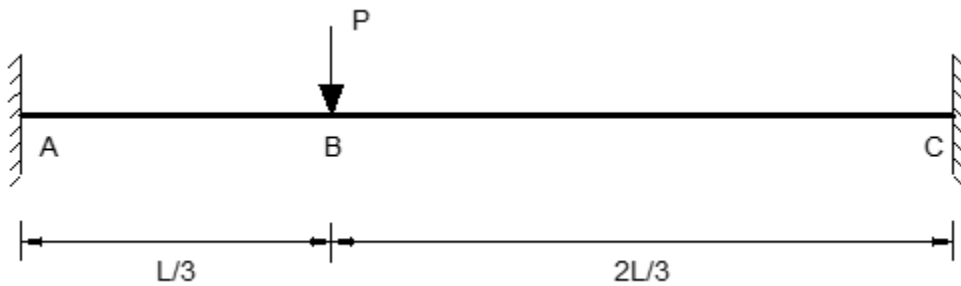
Fig. 3.5 Load vs. deflection curves for “fixed-fixed”: (a) $\lambda = 50$, (b) $\lambda = 100$,(c) $\lambda = 150$ 

Fig. 3.6 A single fixed-ended beam under a member point load

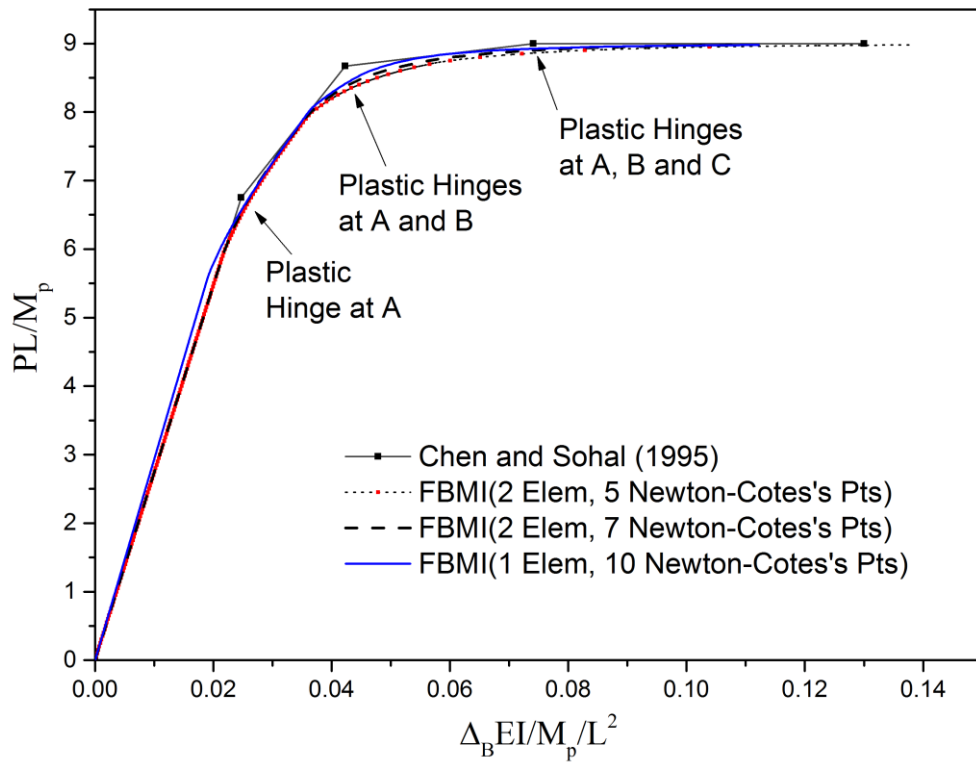


Fig. 3.7 Load-displacement curves of point B

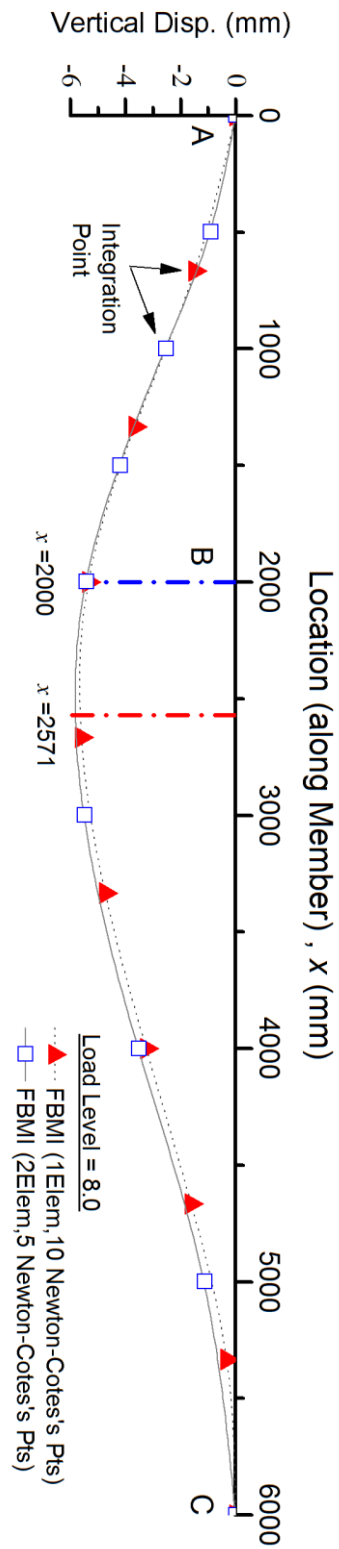


Fig. 3.8 Deformation of integration points along the member

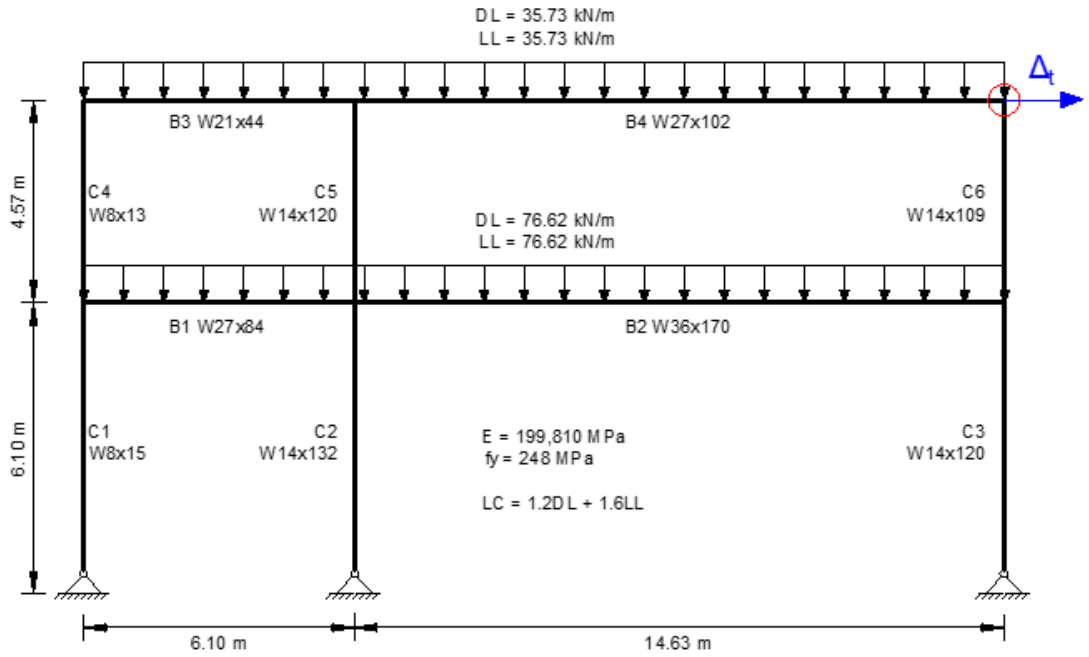


Fig. 3.9 Layout and load pattern of the planar frame by Ziemian and McGuire (2002)

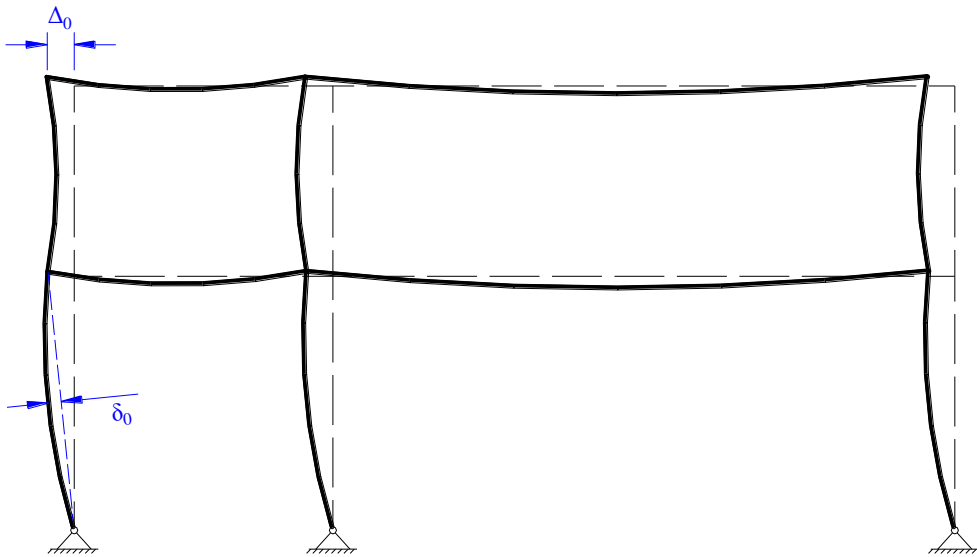


Fig. 3.10 Imperfection pattern of the planar frame by Ziemian and McGuire (2002)

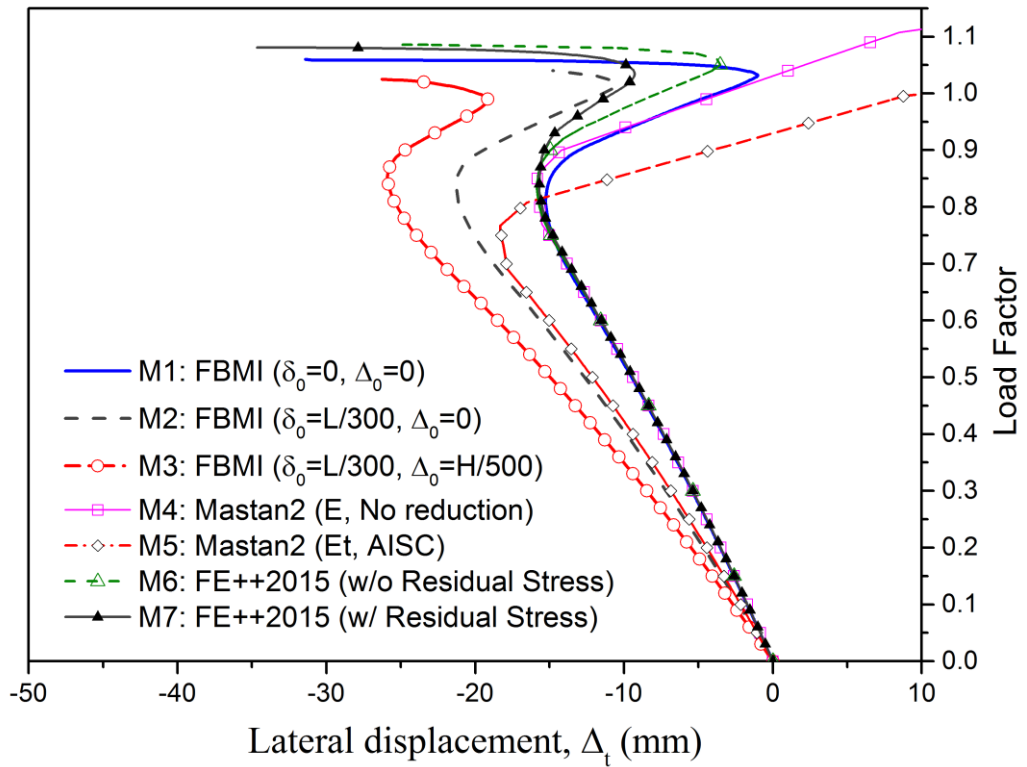


Fig. 3.11 Response curves of the frame by Ziemian and McGuire (2002)

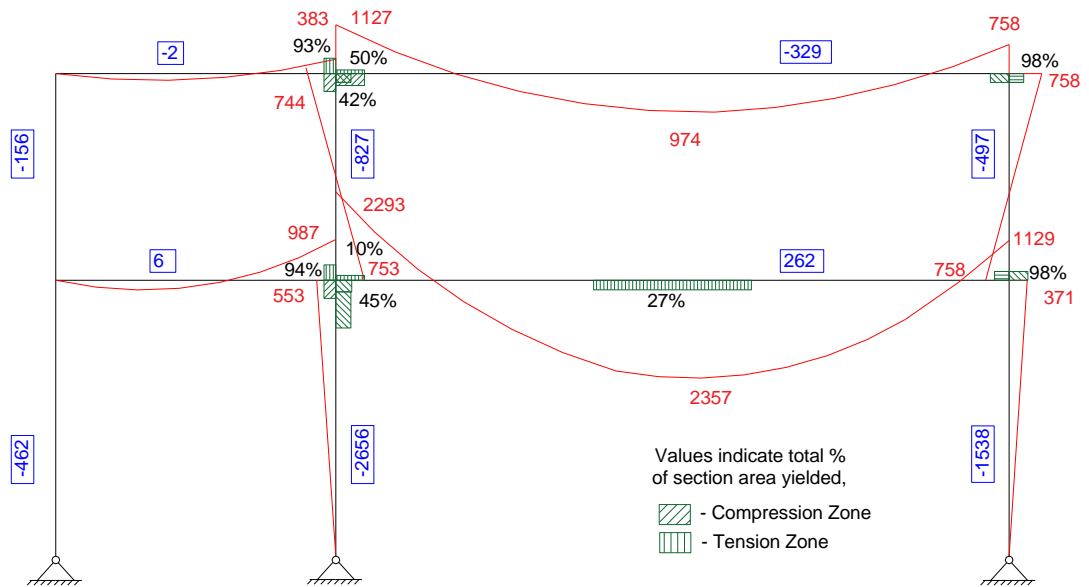


Fig. 3.12 Bending moment, axial force and percentage of the cross-section yielded

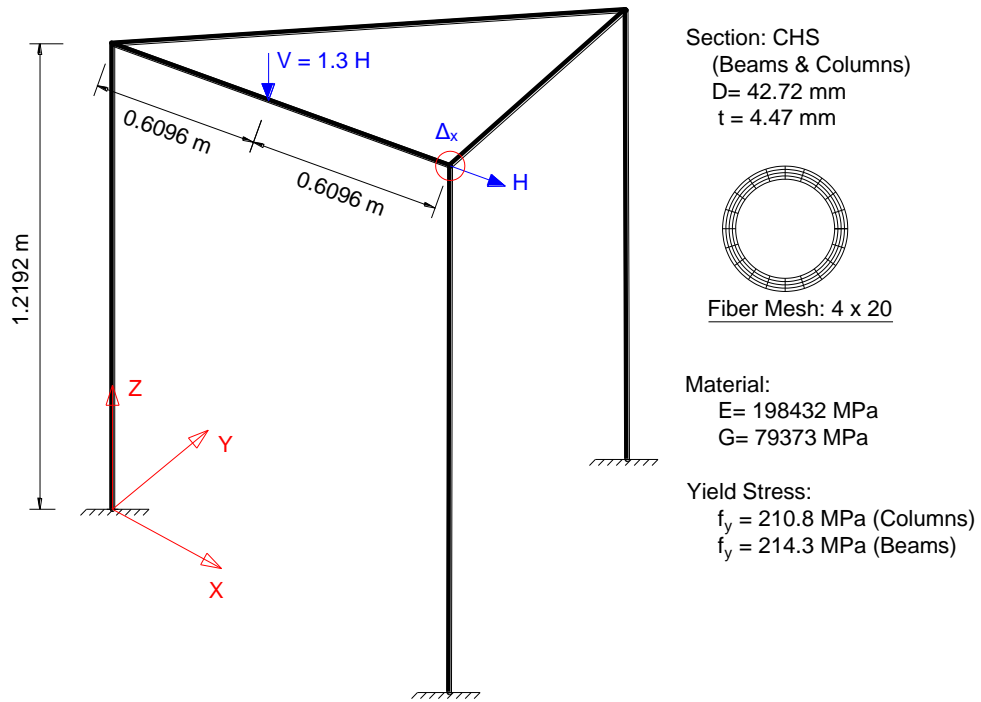


Fig. 3.13 Layout and load pattern of Harrison's space frame

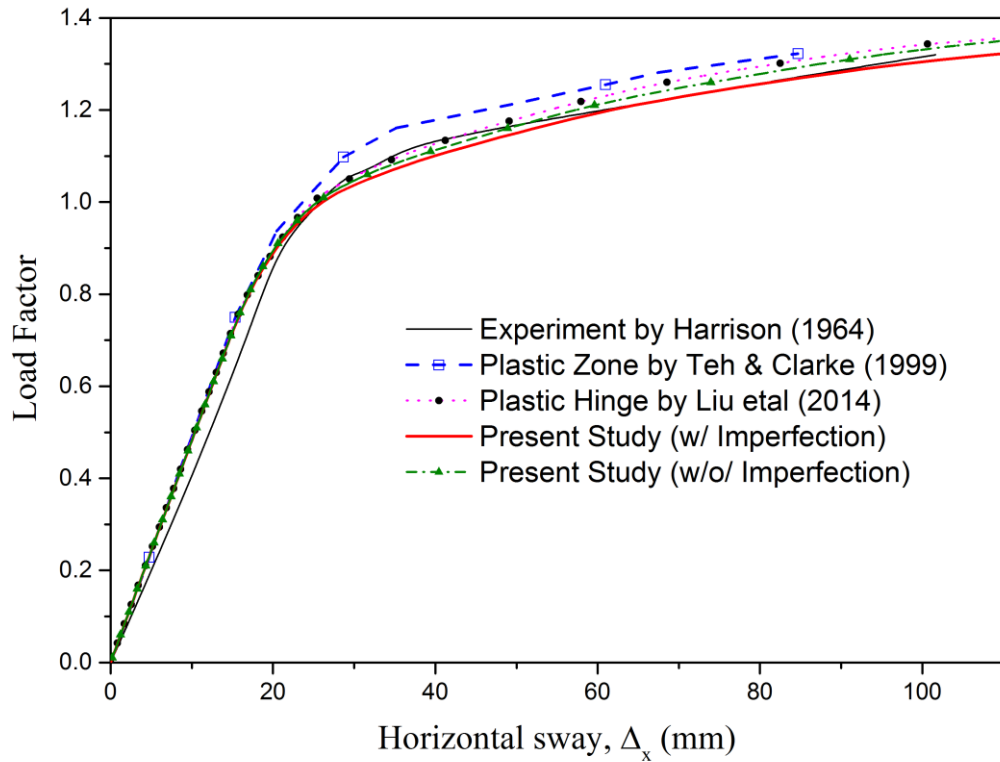


Fig. 3.14 Horizontal displacement of the top point

TABLES

Table 3-1 Numerical integration methods for flexibility-based beam-column element

Integration Method	Order of Accuracy	Number and Location of Integration Point
Newton-Cotes	$N-1$	N points uniformly along the element including both two ends
Gauss-Lobatto	$2N-3$	N points along the element including both two ends
Gauss-Radau	$2N-2$	N points along the element including one end only
Gauss-Legendre	$2N-1$	N points along the element not including two ends

Note: N is the number of integration points whose locations are depended on the integration method used.

Table 3-2 Numerical integration methods for flexibility-based beam-column element

Integration Method	Number of Integration Point per member	Number of elements
Newton-Cotes	10	1
Newton-Cotes	5	2
Newton-Cotes	7	2

Table 3-3 Theory results of a fixed-ended beam under different point loads

Hinge Sequence	Applied Load, P	Deflection, Δ_B
A	$6.75 \frac{M_p}{L}$	$0.0247 \frac{M_p L^2}{EI}$
A and B	$8.67 \frac{M_p}{L}$	$0.0423 \frac{M_p L^2}{EI}$
A, B and C	$9.0 \frac{M_p}{L}$	$0.0741 \frac{M_p L^2}{EI}$

Table 3-4 Models (M1~M7) for the planar frame by Ziemian and McGuire (2002)

Model	General Description	Local Imperfection	Global Imperfection	Plastic Method
M1	Present study, without imperfections, one element per member	$\delta_0 = 0$	$\Delta_0 = 0$	Plastic zone
M2	Present study, only local imperfections, one element per member	$\delta_0 = L/300$	$\Delta_0 = 0$	Plastic zone
M3	Present study, with local and global imperfections, one element per member	$\delta_0 = L/300$	$\Delta_0 = H/500$	Plastic zone
M4	Calculated by MASTAN2, 4 elements per beam, 2 elements per column	No reduction on modulus	$\Delta_0 = 0$	Plastic hinge
M5	Calculated by MASTAN2, 4 elements per beam, 2 elements per column	Modified modulus	$\Delta_0 = 0$	Plastic hinge
M6	Calculated by FE++2015, 16 elements per beam, 8 elements per column	Without residual stress	$\Delta_0 = 0$	Plastic zone
M7	Calculated by FE++2015, 16 elements per beam, 8 elements per column	With residual stress	$\Delta_0 = 0$	Plastic zone

Note: δ_0 and Δ_0 are the magnitudes of initial local and global geometrical imperfection respectively, L represents the member length, H is the frame height.

CHAPTER 4. TWO PLASTICITY MODELS FOR MATERIAL NONLINEARITY

4.1 Introduction

Many modern design codes, such as AISC360 (2016) and Eurocode-3 (2005), have specified “Direct analysis”, “Second-order Analysis” or “Advanced Analysis” for daily design of steel structures, through which the structural stability and safety can be assessed by checking the members and the system in an integrated manner rather than checking individual member using the effective length method (ELM). The ELM is simply based on the first-order linear analysis without consideration of many effects while the direct analysis method (DAM) considers the important factors affecting member and system strength, such as the second-order $P-\delta$ and $P-\Delta$ effects, initial geometrical imperfections, residual stress, material yielding and joint behavior.

Several different beam-column elements have been proposed to incorporate initial geometrical imperfection at the element level. Chan and Zhou (1995) and Liu *et al.* (2014a, 2014b) proposed stiffness-based beam-column elements considering initial bowing for second-order direct analysis, which show high computational efficiency and accuracy. Chiorean (2017) and Du *et al.* (2017) proposed two flexibility-based elements which can also directly incorporate initial imperfection in different manners and exhibit high performance when using one-element-per-member modeling.

Regarding material nonlinearity, there are two widely used methods, i.e., plastic hinge method and plastic zone method. The plastic hinge method (also named as concentrated plasticity method) is widely adopted in the stiffness-based beam-column elements due to its simplicity and computational efficiency, while the plastic zone

method (also well-known as distributed plasticity method) is usually used to calibrate the accuracy of plastic hinge method in previous research. Although the latter can obtain more accurate results, it costs more computer time as well as computer storage in the analysis as it is required to mesh a section into some fibers and several integration points are needed along the member length. This problem will be more serious in the nonlinear dynamic (time-history) analysis. With the recently fast development of computer hardware, it is possible to adopt the plastic zone method in the second-order inelastic analysis so that the structural behavior can be well predicted. However, the lack of consideration of initial imperfection in traditional flexibility-based elements and tedious determination of fiber state require too many computer resources, especially in high-rise buildings and long-span structures. Thus, it is urgent to improve the current analysis method so that more accurate results can be provided for design purpose with enhancement of computational efficiency.

Generalized plasticity method was firstly proposed by Auricchio and Taylor (1995) for material yielding and then extended to a stress resultant section model used in beam-column element developed by Kostic *et al.* (2013). Their element adopts concentrated plasticity model, whose feature is described by generalized plasticity using yield and limit surfaces. Thus, their method can take the benefit of well-accepted interaction functions between the axial force and the bending moments specified in design codes or more accurate yield functions in literature. However, the plastic hinges can be only formed at the ends of the element. It means that more elements are required if one or more plastic hinges are formed along the member. Further, their study does not take the $P-\delta$ effect into account and as a result their outcome cannot fulfill the requirement of direct analysis.

This thesis is intended to improve the computational efficiency of the flexibility-based element with distributed plasticity proposed by Du *et al.* (2017). The time-consuming fiber section integration will be replaced by the robust stress-resultant plasticity model based on the concept of the generalized plasticity method. As the discretization of cross-section into fibers is no longer required, the proposed method will significantly enhance the computational efficiency by directly using the relationship between section deformations and stress resultants. Also, good numerical convergence is observed when using the backward-Euler algorithm in the determination of section state. Thus, a practical solution will be proposed for second-order inelastic analysis through which a safer and more economical design can be achieved.

4.2 Distributed plasticity analysis

Comparing with displacement-based beam-column elements with high numerical efficiency, the biggest advantage of flexibility-based beam-column elements is the excellent performance in the second-order inelastic analysis. This highlighted feature is carried out by distributed plasticity method with fiber section technique. This technique is widely adopted in flexibility-based elements to consider distributed plasticity along the section height and member length, as seen in Fig. 4.1. Along the element, numerical integration scheme is used to represent the member with several integration points located in special locations. The cross-section is discretized into some fibers as integration points as shown in Fig. 4.2. For arbitrary shapes of cross-sections, the Blossom-Quad algorithm (2013) can be used to mesh them into quadrilateral fibers. Each of them is an independent region, which is defined by its centroid coordinates (y_j, z_j) and area (A_j) . Their mechanics behaviors are modeled

by the nonlinear stress-strain relationship. The stress resultants and tangent stiffness of the cross-section can be obtained by integration of these fibers as

$$\mathbf{S}(\xi_i) = \begin{Bmatrix} N(\xi_i) \\ M_z(\xi_i) \\ M_y(\xi_i) \\ T \end{Bmatrix} = \begin{Bmatrix} \sum_{j=1}^m (\sigma_j A_j) \\ \sum_{j=1}^m (-y_j \sigma_j A_j) \\ \sum_{j=1}^m (z_j \sigma_j A_j) \\ GJ\varphi' \end{Bmatrix} \quad (4.1)$$

$$\mathbf{k}_s(\xi_i) = \begin{bmatrix} \sum_{j=1}^m (E_{tj} A_j) & \sum_{j=1}^m (-y_j E_{tj} A_j) & \sum_{j=1}^m (z_j E_{tj} A_j) & 0 \\ \sum_{j=1}^m (-y_j E_{tj} A_j) & \sum_{j=1}^m (y_j^2 E_{tj} A_j) & \sum_{j=1}^m (-y_j z_j E_{tj} A_j) & 0 \\ \sum_{j=1}^m (z_j E_{tj} A_j) & \sum_{j=1}^m (-y_j z_j E_{tj} A_j) & \sum_{j=1}^m (z_j^2 E_{tj} A_j) & 0 \\ 0 & 0 & 0 & GJ \end{bmatrix} \quad (4.2)$$

in which, E_{tj} is the material tangent modulus of the fiber j corresponding to current stress state. The nonlinear stress-strain curve of material can be adopted by Equation (4.2) to trace the progressive yielding of the cross-section. When conducting second-order elastic analysis, the Equation (4.2) can be rewritten in a simple form as

$$\mathbf{k}_s(\xi_i) = \begin{bmatrix} EA & 0 & 0 & 0 \\ 0 & EI_z & 0 & 0 \\ 0 & 0 & EI_y & 0 \\ 0 & 0 & 0 & GJ \end{bmatrix} \quad (4.3)$$

4.3 Stress-resultant plasticity model

A natural idea to resolve this problem presented in the last sub-section is to treat the cross-section as a whole without discretization. One successful application of this idea is the plastic hinge method which has been widely used in the stiffness-based elements, for example, Liu *et al.* (2014a, 2014b). However, their method needs to increase the

load step with small increment so that the progressively yielding behavior can be captured. It will significantly increase computer time. Meanwhile, their method ignores the coupling effect between axial force and bending moments.

In this thesis, a stress-resultant plasticity model is proposed to reflect the relationship between the section deformations and the stress resultants directly, which is extended from the generalized plasticity material model introduced by Auricchio and Taylor (1995) and Lubliner *et al.* (1994, 1995, 1993). This model is also studied by Kostic *et al.* (2013, 2016) to investigate the inelastic response of plastic hinge. With the yield function f and limit function F as shown in Fig. 4.3, the stress-resultant plasticity model is able to model the progressive yielding of the cross-section. The functions f and F divide the space in terms of P-My-Mz into three regions:

- 1) Region 1: $f < 0$ and $F < 0$, the section is in the elastic state;
- 2) Region 2: $f > 0$ and $F < 0$, the section is in the inelastic state, or elastic state under unloading;
- 3) Region 3: $f > 0$ and $F > 0$, the section is in the inadmissible state.

Unlike the fiber section model which needs numerous variables to record material history state of every fiber during the analysis, the stress-resultant plasticity model only needs a few variables to represent the section state. Thus, this model will save much computer storage and cost less computer time in the determination of section state. Further, as the proposed flexibility-based element has taken the initial geometrical imperfections and P- δ effect into account, only one element per member can provide accurate responses for design which will significantly reduce the degrees of freedom and enhance computational efficiency.

To distinguish section state between elastic and inelastic behaviors, the yield function of the metal material is expressed regarding stress when using fiber section approach.

As an extension of this concept, the fully yield function of a section at the integration point along a member can be expressed regarding section stress-resultant \mathbf{p} as

$$f(\mathbf{p}) = \Phi(\mathbf{p} - \mathbf{a}) - H_{iso}\alpha \quad (4.4)$$

in which, \mathbf{a} is the center point of the yield surface to consider the Kinematic hardening effect; H_{iso} is the isotropic plastic hardening parameter; α is the equivalent plastic strain.

The gradually yielding process is described by a limit function as given in Equation (4.5), which is originally proposed for generalized plasticity model.

$$F = h(f) \frac{d\Phi}{dt} - \dot{\lambda} \quad (4.5)$$

$$\text{with } h(f) = \frac{f}{\delta(\beta-f)} \quad (4.6)$$

in which, $\dot{\lambda}$ is the plastic strain-rate multiplier; δ and β are two non-dimensional positive constants, and the former controls the speed from elastic status to fully plastic status while the latter represents the region of elastic-plastic status.

When the section force exceeds the yield surface, plastic deformation will happen.

Plastic deformation is determined by an associated plastic flow rule as

$$\mathbf{d}^p = \dot{\lambda} \frac{\partial f}{\partial \mathbf{p}} \quad (4.7)$$

According to the plastic theory, the Kuhn-Tucker complementarity conditions can be used to convert the plastic problem to a constrained optimization problem. The complementarity conditions are expressed as

$$\dot{\lambda} \geq 0, \quad F \leq 0 \quad \dot{\lambda}F = 0 \quad (4.8)$$

Hence, the limit function in Equation (4.5) should satisfy the following equation.

$$F = h(f) \frac{d\Phi}{dt} - \dot{\lambda} = 0 \quad (4.9)$$

4.4 Integration of rate equations and section tangent stiffness

4.4.1 Integration algorithm

The section deformations can be decomposed into the elastic deformations and the plastic deformations as

$$\mathbf{d} = \mathbf{d}^e + \mathbf{d}^p \quad (4.10)$$

During the integration process, the section forces and the section deformations are assumed to be known at time step t_n . The relationship between the generalized strain field and stress resultants is given as

$$\mathbf{s}_n = \mathbf{k}_{se}(\mathbf{d}_n - \mathbf{d}_n^p) \quad (4.11)$$

in which, \mathbf{k}_{se} is the elastic section tangent stiffness matrix; \mathbf{d}_n and \mathbf{d}_n^p are the total section deformations and plastic section deformations respectively; \mathbf{s}_n is the section forces excluding the torsional moment.

If the increment of section deformations is expressed as $\Delta\mathbf{d}$ at time step t_{n+1} , the total section deformations can be determined as

$$\mathbf{d}_{n+1} = \mathbf{d}_n + \Delta\mathbf{d} \quad (4.12)$$

From the above, the only unknown variable for determination of section state is the plastic section deformations \mathbf{d}_{n+1}^p . In this thesis, the backward-Euler numerical integration algorithm will be adopted to find the plastic section deformations. This method is based on the following equation,

$$\mathbf{d}_{n+1}^p = \mathbf{d}_n^p + \mathbf{r}_{n+1}(\mathbf{s}_{n+1})\Delta\lambda \quad (4.13)$$

in which,

$$\mathbf{r}(\mathbf{s}) = \frac{\partial f}{\partial \mathbf{s}} \quad (4.14)$$

The incremental form of the Kuhn-Tucker conditions can be written as

$$\Delta\lambda \geq 0, \quad F_{n+1} \leq 0 \quad \Delta\lambda F = 0 \quad (4.15)$$

Similarly, the continuous form of the limit function in Equation (4.9) can be rewritten to a discrete form as

$$h(f)(\Phi_{n+1} - \Phi_n) - \Delta\lambda = 0 \quad (4.16)$$

in which,

$$\Delta\lambda = \int_{t_n}^{t_{n+1}} \lambda dt \quad (4.17)$$

4.4.2 Return mapping algorithm

Elastic predictor-plastic corrector integration strategy is adopted as the force integration algorithm. When the moment-axial force point lies outside the full yield surface, the procedure of return mapping algorithm as shown in Fig. 4.4 should be used to correct the section state. The position A is the starting point while the final position can be determined by the following three steps.

Step 1: Prediction procedure

In the first step, the trial position B is located by the elastic relationship between the section deformations and stress resultants given in Equation (4.18)

$$\mathbf{s}_{n+1}^{trial} = \mathbf{k}_{se}(\mathbf{d}_{n+1} - \mathbf{d}_n^p) \quad (4.18)$$

The plastic deformations are assumed to be constant from time step t_n to t_{n+1} .

Hence, the plastic deformations at the time step t_{n+1} are equal to that at the time step t_n as shown in Equation (4.19), and $\Delta\lambda = 0$.

$$\mathbf{d}_{n+1}^{p,trial} = \mathbf{d}_n^p \quad (4.19)$$

Further, the yield function in Equation (4.4) will be updated with the trial stress resultants \mathbf{s}_{n+1}^{trial} as

$$f_{n+1}^{trial} = \Phi_{n+1}^{trial} - H_{iso}\alpha \quad (4.20)$$

Step 2: State check

After trial point **B** and trial section state are determined from step 1, the trial location should be checked if the conditions in Equation (4.15) are satisfied or not. As the plastic flow is frozen at step 1 with $\Delta\lambda = 0$, the conditions can be rewritten as

$$f_{n+1}^{trial} < 0, \quad or \quad f_{n+1}^{trial}(\Phi_{n+1}^{trial} - \Phi_n) \leq 0 \quad (4.21)$$

The first condition in Equation (4.21) represents the state that the stress resultants do not violate the yield surface, and the second one is for the unloading state. If one of the conditions is satisfied, the plastic deformations, stress resultants and the tangent stiffness of the section can be updated by Equations (4.22) to (4.24) using the trial results from step 1, and then exit the whole return procedure. If both conditions are not satisfied, it should go to step 3 to perform the correction procedure.

$$\mathbf{d}_{n+1}^p = \mathbf{d}_n^p \quad (4.22)$$

$$\mathbf{s}_{n+1} = \mathbf{s}_{n+1}^{trial} \quad (4.23)$$

$$\mathbf{k}_{n+1} = \mathbf{k}_{se} \quad (4.24)$$

Step 3: Correction procedure

From step 2, it is known that the trial position **B** is not the balanced point and further iterative procedure is needed to satisfy the conditions in Equation (4.15). The difference between the current deformations and the backward-Euler deformations is represented by a vector **R** which can be determined from Equation (4.25) for time step t_{n+1} .

$$\mathbf{R}_{n+1} = -\mathbf{d}_{n+1}^p + \mathbf{d}_n^p + \mathbf{r}_{n+1}\Delta\lambda \quad (4.25)$$

To find the final deformations meeting the requirements in Equation (4.15), all elements in vector **R** should be less than a tolerance. For the trial plastic deformations,

\mathbf{d}_n^p being fixed, a truncated Taylor expansion can be applied to Equation (4.25) such that a new residual, \mathbf{R}^k , can be produced as

$$\mathbf{R}^k = \mathbf{R}^0 - \mathbf{d}_{n+1}^p + \Delta\lambda\mathbf{Q}\dot{\mathbf{s}} + \dot{\lambda}\mathbf{r} \quad (4.26)$$

with

$$\mathbf{Q}(\mathbf{s}) = \frac{\partial^2 f}{\partial \mathbf{s}^2}, \quad \dot{\mathbf{s}} = -\mathbf{k}_{se}\dot{\mathbf{d}}_{n+1}^p \quad (4.27)$$

in which, $\dot{\mathbf{s}}$ is the change in \mathbf{s} ; $\dot{\lambda}$ is the change in $\Delta\lambda$. Setting \mathbf{R}^k to zero, it gives

$$\dot{\mathbf{d}}_{n+1}^p = (\mathbf{I} + \Delta\lambda\mathbf{Q}\mathbf{k}_{se})^{-1}(\mathbf{R}^0 + \dot{\lambda}\mathbf{r}) \quad (4.28)$$

With Equation (4.28), a truncated Taylor series on Equation (4.15) will produce

$$a\Delta\Delta\lambda + b\Delta\Delta\lambda + c = 0 \quad (4.29)$$

in which,

$$a = (\delta - \mathbf{r}^T\mathbf{C}\mathbf{r})(\mathbf{r}^T\mathbf{C}\mathbf{r}) \quad (4.30)$$

$$b = \delta\Delta\lambda(\mathbf{r}^T\mathbf{C}\mathbf{r}) + \delta(\beta - f^{trial} + \mathbf{r}^T\mathbf{C}\mathbf{R}_1) + (f^{trial} + \Phi^{trial} - 2\mathbf{r}^T\mathbf{C}\mathbf{R}_1 - \Phi_n)(\mathbf{r}^T\mathbf{C}\mathbf{r}) \quad (4.31)$$

$$c = \delta\Delta\lambda(\beta - f^{trial} + \mathbf{r}^T\mathbf{C}\mathbf{R}_1) - (f^{trial} - \mathbf{r}^T\mathbf{C}\mathbf{R}_1)(\Phi^{trial} - \mathbf{r}^T\mathbf{C}\mathbf{R}_1 - \Phi_n) \quad (4.32)$$

$$\mathbf{C} = (\mathbf{k}_{se}^{-1} + \Delta\lambda\mathbf{Q})^{-1} \quad (4.33)$$

The smaller positive solution $\Delta\Delta\lambda$ in Equation (4.29) will be used to update $\Delta\lambda$ on iteration k as

$$\Delta\lambda_{n+1}^{k+1} = \Delta\lambda_{n+1}^k + \Delta\Delta\lambda_{n+1}^k \quad (4.34)$$

When $\Delta\Delta\lambda$ is less than the given tolerance, the final force position is located and the whole process is terminated. Otherwise, the iterative procedure using Equation (4.34) should be continued until $\Delta\Delta\lambda$ meets the convergent condition.

4.4.3 Section tangent stiffness matrix

After determination of the section state by the return mapping algorithm above, the section tangent stiffness can be calculated. The standard backward-Euler algorithm in Equation (4.13) can be rewritten as

$$\mathbf{s}_{n+1} = \mathbf{s}_{n+1}^{trial} - \Delta\lambda \mathbf{k}_{se} \mathbf{r} \quad (4.35)$$

Taking the derivative of Equation (4.35) it gives

$$\dot{\mathbf{s}}_{n+1} = \mathbf{k}_{se} \dot{\mathbf{d}} - \dot{\lambda} \mathbf{k}_{se} \mathbf{r} - \Delta\lambda \mathbf{k}_{se} \dot{\mathbf{s}}_{n+1} \quad (4.36)$$

To satisfy Equation (4.16), the consistent tangent matrix can be derived as

$$\mathbf{k}_{n+1} = \mathbf{C}_{n+1} - k \mathbf{C}_{n+1} \mathbf{r}_{n+1} \mathbf{r}_{n+1}^T \mathbf{C}_{n+1} \quad (4.37)$$

in which,

$$k = \frac{(f_{n+1} + \Phi_{n+1} - \Phi_n + \delta\Delta\lambda_{n+1})}{\delta(\beta - f_{n+1}) + (f_{n+1} + \Phi_{n+1} - \Phi_n + \delta\Delta\lambda_{n+1}) \mathbf{r}_{n+1}^T \mathbf{C}_{n+1} \mathbf{r}} \quad (4.38)$$

4.5 Verification examples

For the steel member with the wide-flange compact section, Orbison (1982) proposed a yield function which is reproduced in Equations (4.39) and (4.40) below to trace the material nonlinearity,

$$\Phi(F) = 1.15p^2 + m_z^2 + m_y^2 + 3.67p^2 m_z^2 + 3p^6 m_y^2 + 4.65m_y^2 m_z^4 = 1 \quad (4.39)$$

$$F(P, M_z, M_y) = \begin{bmatrix} p \\ m_z \\ m_y \end{bmatrix} = \begin{bmatrix} \frac{P}{P_y} \\ \frac{M_z}{M_{pz}} \\ \frac{M_y}{M_{py}} \end{bmatrix} \quad (4.40)$$

in which, P_y is the axial resistance, M_{pz} and M_{py} are the plastic moment resistance about z- and y-axis respectively. For easy comparison, the Kinematic and isotropic

hardening effects in Equation (21) are ignored in the following examples. The full surface under the interaction of force resultants is shown in Fig. 4.5.

For fair comparison regarding computational efficiency, all examples were analyzed in the same personal computer with an Intel® Core™ i7-3770 CPU of 3.4 GHz and 16 GB RAM.

4.5.1 A cantilever column subjected to a cyclic axial force

The cantilever column as shown in Fig. 4.6 was firstly studied by Kostic *et al.* (2013) in a beam-column element with end plastic hinges only. In this thesis, this example is used to validate the ability of the proposed element in dealing with material and geometrical nonlinearity using the stress-resultant plasticity model. The fiber section plasticity model will be used for comparison purpose. The layout, section and material properties of the column are shown in Fig. 4.6. Two cases have been studied as follows.

Case 1: The column is subjected to uniaxial tip translation history along the weak y -axis.

Case 2: The column, with or without initial geometrical imperfection $L/300$, is subjected to a variable axial force.

In case 1, both the proposed stress-resultant plasticity model and the fiber section model are used to simulate the column behavior. Only one flexibility-based element is used in the two methods for easy comparison.

The hysteresis curves of bending moment versus rotation on the bottom of the column, predicted by two different models, are shown in Fig. 4.7. It can be seen that the results from the stress-resultant plasticity model are remarkably close to the fiber section model. It demonstrates that the proposed model can capture the gradually yielding of the cross section with acceptable accuracy.

In case 2, the column, with and without initial geometrical imperfection, is modeled by one proposed flexibility-based element using the stress-resultant plasticity model. The initial bowing of the column is taken as $L/300$, which L is the member length. This case aims to study the influence of initial imperfection on the structural behavior. The hysteresis curves of bending moment versus rotation at the bottom of the column with and without consideration of imperfection are plotted in Fig. 4.8. It is interesting to find that the initial imperfection has little effect on tension capacity, but it will weaken the column's compressive capacity and alter the structural behavior. It also demonstrates that the proposed flexibility-based element with the stress-resultant plasticity model has good performance under the pseudo-static load.

4.5.2 Vogel six-story steel frame

A two-bay six-story 2D steel frame subjected to distributed gravity loads and concentrated lateral loads at each story level was firstly studied by Vogel (1985). The layout, applied loads, section and material properties of the structure are given in Fig. 4.9. This frame will be used to calibrate accuracy and numerical stability of the proposed method with the stress-resultant plasticity model. The result using several flexibility-based elements per member with fiber section model is believed as a sufficiently accurate response for calibration purpose. The influence of initial out-of-plumb straightness is neglected for easy comparison. Two simulation strategies are designed as follows:

Case 1: All beams and columns are modeled by one flexibility-based element with the stress-resultant plasticity model. Seven Gauss-Lobatto integration points along each element are employed.

Case 2: All beams are modeled by four proposed elements while all columns are modeled by two flexibility-based elements. The fiber section model is adopted for consideration of material nonlinearity. Seven Gauss-Lobatto integration points along each element are employed.

The load-deflection curve of the node A at the top level is plotted in Fig. 4.10. It can be seen that the proposed method produces very close results compared with the more accurate fiber section approach which generally consumes more computer time. Thus, this example demonstrates that the proposed method can accurately predict the responses of practical structures with one-element-per-member modeling.

4.5.3 Two-story high strength steel frame

Six full-scale tests of single-bay two-story frames under cyclic loading were conducted by Hu *et al.* (2017) to study the seismic behavior of high strength steel frames. In this thesis, the specimen B460-C460-2 with a clear presentation of results as comparison purpose is selected to verify the proposed element with the stress-resultant plasticity model. The layout, section and material properties of the specimen are shown in Fig. 4.11.

A constant axial load of 756 kN is applied on the top of each column. The point A is subjected to a lateral cyclic displacement as shown in Fig. 4.12. At the same time, a variable force F_B is applied on point B. The force F_B is taken as one twentieth of the lateral reaction force of point A, which is resistant force determined in the last cycle. All beams and columns are modeled by one flexibility-based element. The yielding behavior of the frame is captured by the stress-resultant plasticity model.

The hysteresis results of the base shear versus controlled overall drift ratio against the experimental results are plotted in Fig. 4.13. Generally speaking, the proposed method

can predict the energy absorbing ability through the inelastic behavior of steel members. The numerical simulation results by the proposed method are slightly higher than experimental results. It may be due to ignorance of the contribution of connections on the absorption of energy in a numerical study.

4.5.4 Four-story 3D steel frame

As shown in Fig. 4.14, the four-story 3D steel frame with irregular layout both in plan and elevation under different ground motions is used to study the computational efficiency of the proposed method against the conventional fiber section approach. The structural geometry, section sizes, and material properties are detailed in Fig. 4.14. For simplicity, the static loads on the frame consist of self-weight (SW), five kPa of dead loads (DL) and 2 kPa of live loads (LL) applied at each floor. The combination of static loads is $1.0(\text{SW}+\text{DL}) + 0.5\text{LL}$, which is also used as the input of mass sources. For the ground motions, four earthquake records are studied here, i.e., the El-Centro 1940, the San Fernando 1971, the Loma Prieta 1989 and the Northridge 1994.

All beams and columns are modeled by one proposed element. The material nonlinearity is considered by the stress-resultant plasticity model and fiber section model respectively so that the advantage of the proposed method can be quantified based on their computer time cost. The Newmark method with $\gamma = 0.5$ and $\beta = 0.25$ is adopted for time integration. The Rayleigh damping is calculated by the first two frequencies of the elastic structure. The time increment is 0.02 second.

The base shear F_x and displacement U_x at the roof level are shown in Fig. 4.15 and Fig. 4.16. It can be seen that both the base shears and the roof displacements from the proposed method are well agreed with the fiber section model.

The time consumed using two different methods related to four ground motions is shown in Fig. 4.17. It is observed that the total computer times obtained from the proposed method are shorter than the fiber approach and the minimum time saving is above 25%. Thus, the proposed method can provide sufficiently accurate results with a significant reduction in computational cost. This method is ready for the design of practical structures.

4.6 Concluding remarks

The conventional flexibility-based beam-column elements show high accuracy in inelastic analysis, but they are rarely adopted in a global analysis of engineering structures due to huge consumption of computer time and storage. Also, the conventional method did not take the member initial imperfection into account and, as a result, they require several elements per member to capture the real behavior and fulfill the design code requirement for direct analysis.

This thesis fills the gap between the research and the practical application and a better analysis method regarding safety, efficiency, robustness, and economy can be achieved. The stress-resultant plasticity model is introduced to a robust flexibility-based element developed by the authors to replace the commonly used fiber section model which generally consumes more computer time. Several integration points along an element are used to trace the distributed plasticity. The backward-Euler algorithm is adopted to determine complex section state which may undergo loading, unloading and re-loading behavior. This algorithm is reliable with good numerical convergence.

The numerical examples show that the proposed method produces not only accurate results when compared with the conventional fiber section model, but also reduces

significantly the computational cost. Thus, this innovative solution, complying with the codified requirement of second-order direct analysis, is readily applicable to the design of practical steel structures.

FIGURES

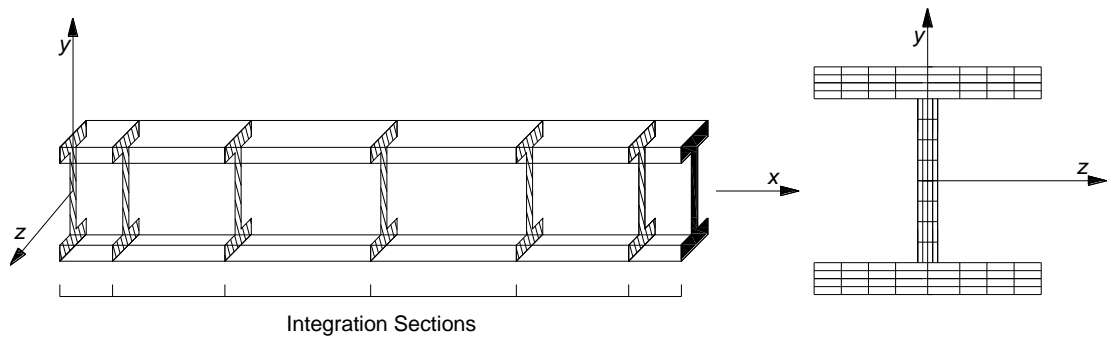


Fig. 4.1 Distributed plasticity by fiber section approach

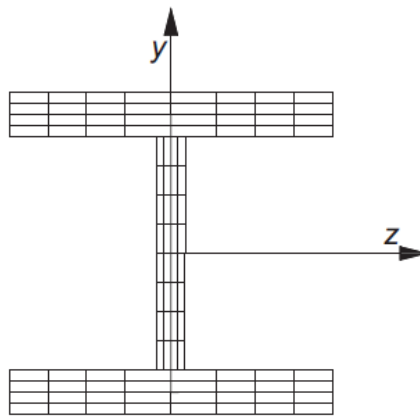


Fig. 4.2 Fiber discretization for wide-flange section

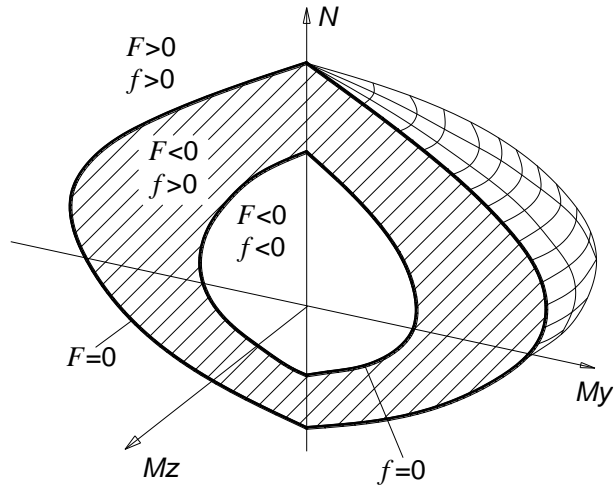


Fig. 4.3 Yield function and limit function for section state

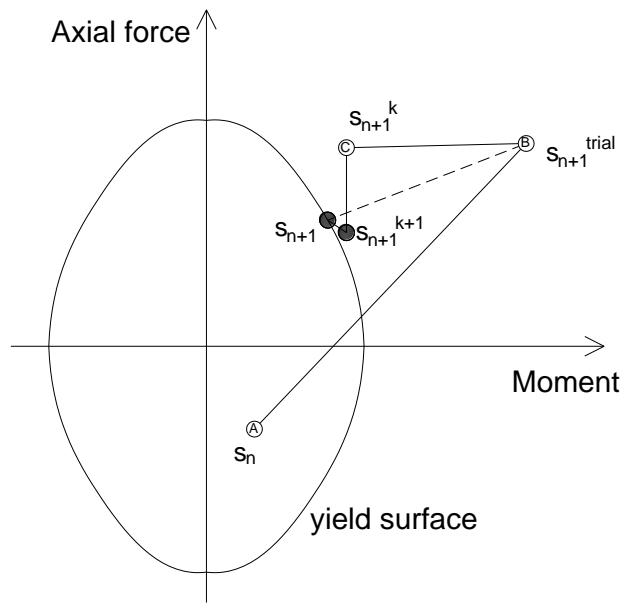


Fig. 4.4 Backward-Euler return procedure

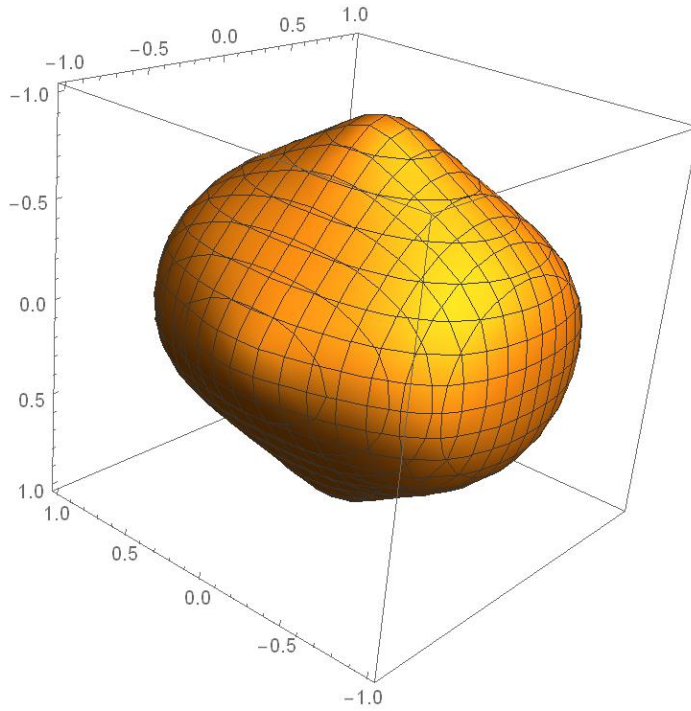


Fig. 4.5. Full surface under interaction of force resultants

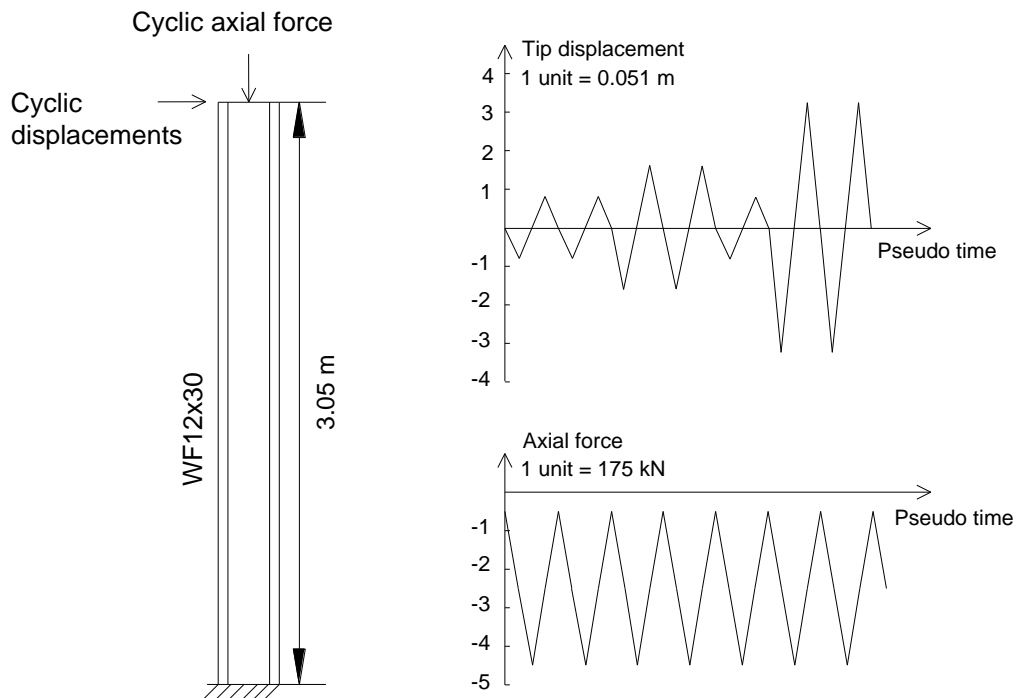


Fig. 4.6 Layout of cantilever column and loading patterns

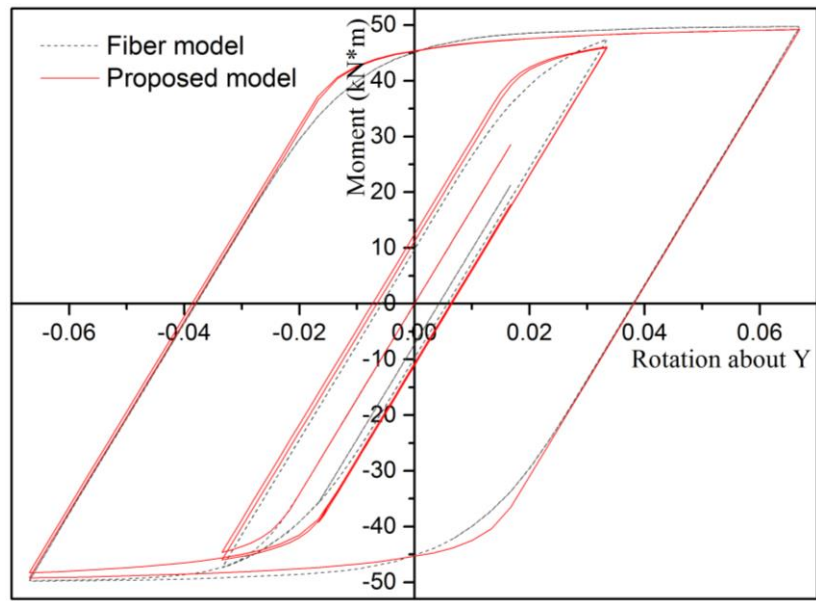


Fig. 4.7 Bending moment-plastic rotation about y-axis for case 1

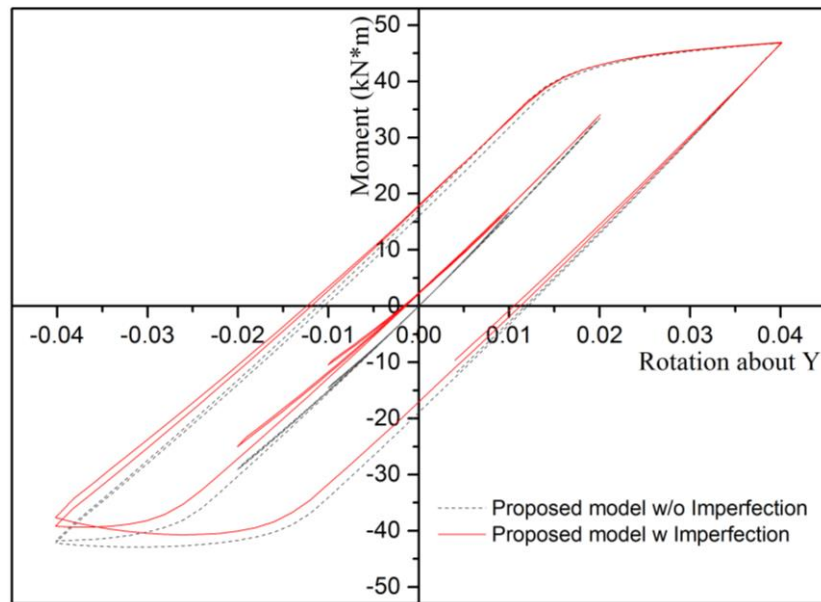


Fig. 4.8 Bending moment-plastic rotation about y-axis for case 2

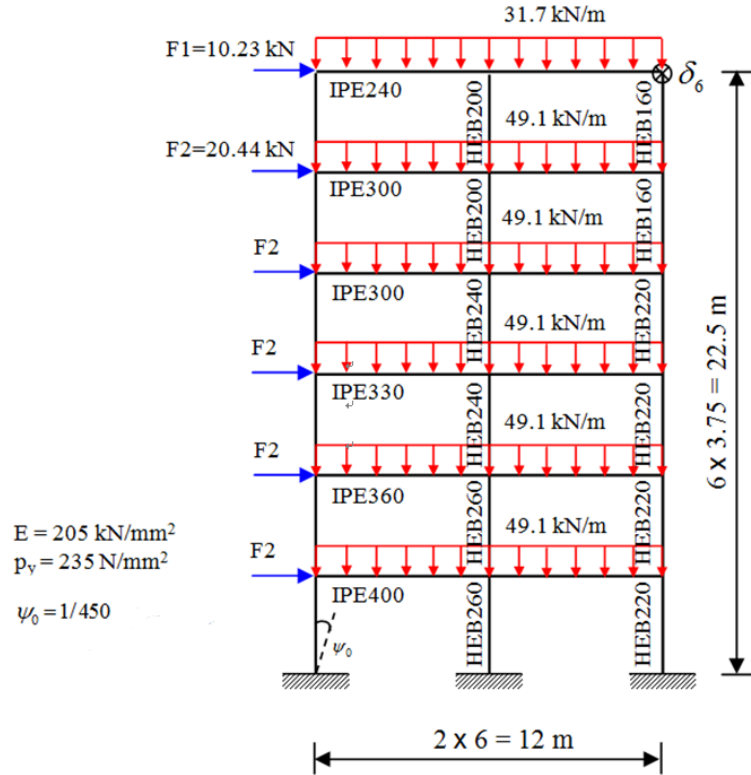


Fig. 4.9 Layout and loading pattern of the Vogel's six-story frame

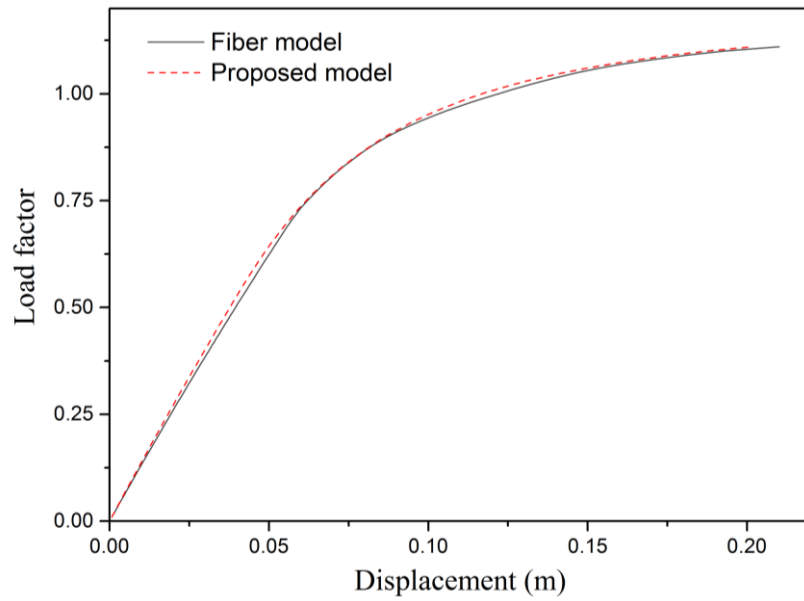


Fig. 4.10 Horizontal displacement of the Vogel's six-story frame

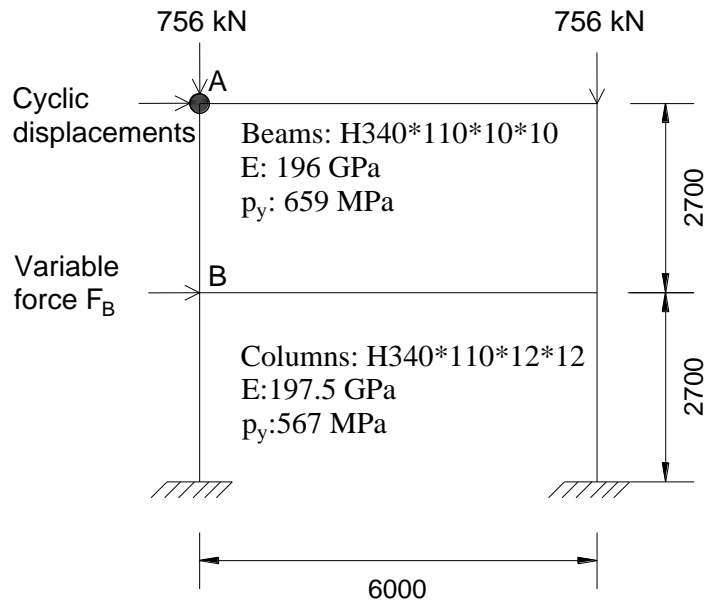


Fig. 4.11 Layout and loading pattern of the high strength steel frame (Unit: mm)

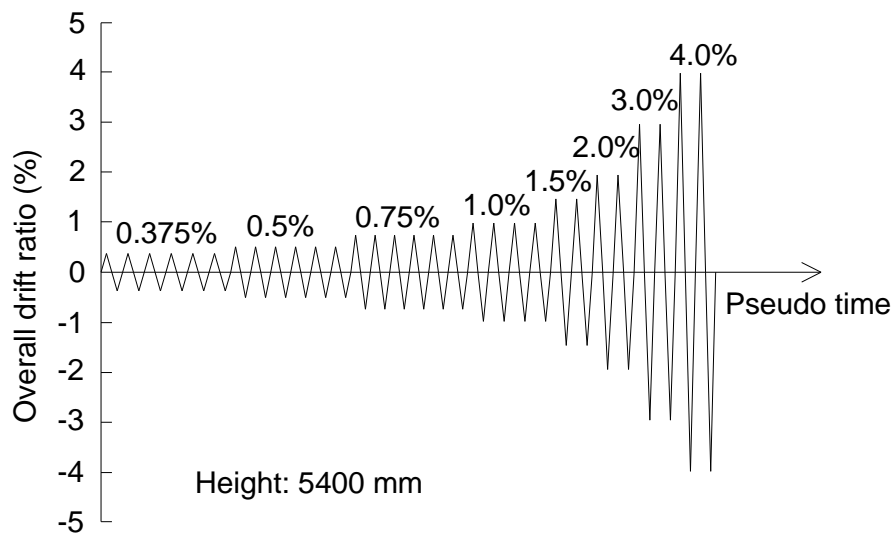


Fig. 4.12 Loading protocol for the top displacement

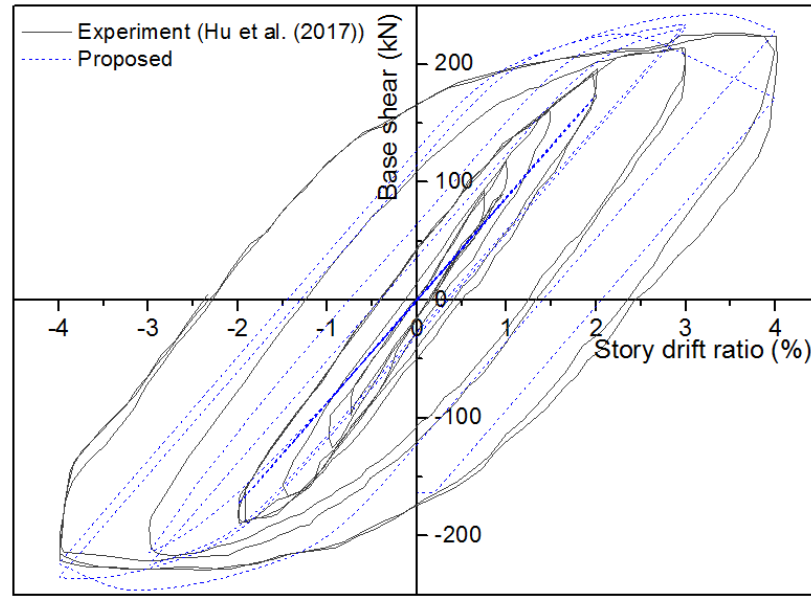


Fig. 4.13 Base shear versus overall drift ratio

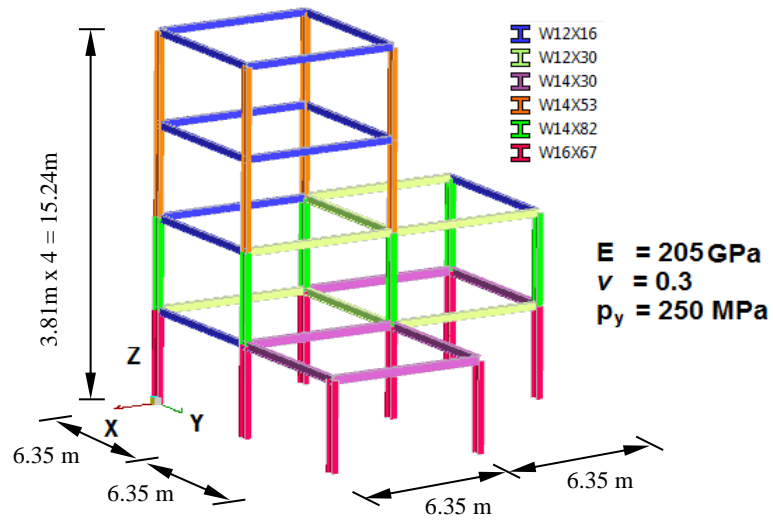
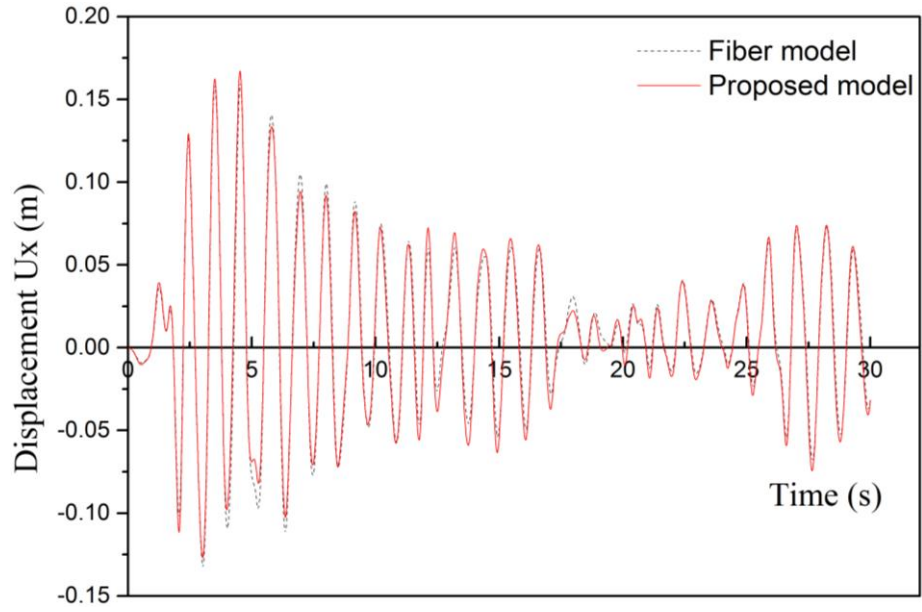
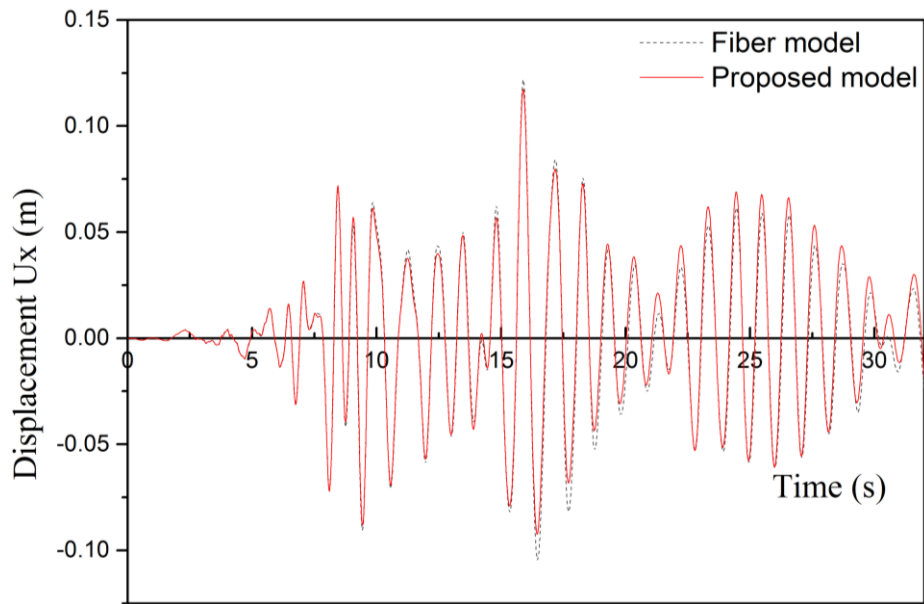


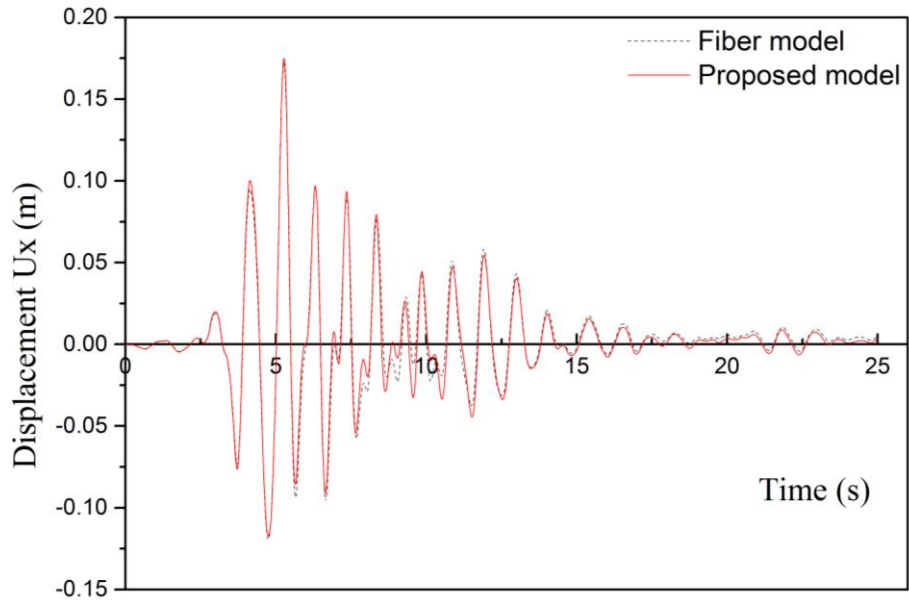
Fig. 4.14 Layout of four-story 3D steel frame



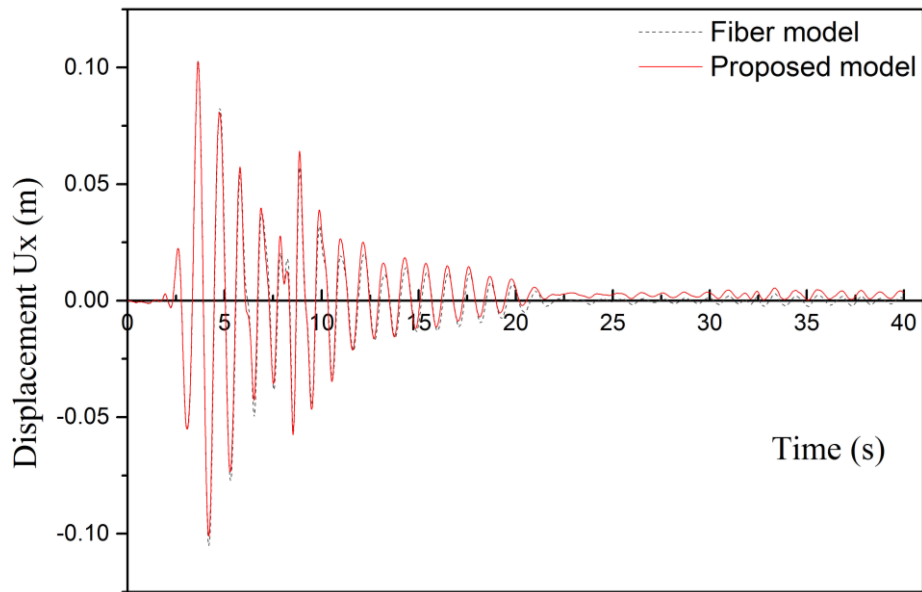
(a) El Centro 1940



(b) Loma Prieta 1989

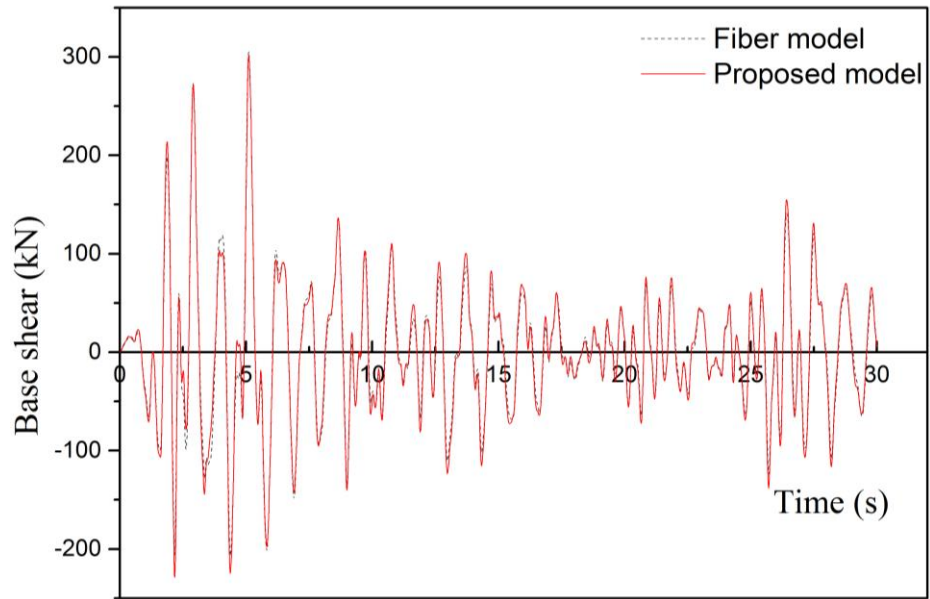


(c) Northridge 1994

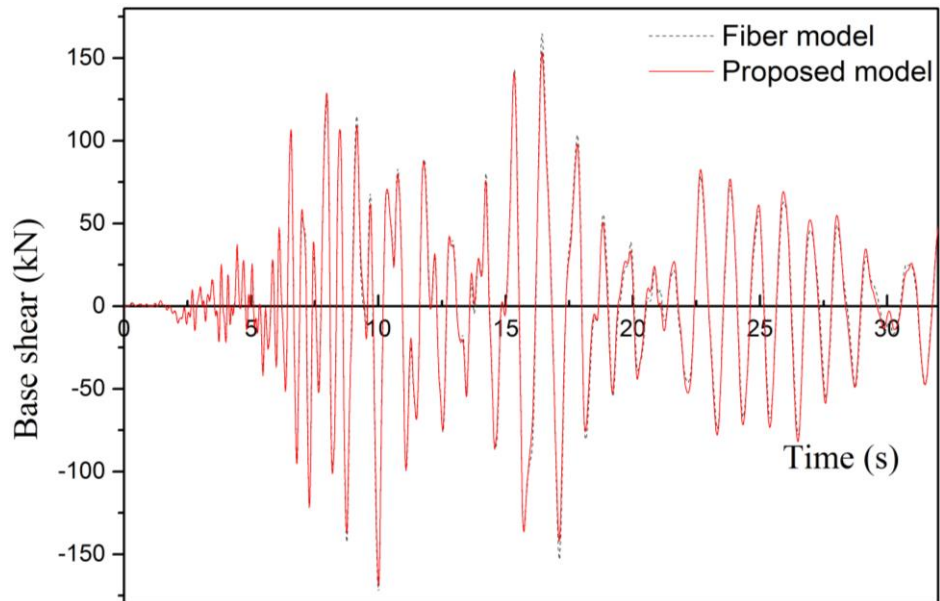


(d) San Fernando 1971

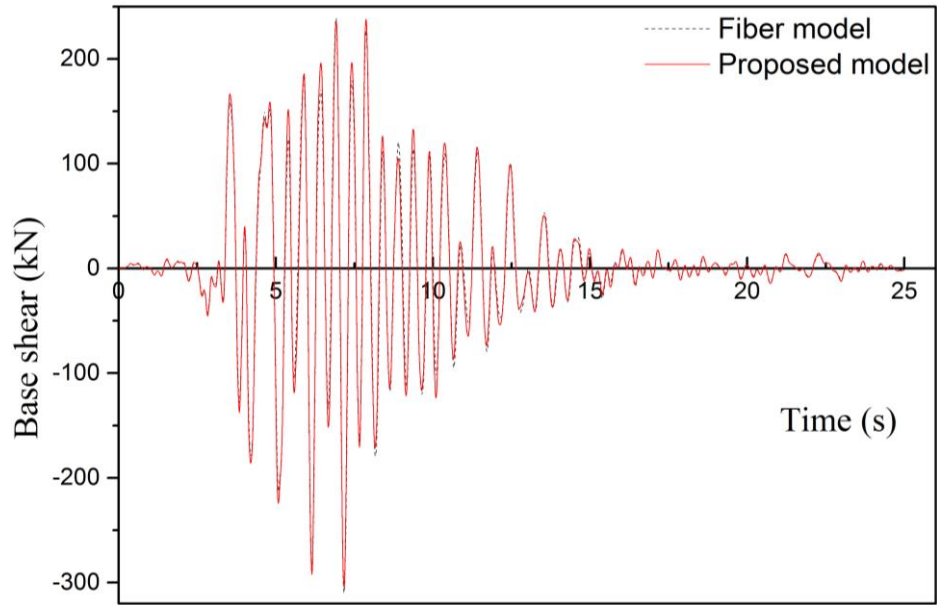
Fig. 4.15 Displacement under four earthquakes



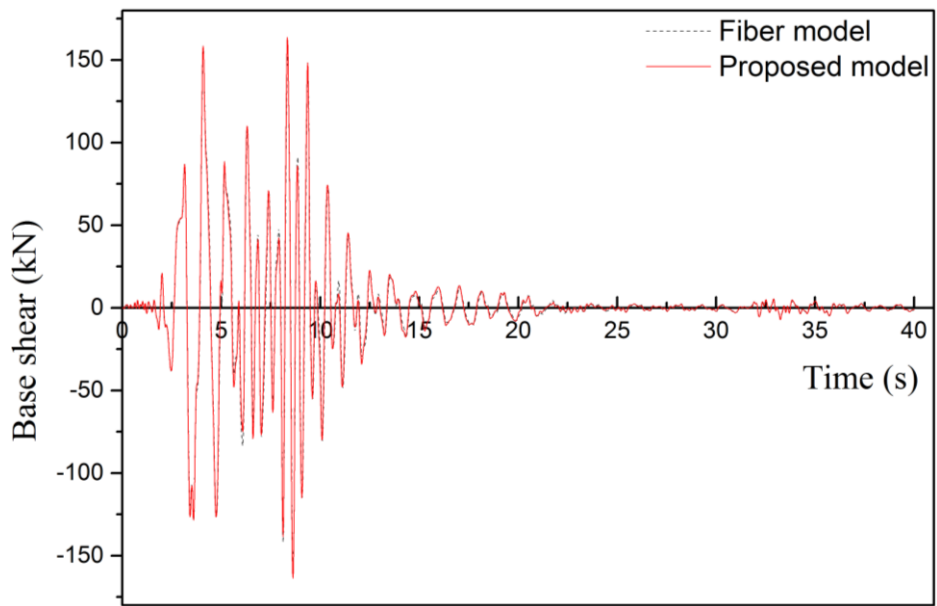
(a) El Centro 1940



(b) Loma Prieta 1989



(c) Northridge 1994



(d) San Fernando 1971

Fig. 4.16 Base Shear under four earthquakes

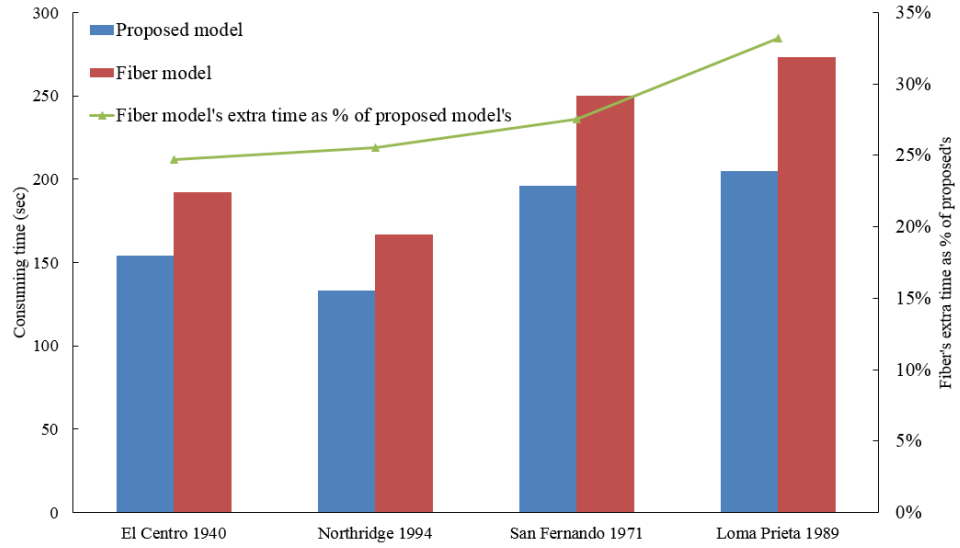


Fig. 4.17 Consuming time of time history analysis under four earthquakes

CHAPTER 5. SEMI-RIGID CONNECTIONS

UNDER MONOTONIC AND CYCLIC LOADS

5.1 Introduction

Connection systems play important role in the skeletal space structures. A large number of connection details have been proposed in the practical projects with great success, such as solid ball joint systems, socket joint systems, plate joint systems, slot joint systems and so on. These joint systems are usually analyzed and designed with the simple assumption that they are either perfectly rigid or frictionlessly pinned for convenience. In fact, the actual joints may have completely different features compared with the rigid and pinned joints. This lead to increasing concerns on the joint behaviors as many collapse events were initiated by connection failure. To satisfy the moment transfer between the beams and the columns, heavily detailed connections between these members are required, which cause larger size of beams required. Extra lateral resisting systems are needed in the pinned-joint structures due to zero rotational connection stiffness between these members. Noted that, connection systems will certainly affect the overall behavior of the entire structure. Many national steel design codes, such as AISC360 (2016) and Eurocode-3-1-8 (2005), have the provisions of semi-rigid connections to consider joint flexibility to overcome the drawbacks described above. Many scholars have noticed this phenomenon and conducted many experimental tests to explore the overall effects of joint flexibility. For example, Csébfalvi (2007) used an optimal method to design structures with consideration of semi-rigid joints, which lead to the redistribution of the internal forces between

members. Ahmadizadeh and Maalek (2014) investigated the effects of socket joint flexibility on the overall behavior of full-scale space structures and demonstrated that the rigid-connection assumption made unsafe prediction of displacements and ultimate load-carrying capacity of the studied structure. Thus, they suggested that the analysis and design of space structures should directly include the effects of socket joint flexibility. Sagiroglu and Aydin (2015) reported that the semi-rigid connection design could lead to a better prediction of the response and reliability of structures. Truong *et al.* (2017) utilized the zero-length element model to simulate the nonlinear behavior of steel connection when optimizing space steel frames with the micro-genetic algorithm. During the optimization process, the type of semi-rigid connection was also a variable. They reported that the column sizes should be increased due to the degradation of connection stiffness. In summary, the joint flexibility should be reflected in the direct analysis with proper beam-column elements.

In this chapter, the modeling methods for the connections under static and cyclic loads will be introduced. Further, the semi-rigid models will be directly incorporated into the proposed element as described in Chapter 3. Several numerical examples will be studied to verify the practicability and accuracy of the proposed approach. Finally, several concluding remarks will be listed to highlight the priorities.

5.2 Modeling of connection behavior under monotonic loading

To consider the joint flexibility in numerical analysis, several linear or nonlinear models have been proposed in the past decades. Generally, the models for static analysis ignored the unloading phase. There are three methods to get the moment-

rotation or force-displacement curves for modeling of semi-rigid connection, i.e. experimental approaches, empirical approaches, and numerical approaches.

5.2.1 Experimental approaches

Among all approaches exploring joint behaviors, the experimental approaches are the accurate way to investigate the characterization of joints. In the past few decades, many monotonic loading tests have been conducted to study the moment-rotation curves of different types of beam-column connections including single/double web cleats, header plates, top and seat angles, extend/flush end plates, etc. These rich experimental results can provide accurate and reliable data for modeling the different types of beam-column connections. Nevertheless, the cost of these experiments was high compared with other approaches, and it was hard to cover all the circumstances. Although there are many disadvantages of these approaches, the basic data regarding joint systems are vital for other methods as the benchmark and calibration purposes.

5.2.2 Empirical approaches

The models from empirical approaches are often calibrated by the experimental test results. By collecting numerous test results, the moment versus rotation curves of various connection types were proposed which can be used for mathematical modeling of beam-column connections. Because these moment-rotation curves are obtained from the limited experimental data, it may not be that accurate for studying the real connection behavior. Moreover, it is difficult to propose an appropriate model for the uncommonly used connection type due to the lack of data.

5.2.2.1 Component method

Eurocode-3-1-8 (2005) introduces an approach called the component method to represent the rotational behavior of extended end plate connections. The stiffness of connection components, such as column web, column flanges, end plates, and bolts, are calculated and then combined together to the overall joint rotational stiffness. Faella (1997) proposed a modified version of this component model. In the modified model, the joint rotational stiffness is determined by the stiffness of the connected beams as

$$K_{\varphi} = \frac{EI_b}{L_e} = \frac{EI_b}{\eta d_b} \quad (5.1)$$

in which, I_b is the inertia moment of the beams; L_e is the equivalent beam length which affects the joint performance; d_b is the depth of the beam; and η is a constant parameter.

5.2.2.2 Neural network method

With the aim of exploring the tolerance for uncertainty, a methodology entitled soft-computing is utilized to attain tractability at low computational cost. Soft-computing has been widely used in various application fields. The basic model of soft-computing is based on the human mind, which is achieved by a neural network (NN). Some scholars such as Abdalla and Stavroulakis (1995) and Güneyisi *et al.* (2014), introduced this method to build models for the joint flexibility. This type of models is based on rich experimental connection data. Its function is composed of three components: weights, bias and an activation function. The function is given as

$$U_k = Bias_k + \sum_{j=1}^n (w_{j,k} I_k) \quad (5.2)$$

in which, I_k is the input parameter; $w_{j,k}$ is the weight; $Bias_k$ is the bias; and U_k is the output value. Before training a NN, the database of experimental tests is collected. Then the mathematical formulation is used to generate the artificial neural network. The training quality is generally evaluated by the mean square errors and correlation coefficients. After training, equation (5.1) can be used to predict the ultimate moment and rotation values.

Though the neural network method is an alternative method for modeling joint connections, this method is case-dependent and drastically influenced by the optimal choice of the network configuration. Meanwhile, the speed of the learning procedure is also a critical problem.

5.2.3 Numerical approaches

Based on the concepts of mechanics theory, such as equilibrium equations, compatibility equations and material properties, the relationship between the joint rotational stiffness and the moment resistance can be derived. Compared with the empirical approaches which should be mainly depended on experiments, the numerical approaches have several advantages: (1) due to their lower computational expense, sufficient data can be obtained quickly and conveniently, as opposed to conducting numerous experimental tests; (2) the local behavior of joints can be investigated while this is difficult for experimental approaches because of the limited observation instruments; (3) parametric analysis can be conducted by numerical approaches to study joint behavior more thoroughly.

Finite element method (FEM) is widely used to explore the relationship between the moment and rotation of joints. Generally, the joints are simulated by solid elements or shell elements, and contact elements with full size geometric dimensioning and nonlinear materials shown in Fig. 5.1 and Fig. 5.2. Large deformation, strain, buckling, and strain-hardening of joints can be captured by proper input. In particular, highly nonlinear behavior, such as slip, friction, and interaction between bolts and plate components, can be reflected in the numerical simulation.

A refined finite element model can produce relatively accurate joint behaviors. FEM is a well-recognized and powerful tool for study of joint behaviors. Through this method, the moment and rotation curves of the conventional and newly-developed joints can be obtained. However, the models as shown in Fig. 5.1 and Fig. 5.2 require large amounts of modeling and computational time. There is a large drawback to apply it in practical design by engineers. Moreover, highly nonlinear problems involve various analysis settings to control numerical convergence, which limits its application, especially in large-scale structure design.

5.2.4 Formulation for the moment-rotation curve

Several models can be used to simulate joint stiffness: the linear model, multi-linear model, polynomial model, three parameter power model and other nonlinear models. The linear and multi-linear model are easy to use but may lead to inaccurate results. The nonlinear models can provide better approximations for joint. However, these moment-rotation curves often require many parameters which are hard to be determined. The commonly used beam-column connection models will be detailly introduced in this section.

5.2.4.1 Linear model

The linear model provides the simplest moment-rotation curve and only requires one parameter. The $M - \phi_c$ curve can be written as

$$M = S_c^o \phi_c \quad (5.3)$$

in which S_c^o is a constant value representing the initial connection stiffness and can be obtained from experimental results. According to Lightfoot and LeMessurier's assumption (1974), the initial stiffness can be expressed as

$$S_c^o = \lambda \frac{4EI}{L} \quad (5.4)$$

in which, λ is the rigidity index which indicates the degree of connection flexibility. The value of λ varies from zero to infinite based on the joint type. Alternatively, S_c^o can be written as

$$S_c^o = \frac{\eta}{1-\eta} \left(\frac{4EI}{L} \right) \quad (5.5)$$

in which, η is a fixity factor proposed by Romstad and Subramanian (1970) and Yu and Shanmugam (1986). The factor η is zero for a pinned joint and unity for a rigid joint.

5.2.4.2 Multi-linear model

The linear model can be used only on the premise of small joint deflection. Regarding large deflection, the degradation of the connection stiffness should be considered. Therefore, the multi-linear model is proposed to improve the accuracy of connection behavior and model the degradation of the stiffness of connections in the large

deflection problem. In fact, another nonlinear model can be described approximately by the multi-linear model with sufficient segmentations.

5.2.4.3 Polynomial model

The first non-dimensional polynomial model of connection behavior was proposed by Frye and Morris (1975). This model can provide a smoother moment-rotation curve and is included in IS: 800 (1893). The original form is

$$\phi_c = C_1(K M)^1 + C_2(K M)^3 + C_3(K M)^5 \quad (5.6)$$

where K is a constant parameter determined by geometrical characteristics, such as member size, throat thickness and so on; M is the moment applied on the joint; C_1 , C_2 , and C_3 are fitting parameters; and ϕ_c is the joint rotation. The Frye-Morris model provides a generalized form that can be extended to different connection types. For example, Prabha *et al.* (2010) proposed a polynomial model for pallet rack connection based on this model with K defined by the thickness of columns (t_u), depth of beams (d_b) and the depth of the connector (d_c).

Generally, the polynomial model exhibits good performance in the initial stiffness prediction, but less accuracy in the ultimate capacity of the connection. Also, the stiffness of the connection is derived by Equation (5.6), which may lead to negative stiffness. This case does not conform to reality and causes difficulty in numerical computation.

5.2.4.4 Three-parameter power model

Kishi and Chen (1987a, 1987b) proposed a three-parameter power model as

$$S_c = K_i \left[1 - \left(\frac{M}{M_u} \right)^n \right]^{(n+1)/n} \quad (5.7)$$

in which, the parameters K_i , M_u and n are the initial stiffness, the ultimate moment capacity and the shape parameter of the $M - \phi_c$ curve respectively.

The power model can always produce positive connection stiffness and has a better numerical performance compared with the polynomial model. Meanwhile, this model is convenient to engineers for practical design due to the reduced number of parameters obtained from experiments. However, it sometimes may have less accuracy in predicting the stiffness of joint connections when remaining elastic.

5.3 Modeling of connection behavior under cyclic loading

5.3.1 $M-\phi$ approach

5.3.1.1 Connection models without degradation

The concept of the constitutive relationship between stress and strain can be extended to generate new $M-\phi$ models. Taking the Giuffr -Menegotto-Pinto hysteretic material model (1983) for example, it is a uni-axial material with isotropic strain hardening for steel material. The smooth transition of stiffness is widely adopted in nonlinear analysis. When rewriting this relationship for moment and rotation, the transitional portion from elastic to plastic state is as given in Equation (5.8) below.

$$M^* = b\varepsilon^* + \frac{(1-b)\phi^*}{(1+\phi^{*R})^{\frac{1}{R}}} \quad (5.8)$$

in which, M^* and ϕ^* are the normalized moment and rotation respectively; and b is the strain hardening ratio between the post-yield tangent and initial elastic tangent;

R is the parameter to adjust the shape of the transition curve and should be determined by the parameters R_0 , a_1 and a_2 during the cyclic loading to reflect the Bauschinger effect. More details regarding this model can be found in Filippou *et al.* (1983).

This model is capable of modeling the joint behavior without strength degradation. Isotropic hardening, compression hardening, and tension hardening can be achieved by setting suitable hardening parameters. Meanwhile, the transition shape can be adjusted according to the joint connection types. This model can be used in the dynamic analysis if its parameters are verified by experiments.

5.3.1.2 Connection models with degradation

Pinching-type responses generally appear with the bond-slip phenomenon, which was originally proposed for reinforced concrete frames. Though it is developed for modeling stress-strain history by Lowes *et al.* (2003), it was virtually a one-dimensional hysteretic load-deformation relationship, which can be used to model joint connections with degradation. It is composed of three components: the response envelope, unload-reload paths, and hysteric damage rules. They are illustrated in Fig. 5.21. The most important feature of this model is the stiffness degradation. It provides three options to simulate hysteretic damage: unloading stiffness degradation, reloading stiffness degradation and strength degradation. For unloading stiffness degradation, the unloading stiffness k_i is defined as

$$k_i = k_0(1 - \delta k_i) \quad (5.9)$$

where k_0 is the initial unloading stiffness without damage; δk_i is the current damage index of stiffness which can be determined by equation (5.12).

Reloading stiffness degradation is implemented by increasing the maximum historic deformation as,

$$d_{max,i} = d_{max,0}(1 + \delta d_i) \quad (5.10)$$

in which, $d_{max,0}$ is the initial maximum deformation; $d_{max,i}$ is the current maximum deformation after damage; and δd_i is defined by the same way as δk_i .

The strength degradation is defined as,

$$f_{max,i} = f_{max,0}(1 - \delta f_i) \quad (5.11)$$

where $f_{max,0}$ is the initial maximum strength; $f_{max,i}$ is the maximum strength after damage; and δf_i is calculated as δk_i .

The damage indexes such as δk_i , δd_i and δf_i are defined as,

$$\delta k_i = (gK1(d_{max})^{gK3} + gK2 \left(\frac{E_i}{E_{monotonic}} \right)^{gK4}) \leq 1.0 \quad (5.12)$$

with

$$d_{max} = \max \left[\frac{d_{max,i}}{def_{max}}, \frac{d_{min,i}}{def_{min}} \right] \quad (5.13)$$

$$E_i = \int_{load\ history} dE$$

where $gK1$, $gK2$, $gK3$ and $gK4$ are parameters fitting the damage rule to the test data; E is hysteretic energy; E_i is cumulative energy; and $E_{monotonic}$ is failure energy under monotonic loading. def_{max} and def_{min} are the positive and negative deformations respectively; $d_{max,i}$ and $d_{min,i}$ are the maximum and minimum historic deformation respectively. The damage caused by the historical displacement is the damage type called as “cycle”, and “energy” for that is caused by energy accumulation.

This model provides three optional types for modeling degradation, which can be applied for the modeling of RC or composite joint connections after calibration of the model.

5.3.2 *P-My-Mz* approach

All models described in the previous sections are one-dimensional models, ignoring the coupling effect of the axial force and the bending moments. The *P-My-Mz* approach provides a smooth transition from ideally elastic to plastic states of semi-rigid connections. Generally, this method is implemented by integration of fibers along cross-sections as shown in Fig. 4.2. Each fiber can be assigned a one-dimensional stress-strain model according to the properties of joint connections. When updated by the axial strain and curvature about the y- and z- axes, the axial force and bending moments can be integrated along the cross section. Then, the stiffness of connections is determined by the following equation when becoming semi-rigid.

$$k_{i,j} = k_{i,0} \left(\frac{|f_i^p - f_{i,j}|}{|f_{i,j} - f_i^e|} \right) \quad (5.14)$$

in which, $k_{i,0}$ is the initial stiffness of DOF i ; $k_{i,j}$ is the stiffness after the update. $f_{i,j}$ is the input force; f_i^e and f_i^p are the yield force and ultimate plastic force about DOF i of the joint connections. And $f_{i,j}$ ranges from f_i^e to f_i^p . When $f_{i,j}$ is less than f_i^e , the connection remains rigid. If $f_{i,j}$ is larger than f_i^e , the connection becomes semi-rigid.

The *P-My-Mz* approach based on the fiber section concept provides a new solution to consider the coupling effect of the section forces. If the stress-strain relationship of each fiber of the cross-sections is the hysteric type, the *P-My-Mz* model of joint connections is workable for dynamic analysis.

5.4 Flexibility-based beam-column element accounting for semi-rigid joints

Ihaddoudène *et al.* (2017) proposed a 2D beam-column element derived from the stability function which has high accuracy for modeling one member with one element. A joint model was directly incorporated into the beam-column element. However, this 2D element can only be used in plane steel frames. It should be also noted that the coupling effect between the axial force and the bending moment is not considered. Thus, the semi-rigid connection was set in the beams almost without axial force in all calibrated examples in their work. The beam-column element proposed by them shows many limitations and therefore it cannot be used in practical design.

The novelty of the proposed flexibility-based beam-column element with initial geometric imperfection in Chapter 3 (hereafter called FBMI) with a semi-rigid connection not only reserves all excellent quality as described in the previous chapters, but can also consider the effects of the joint flexibility which is an indispensable factor in the modern direct analysis and design. The coupling effect between the axial force and the bending moment, which has been generally ignored in previous studies, is implicitly included in the proposed element. As demonstrated in previous chapter, only one element is required over the length of the element to model the member. This is a marked contribution and the proposed method shows many advantages in terms of simplicity and accuracy in solving practical problems with significant enhancement of computational effort.

It is evident that the gusset plate connection linking a brace and its framing elements exhibits semi-rigid behavior which is different from the conventional fully rigid and ideally pinned behaviors (Hsiao *et al.*, 2012; Uriz *et al.*, 2008; Yoo *et al.*, 2008). The

required strength, stiffness and ductility should be provided when designing a semi-rigid connection. The moment versus rotation ($M - \theta$) curve of a connection representing its semi-rigid behavior can be determined by experimental test, sophisticated finite element analysis or design codes based on an analytical model.

It is a common practice for a joint to be modeled as dimensionless with its location at the intersection of the element centerlines. Furthermore, a rotational spring element satisfying the $M - \theta$ relationship can be inserted into each end of the beam-column element to model the connection behavior. The joint equilibrium condition can be simply expressed as,

$$M_{ik}^b + M_{ik}^c = 0 \quad (5.15)$$

in which M_{ik}^b and M_{ik}^c are the moments at the ends of the members and connection respectively; the subscript i stands for the first or the second end of the brace; the subscript k represents the y- or z- axis, as seen in Fig. 5.3. The internal node is connected to the beam-column element while the external node is associated with the global node.

The connection stiffness S_{ik}^c is related to relative rotations at the connection spring ends by

$$S_{ik}^c = \frac{M_{ik}^b}{(\theta_{ik}^b - \theta_{ik}^c)} = \frac{M_{ik}^c}{(\theta_{ik}^c - \theta_{ik}^b)} \quad (5.16)$$

where θ_{ik}^b and θ_{ik}^c are the conjugate rotations for the moments M_{ik}^b and M_{ik}^c respectively (see Fig. 5.3). Rewriting Equation (5.16) in an incremental form using matrix format, the spring stiffness matrix will be written as

$$\begin{bmatrix} S_{ik}^c & -S_{ik}^c \\ -S_{ik}^c & S_{ik}^c \end{bmatrix} \begin{bmatrix} \Delta\theta_{ik}^b \\ \Delta\theta_{ik}^c \end{bmatrix} = \begin{bmatrix} \Delta M_{ik}^b \\ \Delta M_{ik}^c \end{bmatrix} \quad (5.17)$$

A typical elemental bending stiffness matrix can be expressed as

$$\begin{bmatrix} k_{11} & k_{12} & k_{13} \\ k_{21} & k_{22} & k_{23} \\ k_{31} & k_{32} & k_{33} \end{bmatrix} \begin{bmatrix} \Delta\varepsilon \\ \Delta\theta_{ik}^b \\ \Delta\theta_{jk}^b \end{bmatrix} = \begin{bmatrix} \Delta N \\ \Delta M_{ik}^b \\ \Delta M_{jk}^b \end{bmatrix} \quad (5.18)$$

in which k_{ij} is the stiffness coefficient associated with the axial force and the bending moments about one of the principal axes of the element FBMI given in Equation (3.55). Therefore, a hybrid element can be formed by adding the connection stiffness at two ends to the bending part of FBMI as

$$\begin{bmatrix} k_{11} & 0 & k_{12} & k_{13} & 0 \\ 0 & S_{ik}^c & -S_{ik}^c & 0 & 0 \\ k_{21} & -S_{ik}^c & S_{ik}^c + k_{22} & k_{23} & 0 \\ k_{31} & 0 & k_{32} & S_{jk}^c + k_{33} & -S_{jk}^c \\ 0 & 0 & 0 & -S_{jk}^c & S_{jk}^c \end{bmatrix} \begin{bmatrix} \Delta u \\ \Delta\theta_{ik}^c \\ \Delta\theta_{ik}^b \\ \Delta\theta_{jk}^b \\ \Delta\theta_{jk}^c \end{bmatrix} = \begin{bmatrix} \Delta N \\ \Delta M_{ik}^c \\ \Delta M_{ik}^b \\ \Delta M_{jk}^b \\ \Delta M_{jk}^c \end{bmatrix} \quad (5.19)$$

in which the subscripts i and j refers to nodes i and j respectively; the subscript k refers to the y - or z -axis. To eliminate internal degrees of freedom due to the connection spring, the standard static condensation procedure in the finite element textbook should be adopted. Finally, the hybrid element's stiffness expression with a pair of springs at both ends about one of the principal axes can be written as

$$[k_c][\Delta D_c] = [\Delta P_c] \quad (5.20)$$

in which

$$[\Delta D_c] = [\Delta u \quad \Delta\theta_{ik}^c \quad \Delta\theta_{jk}^c]^T, \quad [\Delta P_c] = [\Delta N \quad \Delta M_{ik}^c \quad \Delta M_{jk}^c]^T \quad (5.21)$$

$$[k_c]$$

$$= \begin{bmatrix} k_{11} & 0 & 0 \\ 0 & S_{ik}^c & 0 \\ 0 & 0 & S_{jk}^c \end{bmatrix} \quad (5.22)$$

$$+ \begin{bmatrix} k_{12} & k_{13} \\ -S_{ik}^c & 0 \\ 0 & -S_{jk}^c \end{bmatrix} \begin{bmatrix} S_{ik}^c + k_{22} & k_{23} \\ k_{32} & S_{jk}^c + k_{33} \end{bmatrix}^{-1} \begin{bmatrix} k_{21} & -S_{ik}^c & 0 \\ k_{32} & 0 & -S_{jk}^c \end{bmatrix}$$

where S_{ik}^c and S_{jk}^c are the connection stiffness values at nodes i and j , respectively.

Specially, when the spring stiffness S^c is zero, it means that the corresponding end

is an ideally pinned end; when the spring stiffness S^c is infinite, it means that the corresponding end is a fully rigid end. For the semi-rigid case, the spring stiffness S^c can be determined by the given $M-\theta$ function from the experimental test, continuum finite element analysis and so on. The complete stiffness matrix \mathbf{K}_c considering both principal axes can be simply expanded from Equation (5.22) and is not shown here.

It is worth emphasizing that the coupling effect of the axial force and bending moments, which was generally overlooked in previous research studies, has been considered in Equation (5.22). In previous studies, the semi-rigid connections were mainly applied at the beam ends dominated by the bending moment so that the influence of the axial force on the connection can be ignored. However, some members, such as the braces in SCBFs, undergo considerably large axial forces and dissipate energy through tensile yielding, buckling and post-buckling behaviors. In this study, the member stiffness coefficients k_{ij} ($i = 1, j = 2, 3; j = 1, i = 2, 3;$) due to bending moments may be not be zero as in previous research studies. This means that their interaction can be considered at the element level. This proposed stiffness expression in Equation (5.22) can be applied not only in the connections of braces but also in those of beams and columns if the associated connections cannot be simply classified as pinned or rigid.

5.5 Numerical examples

To validate the proposed approach described in this chapter, several static and dynamic examples, which have been widely studied by other scholars, will be analyzed by the proposed element FBMI considering joint flexibility. In addition, a new example will

be introduced to demonstrate the influence of joint stiffness on the stability of the entire structure.

5.5.1 Non-sway frame under static loads

The structural layout of the non-sway frame steel frame as shown in Fig. 5.4 was originally studied by Mageirou *et al.* (2006). In Fig. 5.4(a), the lower of the column is pinned and the upper is connected with a semi-rigid joint. The right joint of the beam is also fixed. The length of a column is 10 m, and the EI and EA are $9.0699e^4$ kN*m² and $1.2726e^6$ kN respectively. The length of the beam is 20 m, and the EI and EA are $4.8573e^4$ kN*m² and $8.9649e^5$ kN respectively. The stiffness of the joint connecting a beam and column is assumed to be linear with $k_l = 150$ kN*m/rad. This example is designed to explore the influence of the semi-rigid connection on column stability. Therefore, the only difference between Model B and Model C as shown in Fig. 5.4(b) and Fig. 5.4(c) is the right boundary condition of a beam. The stiffness of the right connection is 500 kN*m/rad in Model 2. All connections of the beam in Model 3 are rigid. Whether it will affect the critical loading will be analyzed by comparing the results obtained from two cases. All members are modeled using the one-member-one-element strategy by the proposed method.

Table 5-1 shows the critical load for Model A and Model B from the prediction of the proposed method, as well as that from Mageirou *et al.* (2006). From the table, the proposed method obtains similar results. It is worth noting that F.E.M-MS-C-NASTRAN used 3D solid elements to model this simple frame. Accurate results can be produced, but it requires huge computer time, which is hard to apply in practical design. In contrast, the proposed method can obtain accurate results at the same level with lower computational cost.

Fig. 5.5 shows the curves of applied force vs. displacements about the top point of a column. From the figure, the end condition of the right joint of a beam has less effect on the ultimate bearing capacity of the frame. However, the joint flexibility between a beam and column makes a large difference in the frame capacity. The ultimate load of a rigid connection is 10377 kN, which is improved 13% compared with a semi-rigid connection. Thus, it may lead to an overestimated design if assuming the connections between beams and columns are assumed to be rigid in this situation.

5.5.2 Sway and non-sway frame subjected to static loads

Fig. 5.6(a) and (b) show a one-story non-sway frame and a one-story sway frame, which have been studied by Mageirou *et al.* (2006) and Ihaddoudène *et al.* (2017) respectively. In both models, the length of a beam is 20 m, and the length of a column is 10 m. The section of all columns is HEB360 with a moment of inertia of $4.319 \times 10^{-4} \text{ m}^4$. The section of all beams is IPE400 with a moment of inertia of $2.313 \times 10^{-4} \text{ m}^4$. The bottom end conditions of all columns are considered to be pinned. The joint connections between beams and columns are assumed to be semi-rigid with a linear stiffness of 150 kN*m. In model B, there is a horizontal support on the right node of the beam. The Young's modulus is $2.1 \times 10^8 \text{ kN/m}^2$. All members are modeled using the one-member-one-element strategy by the proposed method.

Table 5-2 shows the critical load for Model A and Model B from the prediction of the proposed method, as well as from Ihaddoudène *et al.* (2017). The beam-column element allowing for joint flexibility proposed by this study makes a similar prediction of ultimate loading capacity as the refined modeling with F.E.M-MSC-NASTRAN. Nevertheless, the proposed method can save much modeling time as well as computational time.

Fig. 5.7(a) and (b) show the applied force vs. displacement curves. From the figure, the lateral support largely improves the critical loading of the frame. Though the stiffness of connections can provide a lateral resisting system like moment frame, its contribution is limited. The sway frame becomes unstable when the applied force reaches 12 kN. Thus, it is important to assume the boundary conditions to determine whether the frame is a sway or non-sway frame.

5.5.3 Multistory sway and non-sway frame under static loads

In this example, three-story sway and non-sway frames will be adopted to study the influence of joint flexibility on multistory buildings, as shown in Fig. 5.8(a) and Fig. 5.8(b). The cross-section of all columns is HEB360 with moment of inertia of $4.319 \times 10^{-4} \text{ m}^4$. The cross-section of all beams is IPE400 with a moment of inertia of $2.313 \times 10^{-4} \text{ m}^4$. The material of all members is made of steel with Young's modulus $E = 2.1 \times 10^8 \text{ kN/m}^2$. All end connections of beams are assumed to be semi-rigid with a linear stiffness of $150 \text{ kN}\cdot\text{m}$. Concentrated point loads are applied on each joint of beam-column connections. In the numerical model, the material is assumed to be elastic, and the one-element-per-member strategy is adopted. The displacement control method with a constant displacement increment of the monitoring node is used to find the nonlinear solution.

Table 5-3 shows the critical load for Model A and Model B from the prediction of the proposed method, as well as from Ihaddoudène *et al.* (2017). Compared with results from F.E.M-MS-C-NASTRAN, the beam-column element with joint flexibility proposed by this study makes a relatively accurate prediction of ultimate loading capacity with a relative error within 0.6%. Nevertheless, the proposed method can save much modeling time, as well as computational time.

Fig. 5.9(a) and (b) show the curves for applied force vs. horizontal displacement. The sway frame is more sensitive to stability, and it is unstable when the applied force reaches 5.5 kN. Meanwhile, the non-sway frame is more stable when the critical load is more than 3500 kN.

5.5.4 William's toggle frame with semi-rigid connection under static load

The layout and applied load of the William's toggle frame (1964) is shown in Fig. 5.10. This frame represents a typical roof structure. It has a special buckling mode, the snap-through buckling mode, and exhibits highly geometrical and material nonlinearity. It has attracted extensive attentions to explore its static behaviors. In this study, this frame will be explored by static analysis with different connection settings. All connections of the members are assumed to be rigid in Model 1 as shown in Fig. 5.10 (a). Model 2 assumes that the middle top connection is semi-rigid with linear connection stiffness, 6877.4 lb·in as shown in Fig. 5.10 (b). Two base joint connections of Model 3 are set as semi-rigid with linear connection stiffness, 6877.4 lb·in as shown in Fig. 5.10 (c). All joint connections are assumed to be semi-rigid with linear connection stiffness, 6877.4 lb·in as shown in Fig. 5.10 (d). For comparison, Model 5 and Model 6 are assumed to be pinned as shown in Fig. 5.10 (e) and Fig. 5.10 (f). All models are applied with a concentrated point load P at the middle top point.

5.5.5 William's toggle frame with semi-rigid connection under dynamic load

Fig. 5.13 shows the layout and pattern load of a planar frame, the famous William's toggle frame (1964). The last example has explored its static properties. In this example, this frame will be studied by dynamic analysis with different connection

settings. All connections of members are assumed to be rigid in Model 1 as shown in Fig. 5.13 (a). Model 2 assumes two base connections are semi-rigid with linear connection stiffness 687.74 lb·in as shown in Fig. 5.13 (b). Two base joint connections of Model 3 are set as pinned in Fig. 5.13 (c). All models are applied with a concentrated point load $F(t)$ at the middle top point. The density of all members is $2.54e^{-4}$ lb·sec²/in⁴. For models 1, 2 and 3, results from the proposed method agree with those from another scholar using several elements to model one member, as shown in Fig. 5.14(a)~(b). From the figures, the joint flexibility reduces the stiffness of the structural system and then increases the structural natural frequency. Meanwhile, the joint flexibility also boosts the vertical displacement under the dynamic loading. Therefore, it is necessary to consider the joint flexibility in the seismic design of frame structures.

5.5.6 Buckling and vibration analysis of one-story frame with semi-rigid joints

In this example, a planar frame with semi-rigid joints will be studied with buckling and vibration analysis. Its layout is shown in Fig. 5.15. The section of all columns is 305x305x97 UC. The section of beams is 457x191x98 UB. The stiffness of beam-column connections varies from pinned to rigid to assess how the natural frequency of a frame varies against the joint stiffness. The half mass of the beams and columns is concentrated into the top points respectively. The mass factor is assumed to be 1 times, 5 times and 10 times to explore the influence of mass on the vibration behavior of the frame.

Fig. 5.16 (a) and (b) the natural frequency of the frame under connection stiffness and mass. From the figure, the natural frequency increases as the stiffness of the beam-column connections become rigid and decreases as the mass factor increases. In practice, the stiffness of connection types, such as extended end plate connections, the

flexible joint detail of angle web cleats and the flush end plate, varies between rigid and pinned. Therefore, it is necessary to consider joint flexibility when conducting vibration analysis.

5.5.7 Dynamic analysis of a one-story frame with semi-rigid connection

This example has the same layout as the last example, as shown in Fig. 5.17. Dynamic analysis is conducted to explore its dynamic properties. Sections of all members remain unchanged from the last example. All beam-column connections are assumed to be semi-rigid with linear stiffness, $1.17e^4$ kN*m. Dynamic horizontal loading, $F(t) = 300$ kN, is applied on the left top joint. To explore the influence of the second-order effect on the dynamic response, a constant vertical load, 0 kN, 1000 kN or 2000 kN, is applied on the top of columns.

The responses for the frame under different vertical loads are plotted in Fig. 5.18. From the figure, the responses of the frame vary greatly. The maximum deflections under the dynamic loads are different. The P- Δ effect produces a larger lateral drift. Meanwhile, it reduces the frame stiffness and thus the structural frequency.

5.5.8 A column with semi-rigid connection under dynamic load

Fig. 5.19 shows a column with only the vertical DOF being free. This example is provided on the OpenSees website (2009) to illustrate the properties of Pinching4Material. In this study, the column is modeled by the proposed element with a rigid material. The end connection between column and base is assumed to be semi-rigid on the axial DOF. The semi-rigid model, as described in section 5.3 is adopted. Fig. 5.20 shows a cyclic load history applied on the free node of the column.

Plotted on the Fig. 5.22 shows the responses of columns under different parameters settings of the semi-rigid model. Fig. 5.22 (a) shows the response of the column with no damage to the semi-rigid connection. The unloading stiffness degradation of the semi-rigid connection is shown in Fig. 5.22 (b). The stiffness of the joint connection degrades during the unloading process. Fig. 5.22 (c) and (d) shows the response with re-loading stiffness degradation and yielding strength degradation. Fig. 5.22 (e) and (f) shows two damage types: “Energy” and “Cycle”. This example illustrates that the proposed element with semi-rigid joints can be used to model the complex behavior of semi-rigid joint connections.

5.6 Concluding remarks

The mechanical characteristics of steel structures should consider the influence of joint flexibility. It can be concluded that the analytical approach of semi-rigid connections presented in this study can provide a reasonable representation of the flexibility behavior of different joint systems. Several meaningful conclusions are drawn:

- (1) A second-order beam-column element allowing the flexibility of joint connections is proposed.
- (2) The coupling effect between the axial force and the bending moment of joint connections is considered in the proposed element.
- (3) The flexibility of joint connections has a significant influence on the static and dynamic performance of structural systems.
- (4) The properties of joint flexibility can be assumed to be linear or nonlinear to model different connection types, which can be integrated into the proposed element and then applied in the practical design.

FIGURES

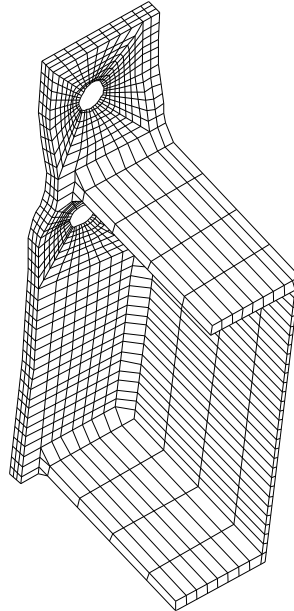


Fig. 5.1 Finite element model of the end-plate connection using solid elements

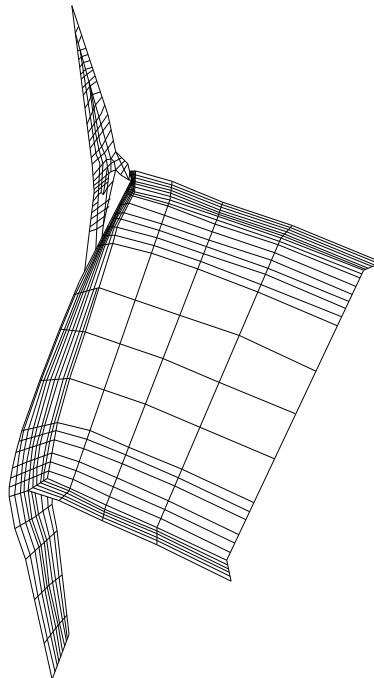


Fig. 5.2 Finite element model of the end-plate connection using shell elements

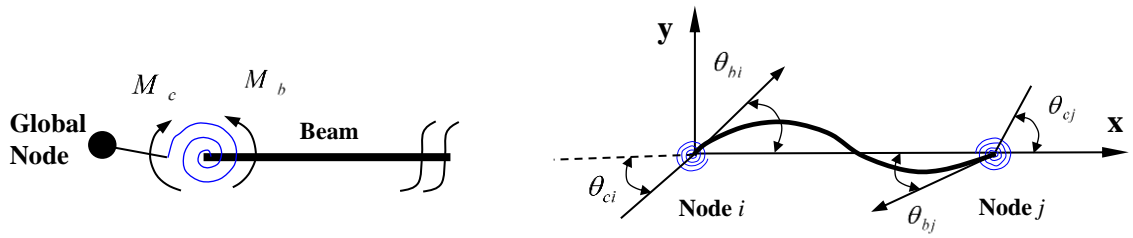
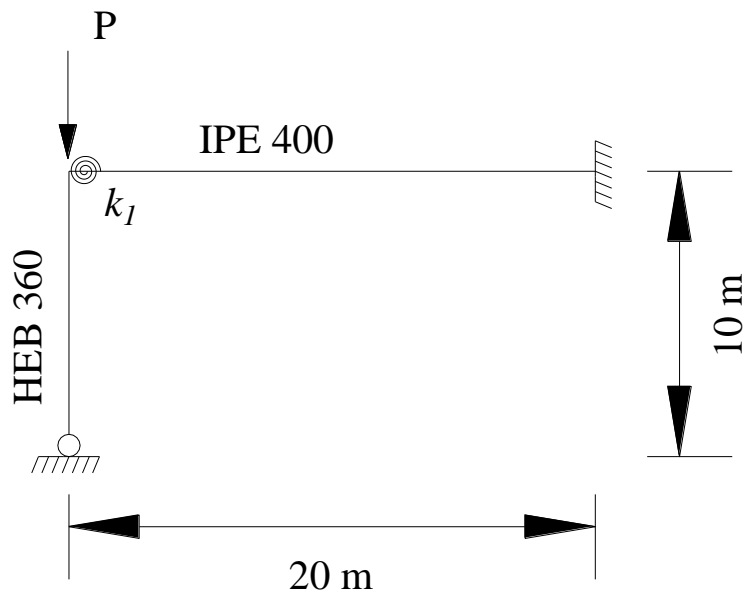
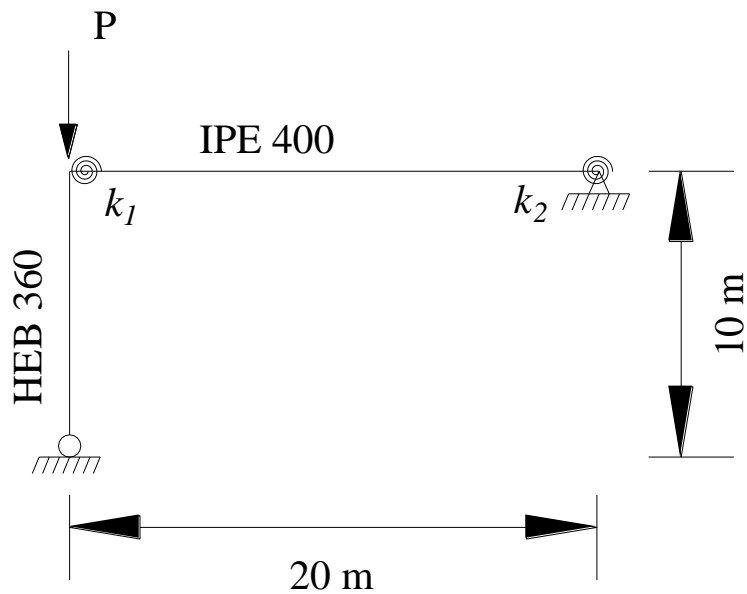


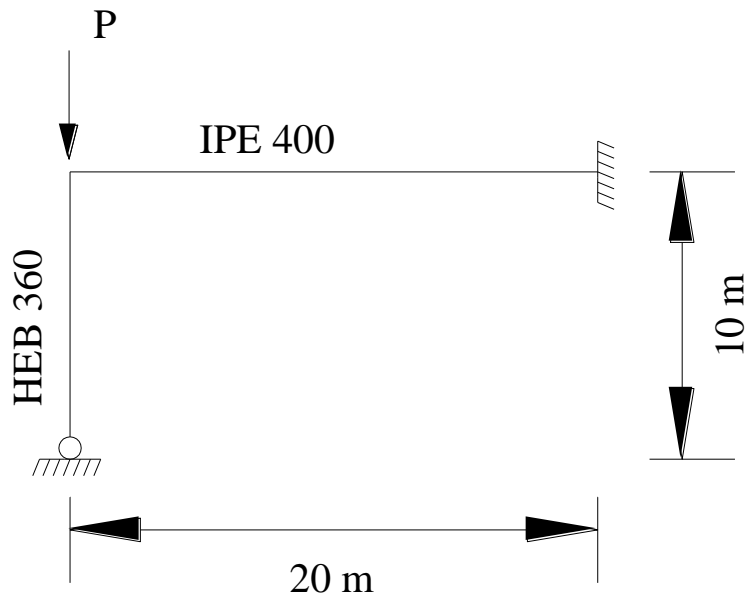
Fig. 5.3 Modeling of a semi-rigid jointed member



(a) Model A



(b) Model B



(c) Model C

Fig. 5.4 Layouts and load patterns of the frames

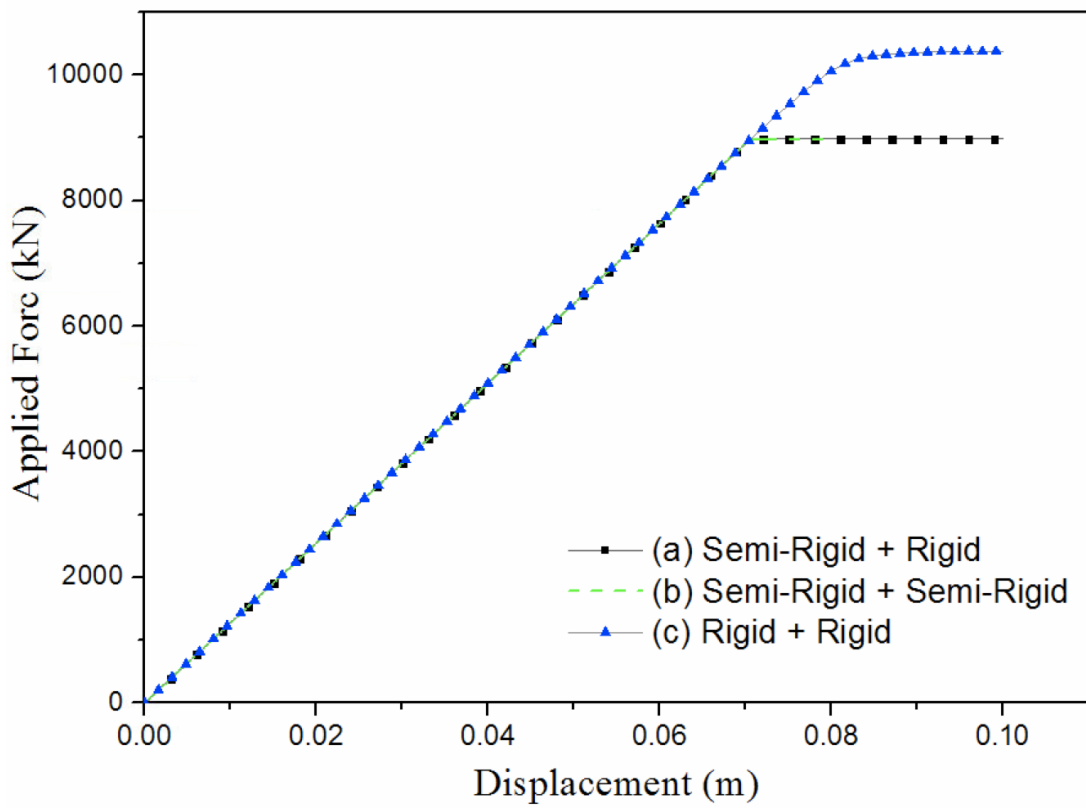
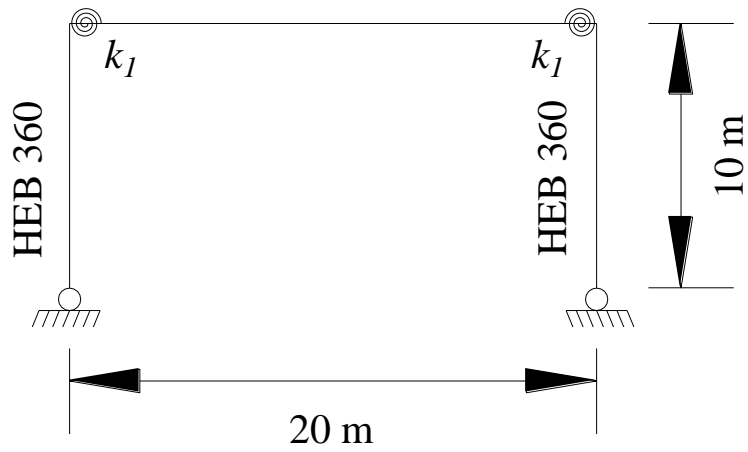
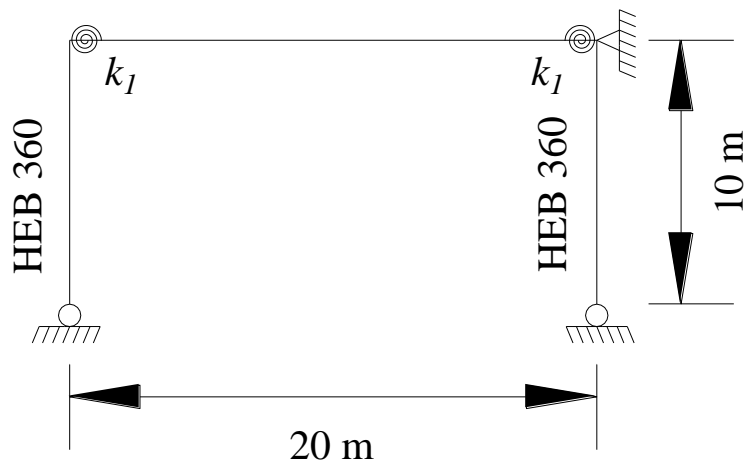


Fig. 5.5 Loading-deflection curves of models with various connection types

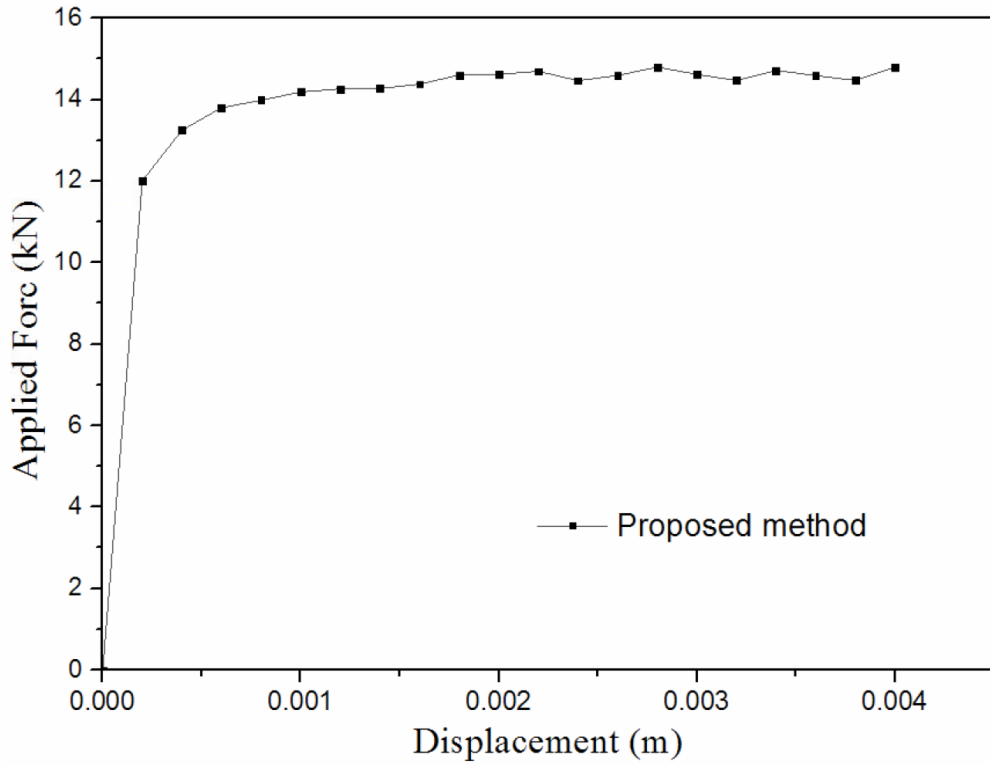


(a) Model A

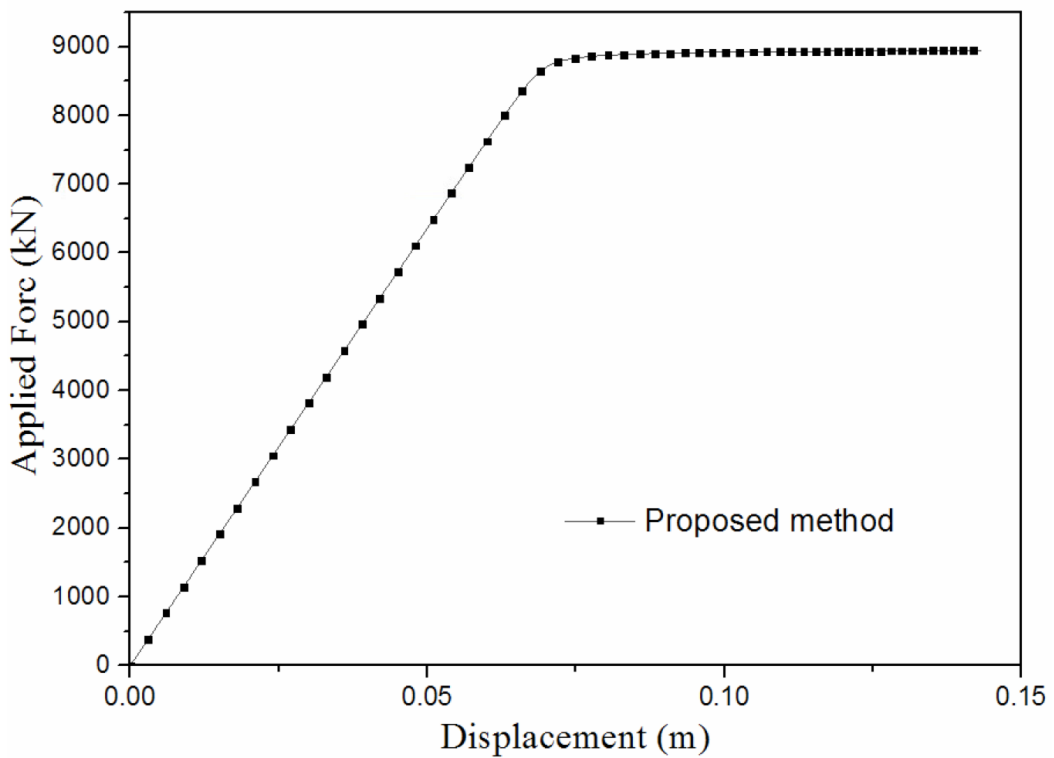


(b) Model B

Fig. 5.6 Layouts of sway and non-sway frames

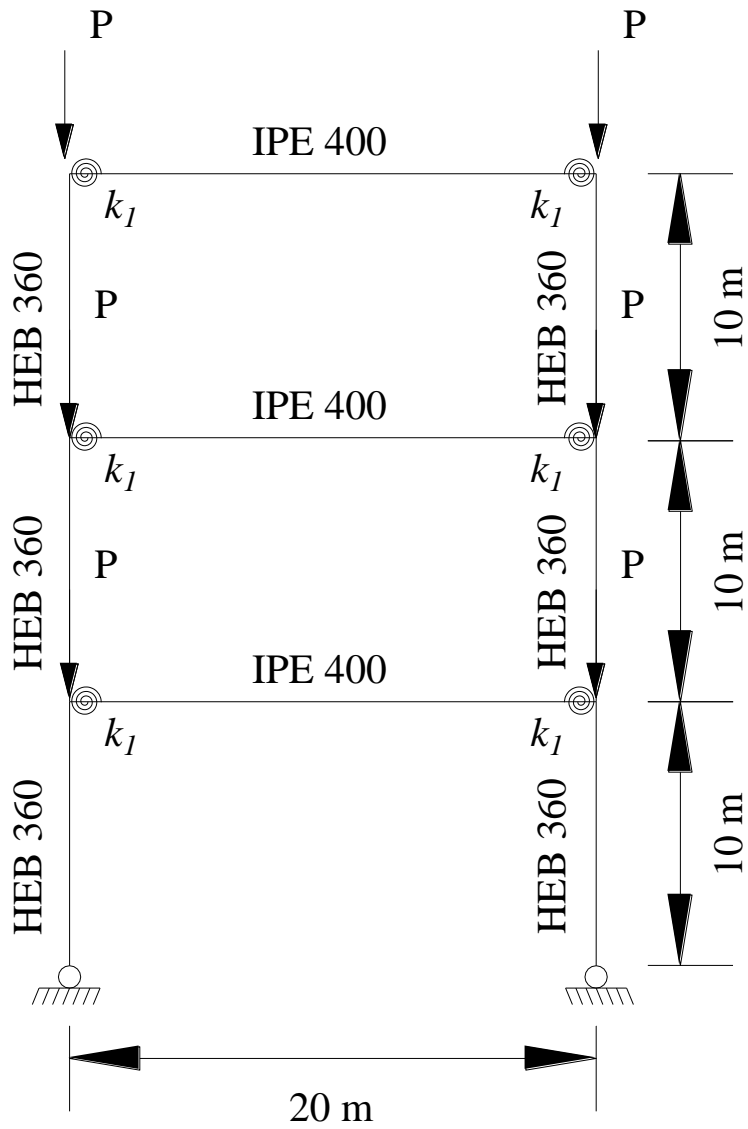


(a) Applied force vs. horizontal displacement for model A

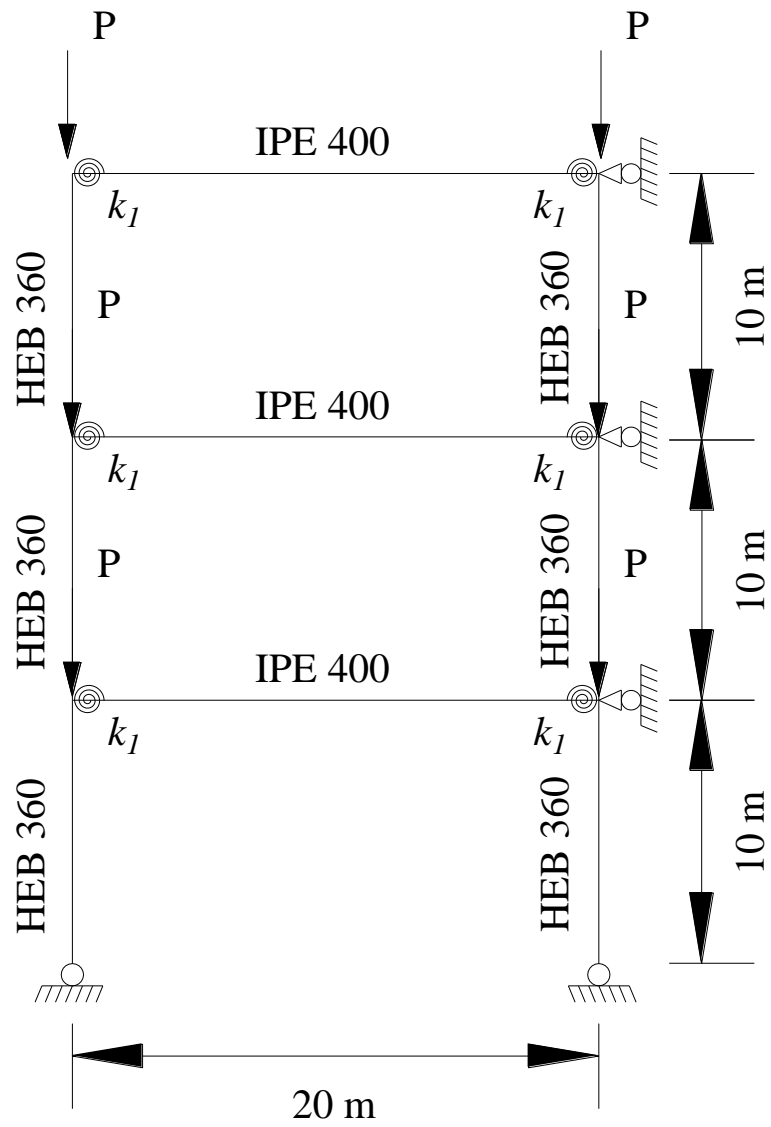


(b) Applied force vs. horizontal displacement for model B

Fig. 5.7 Applied force vs. horizontal displacement

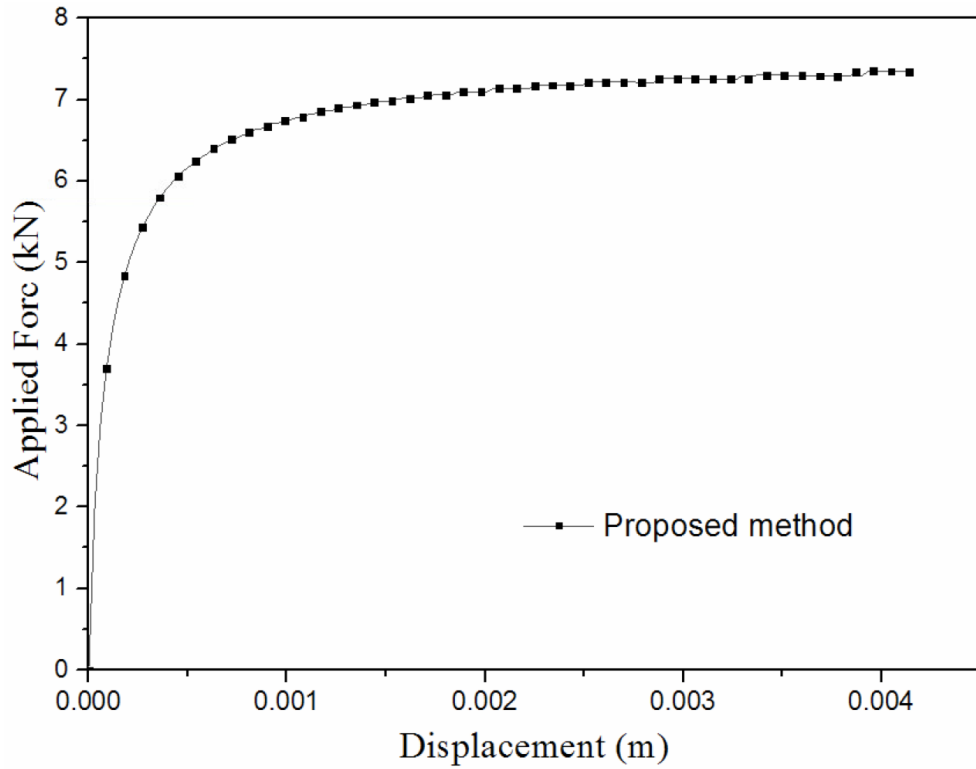


(a) Model A

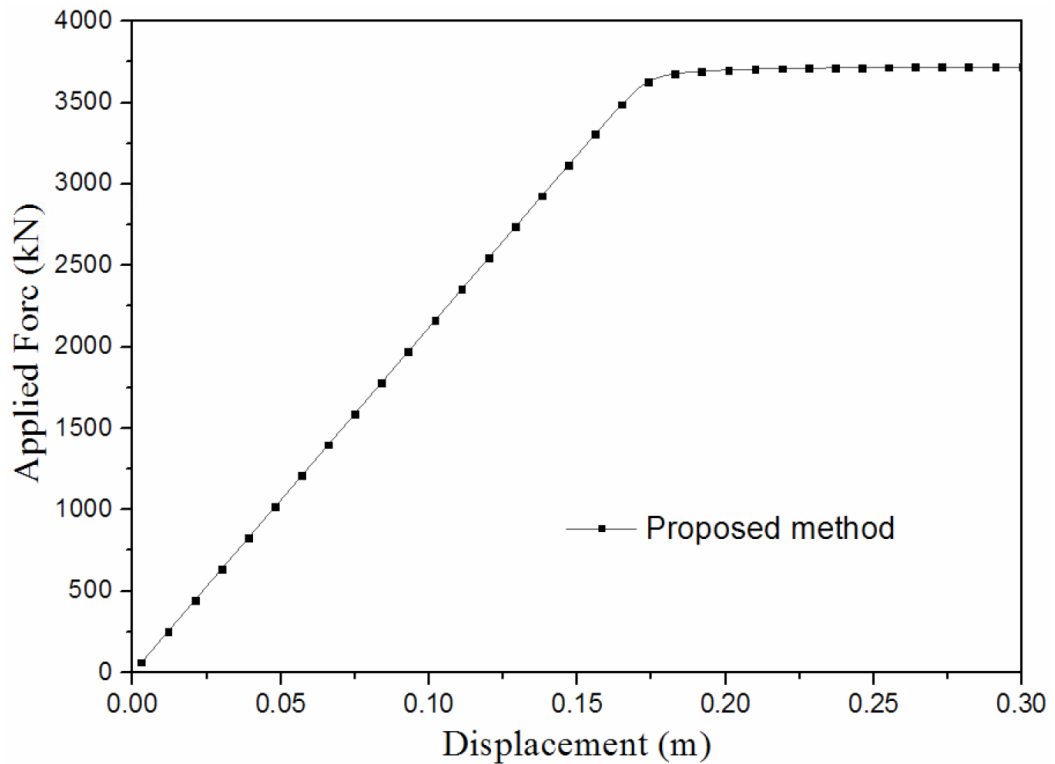


(b) Model B

Fig. 5.8 Layouts and load patterns of three-story sway frames

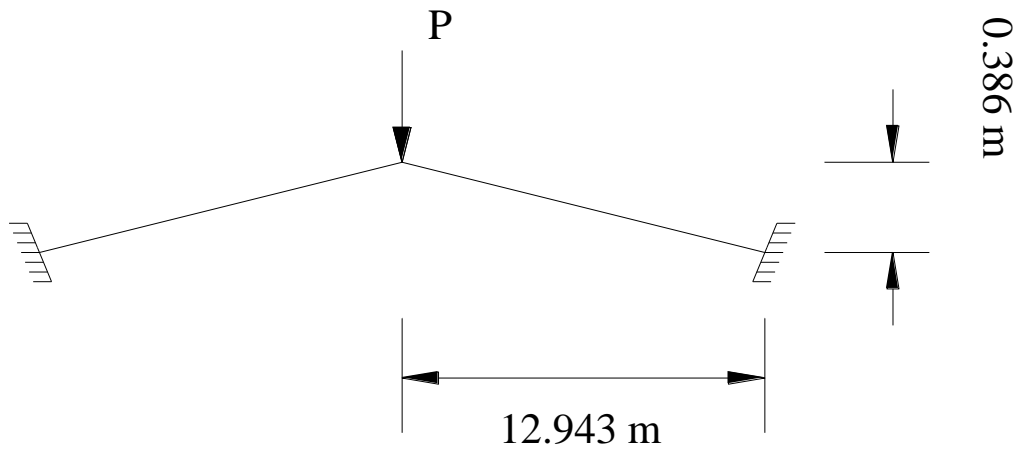


(a) Applied force vs. horizontal displacement for model A

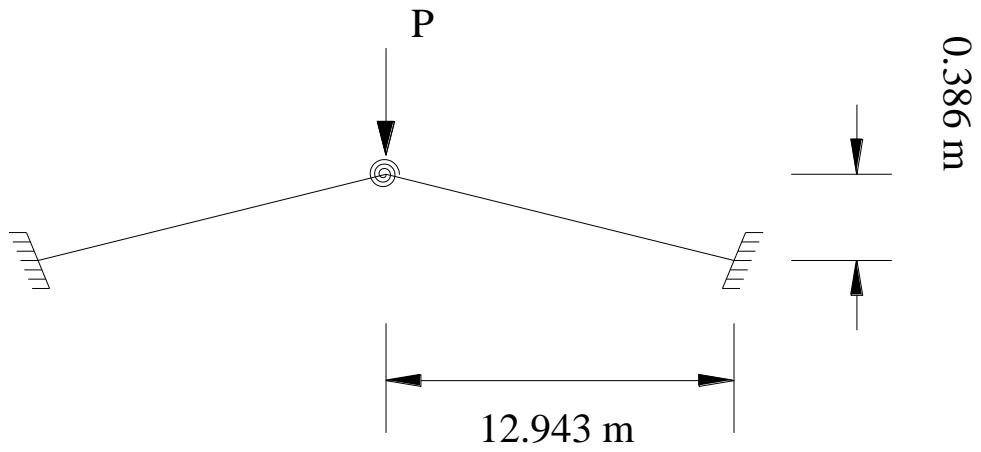


(b) Applied force vs. horizontal displacement for model B

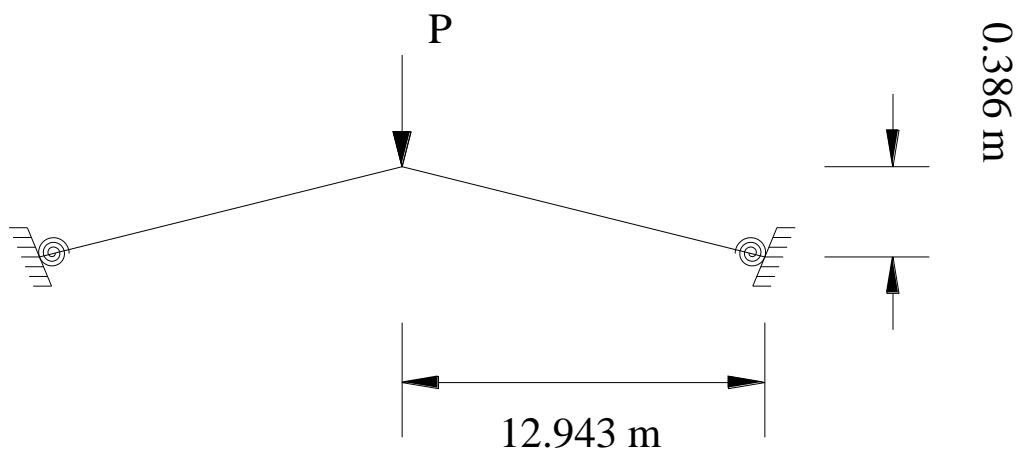
Fig. 5.9 Loading-deflection curves for models of three-story sway frames



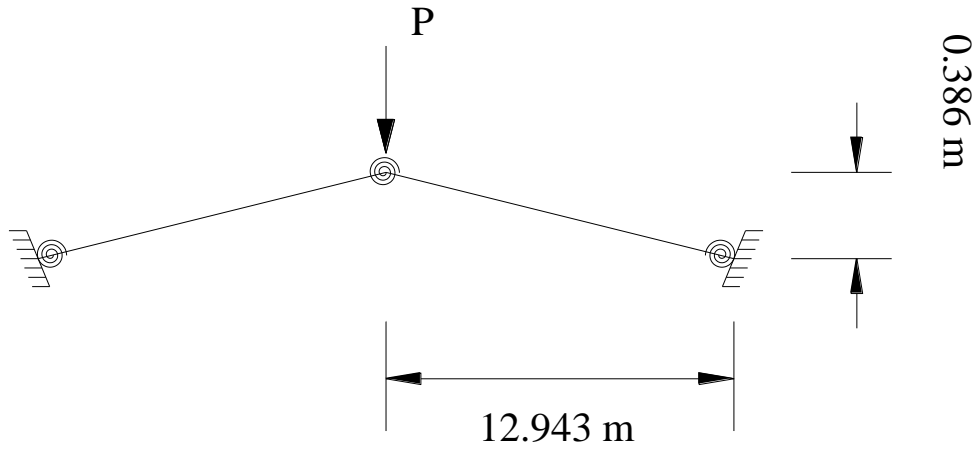
(a) Model 1



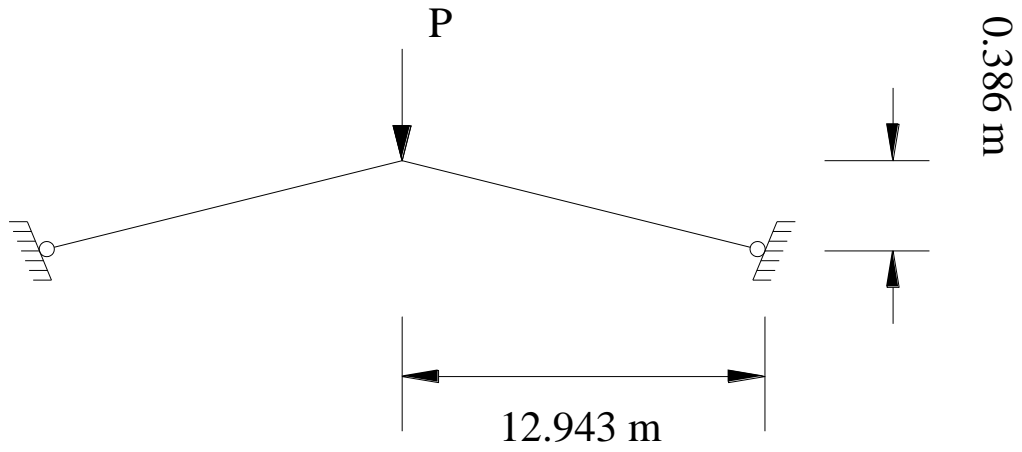
(b) Model 2



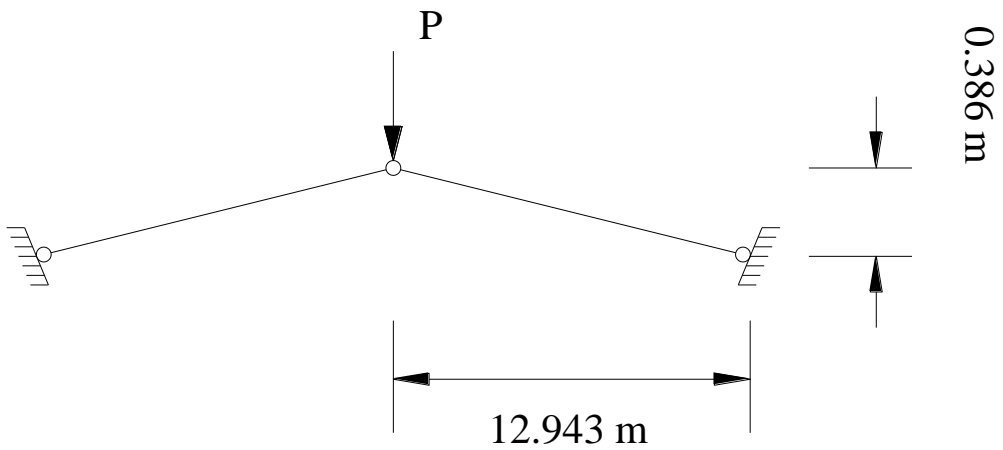
(c) Model 3



(d) Model 4

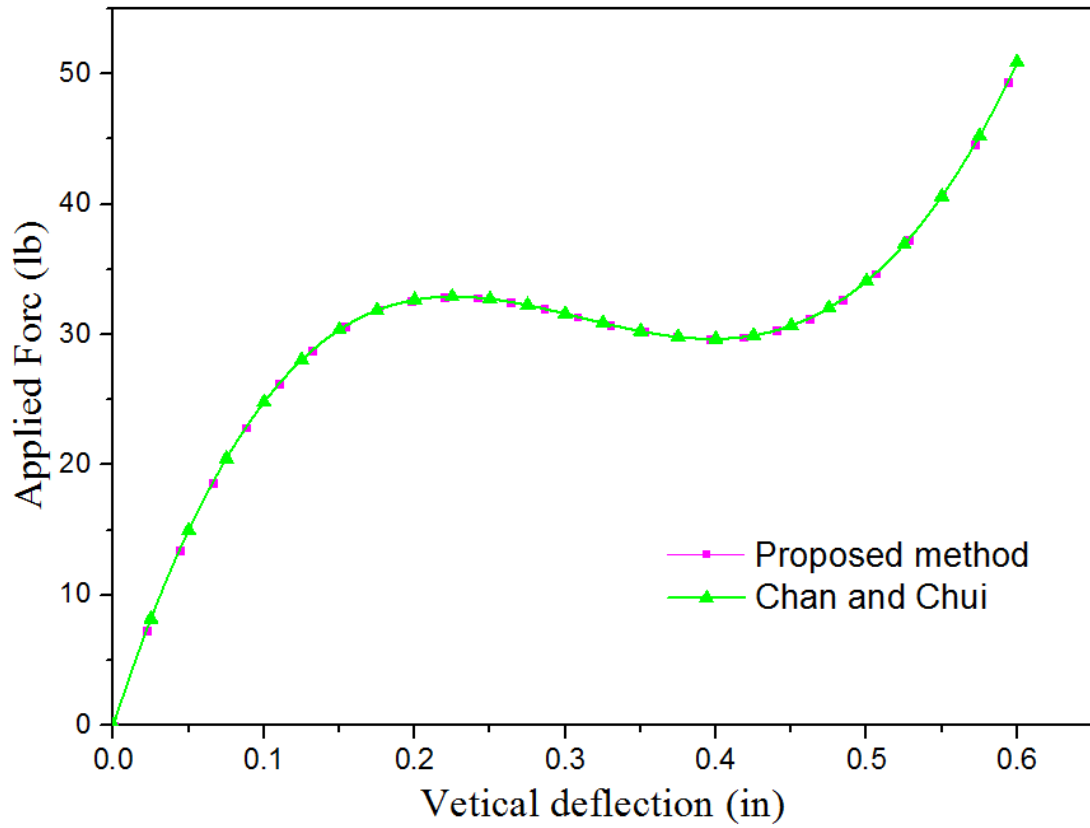


(e) Model 5

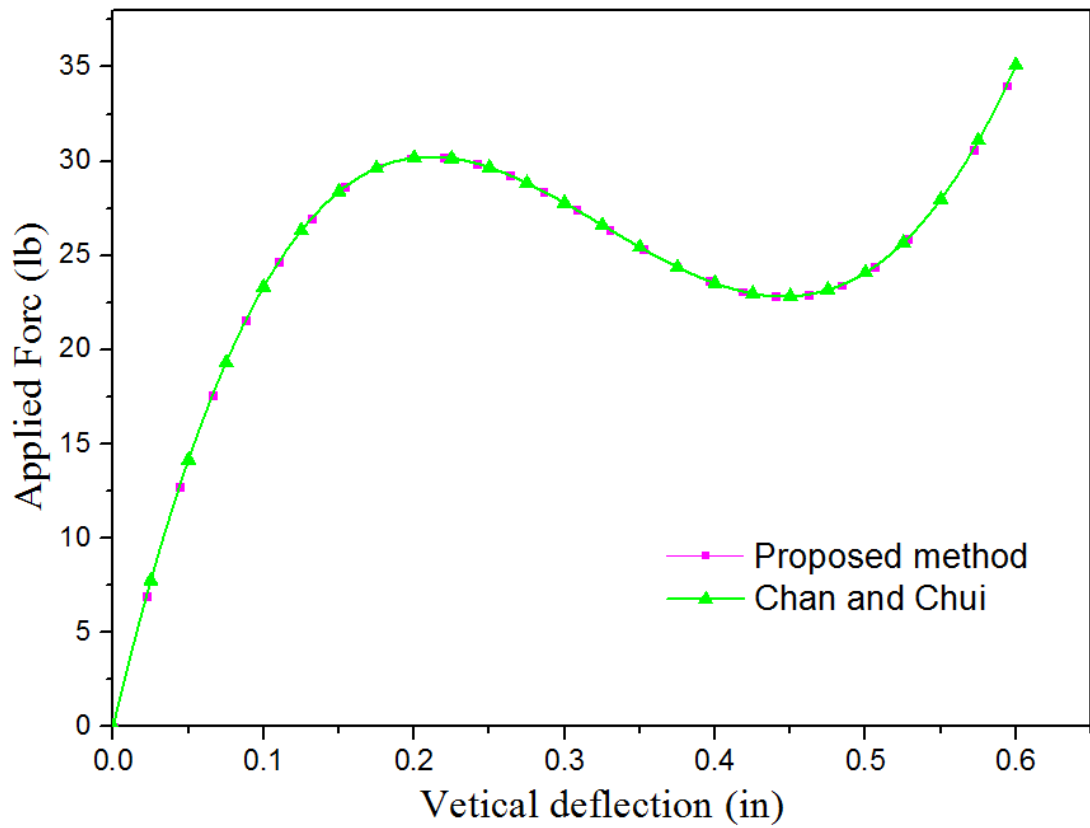


(f) Model 6

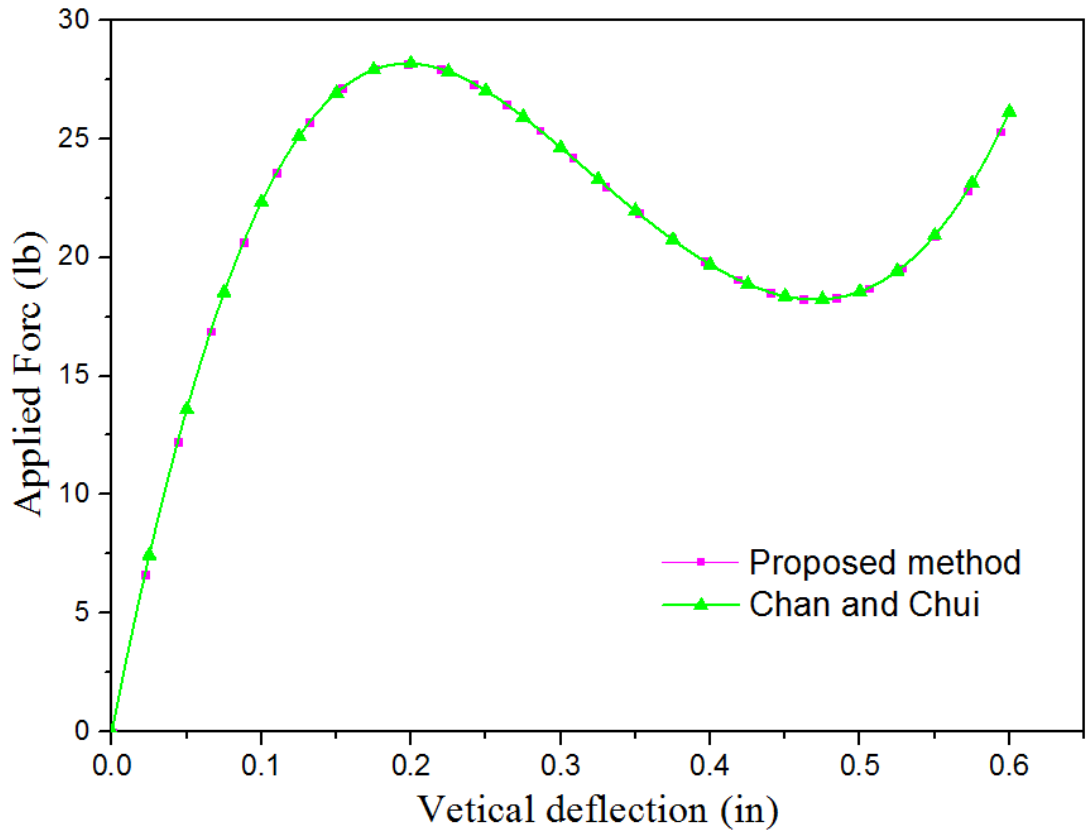
Fig. 5.10 Layouts and load patterns for William's toggle frame



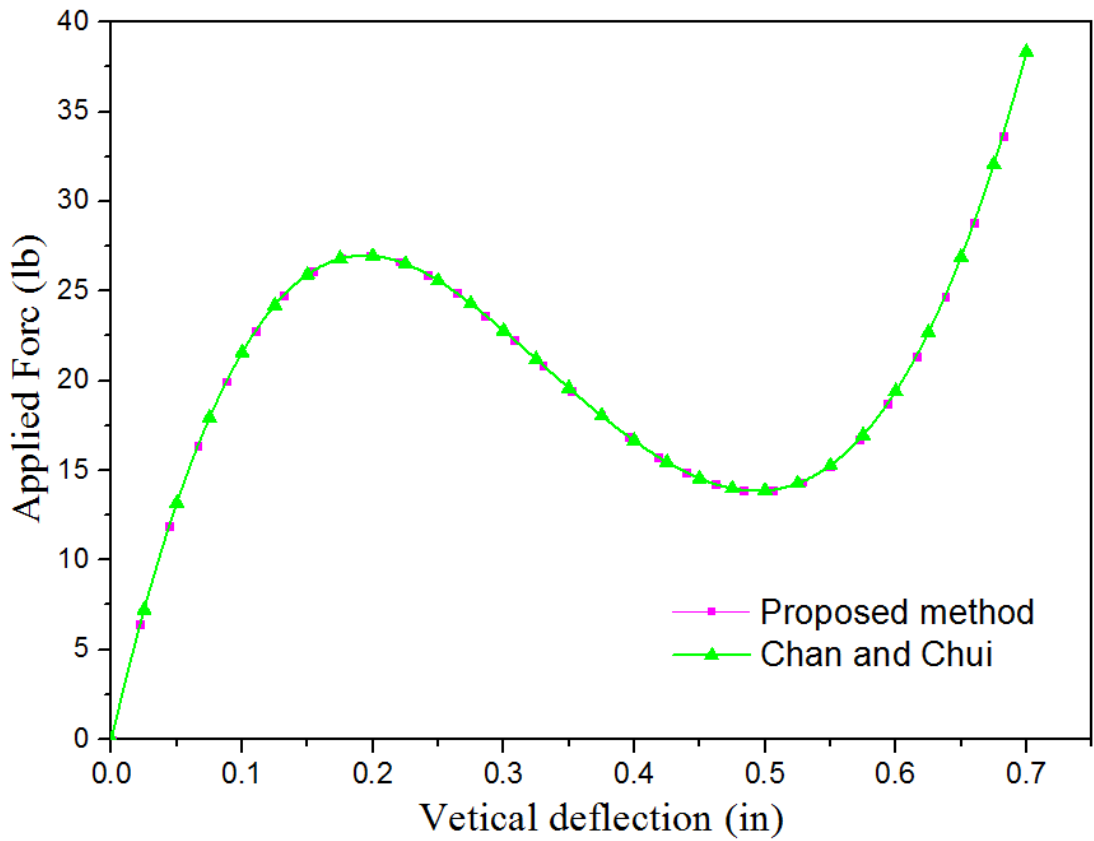
(a) Response for Model 1



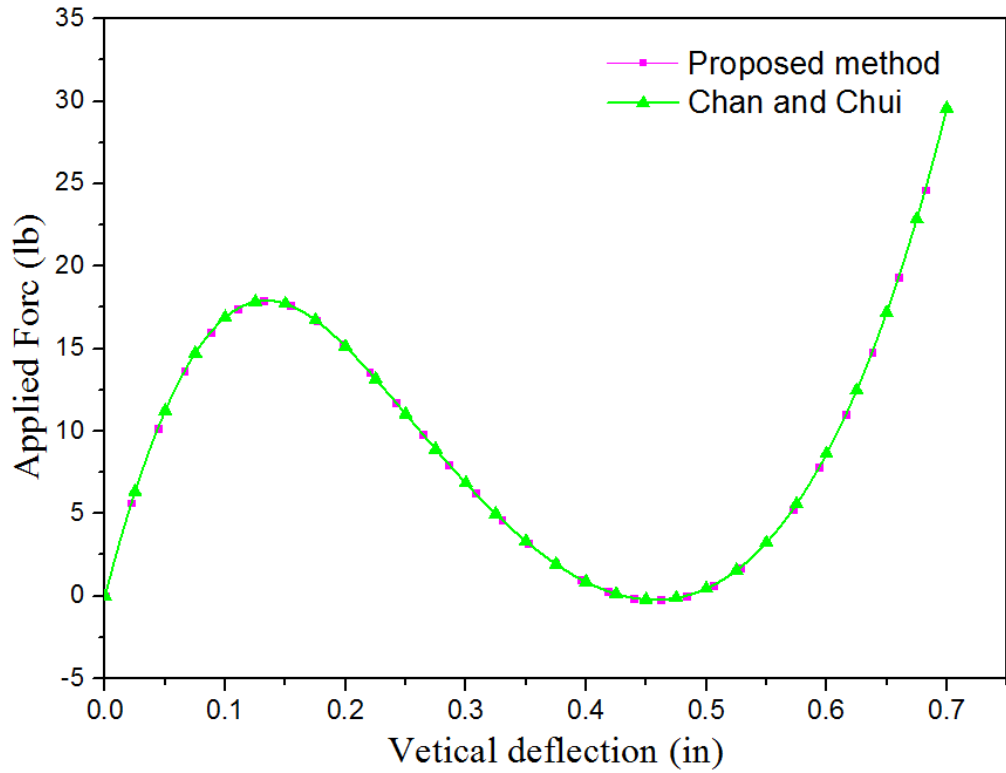
(b) Response for Model 2



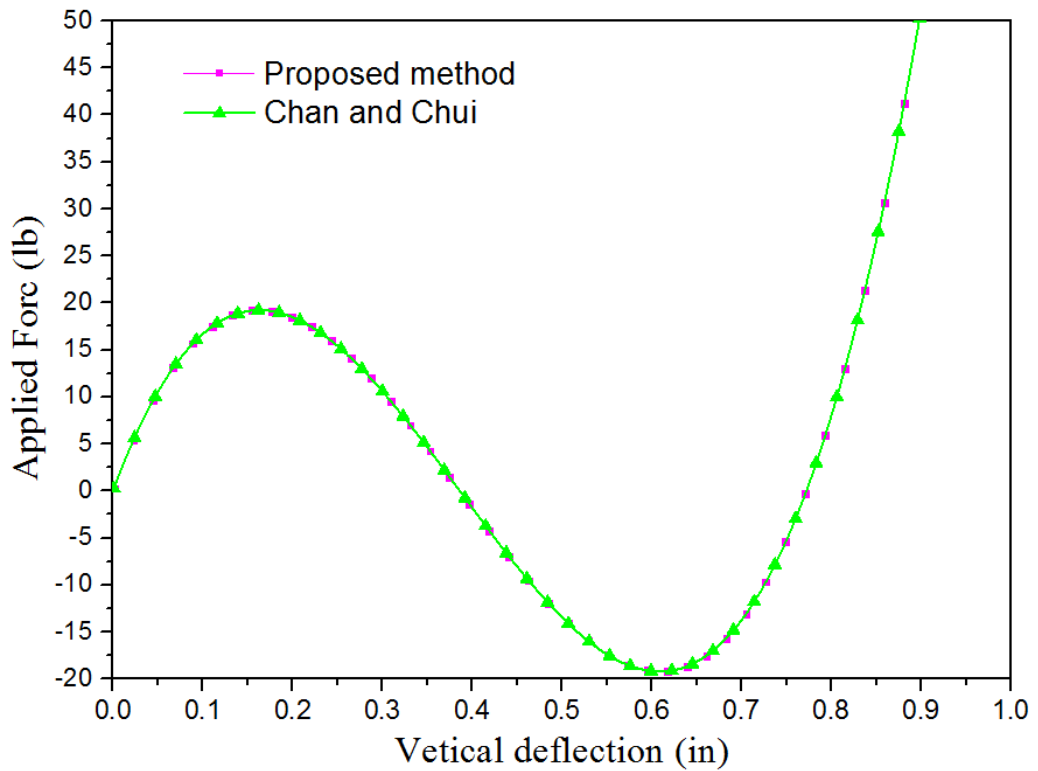
(c) Response for Model 3



(d) Response for Model 4



(e) Response for Model 5



(f) Response for Model 6

Fig. 5.11 Loading-deflection curves of William's toggle frame

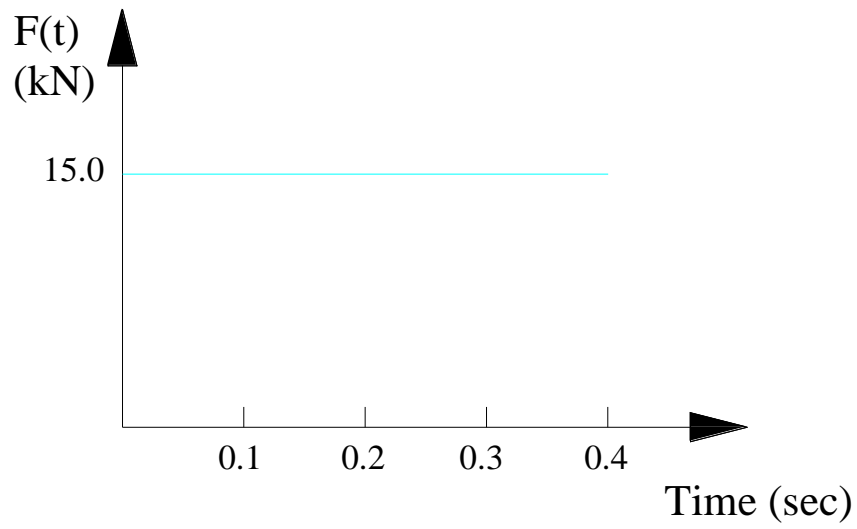
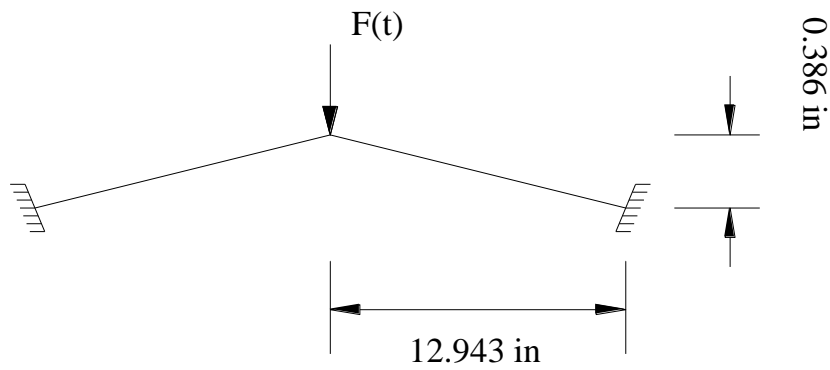
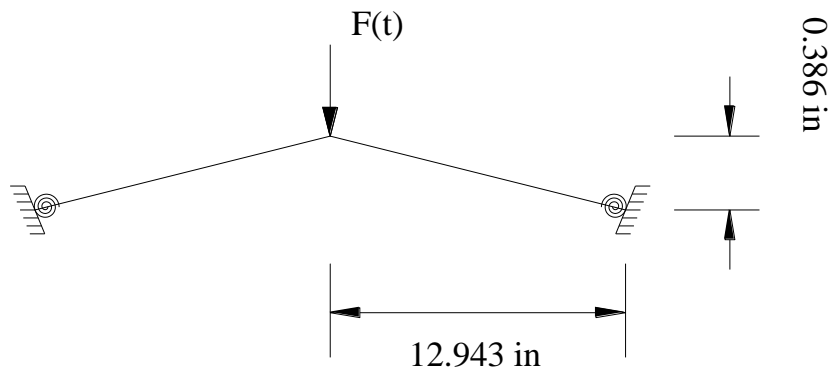


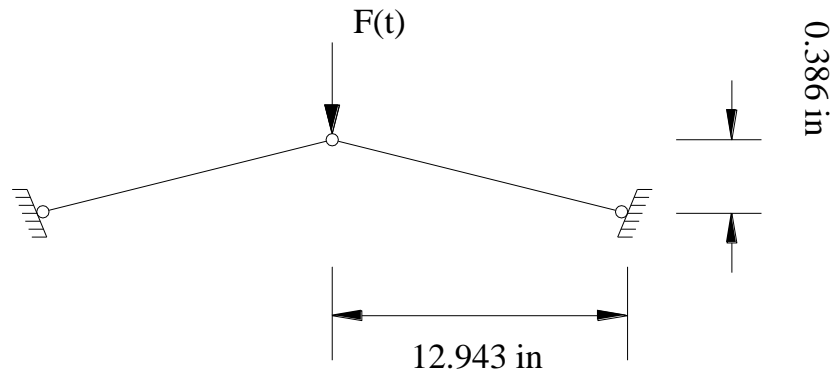
Fig. 5.12 Vertical load history



(a) Model 1

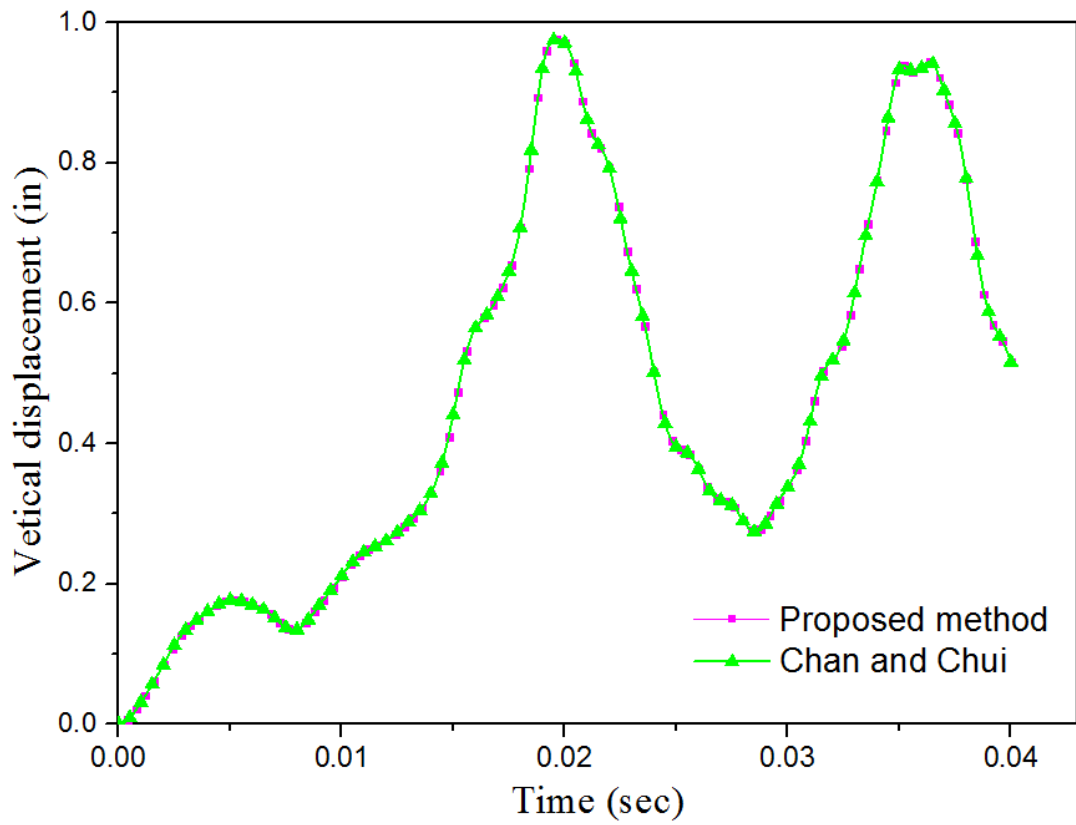


(b) Model 2

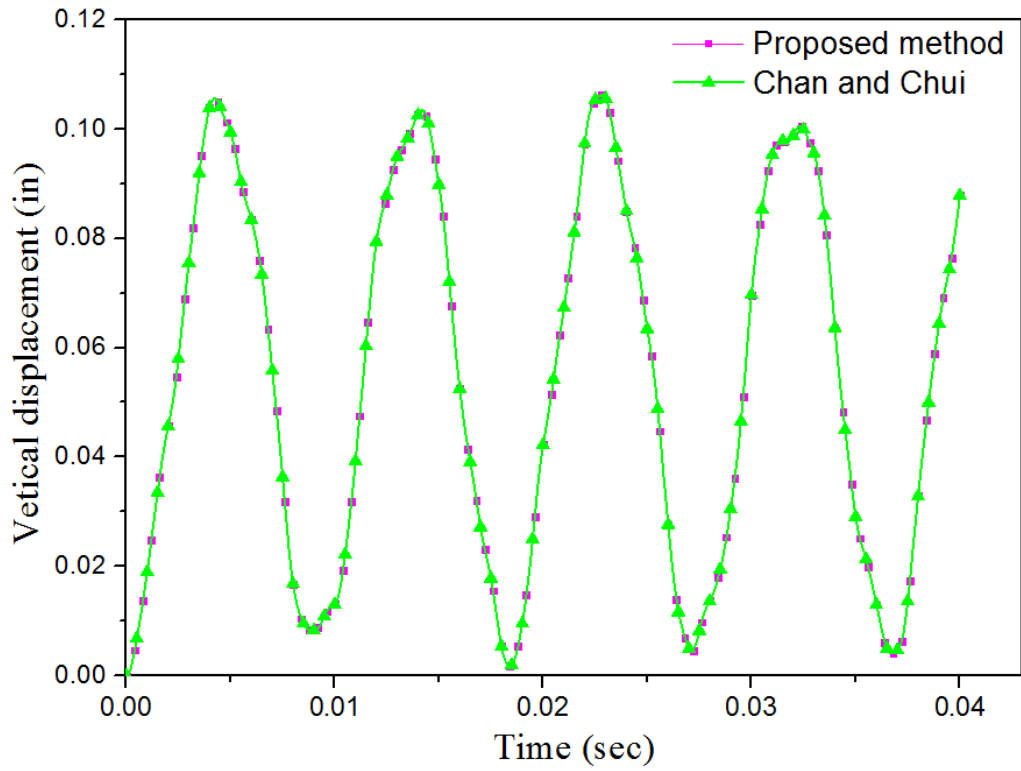


(c) Model 3

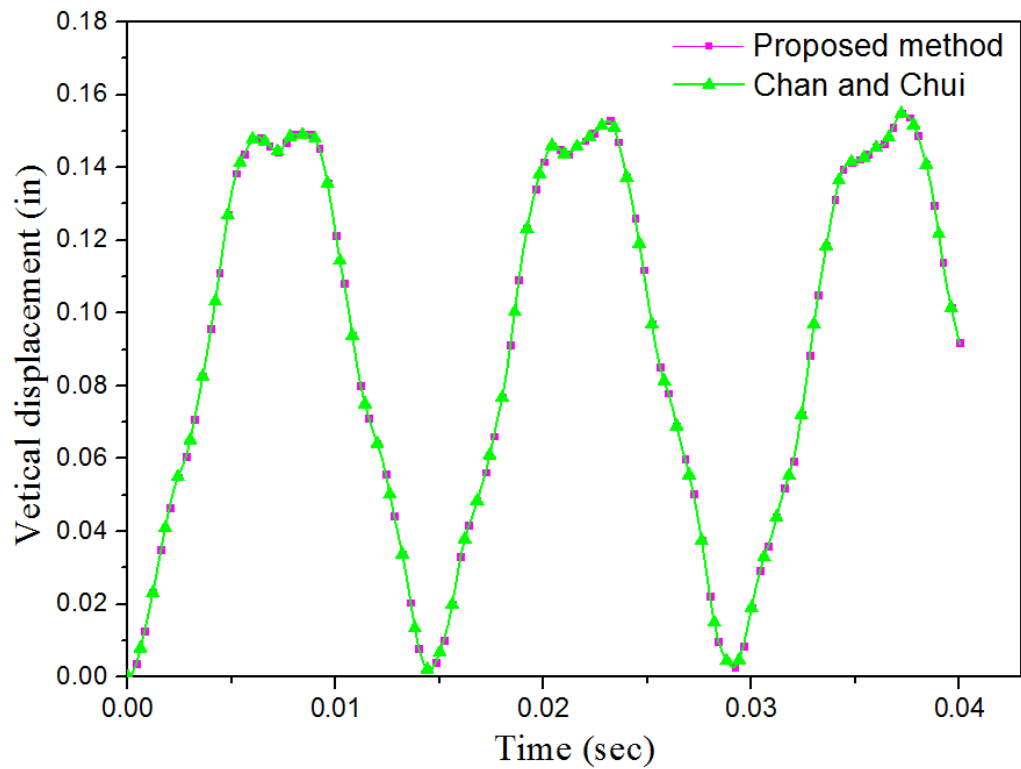
Fig. 5.13 Layouts and dynamic loadings for William's toggle frame



(a) Response for Model 1



(b) Response for Model 2



(c) Response for Model 3

Fig. 5.14 The transient response of William's toggle frame

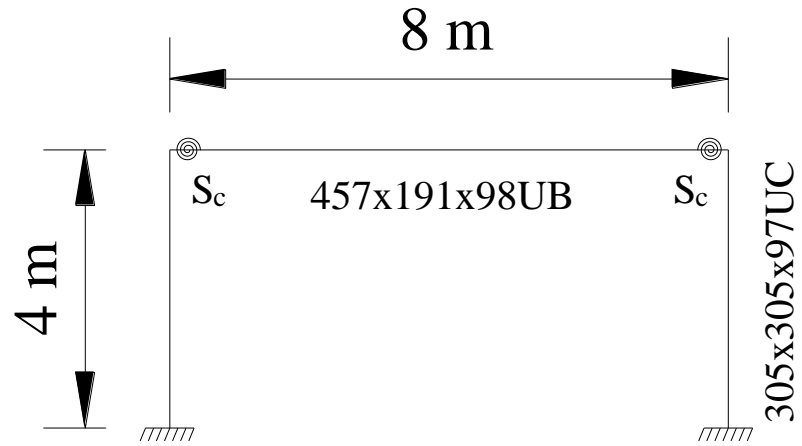
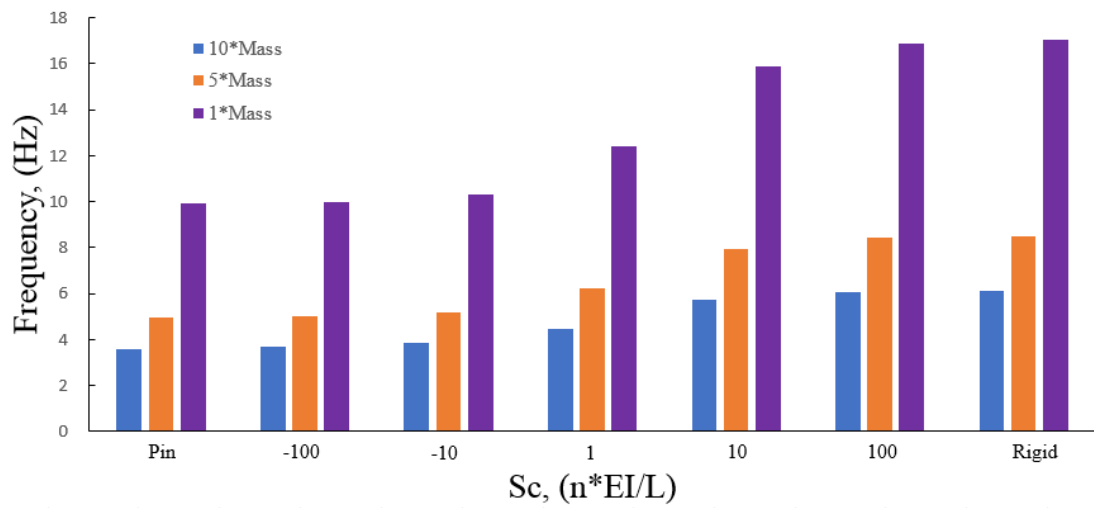
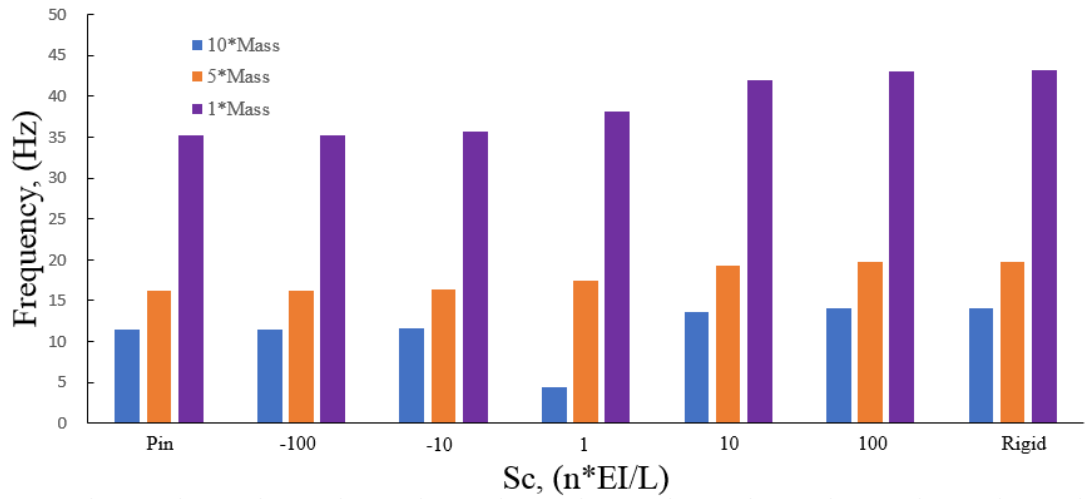


Fig. 5.15 Layout of one-story frame



(a) 1st mode



(b) 2nd mode

Fig. 5.16 Frequency against joint stiffness

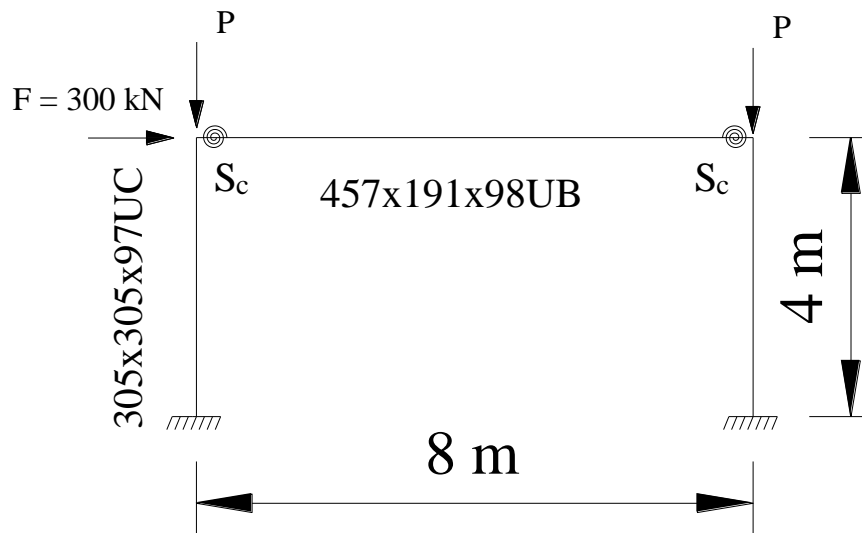
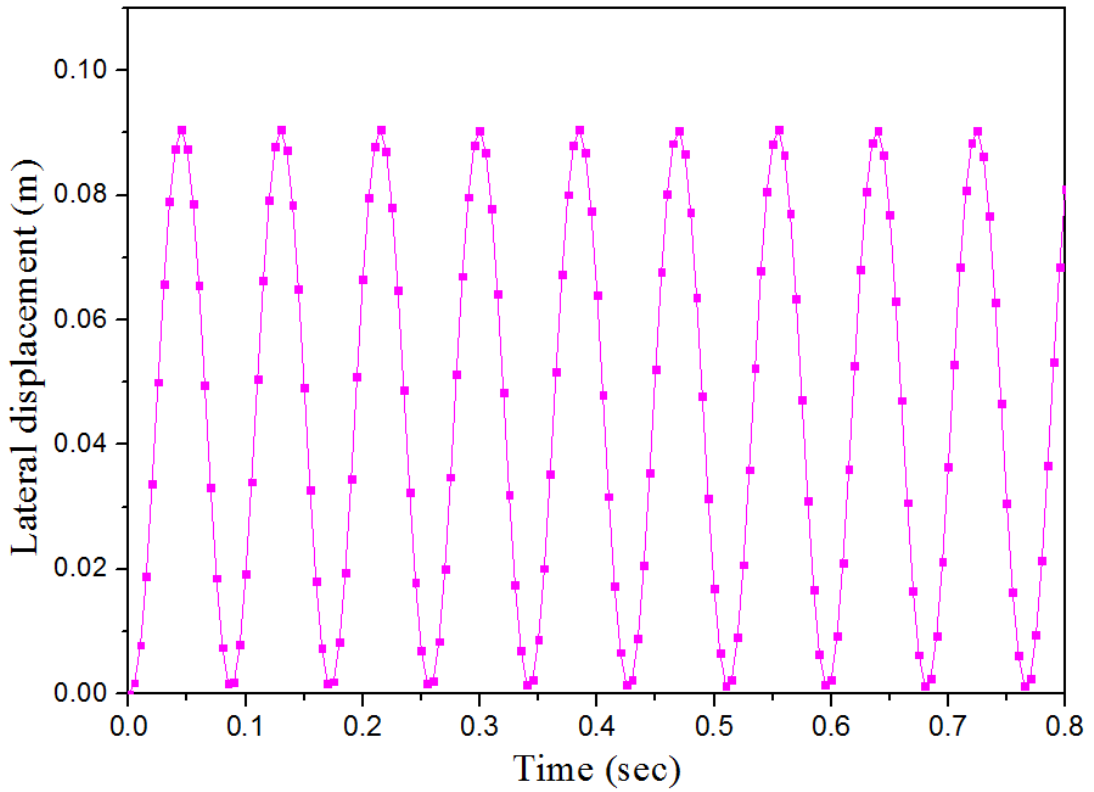
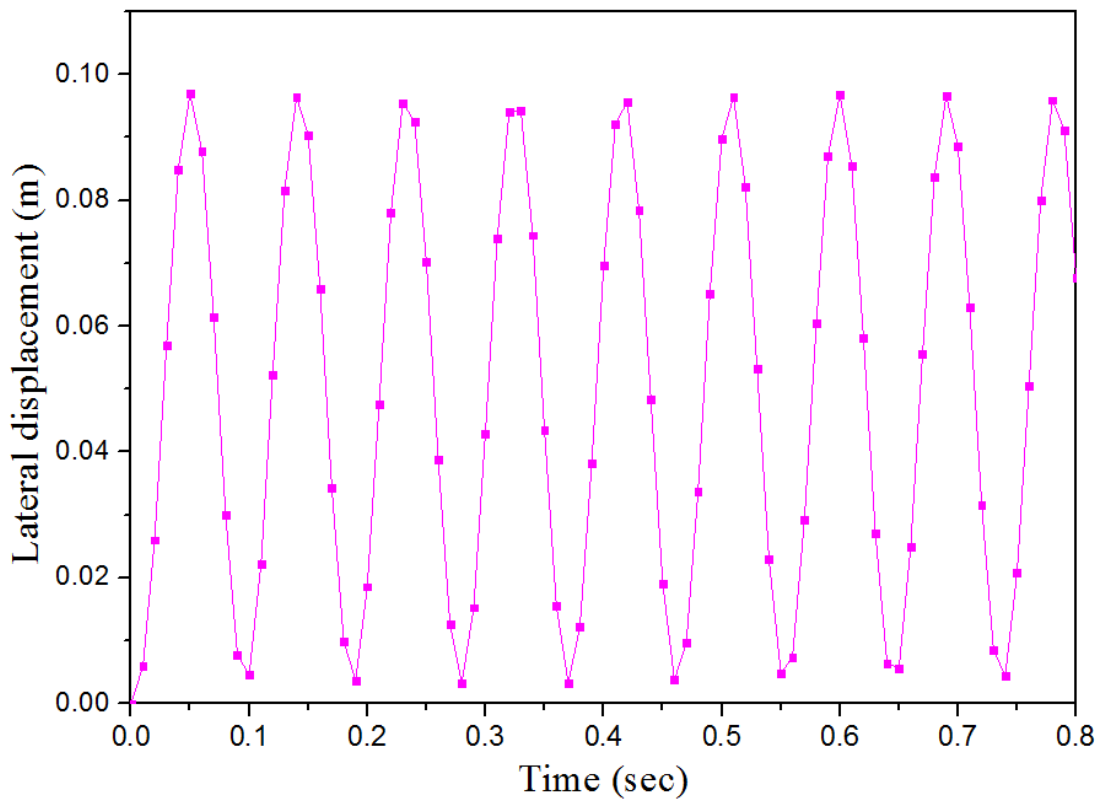


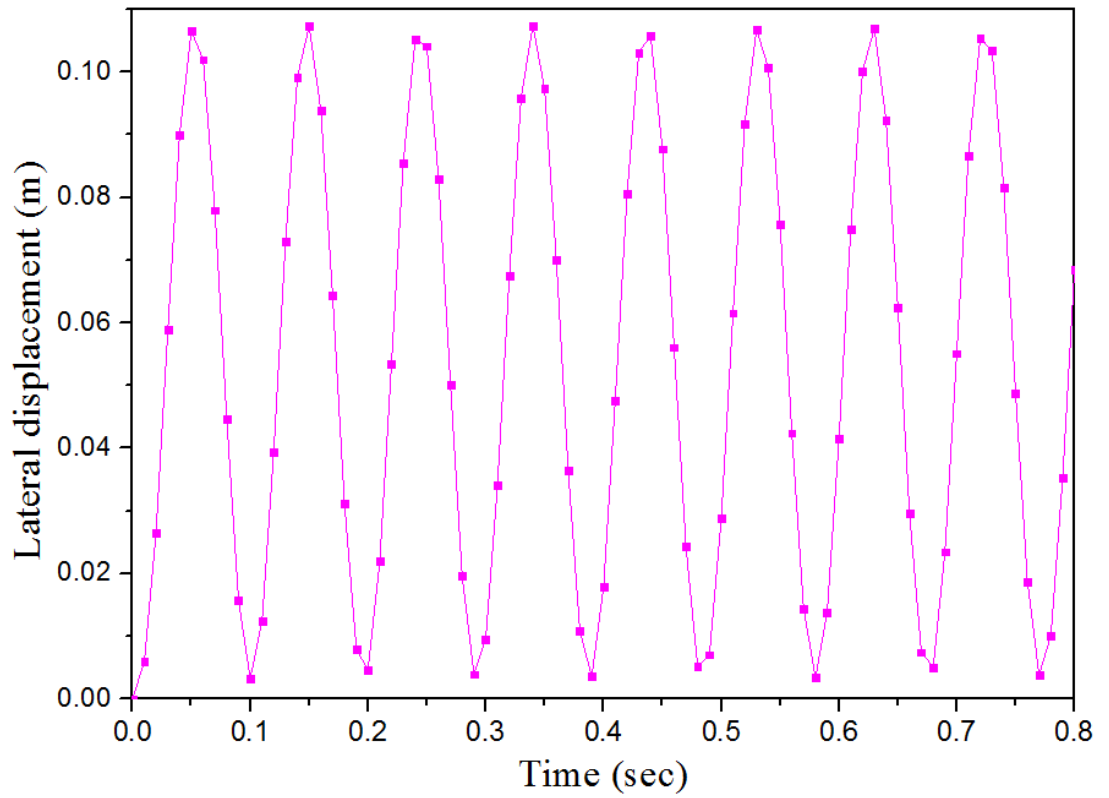
Fig. 5.17 Layout and load pattern of one-story frame



(a) 0 kN



(b) 1000 kN



(c) 2000 kN

Fig. 5.18 The transient response of the frame

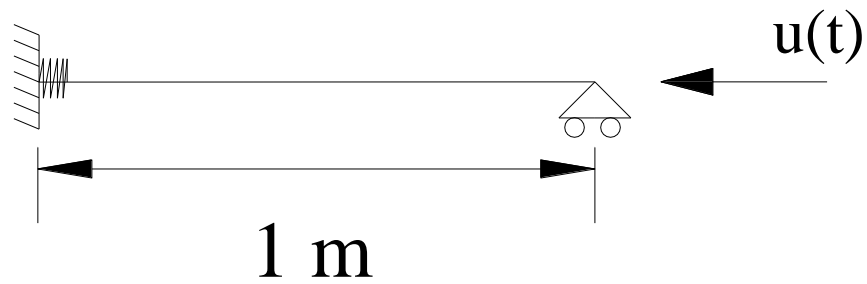


Fig. 5.19 Layout and load pattern of a column

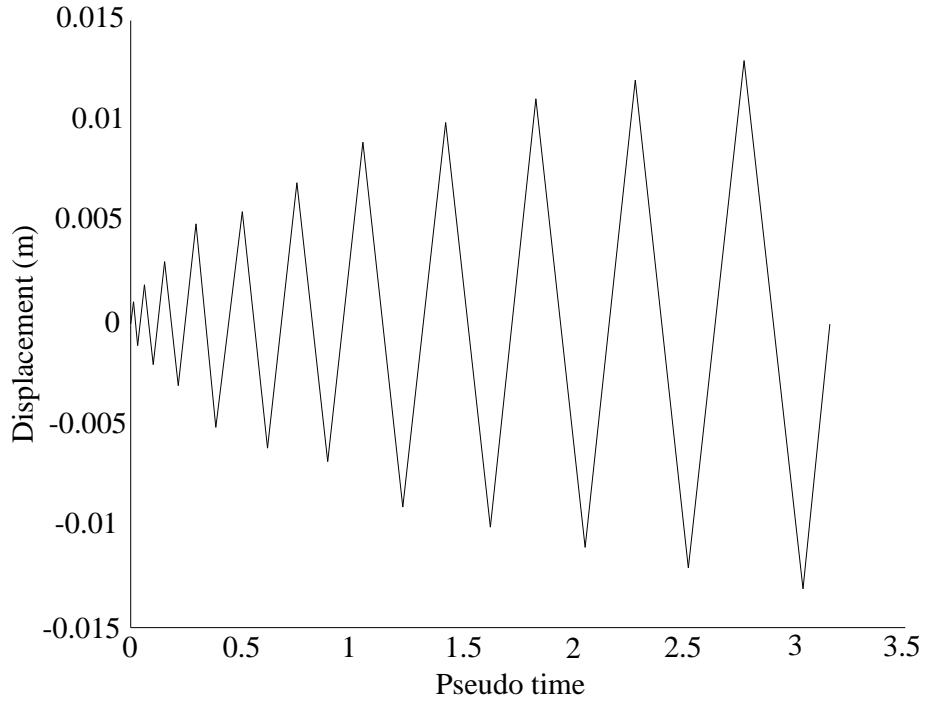


Fig. 5.20 Cyclic load history

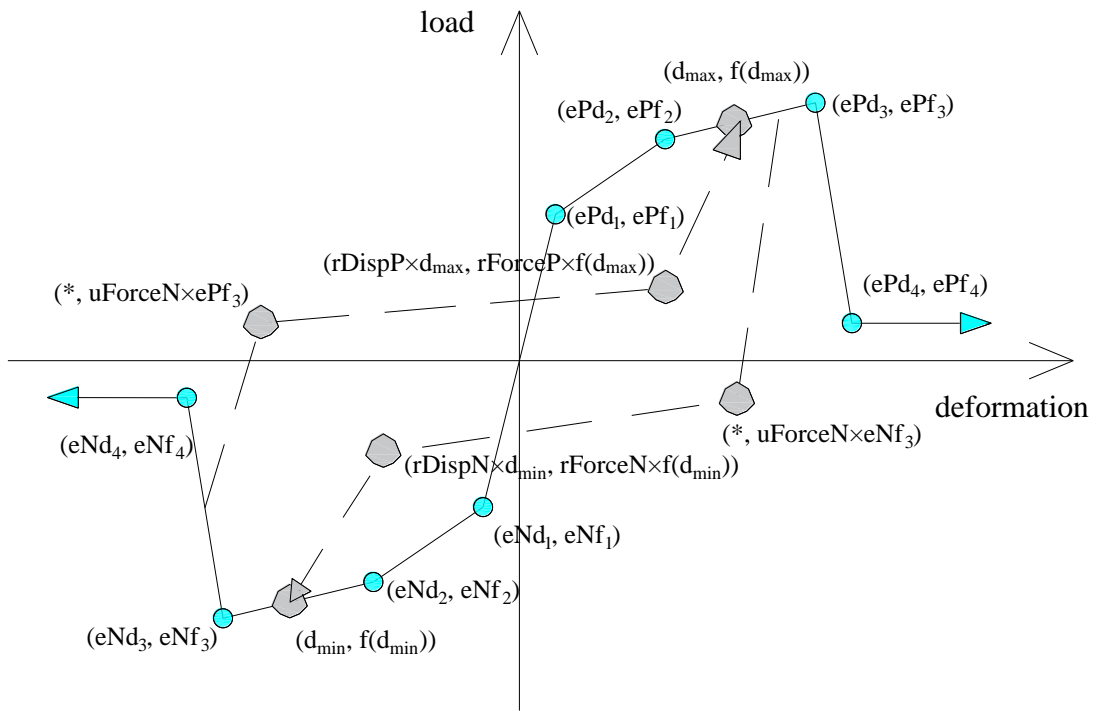
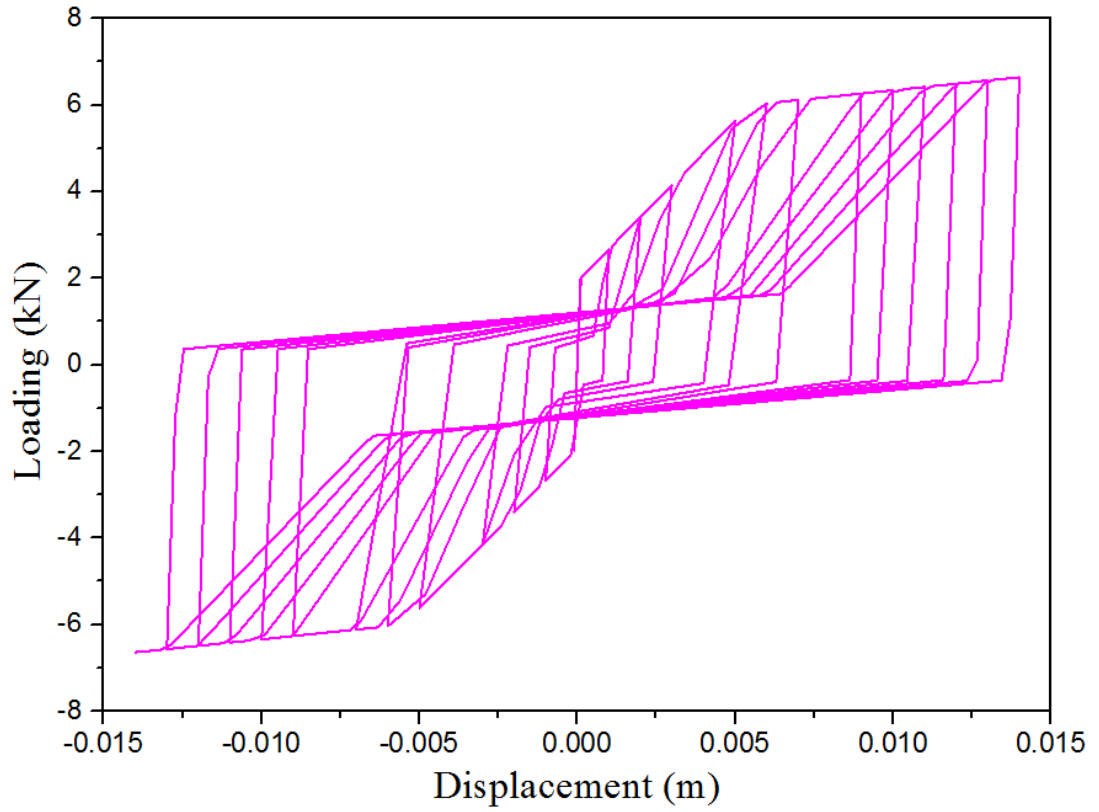
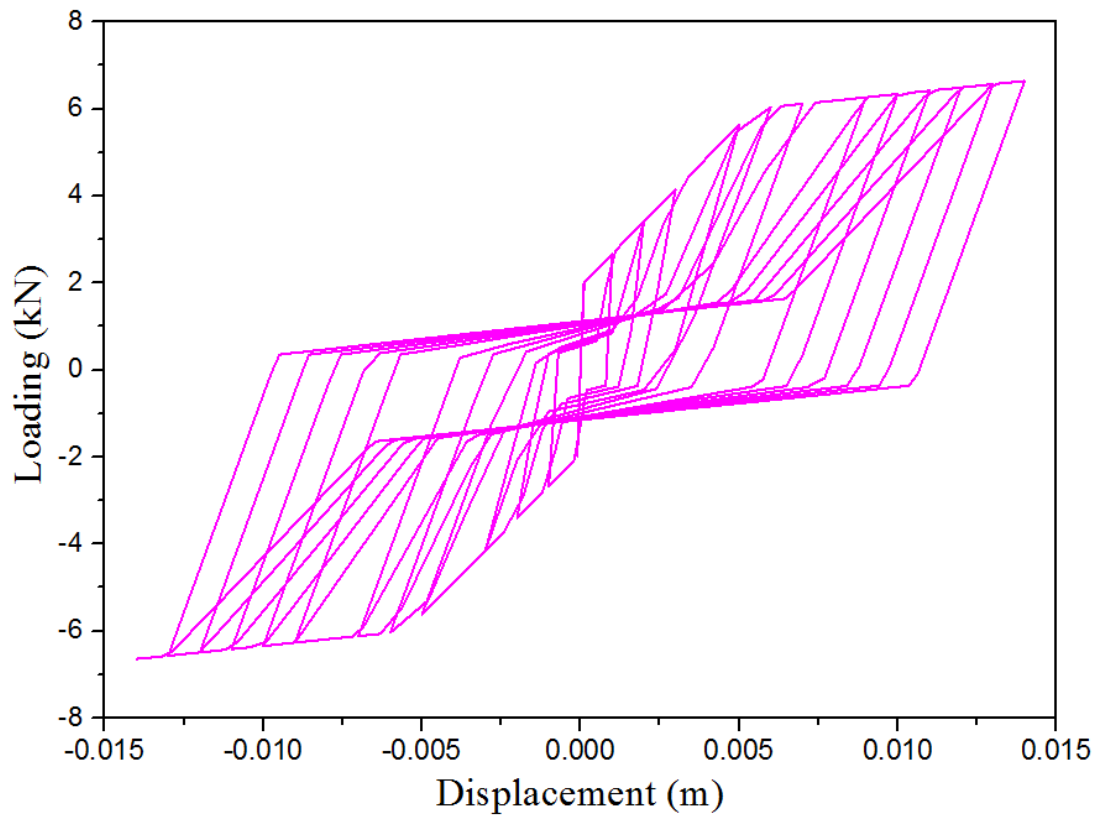


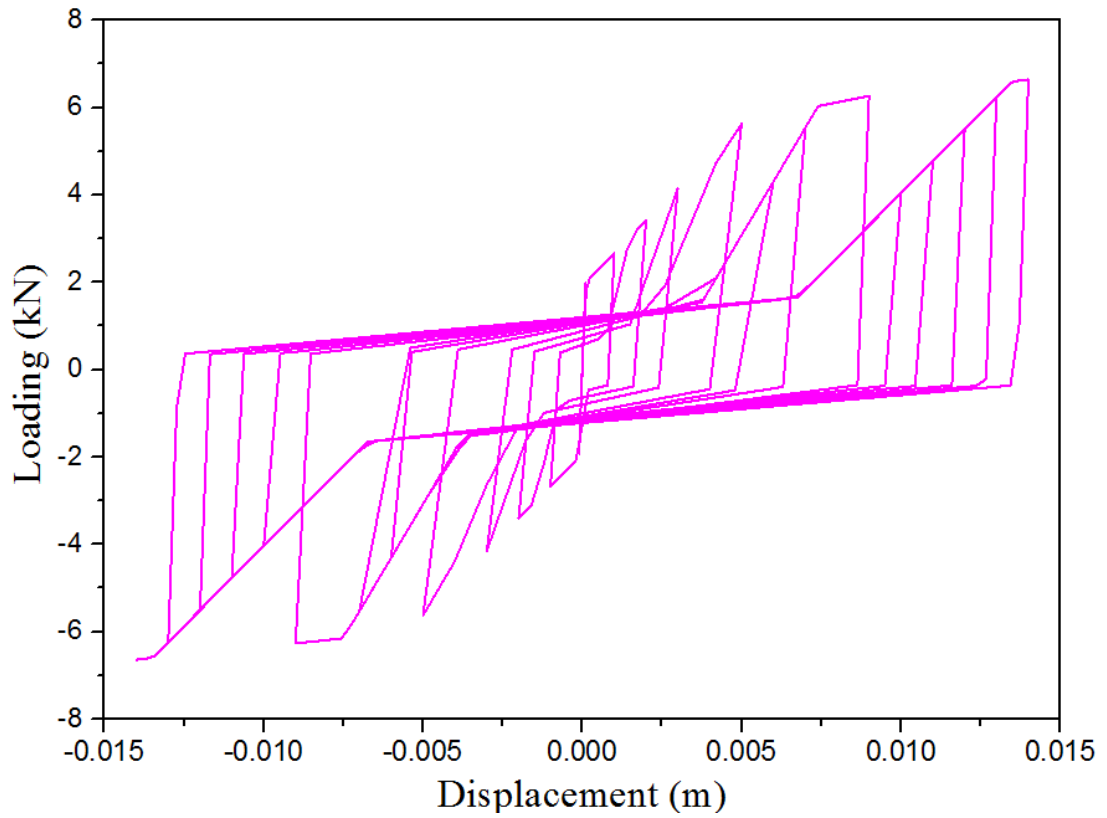
Fig. 5.21 Load-deformation response of the Pinch type model



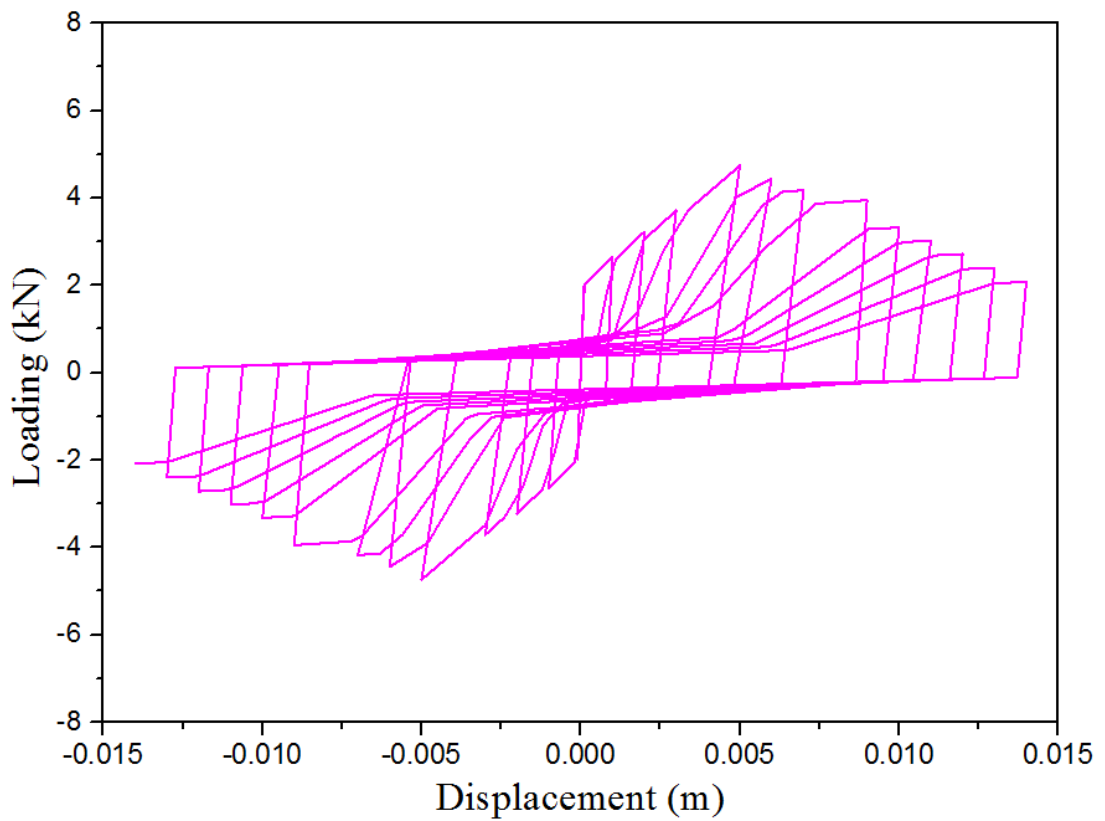
(a) Response of the pinch type model without degradation



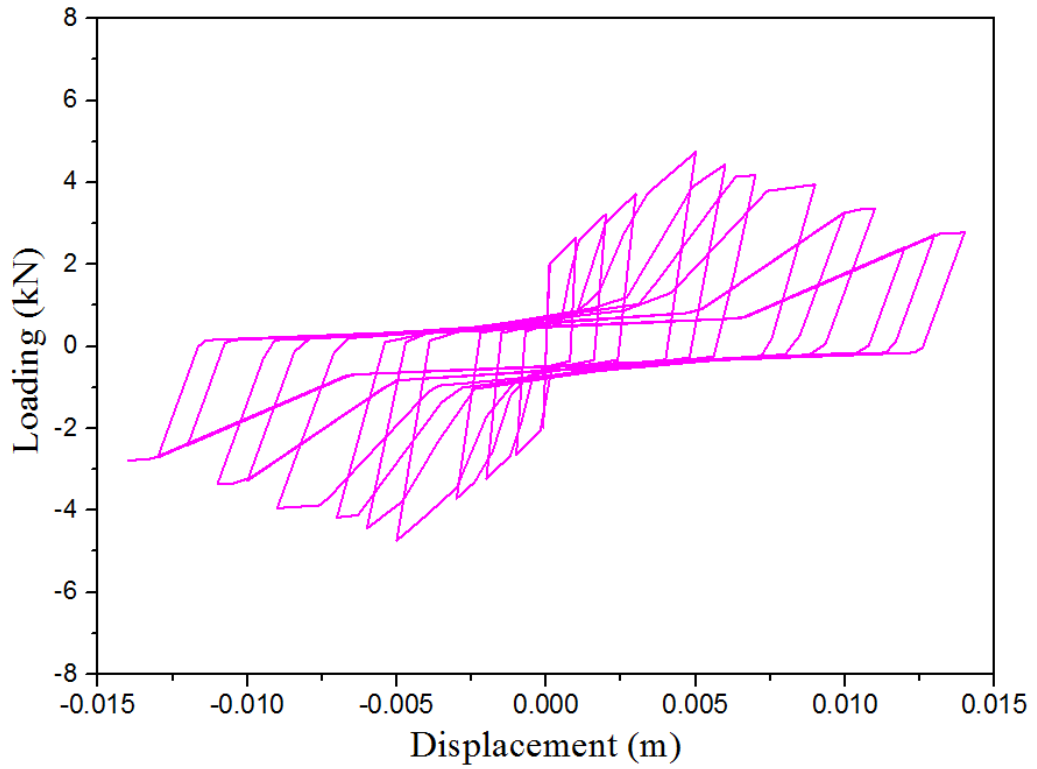
(b) Response of the pinch type model with unloading degradation



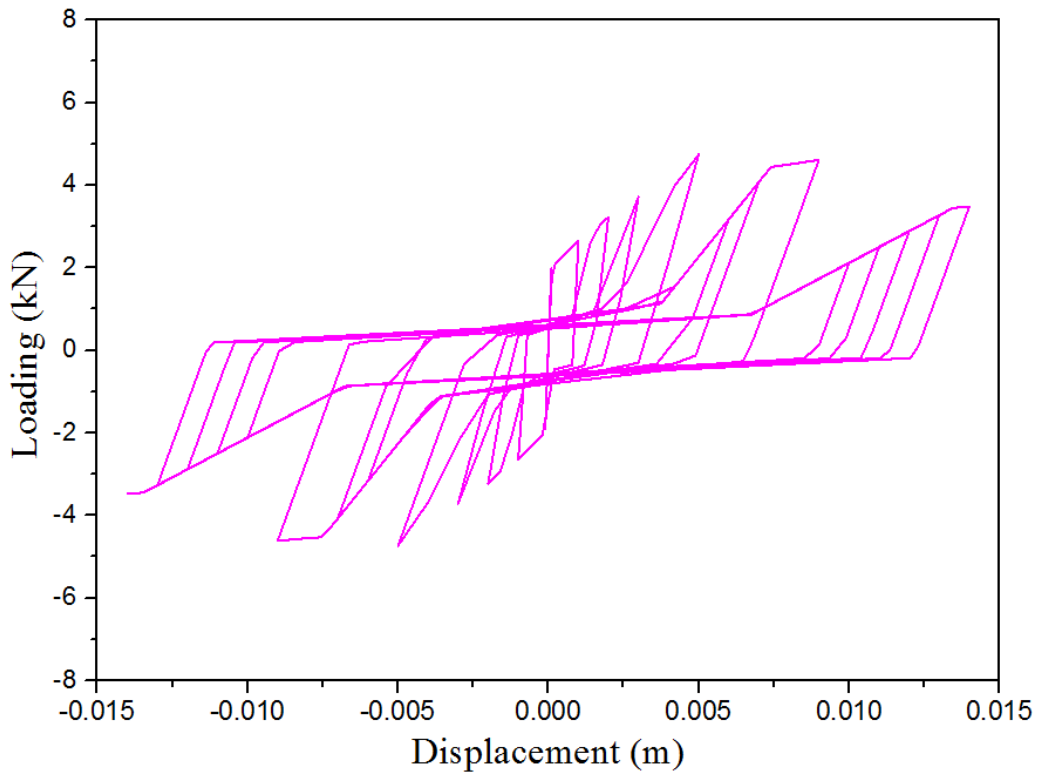
(c) Response of the pinch type model with reloading degradation



(d) Response of the pinch type model with strength degradation



(e) Response of the pinch type model with "energy" damage



(f) Response of the pinch type model with "cycle" damage

Fig. 5.22 The load-displacement histories of various pinch type models

TABLES

Table 5-1 Comparison of the critical load values for a non-sway frame

End Conditions	Methods Used	Critical load (kN)
(a)	F.E.M-MSC-NASTRAN	8981.58
	Proposed method	8981.67
(b)	F.E.M-MSC-NASTRAN	8981.02
	Proposed method	8981.01

Table 5-2 Comparison of the critical load values for a sway frame

End Conditions	Methods Used	Critical load (kN)
(a)	F.E.M-MSC-NASTRAN	14.77
	Proposed method	14.79
(b)	F.E.M-MSC-NASTRAN	8980.67
	Proposed method	8944.63

Table 5-3 Comparison of the critical load values for multistory sway frame

End Conditions	Methods Used	Critical load (kN)
(a)	F.E.M-MSC-NASTRAN	7.34
	Proposed method	7.34
(b)	F.E.M-MSC-NASTRAN	3745.92
	Proposed method	3726.00

CHAPTER 6. DIRECT ANALYSIS OF NONCOMPACT AND SLENDER CFT MEMBERS

6.1 Introduction

Concrete-filled steel tube (CFT) members are widely designed to sustain axial compression, flexure, or their combination due to structural efficiency compared with bare steel and reinforced concrete members. The outer steel tube in rectangular or circular shape often serves as formworks during the concrete casting period to reduce labor costs. This innovative structural member makes full use of steel tubes and the concrete infill. The local buckling of outer steel tubes can be restricted by the concrete infill whose strength will be improved by the confinement effect from steel tubes in return.

To account for local buckling, the steel tubes of CFT members can be classified as compact, noncompact, or slender section according to the limiting width-to-thickness ratios specified in Table I1.1a and I1.1b of AISC 360-16 (2016), which is also reproduced in Table 6-1 for easy reference. In AISC 360-16, the compressive strength f'_c of the concrete infill is limited from 21 MPa to 69 MPa and 41 MPa for normal weight concrete and light weight concrete, respectively. The yield stress of the steel tube shall not exceed 525 MPa. Eurocode 4 (2004) makes no distinction between compact, noncompact, and slender section, but simply gives limiting width-to-thickness ratios. For example, D/t is limited to $90 \sqrt{\frac{235}{f_y}}$ for circular CFT members;

h/t and b/t are limited to $52 \sqrt{\frac{235}{f_y}}$ for rectangular CFT members. Compared with AISC 360-16 (2016), the sections of CFT members are required to be more compact in Eurocode 4 (2004).

Generally, the noncompact and slender CFT members experience complex behaviors such as yielding and local buckling of steel tube, confinement and crack of concrete, and slippage between the steel tube and the concrete infill. Thus, it is a challenging task to model a CFT member by conventional numerical methods. The three-dimensional (3D) finite solid element analysis and the one-dimensional beam-column element analysis are two well-recognized methods.

The first method can explicitly account for the effects of local buckling and hoop stresses in the steel tube as well as the effects of confinement on the concrete infill. However, as this method requires many modeling skills and involves huge computer time with difficult interpretation results for engineers, it is rarely adopted in routine design. This method is mainly used to conduct parametric studies with limited experimental results or calibrate new numerical modeling methods. Lai *et al.* (2014) built detailed 3D finite element models to study noncompact or slender rectangular CFT members and address the gaps in the experimental database. Lai and Varma (2015) conducted parametric studies on noncompact and slender circular CFT members by 3D finite element models. Lam *et al.* (2012) adopted 8-node solid elements to model the stub concrete-filled steel tubular column with tapered members, and similar work has been done by Hassan *et al.* (2016). Liew and Xiong (2009) used continuum solid and shell elements to study the behavior of CFT members with initial preload. Du *et al.* (2017), Ding *et al.* (2017), Javed *et al.* (2017) and Aslani *et al.* (2016) adopted 8-node brick elements with reduced integration to study the behaviors of CFT members.

The second method adopts the one-dimensional beam-column elements to explicitly or implicitly consider the complex behaviors of CFT members. The explicit one adds extra degrees of freedom (DOFs) to the end nodes of beam-column elements. Tort and Hajjar (2010) extended the conventional 12 DOFs beam element into 18 DOFs beam element to consider the slip deformation between the steel tube and the concrete infill of rectangular CFT members. Lee and Filippou (2015) proposed a composite frame element to capture the bond-slip behavior at the interface between the steel tube and concrete infill based on an extension of the Hu-Washizu variational principle. The underlying theory of this method is the exact interpolation of the total section forces. Noted that to solve these particular problems, additional DOFs need to be introduced in the special beam-column element and further condensed at the elemental level. The whole procedure involves complicated numerical operations. In contrast, the implicit approach simply adopts fiber-based beam-column elements with effective stress-strain relationships to indirectly simulate the complex behaviors of CFT members. The whole analysis and design procedure is simple without additional numerical work and requires less computer time. Thus, this method is more competent than other methods in the daily design of CFT members.

Regarding CFT members with compact sections, several effective stress-strain relationships are available for the fiber-based beam-column elements, for instance, Tort and Hajja (2010), Sakino *et al.* (2004), Han *et al.* (2005) and Liang (2009). As for noncompact and slender CFT members, few effective stress-strain relationships can be used for design purpose. Lai and Varma (2016) proposed effective stress-strain relationships for noncompact and slender circular and rectangular CFT members. They also proposed a nonlinear fiber analysis (NFA) macro model to design CFT members. However, their model is only for two-dimensional problems with axial force

and uni-axial moment but not for spatial CFT members subjected to bi-axial moments. The latter is a common case, for example, the corner columns. Furthermore, their model needs to divide one single CFT member into several segments, which brings inconvenience in structural modeling and also significantly increases the computer time.

AISC 360-16 (2016) firstly provides three methods for design of noncompact and slender CFT members. The first two methods use interaction equations for strength checking with stability design by effective length method. The system stiffness is approximately simulated based on reduced or effective member stiffness, and therefore they cannot accurately capture the structural behaviors. The third method uses effective stress-strain relationships, which reflect the fundamental behaviors and strengths of CFT members with sufficient accuracy in a simple manner, for practical design. Noted that this method ignores the influence of slenderness effects and therefore the traditional effective length method is still needed for stability check. Alternatively, the member initial imperfections can be included in the direct analysis so that the effective length assumption is no longer required. However, the magnitude of member imperfection for noncompact/slender CFT members should be further studied.

In this chapter, a second-order flexibility-based beam-column with member imperfections and incorporates the effective stress-strain models into the fiber section is proposed for direct analysis of noncompact/slender CFT members. The gradual change of member stiffness and the actual section capacity can be accurately reflected in the analysis process and as a result, the traditional effective length method is no longer required in the proposed direct analysis. It is also found that the initial imperfection of $L/1000$ is insufficient for CFT members.

The outline of this chapter is as follows. Firstly, three design methods suggested by AISC 360-16 (2016) are presented and discussed. Next, a comprehensive direct analysis method for CFT members made of noncompact or slender sections is introduced. At last, several experimental tests from literatures are used to verify the proposed method.

6.2 Design methods for CFT members with noncompact or slender sections in AISC360

The design methods for compact CFT members can be found in the extensive research papers and design codes such as Eurocode 4 (2004) and AISC 360-16 (2016), and therefore they will be not repeated here. In contrast, the design methods, especially the effective stress-strain method, for noncompact and slender CFT members are newly developed and firstly specified in AISC 360-16 (2016). The practical design tools and the applications are limited. Thus, it is worth to conduct more research on this topic and provide more comprehensive solutions or recommendations for structural engineers to design noncompact and slender CFT members. In this section, the available design methods will be briefly introduced.

6.2.1 General interaction method

AISC 360-16 (2016) provides a general method for the design of doubly symmetric CFT members subjected to compression and flexure. Equations (6.1a) and (6.1b) are the interaction equations considering different levels of axial force, which is directly extended from bare steel members to compact, noncompact and slender CFT members.

$$\frac{P_r}{P_c} + \frac{8}{9} \left(\frac{M_{rx}}{M_{cx}} + \frac{M_{ry}}{M_{cy}} \right) \leq 1.0, \text{ for } \frac{P_r}{P_c} \geq 0.2, \quad (6.1a)$$

$$\frac{P_r}{2P_c} + \frac{8}{9} \left(\frac{M_{rx}}{M_{cx}} + \frac{M_{ry}}{M_{cy}} \right) \leq 1.0, \text{ for } \frac{P_r}{P_c} < 0.2 \quad (6.1b)$$

in which, P_c is the available axial strength; M_{cx} and M_{cy} are the major and minor flexural strengths; P_r is the required axial strength; M_{rx} and M_{ry} are the major and minor required flexural strength.

Clearly, although these equations can consider bi-axially bending problems, the beneficial effect of axial compression on the flexural strength has been ignored. It was reported by Lai *et al.* (2015) that these equations are over-conservative for checking the strength of noncompact and slender CFT members. Therefore, this method belongs to one of optional methods for the design of compact and noncompact/slender CFT members in AISC 360-16 (2016).

Both the direct analysis method and first-order analysis method can be used to determine the required strengths P_r , M_{rx} and M_{ry} . When using the former for the ultimate limit state, the deduced stiffness for compression and flexure given in Equation (6.2) should be adopted in the second-order elastic analysis.

$$EA^{II} = 0.8(E_s A_s + E_s A_{sr} + E_c A_c) \quad (6.2a)$$

$$EI^{II} = 0.8\tau_b EI_{eff} \text{ with } \tau_b = 0.8 \quad (6.2b)$$

$$EI_{eff} = E_s I_s + E_s I_{sr} + C_1 E_c I_c \quad (6.2c)$$

$$C_1 = 0.25 + \frac{A_s + A_{sr}}{A_g} \leq 0.7 \quad (6.2d)$$

in which, E_s and E_c are Young's moduli of steel and concrete respectively; A_s , A_c and A_{sr} are the total areas of the steel tube, concrete infill, and reinforcement respectively while A_g is the total area of all components; I_s , I_c and I_{sr} are the second moment of areas of the steel tube, concrete infill and reinforcement respectively.

Denavit *et al.* (2015) confirmed that the stiffness in Equation (6.2) does not always give a conservative design. However, AISC 360-16 (2016) does not provide detailed limitation its use.

For the first-order analysis with effective length method, the stiffness given in Equation (6.3) should be employed in the global structural analysis.

$$EA^I = E_s A_s + E_s A_{sr} + E_c A_c \quad (6.3a)$$

$$EI^I = EI_{eff} \quad (6.3b)$$

When using the effective length method to check the flexural buckling, the compressive strength P_c is obtained by multiplying resistance factor or dividing safety factor with nominal compressive strength P_n , which can be calculated from Equation (6.4).

$$P_n = P_{no} 0.658^{P_{no}/P_e}, \text{ for } \frac{P_{no}}{P_e} \leq 2.25 \quad (6.4a)$$

$$P_n = 0.877 P_{no}, \text{ for } \frac{P_{no}}{P_e} > 2.25 \quad (6.4b)$$

$$P_e = \frac{\pi^2 (EI_{eff})}{(KL)^2} \quad (6.4c)$$

in which, P_{no} is the nominal compressive strength without consideration of slenderness effect; P_e is elastic critical buckling load; KL is the effective length.

6.2.2 Direct interaction method

To account for the beneficial effects due to axial compression on limiting crack of infilled concrete and increasing flexural strength by confinement, AISC 360-16 (2016) introduces two coefficients c_p and c_m corresponding to the balance point into Equation (6.1) and then can be rewritten in Equation (6.5) as

$$\frac{P_r}{P_c} + \frac{1 - c_p}{c_m} \left(\frac{M_r}{M_c} \right) \leq 1.0, \text{ for } \frac{P_r}{P_c} \geq c_p \quad (6.5a)$$

$$\left(\frac{1 - c_m}{c_p}\right)\left(\frac{P_r}{P_c}\right) + \frac{M_r}{M_c} \leq 1.0, \text{ for } \frac{P_r}{P_c} < c_p \quad (6.5b)$$

in which, P_c and M_c are the available axial strength and flexural strength respectively; P_r and M_r are the required axial strength and flexural strength respectively. c_p and c_m , as shown in Table 6-2, are coefficients determined by the relative strength ratio c_{sr} between concrete strength and steel strength which can be calculated by Equation (6.6).

$$c_{sr} = \frac{A_s F_y + A_{sr} F_{yr}}{A_c f'_c} \quad (6.6)$$

where F_y and F_{yr} are the steel and reinforcement yield stress; f'_c is the concrete strength.

It should be noted that both the direct analysis method and first-order analysis method should adopt the reduced stiffness in Equation (6.2). It means that unconservative design may be induced due to the approximation of member stiffness.

Similar to the general interaction method, Equation (6.4) should be followed to check the flexural buckling if the first-order analysis method is used.

6.2.3 Effective stress-strain method

AISC 360-16 (2016) allows four methods for the calculation of the nominal strength of composite sections, i.e., plastic stress distribution method, strain compatibility method, elastic stress distribution method and effective stress-strain method. The last one is specially developed for the analysis and design of CFT members made of noncompact and slender cross sections. The fundamental behaviors such as local buckling, yielding, interaction and concrete confinement are accounted for through the effective stress-strain relationships rather than directly include them in a complex

analysis model. Lai and Varma (2016) proposed effective stress-strain relationships for analysis of noncompact and slender filled composite members.

Generally speaking, this method is particularly suitable for the fiber-based element to form sectional tangent stiffness and then perform direct analysis to check the actual section capacity and system resistance without the use of effective length assumption. Most importantly, the inelastic behavior of CFT members can be well captured. The accurate member stiffness can be formed by fiber integration approach rather than the approximate effective stiffness or reduced stiffness used in the interaction methods aforementioned. Although the strain compatibility is required based on beam-column theory, the modified material stress-strain relationships have implicitly considered the macro effects such as local buckling, yielding, and concrete confinement and therefore it provides an innovative solution on structural analysis and design of frame structures with CFT members under the framework of direct analysis.

6.2.4 Discussion on design methods

The general interaction method ignores the beneficial effects due to the restraint of steel tube on the concrete infill while the other methods have been implicitly taken them into account. Thus, the first method generally produces a conservative design regarding strength checking.

It is noted that the two P-M interaction methods need to use reduced or effective stiffness either in direct analysis or in the first-order analysis. It means that the change of member stiffness associated with its complex behaviors is approximately reflected in the analysis process. As a consequence, the traditional effective length should be further adopted for stability checking. It will bring uncertainty in stability design as the effective length is difficult to know due to the changing of system stiffness under

external loads. In the viewpoint of direct analysis, the stability design should be based on system behavior but not simply based on individual member response. Generally speaking, the two methods are only applicable for second-order elastic analysis. The progressive yielding behavior cannot be accurately simulated by them.

The third method adopts effective stress-strain relationships based on the fiber section approach. The effective stress-strain curves are essentially based on limited experimental and numerical tests. As for lack of consideration of slenderness effects and initial geometrical imperfections, this method does not fully fulfill the requirements of direct analysis. However, this method can implicitly account for the complex behaviors of noncompact/slender CFT members, and therefore it forms the solid foundation for direct analysis using beam-column elements. The members with complex local behaviors can be modeled through this method. Thus, it has bright future with the combination use of direct analysis method.

In the next section, a flexibility-based beam-column with member imperfections and incorporating the effective stress-strain curves is proposed for the direct analysis of noncompact/slender CFT members.

6.3 Direct analysis method

The spirit of direct analysis method is to integrate all factors, which may significantly affect the structural behaviors, into the second-order analysis process so that the conventional effective length method is no longer required for member and system stability check. In the viewpoint of finite element analysis, both the geometrical and material nonlinearities should be included unless the effect(s) can be ignored. Along with this thought, Du *et al.* (2017) proposed a new curved flexibility-based beam-column element for direct analysis, which explicitly accounts for member initial

imperfections and distributed plasticity. However, their work was mainly concentrated on bare steel structures.

In this thesis, the element proposed by Du *et al.* (2017) will be extended to model CFT members, especially for noncompact and slender sections by imposing the effective stress-strain relationships into the fiber sections. As a consequence, this element can simulate the complex behaviors of CFT members, such as local buckling, confinement of concrete, etc.

In this section, the element with member imperfections will be briefly introduced. The magnitude of initial imperfection for CFT members will be first discussed. The effective stress-strain relationships proposed by Lai and Varma (2016) for CFT members with noncompact and slender sections will be modified for direct analysis.

6.3.1 Initial geometrical imperfection of CFT members

The member imperfections such as initial out-of-straightness and residual stress may come from the manufacturing process, fabrication and transportation. It affects the member stiffness and causes early buckling and therefore should be considered in direct analysis. Essentially, the member imperfection will induce P- δ moment and then reduce the member capacity and lead to moment redistributions. Relevant provisions are specified in many modern design codes either implicitly or explicitly.

In AISC 360-16 (2016), both the second-order elastic analysis and second-order inelastic analysis shall consider member imperfection. The shape of geometrical imperfection is assumed as a half-sine function with an amplitude equal to δ_0 , which is recommended as $L/1000$ and L is member length. Eurocode 4 (2004) also has particular provisions about member imperfections for composite columns. The magnitude of member

imperfection is $L/300$ when the reinforcement ratio is less than 3% and $L/200$ for the reinforcement ratio being more than 3% but less than 6%.

Noted that it cannot conclude that Eurocode 4 (2004) is more conservative than AISC 360-16 (2016), because the reduced stiffness shown in Equation (6.2b) is used in the latter while the effective stiffness similar to Equation (6.2c) is adopted in the former.

It is further found that the imperfection magnitude of noncompact and slender CFT members does not include in both design codes. This thesis will first study the imperfection magnitude of noncompact and slender CFT members, and aims to propose a practical one for design purpose.

6.3.2 Effective material representation of CFT members

In the fiber-based beam-column element, the section stiffness of a CFT member is obtained by the integration of the fibers along cross section as

$$\mathbf{k}_s(\xi_i) = \begin{bmatrix} \sum_{j=1}^m (E_{tj}A_j) & \sum_{j=1}^m (-y_j E_{tj}A_j) & \sum_{j=1}^m (z_j E_{tj}A_j) & 0 \\ \sum_{j=1}^m (-y_j E_{tj}A_j) & \sum_{j=1}^m (y_j^2 E_{tj}A_j) & \sum_{j=1}^m (-y_j z_j E_{tj}A_j) & 0 \\ \sum_{j=1}^m (z_j E_{tj}A_j) & \sum_{j=1}^m (-y_j z_j E_{tj}A_j) & \sum_{j=1}^m (z_j^2 E_{tj}A_j) & 0 \\ 0 & 0 & 0 & GJ \end{bmatrix} \quad (6.7)$$

in which, ξ_i is the location of the monitoring section; y_j and z_j are the centroid coordinates of fiber j ; E_{tj} is the tangent stiffness of fiber j ; \mathbf{k}_s is the section stiffness matrix which is the inverse of the section flexibility matrix \mathbf{f}_s in Equation (3.39). The typical fiber mesh for rectangular and circular CFT sections are shown in Fig. 6.1. Thus, the member stiffness, section strength, and the resultant stresses can be determined.

Lai and Varma (2016) proposed the uniaxial effective stress-strain relationships for the steel tube and the concrete infill of noncompact and slender CFT members through an extensive parametric study by 3D finite element analysis regarding geometric and material parameters. These relationships are simple for fiber-based analysis with implicitly consideration of CFT members' complex behaviors, such as yielding, local buckling, and concrete confinement. They will be briefly described as follows.

6.3.2.1 Stress-strain relationships of the steel tube

The effective stress-strain relationships of the steel tube for rectangular or circular CFT members are different because the shape of steel shapes affects the local buckling stress as shown in Fig. 6.2.

Fig. 6.2 (a) shows the tensile effective stress-strain relationship curve in trilinear shape for the steel tube of rectangular CFT members. This curve is determined by two anchor points, i.e., the peak stress point and the post-peak point. Larger tube slenderness ratios or yield stress will lead to less peak stress on the steel tube with σ_p defined in Equation (6.8). The post stress σ_2 is affected by infill concrete compressive strength except for tube slenderness ratios and yield stress, and can be calculated by Equation (6.9).

$$\sigma_p = F_y \times (1.12 - 0.11\lambda_{coeff}) \leq F_y \quad (6.8)$$

$$\sigma_2 = F_y \times (0.87 - 0.0055(\frac{b}{t} - \frac{F_y}{f'_c})) \quad (6.9)$$

$$\lambda_{coeff} = \frac{b/t}{\sqrt{E_s/F_y}} \quad (6.10)$$

As for circular CFT members, the post-peak deterioration is negligible, and the compression behavior of the steel tube is assumed to be elastic-perfectly plastic as shown in Fig. 6.2(b), with the peak stress σ_p calculated by Equation (6.11).

$$\sigma_p = 0.9F_y \quad (6.11)$$

For both rectangular and circular CFT members, the tensile stress-strain behavior of the steel tube is modeled by a bilinear curve. In the elastic stage, the steel tube remains elastic with an elasticity modulus E_s and yield stress F_y . In the plastic stage, the steel tube is assumed to be a post-yield linear hardening branch with hardening factor 0.01 as shown in Fig. 6.2.

6.3.2.2 Stress-strain relationships of the concrete infill

The effective stress-strain relationships for rectangular CFT members and circular CFT members are different because the shape of steel shapes affects the confinement of concrete infill as shown in Fig. 6.3. The empirical model by Popovics (1973) is modified to reflect the compression strength of the concrete infill of CFT members. The concrete compressive strength f'_c is replaced by the concrete peak stress f'_{cp} as shown in Equation (6.12). The unconfined concrete peak strain ε_c and the compressive shape factor n are calculated by Equations (6.13) and (6.14) respectively.

$$f_c = f'_{cp} \frac{\varepsilon}{\varepsilon_c} \frac{n}{n - 1 + (\varepsilon/\varepsilon_c)^n} \quad (6.12)$$

$$\varepsilon_c = \frac{f'_c}{E_c} \frac{n}{n - 1} \quad (6.13)$$

$$n = 0.058f'_c + 1.0 \quad (6.14)$$

For the rectangular CFT members, larger tube slenderness ratio or higher ratio between the steel yield stress and the concrete compressive strength improves the concrete peak stress f'_{cp} , which is limited to $1.10f'_c$. Although the steel tube can provide certain confinement on the infill concrete and improve the post-peak ductility of concrete, the

confinement effect is really limited. For this reason, the post-peak behavior of the concrete infill is modeled as the unconfined concrete as shown in Fig. 6.3(a) for conservative.

$$f'_{cp} = f'_c \times \left(0.8 + 0.18 \left(\frac{b/t}{100} + \frac{F_y/f'_c}{30} \right) \right) \quad (6.15)$$

Equation (6.16) defines the concrete peak stress. Unlike the rectangular CFT members, larger tube slenderness ratio degrades the concrete peak stress of the circular CFT members. Besides, the steel tube provides better confinement than that of the rectangular CFT members. Consequently, an elastic-perfectly plastic curve is used to model the post-peak behavior of the infill concrete as shown in Fig. 6.3(b).

$$f'_{cp} = f'_c \times \left(1.0 - 0.11 \left(\frac{D/t}{100} - \frac{F_y/f'_c}{9} \right) \right) \quad (6.16)$$

AISC 360-16 (2016) suggests that the tensile strength of the concrete shall be neglected in the determination of the nominal strength of composite members. Thus, the tensile strength is not considered in tensile stress-strain relationships as shown in Fig. 6.3.

6.4 Validation examples

In this thesis, six experimental tests from literature, including noncompact and slender rectangular or circular CFT members under flexure, axial compression or their combination, are selected to verify the accuracy of the proposed method in line with AISC 360-16 (2016). The strength of steel tube and concrete infill used in the tests satisfies the requirements in design code. The proposed element incorporating the effective stress-strain curves introduced in section 2 was coded into the software NIDA (2018) for this study.

6.4.1 Rectangular CFT member under axial compression

One of the tests labeled as KOM2001 under axial compression only from Kang *et al.* (2001) is studied here. Fig. 6.4 shows the section dimensions and the material properties. The member length is 0.8992 m. The width-to-thickness ratio b/t is 93.75 which is greater than the limit λ_r equal to 75.25 and therefore it belongs to a slender section. One proposed element with seven integration fiber sections is used to model this column. The meshing pattern is shown in Fig. 6.1(a) with N1 and N2 equal to 4 and 8 respectively. The behavior of each fiber is represented by one of the effective stress-strain relationship as described by Equations (6.8) - (6.16) according to the material used. The initial geometric imperfection is set as sinusoidal shape with the magnitude of 0, L/1000, L/500, L/300. The axial shortening versus axial force curves obtained from the proposed direct analysis method are shown in Fig. 6.5. The axial load P_{exp} from experimental test is also plotted by solid line.

It can be seen that when the member initial bowing is taken as 0 or L/1000, the ultimate loads are greater than the test result. Thus, the member imperfection of L/1000 recommended in AISC 360-16 (2016) will overestimate the load resistance of noncompact/slender CFT member. On the contrary, the imperfection of L/300 given in Eurocode 4 (2004) is slightly on the conservative side. The imperfection of L/500 predicts results in good agreement with the test.

6.4.2 Rectangular CFT member under flexure, combined compression and flexure

Jiang *et al.* (2013) conducted a series of tests on rectangular CFT members. The specimen S-150-2.0 is taken as an example and studied in this thesis. The section dimensions and

the material properties are shown in Fig. 6.6(a). The flexural test is conducted by four-point loading schemes as showed in Fig. 6.7(a). The member length is 2.0 m. The width-to-thickness ratio h/t is 75.0 which is greater than the limit λ_p equal to 67.34 and therefore it belongs to a noncompact section. One proposed element with seven integration fiber sections is used to simulate this CFT member. The meshing pattern is shown in Fig. 6.1(a) with N1 and N2 equal to 4 and 8 respectively. The effective stress-strain relationships presented in section 3.2 will be imposed to the fibers.

This test was also studied by Lai *et al.* (2014) using 3D finite solid elements for academic purpose. Unlike their work, one proposed flexibility-based beam-column element is used to simulate the CFT member in this thesis for practical application.

The analysis results predicted by the proposed method are plotted in Fig. 6.8(a) against the experimental results from Jiang *et al.* (2013) and the numerical results from Lai *et al.* (2014). It is no doubt that the 3D finite element model produces more accurate results because it can consider all effects but with expensive computational cost. In contrast, the proposed method provides slightly conservative results with a significant saving of computer time. The behaviors in the elastic stage are almost identical for the two numerical methods. The 3D model can well predict the hardening effect due to the restraint from the steel tube to the concrete infill while the beam-column model can capture the stiffness degradation with sufficient accuracy for practical design.

An experimental test “BRA4-2-5-02” as shown in Fig. 6.6(b) performed by Nakahara and Sakino (2000) is also studied here. Fig. 6.7(b) shows the section dimensions and the material properties. The member length is 0.6 m. The width-to-thickness ratio h/t is 98.04 which is greater than the limit λ_p equal to 84.35 and therefore it belongs to a slender section. The axial force was kept unchanged in the loading process, while the flexure was increased continuously. The fiber mesh is the same as “S-150-2.0”. In this study, one

proposed beam-column element with the initial imperfection of $L/1500$ is used to model this CFT member.

Similarly, the proposed method provides slightly conservative results compared with test results and the numerical results by Lai *et al.* (2014) using 3D solid elements, seen in Fig. 6.8 (b).

6.4.3 Circular CFT member under axial compression

Yoshioka *et al.* (1995) conducted several circular CFT column tests under axial compression. The test “CC4-D-4-1” is selected to verify the proposed method. The column length is 1.349 m, and its section sizes, as well as materials used, are shown in Fig. 6.9. The diameter-to-thickness ratio D/t is 151.45 which is greater than the limit λ_r equal to 134.86 and therefore it belongs to a slender section. Similarly, one proposed element using seven integration points is used to simulate this CFT member. The meshing pattern is shown in Fig. 6.1(b) with N_1 and N_2 equal to 4 and 8 respectively. Each fiber is associated with one effective stress-strain relationship presented in section 3.2. The initial geometric imperfection is set as a sinusoidal shape with the magnitude of 0, $L/1000$, $L/500$, $L/300$ respectively.

The axial shortening versus axial force curves obtained from the proposed direct analysis method are shown in Fig. 6.10. The axial load P_{exp} from the experimental test is also plotted by a solid line. From Fig. 6.10, the model without consideration of initial imperfection will slightly overestimate the ultimate resistance of the circular CFT member. Both the imperfections recommended in AISC 360-16 (2016) and Eurocode 4 (2004) are fair for design purpose.

6.4.4 Circular CFT member under flexure, combined compression and flexure

A circular CFT column, labeled as TB002, under flexure tested by Wheeler and Bridge (2006) is studied here. Fig. 6.11(a) shows its section dimensions as well as material properties. The loading scheme is shown in Fig. 6.12(a). The diameter-to-thickness ratio D/t is 63.44 which is greater than the limit λ_p equal to 51.43 and therefore it belongs to a noncompact section. Only one proposed element with seven integration points is needed to model this CFT member. The meshing pattern is shown in Fig. 6.1(b) with N1 and N2 equal to 4 and 8 respectively. Similarly, each fiber is simulated by one effective stress-strain relationship presented in section 3.2. Lai and Varma (2015) modeled it by 3D solid elements.

For comparison, the load-deflection curves from Lai and Varma (2015) using 3D solid elements and the experimental test are presented in Fig. 6.13(a) with the proposed results. It is found that the responses from Lai and Varma (2015) exhibits slightly stiffer than the test when the CFT member starts to yield and buckle. Also, the ultimate load from the 3D numerical simulation is higher than the test which means on the unsafe side. On the contrary, the present study shows good agreement in the elastic stage and predicts the slightly conservative result in the inelastic stage. Thus, the proposed method is more consistent and conservative and suitable for engineering design.

To further verify the proposed method, a circular CFT beam-column tested by Nishiyama *et al.* (2002) is selected as an example. The CFT member is labeled as EC4-D-4-04 and subjected to combined axial compression and flexure, seen in Fig. 6.11(b). The diameter-to-thickness ratio D/t is 152.03 which is greater than the limit λ_p equal to

134.28 and therefore it belongs to a slender section. Only one proposed element with seven integration points is needed to model this CFT member. The meshing pattern is shown in Fig. 6.1(b) with N_1 and N_2 equal to 4 and 8 respectively. The magnitude of initial geometric imperfection is $L/1000$.

Three set results are shown in Fig. 6.13(b), i.e., numerical model from Denavit and Hajjar (2012), the proposed method and the test by Nishiyama *et al.* (2002). Clearly, the present study is closer to the experimental test than Denavit and Hajjar (2012), but requires fewer computer resources. The two numerical models give slightly conservative ultimate resistance. However, both of them show stiffer behavior in the post-buckling stage.

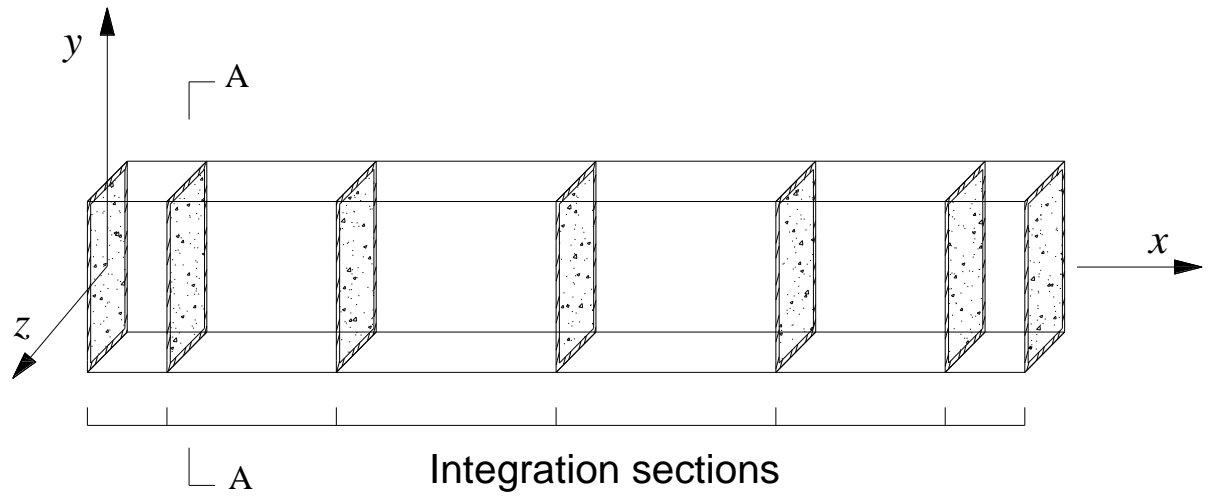
6.5 Concluding remarks

The noncompact/slender concrete-filled steel tube (CFT) members generally exhibit complex behaviors such as local buckling, concrete confinement, and slippage between the steel and concrete components. The latest AISC 360-16 firstly provides two types of methods for design of noncompact/slender CFT members. However, the reduced or effective stiffness method with P-M interaction curves only approximately captures the actual behavior of CFT members. The effective length assumption with many uncertainties is still needed in this method. For the effective stress-strain method, the recommended initial geometrical imperfection is insufficient and may bring unconservative design. In a word, the methods specified in AISC 360-16 are not fully met the requirements of direct analysis. For this reason, a comprehensive method is proposed in this thesis for a direct analysis of frame structures with noncompact/slender CFT members.

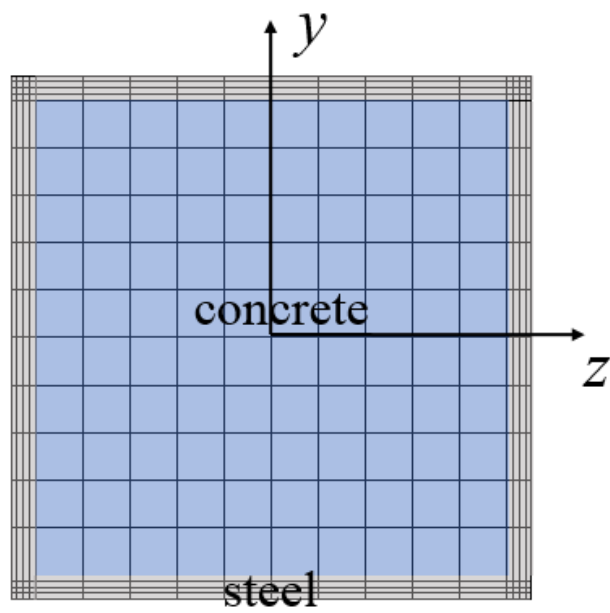
The following conclusions can be drawn from this study.

1. The flexibility-based beam-column with member imperfections and incorporating the effective stress-strain curves is capable for direct analysis of noncompact/slender CFT members.
 2. One proposed element per CFT member is adequate with excellent accuracy and a significant saving of modeling and computational cost.
 3. The effective stress-strain method can implicitly account for the complex behaviors of noncompact/slender CFT members, and therefore it forms the solid foundation for direct analysis using beam-column elements.
 4. The effective length method for flexural buckling check can be completely abandoned in the proposed direct analysis method.
 5. The initial geometrical imperfections recommended in AISC 360-16 (2016) and Eurocode 4 (2004) are on the unconservative and conservative side respectively. The imperfection of $L/500$ is recommended for noncompact/slender CFT members.
- It is also noted the effective stress-strain curves are essentially based on limited experimental and numerical tests. Thus, more test results are recommended to improve the accuracy of the effective stress-strain curves.

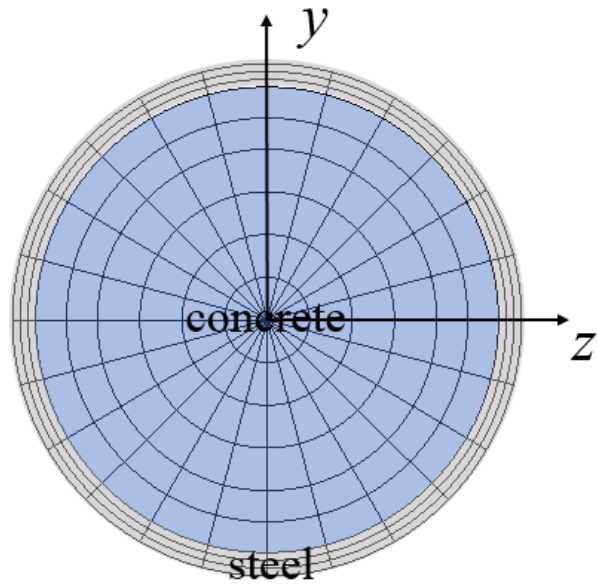
FIGURES



(a) Distributed plasticity by fiber sections

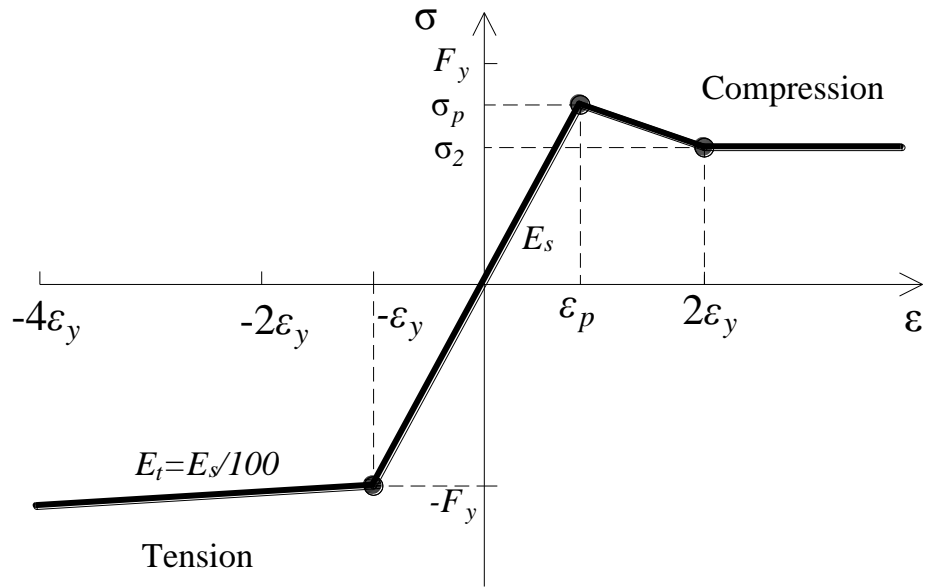


(b) A-A section for rectangular CFT member

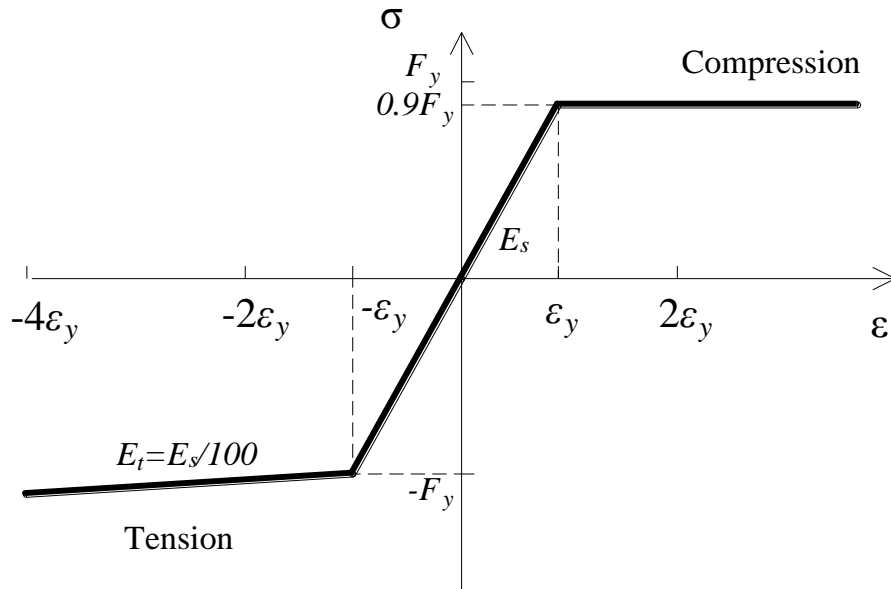


(c) A-A section for circular CFT member

Fig. 6.1. Typical fiber mesh of CFT member

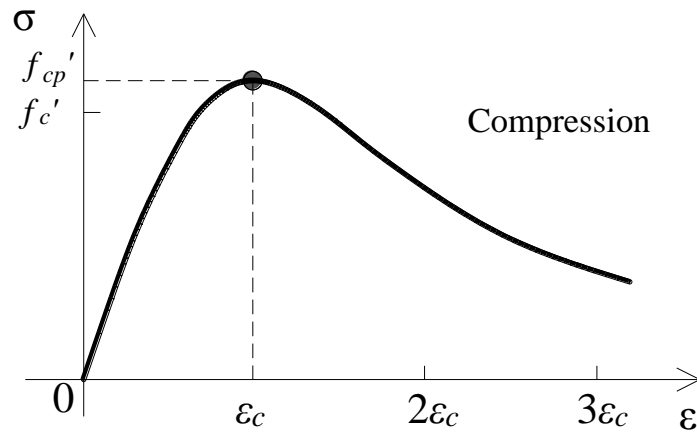


(a) For rectangular CFT members

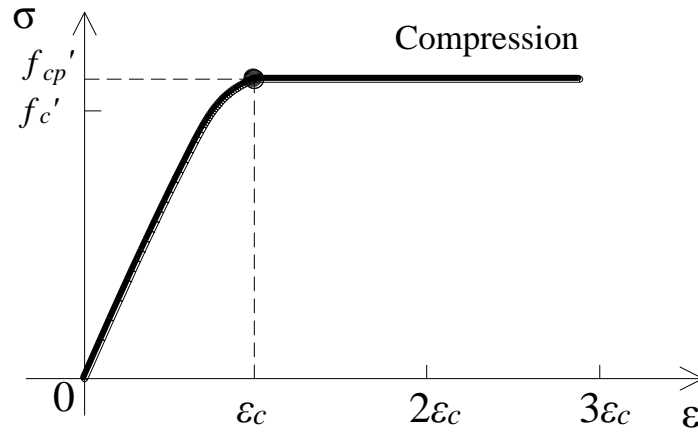


(b) For circular CFT members

Fig. 6.2. Effective stress-strain relationships for steel tube



(a) For rectangular CFT members



(b) For circular CFT members

Fig. 6.3. Effective stress-strain relationships for concrete infill

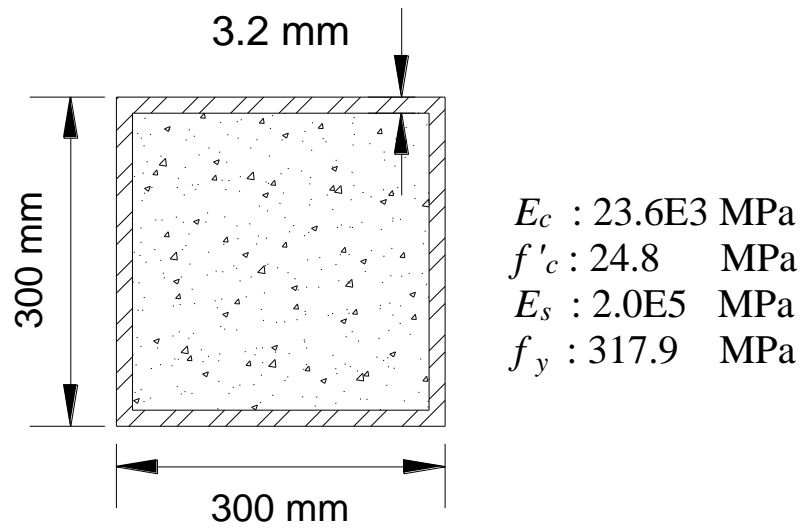


Fig. 6.4. Dimensions and material properties of KOM2001

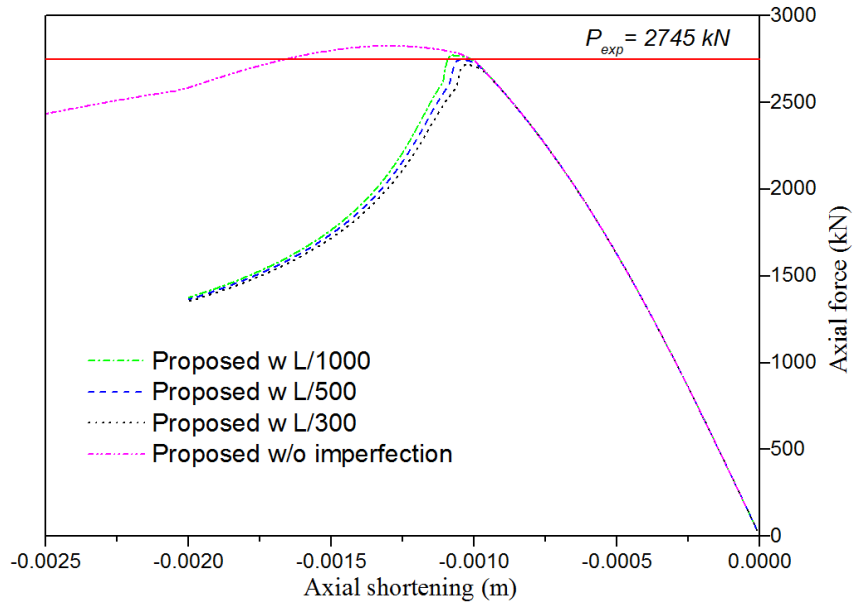
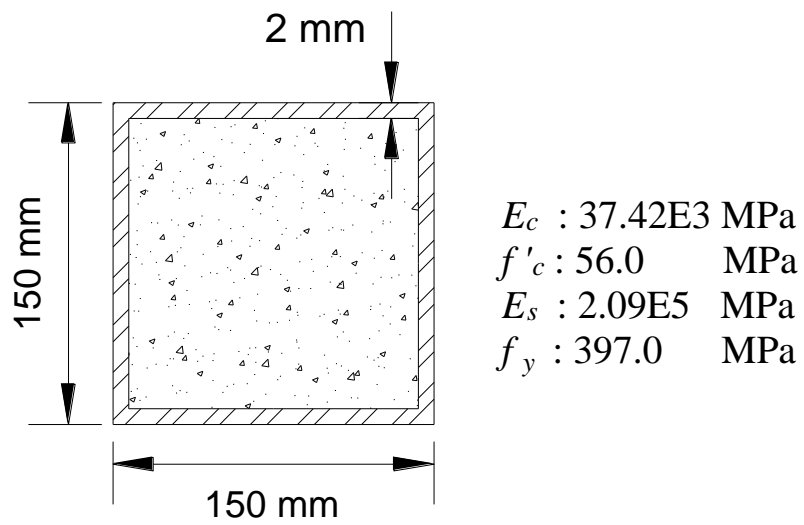
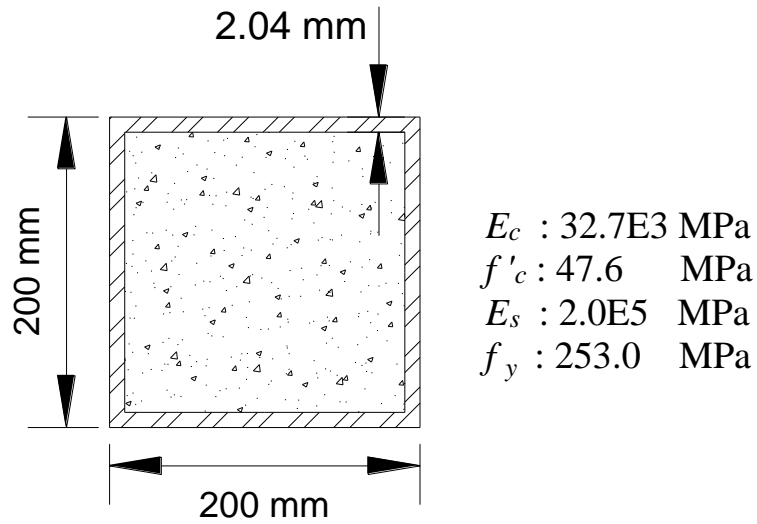


Fig. 6.5. Load-deflection curves of KOM2001

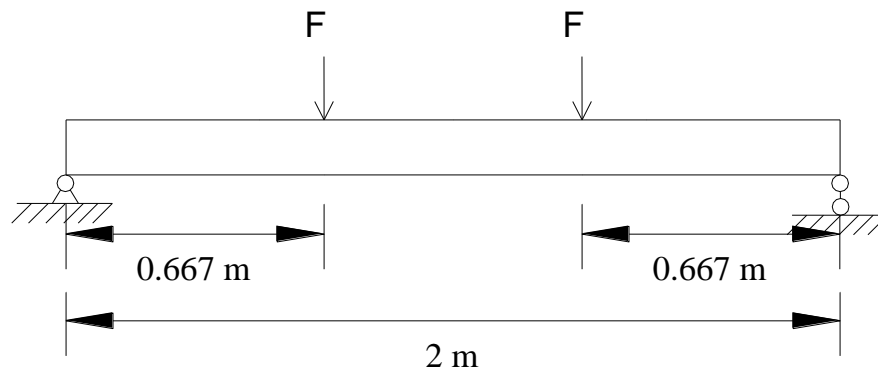


(a) S-150-2.0

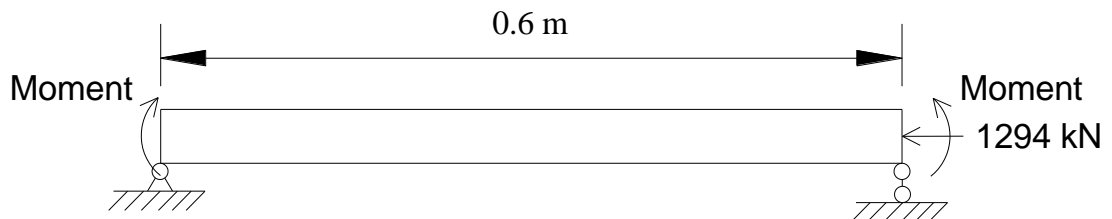


(b) BRA4-2-5-02

Fig. 6.6. Dimensions and material properties for two rectangular CFT members

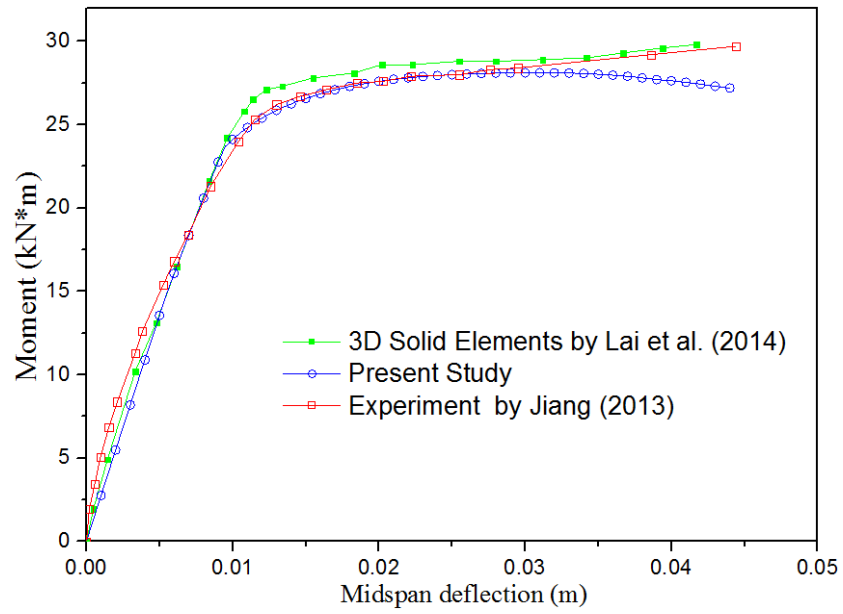


(a) 4-point loading scheme for S-150-2.0

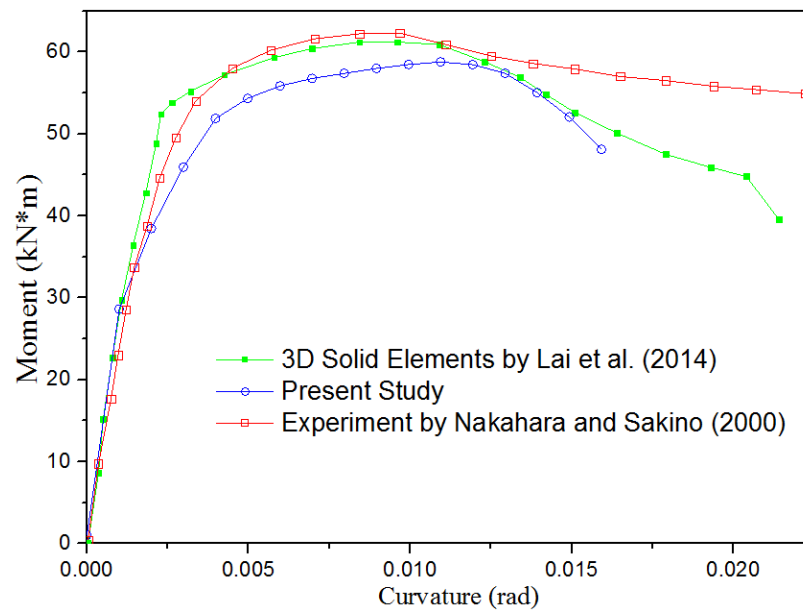


(b) Loading scheme for BRA4-2-5-02

Fig. 6.7. Layout and loading scheme for two rectangular CFT tests



(a) Mid-span deflection vs. moment



(b) Curvature vs. moment

Fig. 6.8. Load-deflection curves for S-150-2.0 and BRA4-2-5-02

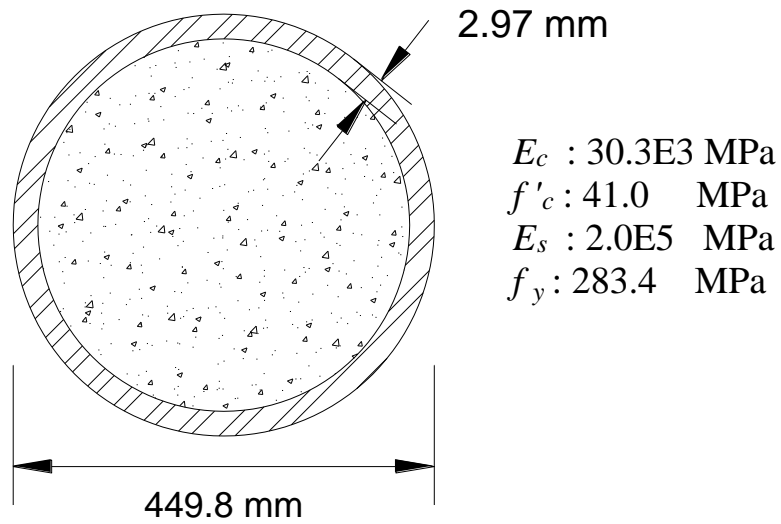


Fig. 6.9. Dimensions and material properties of CC4-D-4-1

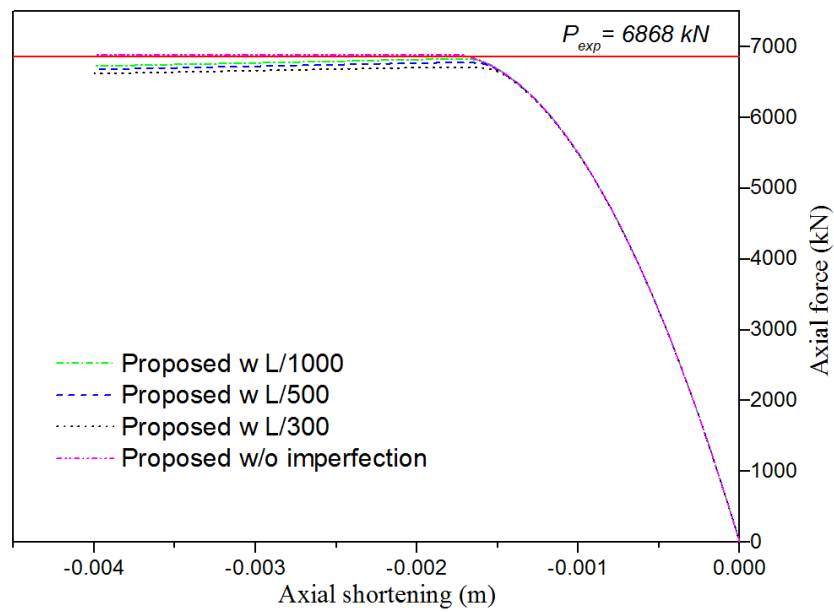
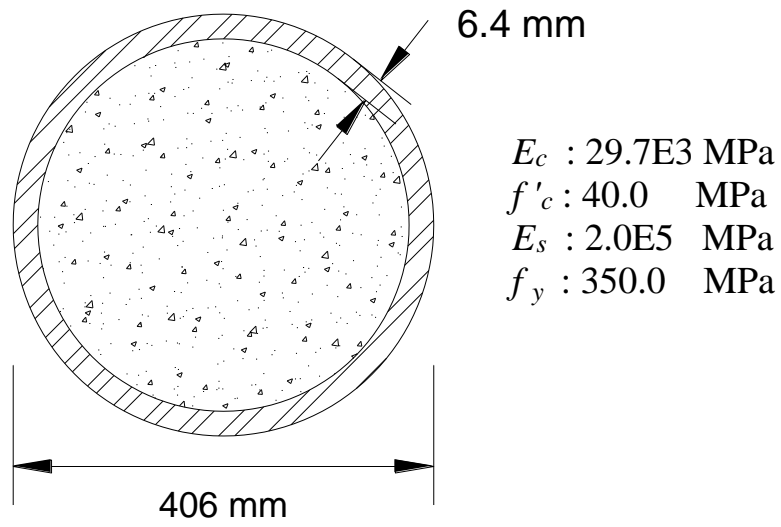
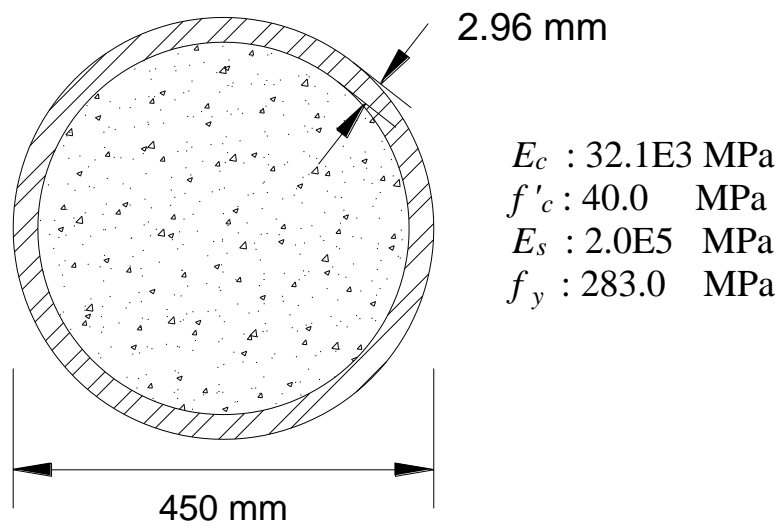


Fig. 6.10. Load-deflection curves for CC4-D-4-1

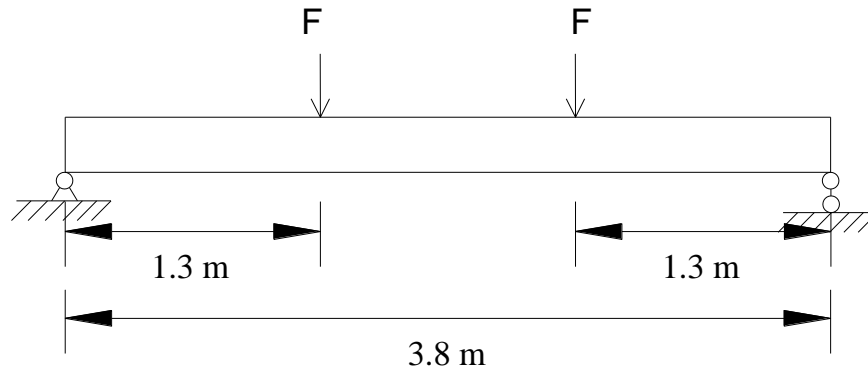


(a) TB002

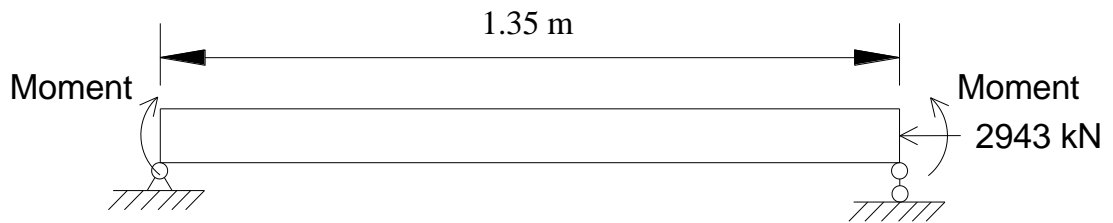


(b) EC4-D-4-04

Fig. 6.11. Dimensions and material properties for two circular CFT members

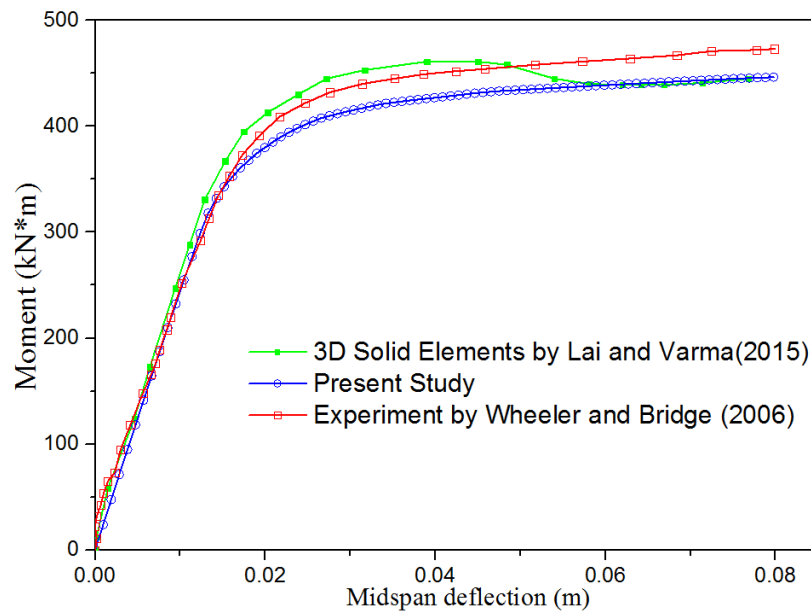


(a) 4-point loading scheme for TB002

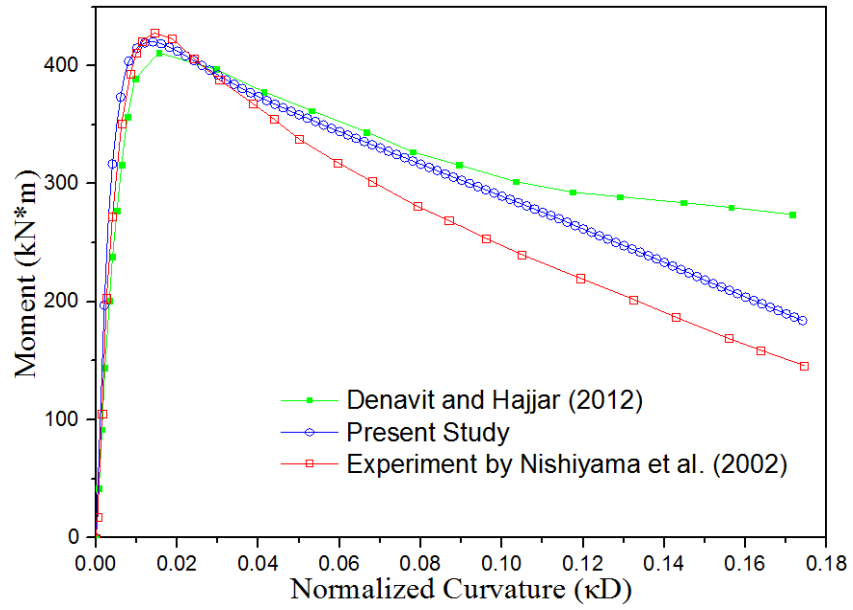


(b) Loading scheme for EC4-D-4-04

Fig. 6.12. Layout and loading scheme for two circular CFT tests



(a) Mid-span deflection vs. moment



(b) Curvature vs. moment

Fig. 6.13. Load-deflection curves for TB002 and EC4-D-4-0

TABLES

Table 6-1 Classification of steel elements in composite members in AISC 360-16

(2016)

Loading status	Shape of steel tube	Width-to thickness ratio	λ_p compact/noncompact	λ_r noncompact/slender	Maximum permitted
Axial Compression	Rectangular HSS or box sections of uniform thickness	b/t	$2.26 \sqrt{E_s/F_y}$	$3.00 \sqrt{E_s/F_y}$	$5.00 \sqrt{E_s/F_y}$
	Round HSS	D/t	$0.15E_s/F_y$	$0.19E_s/F_y$	$0.31E_s/F_y$
Flexural	Rectangular HSS or box sections of uniform thickness	b/t	$2.26 \sqrt{E_s/F_y}$	$3.00 \sqrt{E_s/F_y}$	$5.00 \sqrt{E_s/F_y}$
	Round HSS	h/t	$3.00 \sqrt{E_s/F_y}$	$5.70 \sqrt{E_s/F_y}$	$5.70 \sqrt{E_s/F_y}$
		D/t	$0.09E_s/F_y$	$0.31E_s/F_y$	$0.31E_s/F_y$

Table 6-2. Definitions of c_p and c_m in AISC 360-16 (2016)

Section Shape	c_p	c_m	
		When $c_{sr} \geq 0.5$	When $c_{sr} < 0.5$
Rectangular	$\frac{0.17}{c_{sr}^{0.4}}$	$\frac{1.06}{c_{sr}^{0.11}} \geq 1.0$	$\frac{0.90}{c_{sr}^{0.36}} \leq 1.67$
Circular	$\frac{0.27}{c_{sr}^{0.4}}$	$\frac{1.10}{c_{sr}^{0.08}} \leq 1.0$	$\frac{0.95}{c_{sr}^{0.32}} \leq 1.67$

CHAPTER 7. DIRECT ANALYSIS OF SPECIAL CONCENTRICALLY BRACED FRAMES

7.1 Introduction

Special concentrically braced frames (SCBFs) are extensively employed in high seismicity regions due to structural efficiency and particularly high ductility for energy dissipation through tensile yielding, buckling and post-buckling behaviors of braces. The commonly used configurations of SCBFs are shown in Fig. 2.2. The inverted V-bracing configuration is most welcomed for easy accommodation of doors and windows. Generally, the bracing systems should be designed in pairs to account for tension and compression in both directions. The SCBFs with properly detailed connections can meet various performance levels for performance-based seismic design. The shape of steel brace could be rectangular, square or circular hollow section and H-shape section.

Many experimental tests have been conducted to study the behaviors of isolated components such as braces and gusset plate connections, and the system performance of SCBFs. Fell *et al.* (2009) experimentally investigated the inelastic buckling and fracture behavior of steel braces including square hollow section, pipe and wide-flange H-shape section. Tremblay *et al.* (2003) validated the effective brace slenderness adopted in the design and proposed an empirical model to predict brace fracture by testing fourteen single braces and ten X-braces. Han *et al.* (2007) examined energy dissipation capacity of braces with different width-thickness ratios by quasi-static reversed cyclic experiments. Lehman *et al.* (2008) conducted several full-scale tests of one-story one-bay SCBFs to evaluate the economy and performance of gusset plate

connections. Palmer *et al.* (2012) investigated the seismic behavior of a two-story, one-bay by one-bay frame. Lumpkin *et al.* (2012) explored the seismic response of two three-story SCBFs and proposed several recommendations for enhancing ductility of SCBFs. In summary, the experimental tests provide valuable information for the codified design of SCBFs and motivate the researchers to develop and improve their analytical models so that the routine design should not merely rely on experimental tests which are limited to many idealized conditions.

Extensive works have been carried out on the numerical modeling of braces as well as their connections linking to the framing beams and columns. The researchers attempt to accurately predict the cyclic strength and stiffness deterioration of structural components. The typical structural behavior and the potential failure locations of a single brace are shown in Fig. 2.3. Significant yielding and local plate buckling behaviors are commonly observed. There are four numerical methods proposed for simulation of SCBFs, i.e., phenomenological model (Nilforoushan, 1973), simplified phenomenological model (Soroushian, 1988), fiber-type finite element model (Gunnarsson, 2004) and continuum finite element model (Haddad and Tremblay, 2006). Uriz (2005) pointed out the limitation of the traditional phenomenological model in predicting peak responses of steel braces and proposed a brace component model which can well simulate the post-buckling and fracture of steel braces under cyclic loading. However, his analytical model required several elements to model a brace and introduced a small initial camber which does not fully comply with the code requirement to trigger buckling. Yoo *et al.* (2008) used continuum finite element (FE) model to investigate the behavior of gusset plate connection and the interaction between the connection and framing elements. They pointed out that the proper detailing of gusset plate connection can improve the performance of SCBFs. Uriz and

Mahin (2008) proposed a force-based fiber element to represent the gusset plate connection while Hsiao *et al.* (2012) introduced rotational hinges attached to ends of the beam-column element to model the connections. Their model employed several different types of elements in series to model a brace with end connections which leads to an impractical model for daily use. Generally speaking, the previous researches (Hsiao, 2012, 2013; Karamanci, 2014; Krishnan, 2010; Uriz, 2005) clearly show that the initial curvature of steel braces should be taken into account so that the buckling and post-buckling behavior of steel braces can be captured in numerical analysis. Consequently, several elements per member are compulsively required to simulate the complex behavior of braces. The calibration works with experimental test results can be found in references (Hsiao, 2012, 2013; Karamanci, 2014; Krishnan, 2010). Although Krishnan (2010) has proposed a modified elasto-plastic fiber element, which consists of three fiber segments formed by two external nodes and four internal nodes, to simulate the inelastic behavior of slender columns and braces, it is essential a multi-element per member model (MEPMM) which cannot truly reduce the computer time. The MEPMM not only increases the modeling effort, but also occupies more computer resources, especially in the nonlinear dynamic analysis (NDA, also well known as time history analysis). Most importantly, MEPMM becomes more prone to induce numerical problems when a plastic hinge is formed at the member mid-span in such case the stiffness matrix of the associated node approaches singular. Thus, one-element per member model (OEPMM) is preferred in practical applications.

Theoretically speaking, the three-dimensional solid elements or two-dimensional shell elements can produce more accurate responses for both the components and the SCBF system. However, the two types of finite elements are rarely adopted in a global analysis of engineering structures owing to time-consuming and inconvenience in

codified design. A number of displacement-based beam-column elements (Chan, 1995, 2000; Liu *et al.* 2014) with concentrated plastic hinge method have been proposed for second-order inelastic analysis. Although the elements can account for member initial geometric imperfection, their application on inelastic analysis face challenges because of the inherent shortcomings of displacement-based elements and concentrated plastic hinge assumption. To obtain more accurate results, more elements for the member undergoing significant buckling and plastic behavior such as the braces in SCBFs are inevitably required. Du *et al.* (2017) firstly proposed a flexibility-based beam-column element with initial geometric imperfection for second-order inelastic analysis. However, their work does not take the residual stress, semi-rigid connection, and rigid end-offset into account and therefore their outcome cannot be directly used for the design of SCBFs.

From the above, it can be seen that more efforts are needed to narrow the gap between the research and practical design on SCBFs. First, the previous models required multi-elements per member as well as individual elements for gusset plate connections and rigid end zone. Hence, the models generally lead to more modeling and computational efforts and numerical convergent problem. Second, the influence of initial geometric imperfection and residual stress has not been properly considered in the analysis, and therefore the design of SCBFs may be on the unsafe side. It is also noted that the direct analysis method (DAM) which is well specified in the modern design codes such as AISC360 (2016), Eurocode-3 (2005) and COPHK (2011). However, these codes have not been well linked to the seismic design codes. Thus, this thesis aims to provide a comprehensive solution for the seismic design of SCBFs and, simultaneously, extends the DAM to nonlinear dynamic analysis (NDA) to achieve a consistent design practice.

In this thesis, the element FBMI allowing member initial bowing proposed by Du *et al.* (2017) based on Hellinger-Reissner (HR) functional is modified into a new hybrid element for second-order dynamic analysis of SCBFs. This innovative element considers member initial geometric imperfection, residual stress, finite joint stiffness and rigid end zone at the element level for three-dimensional frame analysis. The proposed element inherits the high accuracy of the original element with consideration of progressive yielding in cross section and along the member length. Fiber section approach is adopted to account for member distributed plasticity with the inclusion of residual stress which has not been reported in the previous SCBFs models. Moreover, the semi-rigid connection technique in the literature was mainly proposed to the beam ends dominated by bending moment and as a result, the influence of axial force on the connection can be ignored. Thus, this conventional method will be improved here as the braces in SCBFs undergo considerably large axial forces.

The layout of this chapter is as follows: the element FBMI allowing member initial imperfection is briefly introduced in section 7.2; the semi-rigid connection technique as well as the treatment of rigid end zone is presented in section 7.3; the material model and residual stress pattern are shown in section 7.4; the comprehensive modeling of SCBFs and the verification works will be presented in section 7.5 and 7.6 respectively. Finally, the conclusions with highlights of this study and several recommendations for SCBF modeling will be made.

7.2 Semi-rigid connection and rigid end zone for gusset plate connections

The gusset plate connection, as an important component of SCBFs connecting brace to beam and column, transfers the axial force and bending moments between the brace and the framing system. It needs to be carefully designed with proper stiffness to tolerate the end rotation of the brace and sustain less damage before the brace fracture. The change of the gusset plate stiffness affects the end conditions of the brace and consequently influences the buckling resistance of the brace. More importantly, the gusset plate connection absorbs a portion of energy from ground motion by hysteretic behavior. Thus, it is worth to capture these features in the analytical model of SCBFs to have a better prediction of SCBFs' behaviors.

Mathematically, a semi-rigid connection can be introduced to reflect the behavior between a brace and a gusset plate connection. To reflect the actual length of the gusset plate connection and the physical length of brace, a rigid zone will be introduced at the end of a brace. The former one technique has been introduced in Chapter 3. The latter one will be incorporated into the proposed FBMI element to form a hybrid element for nonlinear dynamic analysis (NDA) of SCBFs with significant improvement of result accuracy and enhancement of numerical efficiency.

7.2.1 Semi-rigid behavior of gusset plate connection

The bi-linear $M-\theta$ model is widely used in frame analysis to consider semi-rigid behavior for simplicity. To more accurately reflect the hysteretic response of the gusset plates under cyclic loading or strong ground motions, more sophisticated model should be adopted in the design of SCBFs. In this thesis, the $M-\theta$ function of gusset plate connection proposed by Hsiao (2012) with calibration of experimental test results and

the continuum finite element analysis by Yoo (2006) is adopted, as illustrated in Fig. 7.2. The rotational stiffness in elastic stage and the associated bending moment can be calculated as,

$$R_e = \frac{E}{L_{ave}} \left(\frac{W_w t_p^2}{12} \right) \quad (7.1)$$

$$M_y = \left(\frac{W_w t_p^2}{6} \right) F_{y,g} \quad (7.2)$$

in which, E is elasticity modulus; W_w is the whitmore width defined by a 45° projection angle; L_{ave} is the average of L_1 , L_2 , L_3 as shown in Fig. 7.1; t_p is the thickness of the gusset plate; and $F_{y,g}$ is the yield strength.

The beam-to-column shear tab connections are commonly adopted in SCBFs. The semi-rigid behavior of this type of connections can be represented by the multi-linear $M-\theta$ functions proposed by Liu and Astanek-Asl (2004). In their models, the contribution of floor slab can also be considered. More details about the semi-rigid models can be referred to the original reference (Liu and Astanek-Asl, 2004).

7.2.2 Rigid end zone of gusset plate connection

As indicated in Fig. 7.1, the portion of the gusset plate near to the end of the brace is simulated by semi-rigid connection as presented in last sub-section. The remained portion of the gusset plate connected to framing system, undergoing negligible in-plane deformation compared to other deformations of the SCBF, generally exhibits rigid behavior. Thus, a rigid end offset from the intersection point of the beam-to-column connection to the physical end of the brace can be assumed to reflect the gusset plate connection's actual length. Consequently, the nodal displacement vectors \mathbf{D}_i of the intersection point of the beam-to-column connection can be transformed into the physical end of the brace or the other end of the rigid zone as

$$\mathbf{D}_p = \begin{bmatrix} u \\ v \\ w \\ \theta_x \\ \theta_y \\ \theta_z \end{bmatrix}_p = \mathbf{E}_i \mathbf{D}_i = \begin{bmatrix} 1 & 0 & 0 & 0 & 0 & 0 \\ 0 & 1 & 0 & 0 & 0 & e_i \\ 0 & 0 & 1 & 0 & -e_i & 0 \\ 0 & 0 & 0 & 1 & 0 & 0 \\ 0 & 0 & 0 & 0 & 1 & 0 \\ 0 & 0 & 0 & 0 & 0 & 1 \end{bmatrix} \begin{bmatrix} u \\ v \\ w \\ \theta_x \\ \theta_y \\ \theta_z \end{bmatrix}_i \quad (7.3)$$

in which, \mathbf{D}_p is the displacement vector for brace and gusset plate connection; e_i is the distance of the rigid zone between the node i and the associated physical end of the brace.

From the above, the stiffness matrix of the proposed FBMI considering semi-rigid behavior and rigid end zone should be modified as

$$\mathbf{K}_T = \mathbf{L} \mathbf{E}^T (\mathbf{T}^T \mathbf{K}_c \mathbf{T} + \mathbf{N}) \mathbf{E} \mathbf{L}^T \quad (7.4)$$

$$\mathbf{E} = \begin{bmatrix} \mathbf{E}_i & \mathbf{0} \\ \mathbf{0} & \mathbf{E}_j \end{bmatrix} \quad (7.5)$$

in which, \mathbf{K}_c is the stiffness matrix combined with both the brace and the gusset plate connections; \mathbf{E} is the eccentricity transform matrix considering the rigid end zones at two ends. Thus, the stiffness matrix of the hybrid beam-column element as indicated in Fig. 7.1 can be calculated.

7.3 Material representation and residual stress

7.3.1 Material representation

The material representation in the analytical model of SCBFs should be able to capture the typical behaviors of the braces such as buckling, tensile yielding, post-buckling, fracture, and post-fracture. Generally, the multi-axial materials with complex yield criterion are used in continuum finite element models while the uni-axial materials are preferred in the fiber-based frame analysis.

In this thesis, the distributed inelasticity method based on fiber discretization of the cross-section at the integration points along member length is used to simulate the nonlinear material behavior of SCBFs. The spread of yielding is represented through the integration of material responses of fibers over the cross-section. The material of each fiber can be modeled by a uni-axial material, for example, elastic-perfectly plastic material or Giuffr -Menegotto-Pinto hysteretic material (1983). The latter without a sudden change of stiffness is widely adopted in nonlinear analysis, and the transitional portion from elastic to plastic state is given in Equation (7.6) below.

$$\sigma^* = b\varepsilon^* + \frac{(1-b)\varepsilon^*}{(1+\varepsilon^{*R})^{\frac{1}{R}}} \quad (7.6)$$

in which, σ^* and ε^* are the normalized stress and strain respectively; b is the strain hardening ratio between the post-yield tangent and initial elastic tangent; R is the parameter to adjust the shape of the transition curve and should be determined by parameters R_0 , a_1 and a_2 during the cyclic loading to reflect the Bauschinger effect. More details about this material model can be referred to Filippou *et al.* (1983). The preferred failure mode of SCBFs is brace fracture (Hsiao, 2013) as the braces are designed to absorb energy during the earthquake and can be replaced more easily after the earthquake. To capture the fracture effect, the proper fracture material should be selected for the braces. Several fracture material models for braces have been proposed to predict brace behavior. They can be classified into two types based on the response at global level or at local level. For the first one, Lee and Goel (1987) suggested to use an equivalent number of cycles for fracture evaluation. The second one is based on the strain or stress state of braces. Hsiao *et al.* (2013) pointed out that the rupture of braces due to fatigue is correlated to the maximum strain range. For this reason, the

macroscopic fatigue of braces can be simulated through the modified material constitutive model incorporated with fracture criterion as shown in Fig. 7.3.

In summary, the Giuffré-Menegotto-Pinto hysteretic uni-axial material (1983) with consideration of brace fracture proposed by Hsiao *et al.* (2013) is adopted in the proposed analytical model of SCBFs so that the hysteretic behavior of braces can be well predicted. The examples in section 6 will illustrate the validation and accuracy of the proposed method in the design of SCBFs.

7.3.2 Residual stress

Residual stresses always exist in both hot rolled and welded steel members. Residual stresses are self-equilibrium in a member or a component and may come from rolling, cold forming and welding process. The distribution and magnitude of residual stress vary for different types of cross-sections. Typically, the center part of the flange of an I- or H-section is in tension while the remained part of the flange is in compression. For a rectangular hollow section (RHS), the residual stresses at the four corners are in tension while the other portions are in compression. The residual stress patterns for hot rolled square hollow section (SHS) and H-shape section shown in Fig. 7.4 are well-recognized and will be adopted in this study.

The residual tensile stresses at the corners of SHS or RHS will speed up premature fracture of braces while the residual compressive stresses at the center parts will reduce the brace buckling resistance. For this reason, residual stresses are vital in the accurate modeling and practical design of SCBFs. It is found that the influence of residual stress has been generally ignored in previous researches as a result the design may be inadequate.

In this thesis, the residual stresses of frame sections are explicitly modeled and directly incorporated in the analysis through the fiber discretization technology. Initial strain corresponding the residual stress following Fig. 7.4 will pre-set in each fiber. The total stress of each fiber is equal to the sum of the residual stress and the load-induced stress. The tangent stiffness and fracture behavior are determined by the total stress using Giuffré-Menegotto-Pinto material incorporated with the fracture criterion proposed by Hsiao *et al.* (2013). Thus, the actual highly nonlinear behavior of the braces can be well captured.

7.4 Analytical model for SCBF system

A SCBF system dissipates the energy from earthquake through (1) the yielding, buckling and fracture of brace, and (2) yielding of connections and beams. In the point of view of common design practices, the yielding and buckling of columns is not preferred so that the risk of progressive collapse could be minimized. To accurately predict the behavior of SCBF systems, a reliable and efficient analytical model is proposed as shown in Fig. 7.5(b) for practical seismic design of SCBF building, using the technologies described in the above sections. Clearly, the proposed model in Fig. 7.5(b) is much simpler than the conventional one in Fig. 7.5(a). This innovative solution significantly narrows the gap between the academic researches and the engineering applications. The proposed hybrid beam-column element was implemented in the program NIDA (2018) for this study. This new element considers initial geometrical imperfections, residual stress, connection behavior and distributed inelasticity such that a safer and economical design can be obtained.

The national design codes such as AISC360 (2016), Eurocode-3 (2005) and COPHK (2011) highly recommend the direct analysis method (DAM) which requires to

consider initial geometrical imperfections and residual stress so that the member buckling behavior can be directly reflected in the analysis stage rather than separately in the design stage. When using the DAM, the effective length for individual member check is no longer required as the second-order $P-\Delta$ and $P-\delta$ effects have been considered during the analysis process and as a result, only the section capacity check is needed. It should also be pointed out that the local joint behavior should be carefully captured in the analysis if the joint like the gusset plate connection of SCBFs significantly affects the load distribution of the structural system according to the requirement of DAM. However, the DAM is rarely adopted in the seismic design. To some extent, it is because the two design theories were developed and improved in a parallel manner. If the behaviors of members and connections cannot be well represented in the nonlinear dynamic analysis (NDA), the responses for identifying plastic hinges may be inaccurate, and consequently, the more realistic responses of the structural system cannot be predicted which lead to an unsafe design. Being aware of the above, this thesis aims to promote the DAM to seismic design using NDA so that a consistent design method linking the static and dynamic design together can be provided for design office.

The modeling details for braces, gusset plate connections, beams and columns in SCBF system will be introduced in this section. The features and advantages of the proposed model will be highlighted and discussed as followings.

7.4.1 Modeling of beams and columns

In the conventional nonlinear dynamic analysis (NDA), the initial geometrical imperfections and residual stresses, which are inherent in the steel beams and columns, have generally been overlooked. It should be pointed out that the $P-\delta$ effect

associated with member bowing deformation has been partly included in the NDA if a beam-column element with six degrees of freedom per node rather than a truss element is used. When using the effective length method based on undeformed configuration and initial elastic stiffness to check individual member stability, it will bring an inconsistent design.

In this thesis, the proposed FBMI beam-column allowing for the rigid end zone as shown in Fig. 7.5 will be used to model beams and columns. Compared with the conventional NDA, the significant improvement is that one element is adequate to model a steel member (beam or column). Extensive verification works of the element can be referred to Du *et al.* (2017). This will highly enhance the numerical efficiency and greatly reduce the computational expense. By contrast, several elements were used for a beam and a column in Hsiao's modeling (2012) which means more computer time required.

When using the proposed element to model a beam or a column, the length of the rigid end zone at both ends, L_l and L_r can be determined by the connection type. The joint flexibility can also be considered if the associated connection is neither fully rigid nor ideally pinned. Fiber-based approach is employed to monitor the plasticity development of the cross sections at the integration points. The material described in section 4.1 will be used for both beams and columns.

The design codes consider the initial geometrical imperfection and residual stress of steel members in two different ways. In Eurocode-3 (2005) and COPHK (2011), all sources of imperfections will be integrated into an equivalent geometrical imperfection. It should be noted that the amplitude of the initial bow imperfection for a section in a given direction is different in second-order elastic and plastic analysis. Larger initial bowing should be used in the second-order plastic analysis which causes

inconvenience as many members may remain elastic during inelastic analysis. On the contrary, AISC360 (2016) recommends to consider the two sources of imperfections separately. Generally speaking, the former is more welcomed in the stiffness-based beam-column elements with plastic hinge method while the latter is more suitable for flexibility-based beam-column elements with distributed plasticity. In this thesis, the latter will be adopted so that more accurate responses of SCBFs can be obtained.

7.4.2 Modeling of brace and gusset plate connection

The gusset plate connections in SCBFs should be properly designed with detailing requirements specified in AISC341 (2016) so that the brace fracture occurs first and then the connection ruptures. The failure of gusset plate connection early before brace fracture is undesirable as the SCBF will absorb less energy in this situation. The gusset plate connections play an important role in SCBF system, and therefore their behavior should be well represented in the analytical model.

Like the beams and columns, the initial geometrical imperfections and residual stress of braces should be included in the analytical model so that the brace yielding, buckling, and fracture can be precisely captured.

In this thesis, one proposed hybrid element based on FBMI beam-column with rigid end zone, zero-length end spring and initial imperfections is adequate to model a brace with two associated gusset plate connections. Rigid end zones are placed at both ends of the element to reflect the length of connection while two zero-length end springs located between the rigid end zone and the brace are used to simulate the semi-rigid behavior of the gusset plate connections. The associated technologies are described in section 3. The remaining middle part of the element is the actual length of the brace and the fiber-based approach is employed to trace its stability and distributed plasticity.

7.4.3 Highlights of the proposed analytical model

Generally, the proposed analytical model is one of the fiber-type FE (finite element) models with the advantages and disadvantages against other approaches discussed in section 1. However, the proposed model has unique features over other fiber-type FE models. For example, Hsiao *et al.* (2012) proposed a line-element model for SCBFs as shown in Fig. 7.5(a). In their model, an individual link element is required to model the rigid end zone at the end of beam, column or brace; a one-node spring element should be inserted between the link element and the element for brace; several conventional flexibility-based elements without initial geometrical imperfections and residual stress are needed for each beam, column, and brace. To achieve an accurate prediction on brace behavior, ten or more conventional flexibility-based elements are generally required as their element is unable to consider local second-order $P-\delta$ effect as well as initial imperfections. Otherwise, the compressive buckling of the brace cannot be captured.

By contrast, the proposed model requires only one element per member (beam, column, and brace) considering finite joint stiffness. The hybrid element with initial imperfection and semi-rigid connection at the element level not only significantly improves the computational efficiency (especially in nonlinear dynamic analysis) but also effectively alleviates the numerical problems due to the formation of plastic hinge at mid-span, in which the stiffness matrix of the associated node approaches singular when using multi-element per member modeling like Hsiao *et al.* (2012). In such case, an analysis may be terminated due to poor stiffness at the node with plastic hinge, and as a result, the engineer cannot get the whole responses of SCBF building. Also, one-element-per-member modeling is widely accepted in daily design using linear

approach, and therefore the proposed method can significantly reduce modeling efforts but provide an accurate response. The analysis results are directly complied with code requirements, and therefore the individual member check is no longer required. Thus, this is an innovative solution for the seismic design of SCBFs in line with the spirit of direct analysis method (DAM).

7.5 Numerical examples

7.5.1 A single HSS brace subjected to cyclic loading

Fell *et al.* (2009) conducted 18 large-scale tests of special bracing members. The specimen HSS1 made of HSS101.6x101.6x6.4 with a clear presentation of force-drift curve for comparison purpose is selected in this study to validate the proposed hybrid beam-column element. The setup, loading protocols, and dimensions are shown in Fig. 7.6 and Fig. 7.7. The wall thickness of the brace is 6.4 mm while the thickness of gusset plate is 12.7 mm. The hysteretic material response was represented by the Giuffr -Menegotto-Pinto model, with elasticity modulus of 2×10^5 MPa, the yield stress of 450 MPa, and hardening ratio of 0.1%. The drift demand is in relation with the axial deformation of the brace and their conversion can be referred to Fell *et al.* (2009).

As mentioned in previous sections, the end conditions due to flexible connection, initial geometrical imperfection and residual stress in brace should be taken into account for advanced design of SCBFs. Totally four models with different considerations given in Table 7-1 are built to study these factors affecting the brace behavior. For models 1 to 3 (denoted as M1 to M3), both the geometrical imperfection and residual stress are considered. Only the boundary conditions are different so that

the influence of joint flexibility can be clearly observed. For model 4 (denoted as M4), only the geometrical imperfection is considered so that the influence of residual stress can be clearly observed. For all cases, only one proposed hybrid element is used to simulate the single brace. All analysis results are compared with the experimental result from Fell *et al.* (2009), as seen in Fig. 7.8(a-d).

7.5.2 A one story-one bay SCBF

In this example, a one-story one-bay SCBF with chevron configuration of braces is studied, as seen in Fig. 7.9. The gusset plate connection is a tapered plate with thickness of 35 mm and depth of 1245 mm. The framing members (beam and columns) and braces are modeled by one proposed hybrid element per member. The initial geometrical imperfection of brace is assumed as $L/1000$, in which L is the member physical length. The moment-rotation curve is determined by the method proposed by Hsiao (2012) and reproduced in Fig. 2.2(b). For all steel members, the material is assumed as Giuffré-Menegotto-Pinto constitutive model, with the elasticity modulus equal to 2×10^8 kN/m² and hardening ratio equal to 0.003. The yield stresses are taken as 344.74 kN/m² and 317.16 kN/m² for framing members and braces respectively. The earthquake wave Superstition Hills-01 (1987) is used as input for this study.

For comparison, the analysis result by the model recommended in OpenSees (2000) using 10 displacement-based elements per member is presented here. The material model and the moment-rotation curve for the gusset plate connections are same as those in the proposed model. The rigid end zones need to explicitly model by rigid link element in OpenSees (2000). To consider the initial geometrical imperfection of $L/1000$, the coordinates of the nodes along the members should be modified to suit the

half-sine shape. Totally, there are 11 nodes for one brace in the OpenSees model while only 2 nodes for one brace are required in the proposed model.

For fair comparison regarding computational efficiency, the two models will be run in the same personal computer with an Intel® Core™ i7-3770 CPU of 3.4 GHz and 16.0 GB RAM.

The computer time of the proposed model is 29 seconds, while the OpenSees model costs 67 seconds. The base shear versus story drift curves of the SCBF obtained from the two sets models are shown in Fig. 7.10. It can be seen that the result from present study shows good agreement with that OpenSees model which requires multi-element per member.

From this example, the proposed method shows high accuracy with significant enhancement of computational efficiency. An important aspect to be highlighted is that the modeling effort has been greatly reduced as engineers need not divide a brace into a number of elements with modification of node coordinates to account for initial geometrical imperfection.

7.5.3 A single-story frame with a single brace

A full-scale test of a one-story, one-bay frame was conducted by Lehman *et al.* (2008) at the University of Washington, as seen in Fig. 7.11. The steel sections are W12x72, W16x45 and HSS5x5x3/8 for the columns, beams and brace respectively. The thickness of gusset plate is 9.53 mm. Fig. 7.12 shows the analytical model by the proposed method.

A pair of 1557 kN axial loads, to simulate gravity loads from upper stories, were applied on the top joints of the columns. Asymmetry drift history shown on Fig. 7.13 was applied on the top joint of left column in the horizontal direction.

This experiment has been studied by Yoo *et al.* (2008) with continuum FE models and Hsiao *et al.* (2012) with multi-line elements. Unlike their methods, only one proposed hybrid element per member will be used to predict the structural response of the frame in this thesis. In the proposed model, the square hollow structural section and the wide flange sections are discretized with 208 and 96 fibers respectively. The initial sinusoidal out-of-straightness with maximum amplitude δ_0 of $L/1000$ as well as residual stress is included. The $M-\theta$ functions of gusset plate and beam-column connections are determined by method presented in section 3.1. In each element, seven Gauss-Lobatto integration points are used to form the flexibility matrix in Equation (3.39).

The drift ratio versus lateral force hysteretic curve obtained from this study is plotted in Fig. 7.14 against experimental test result. It is evident that the result of the proposed method agrees well with the experimental measurement in a wide range. Both the compressive and tensile behaviors of the brace can match the test result except the brace approaching fracture, at which the brace suffered significant local buckling. This can be further improved if a more refined material fracture model is available.

7.5.4 A three-story one-bay frame

As shown in Fig. 7.15, a three-story one-bay SCBF was experimentally tested by National Center for Research on Earthquake Engineering (NCREE) in Taiwan, and the Universities of Washington (UW), California, and Minnesota (2012). This frame was designed with the balance design procedure proposed by Roeder *et al.* (2011). The configuration and layout of the frame with steel sections used are shown in Fig. 7.16. All braces are HSS5x5x3/8 with gusset plate of 10 mm. Fig. 7.17 shows the

cyclic, pseudo-static, displacement-controlled loading protocol, which was applied on the intersection joint of braces at the top level.

Similarly, only one proposed hybrid element per member will be used to predict the structural response of the frame. Seven Gauss-Lobatto integration points along each member are employed. The square hollow structural section of braces is discretized with 208 fibers, and 96 fibers for wide flange sections. The initial sinusoidal out-of-straightness with maximum amplitude δ_0 of $L/1000$ as well as residual stress is considered. The $M-\theta$ functions of gusset plate connection and beam-to-column connection are determined by the method presented in section 7.2. Specially, there is a 200 mm thickness composite slab placed on the top of steel members. Thus, the $M-\theta$ curve proposed by Liu and Astaneh-Asl (2004) with consideration of composite slab is adopted here.

The global drift versus lateral force hysteretic curves obtained from the proposed method against the measured results are plotted in Fig. 7.18. Generally, the shapes of the hysteretic loops from numerical simulation and experimental test are similar. The hysteretic areas associated with the dissipated energy are also close. The tensile, compressive and buckling behaviors of the braces have been well represented in numerical simulation by one-element per member model. This example further demonstrates that the proposed method is ready for practical use with a significant reduction of modeling expense and increase of computational efficiency.

7.6 Concluding remarks

Special concentrically braced frames (SCBFs) are widely employed in high seismicity regions as seismic-resistant systems due to structural and economic efficiency and

particularly high ductility for energy dissipation. The steel braces are the key members to absorb energy through tensile yield, compressive buckling, post-buckling and fracture behavior. As the braces exhibit highly nonlinear behavior, the previous modeling methods are generally required several elements to simulate a brace with initial curvature. Also, the influence of residual stress on the structural performance of SCBFs has been largely overlooked. Thus, a practical and innovative analytical model is proposed in this thesis for the performance-based seismic design of SCBFs. This new solution provides an accurate prediction with a significant saving of computer time, and therefore it will be extremely helpful for daily design by nonlinear dynamic analysis. The examples verified by experimental test results show the accuracy, efficiency, and validity of the proposed method.

In summary, there are five novel aspects of the proposed model as follows:

- (1) The initial geometrical imperfection and residual stress are explicitly considered at the element level.
- (2) The joint flexibility effect as well as the rigid end zone due to gusset plate connection is explicitly considered at the element level.
- (3) The distributed plasticity with consideration of fatigue fracture allowing for hysteretic behavior has been included in the proposed model.
- (4) One-element-per-member modeling is adequate, and therefore it can significantly reduce the computational cost.
- (5) This thesis extends the direct analysis method (DAM) which is well specified in the modern design codes such as AISC360 (2016), Eurocode-3 (2005) and COPHK (2011) from nonlinear static analysis to dynamic analysis. Thus, a consistent method linking the static and dynamic design together is provided for practical engineering use to achieve a safer and economic design.

FIGURES

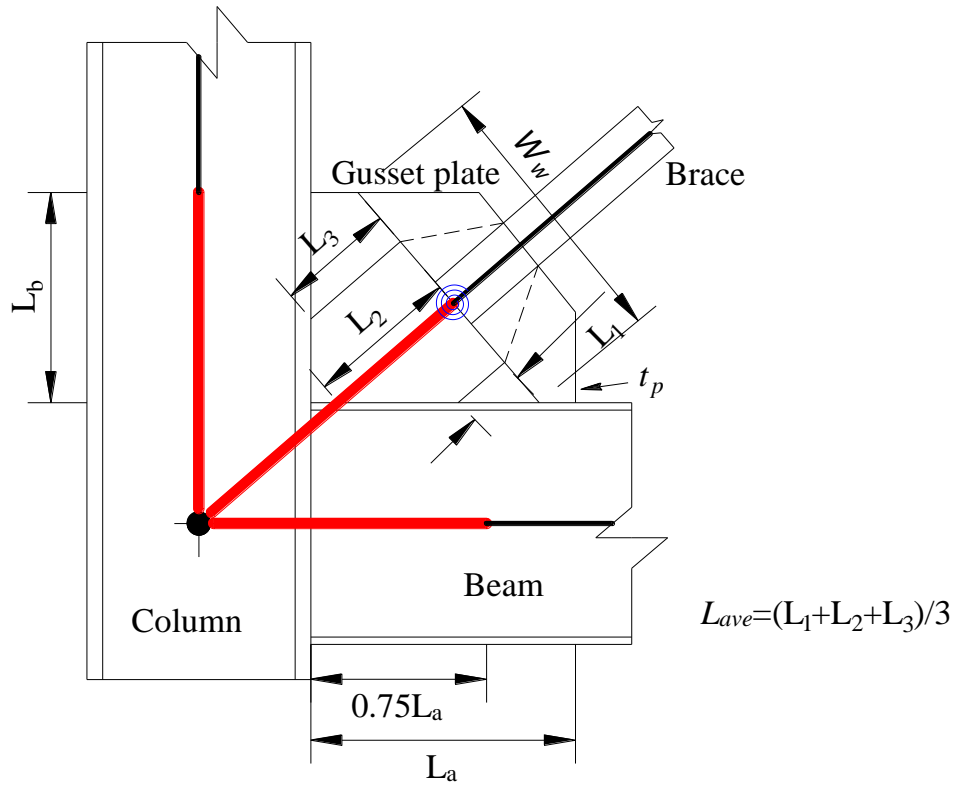


Fig. 7.1 Configuration and modeling of gusset plate connection

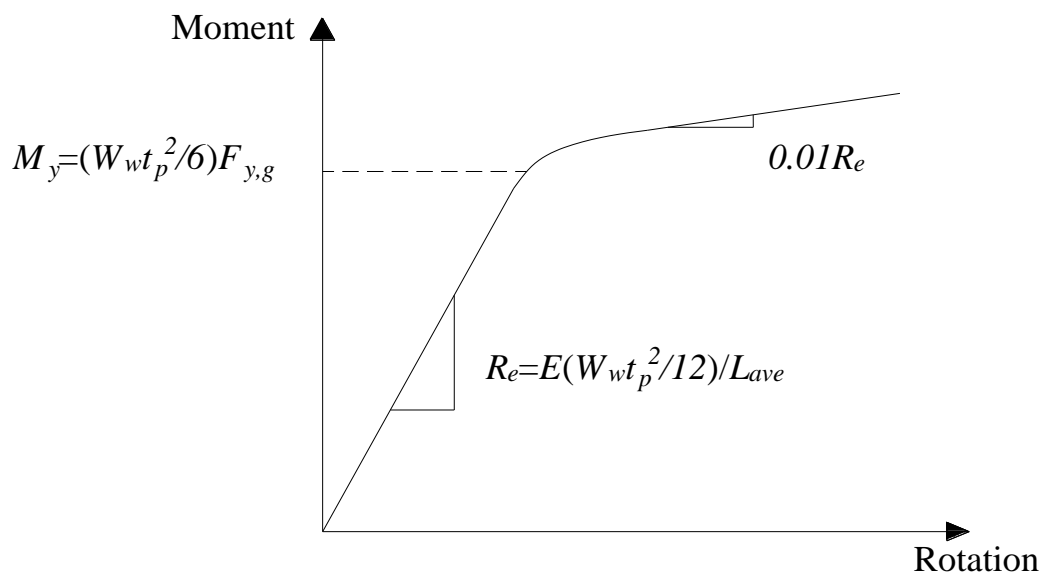
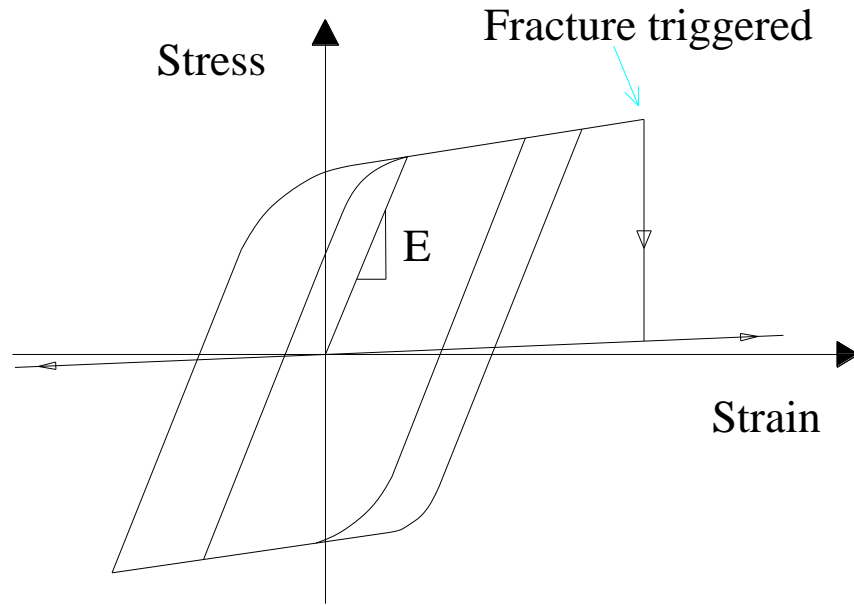
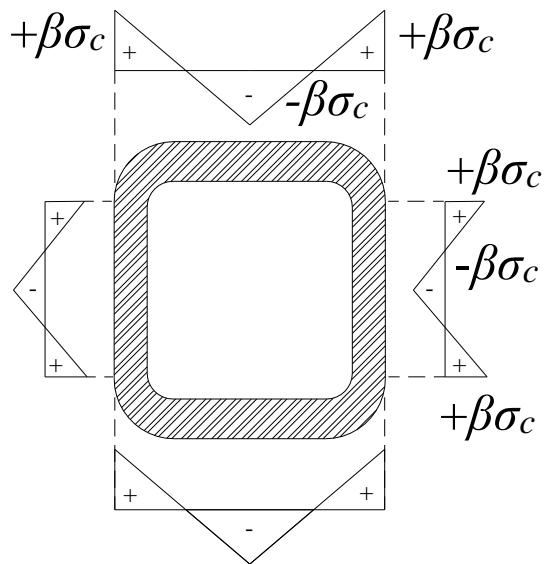


Fig. 7.2 Moment-rotation function of gusset plate connection

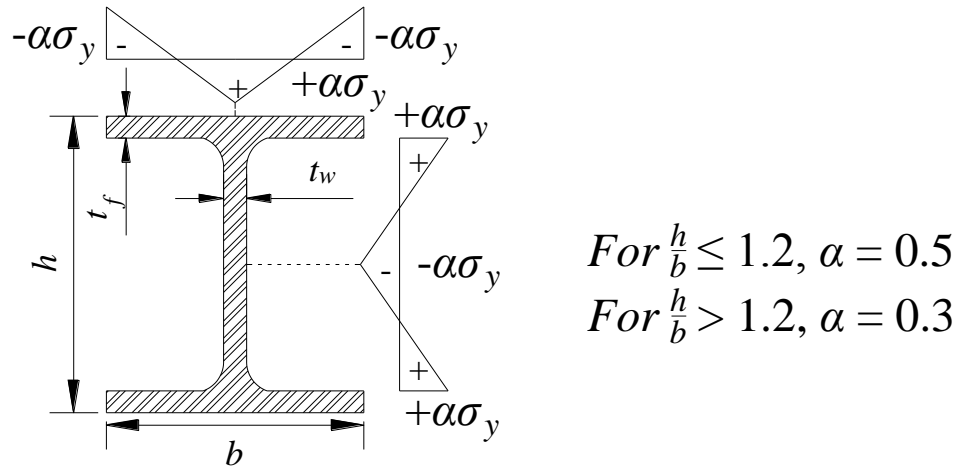


Strain Range Limit

Fig. 7.3 Fracture model of steel material

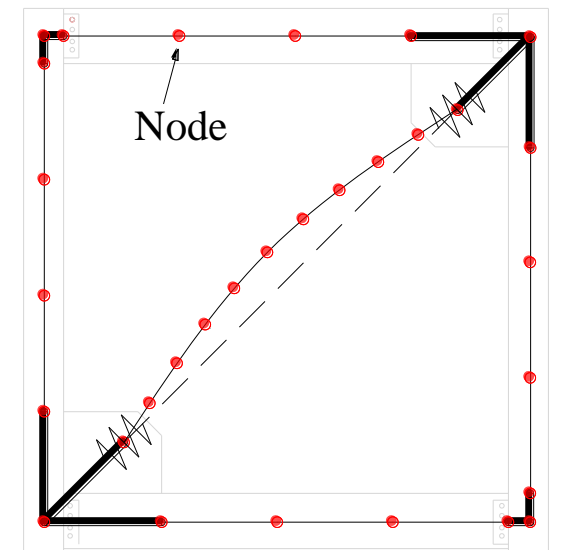


(a) HSS



(b) H-Section

Fig. 7.4 Residual stress patterns



- beam-column element
- rigid link
- ⚡ zero-length spring element

(a) suggested by Hsiao (2012)

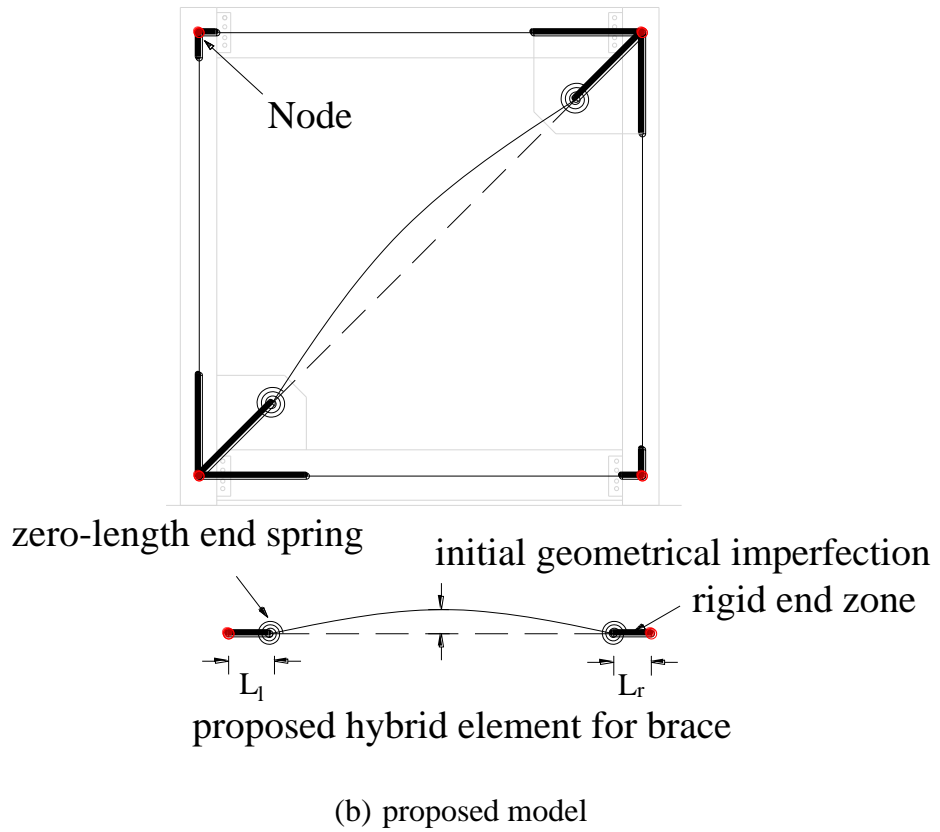


Fig. 7.5 Comparison of analytical models for SCBFs

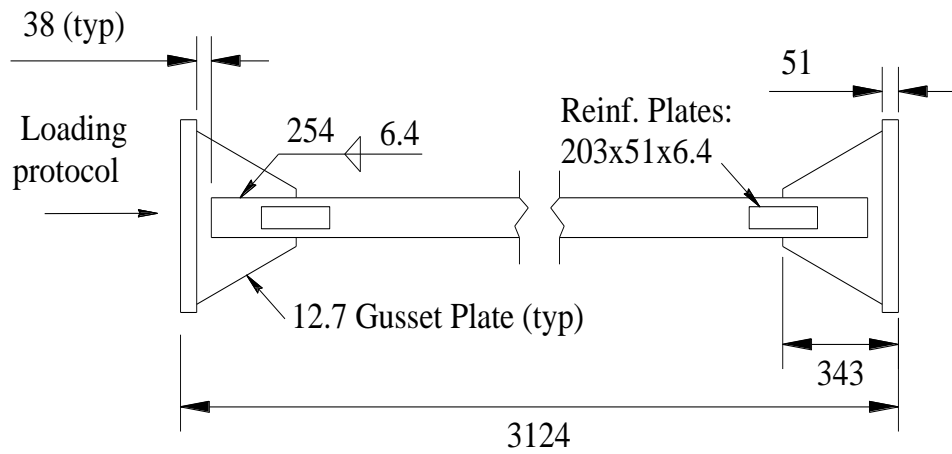


Fig. 7.6 Configuration of a single HSS brace

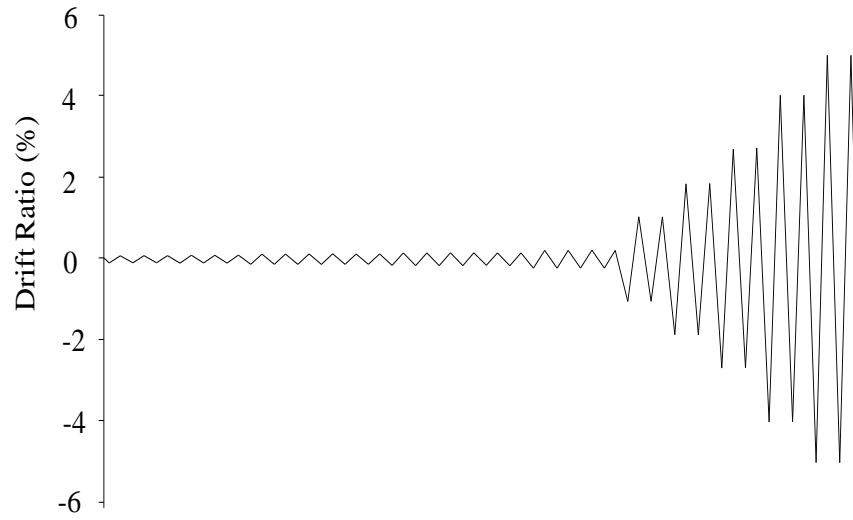
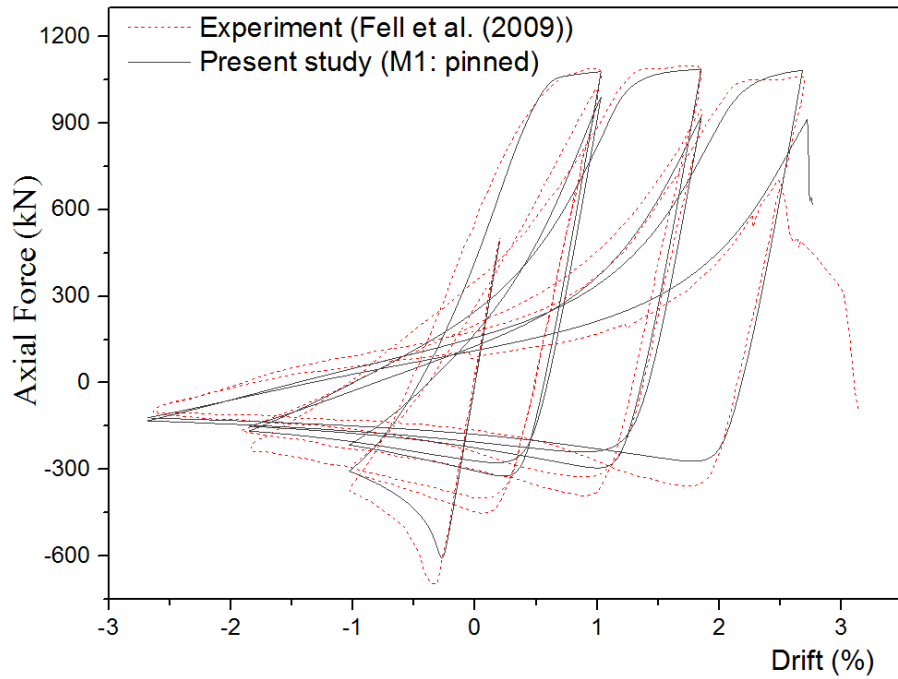
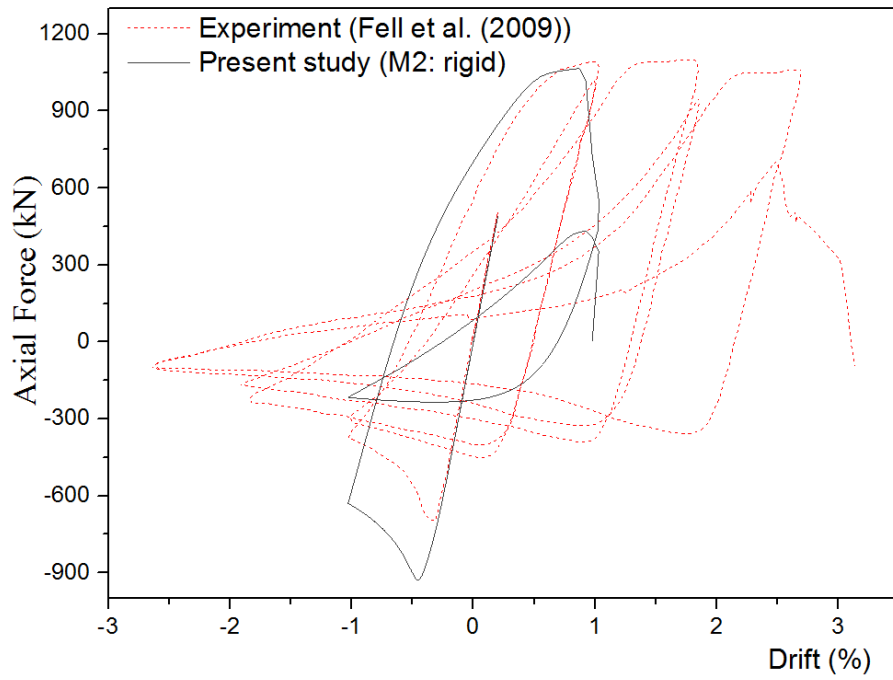


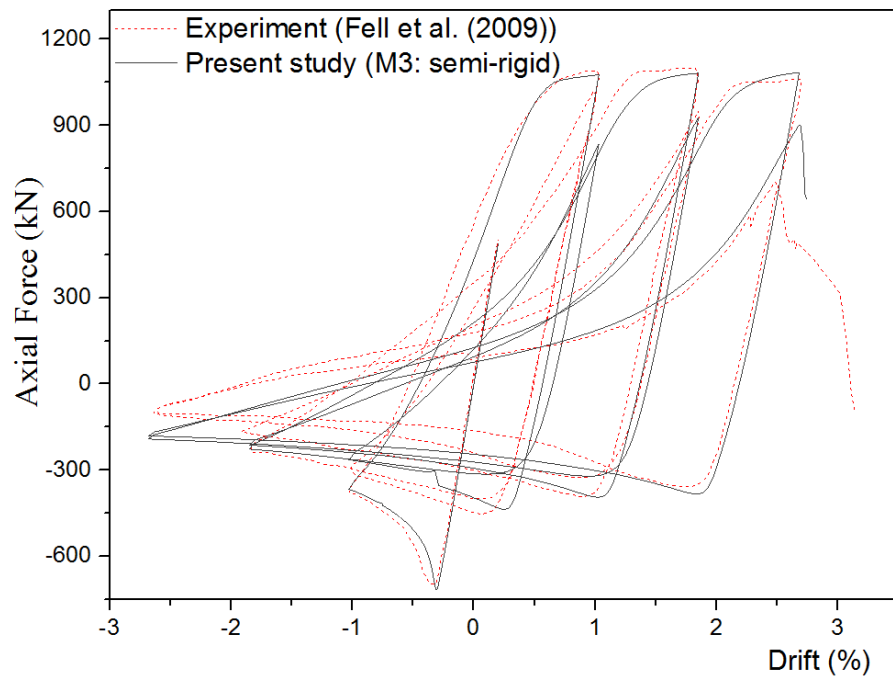
Fig. 7.7 Symmetrical loading protocol



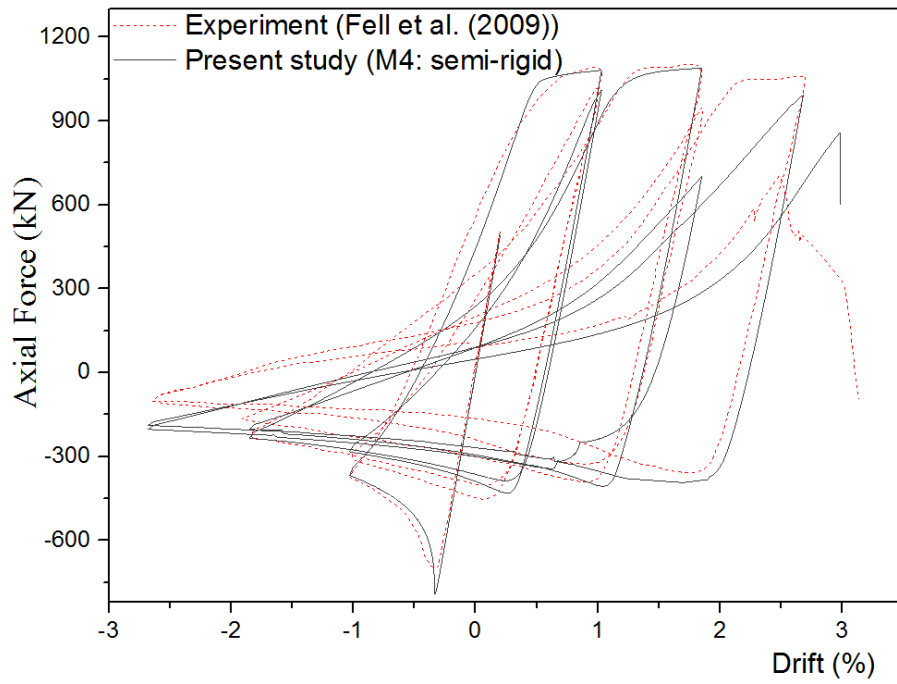
(a)



(b)



(c)



(d)

Fig. 7.8 Brace hysteretic curves for different models: (a) M1, (b) M2, (c) M3 and
(d) M4

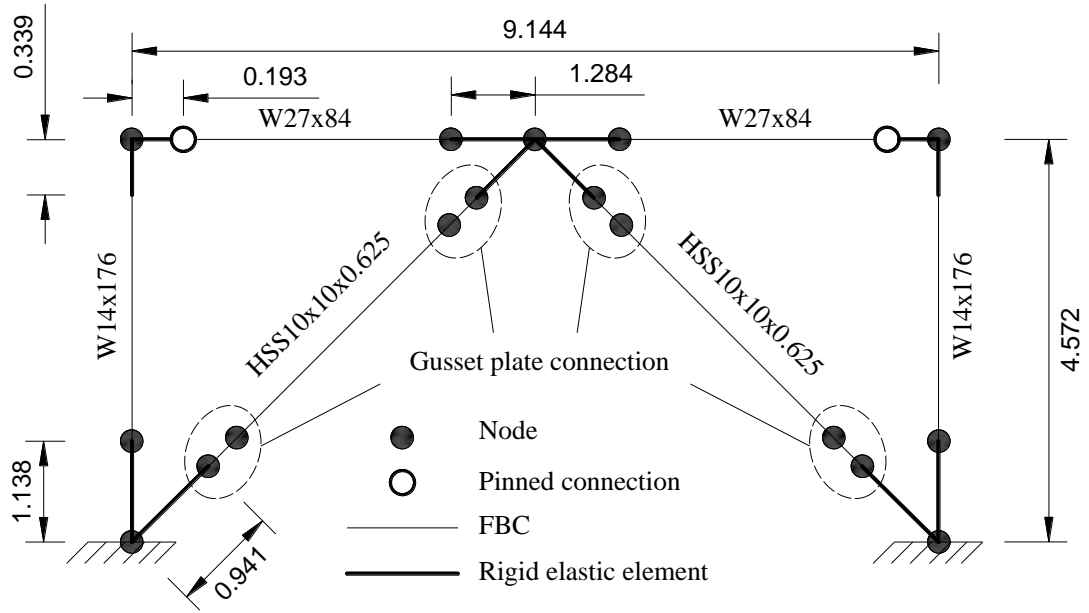


Fig. 7.9 Finite element model of SCBF

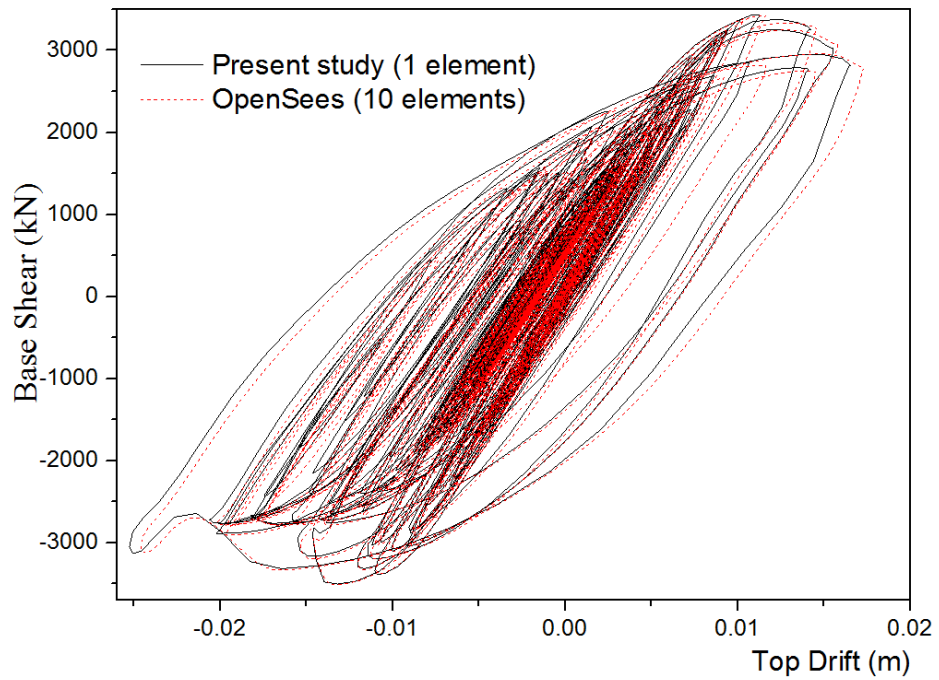


Fig. 7.10 Seismic performance of SCBF with different number of elements

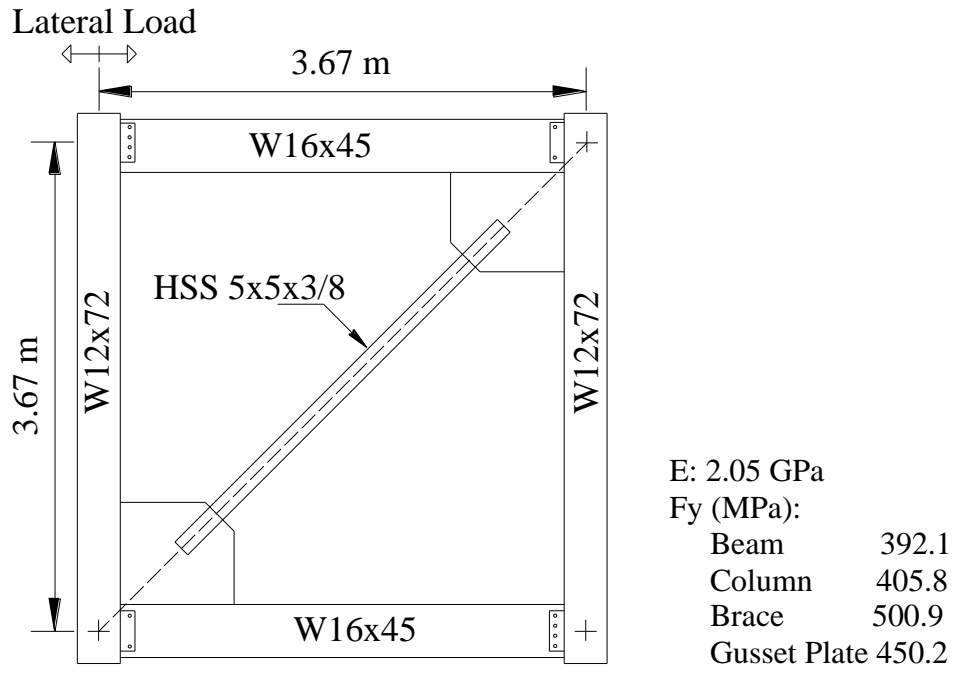


Fig. 7.11 Test specimen of single-story frame

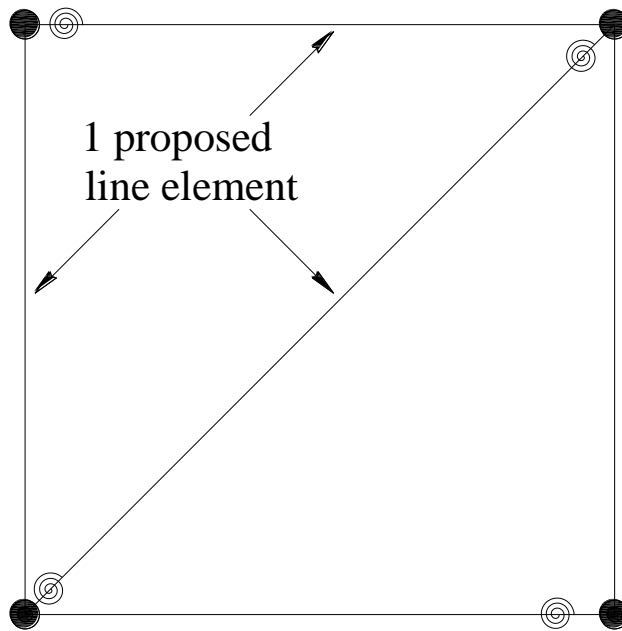


Fig. 7.12 Analytical model

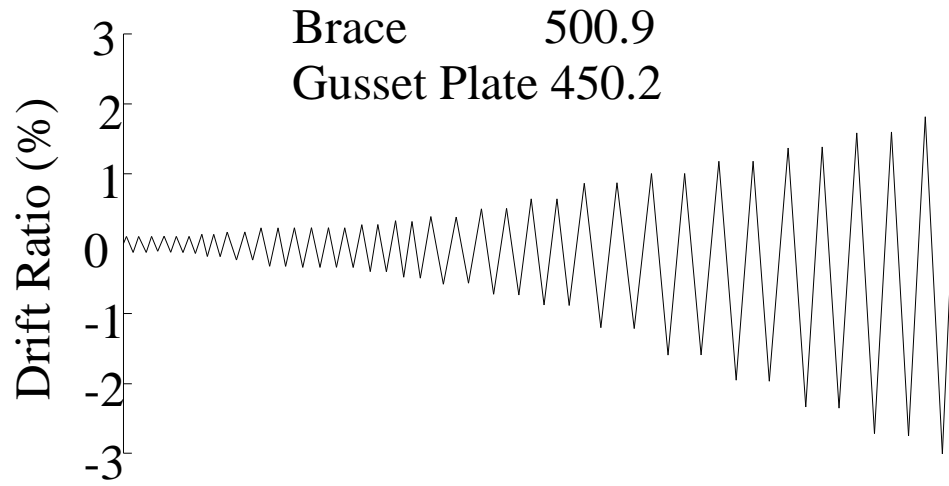


Fig. 7.13 Asymmetrical loading protocol

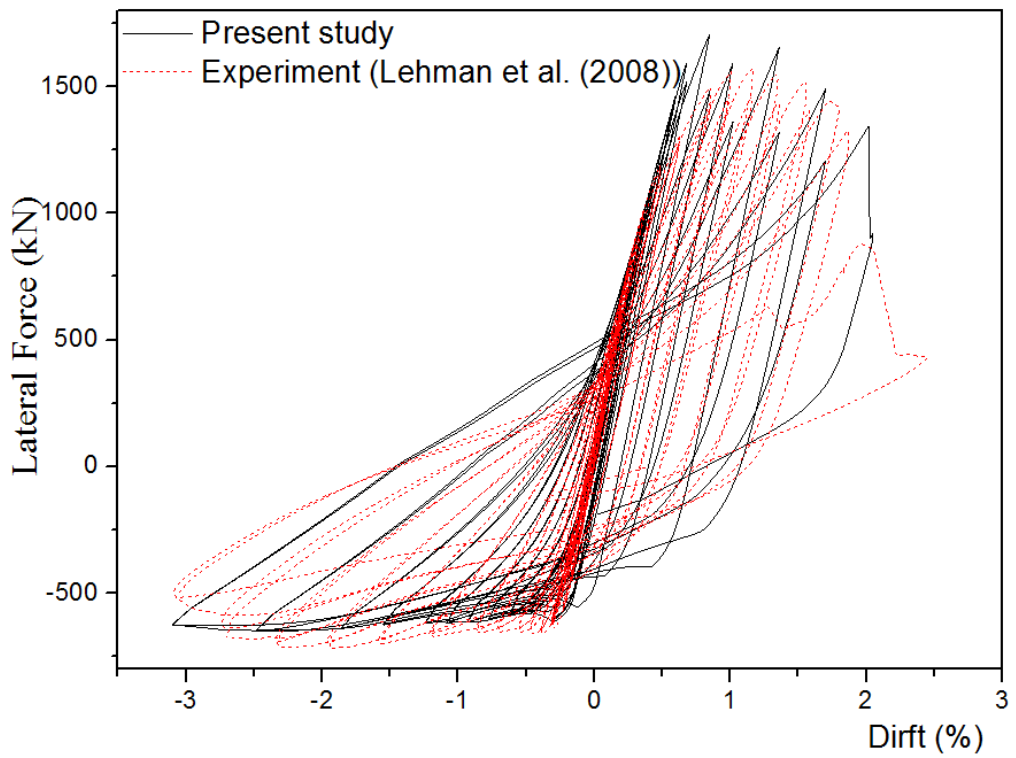


Fig. 7.14 Response of single-story frame

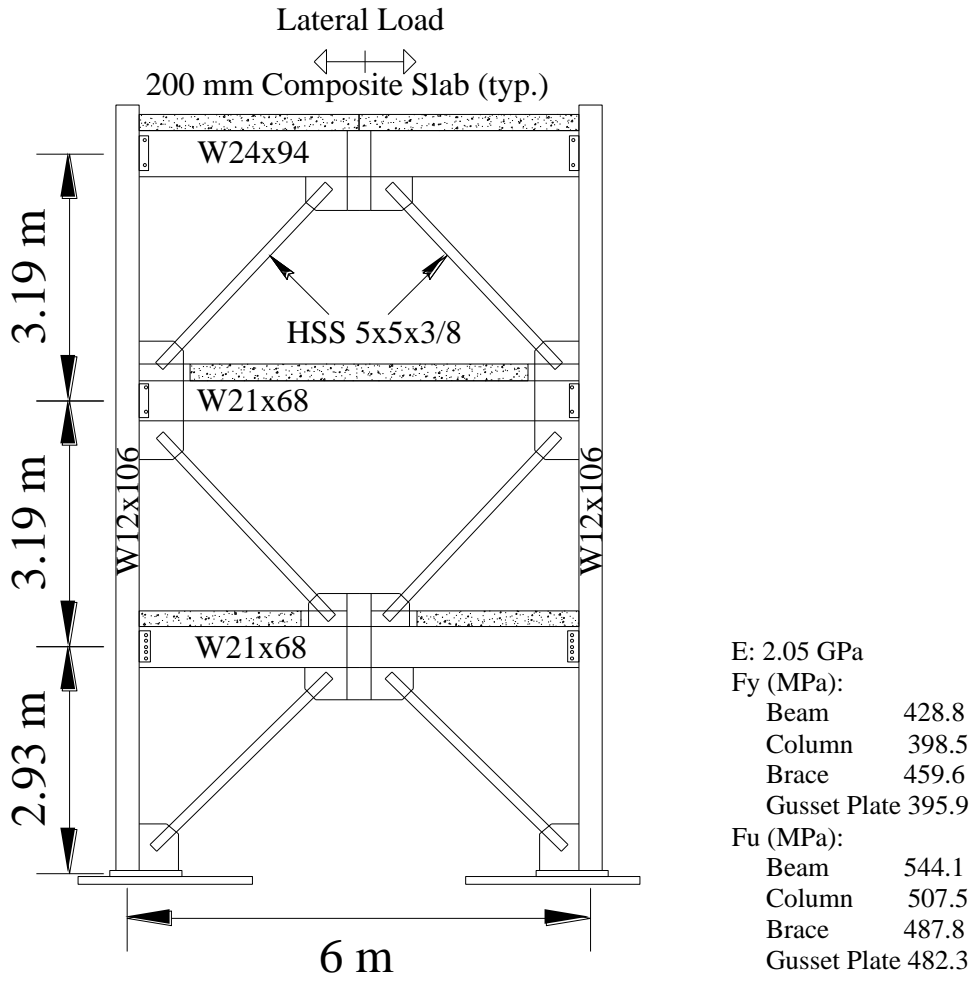


Fig. 7.15 Test specimen of three-story one-bay frame

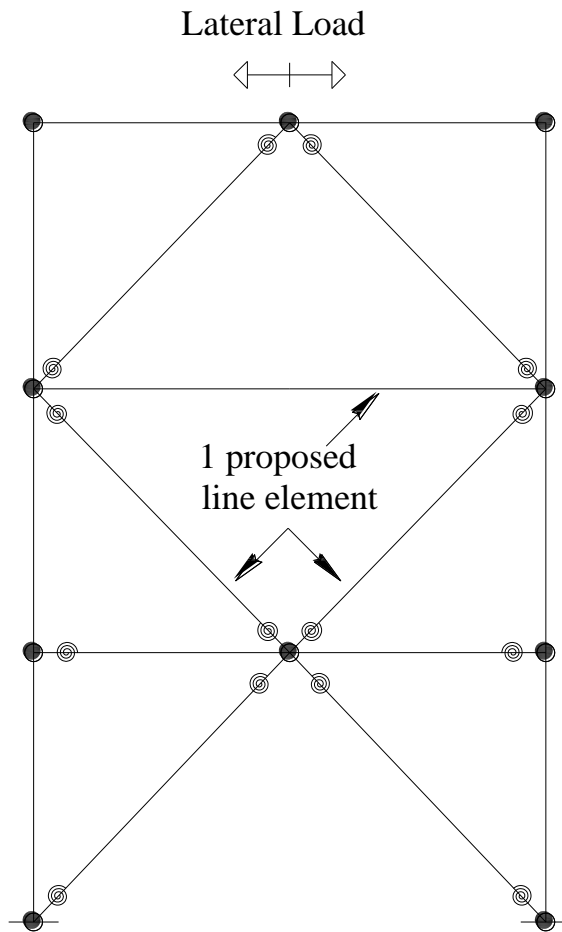


Fig. 7.16 Analytical model

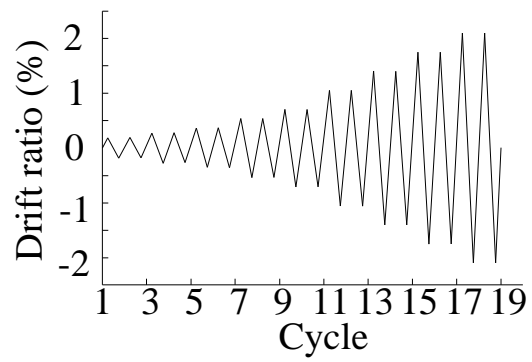


Fig. 7.17 Symmetrical loading protocol

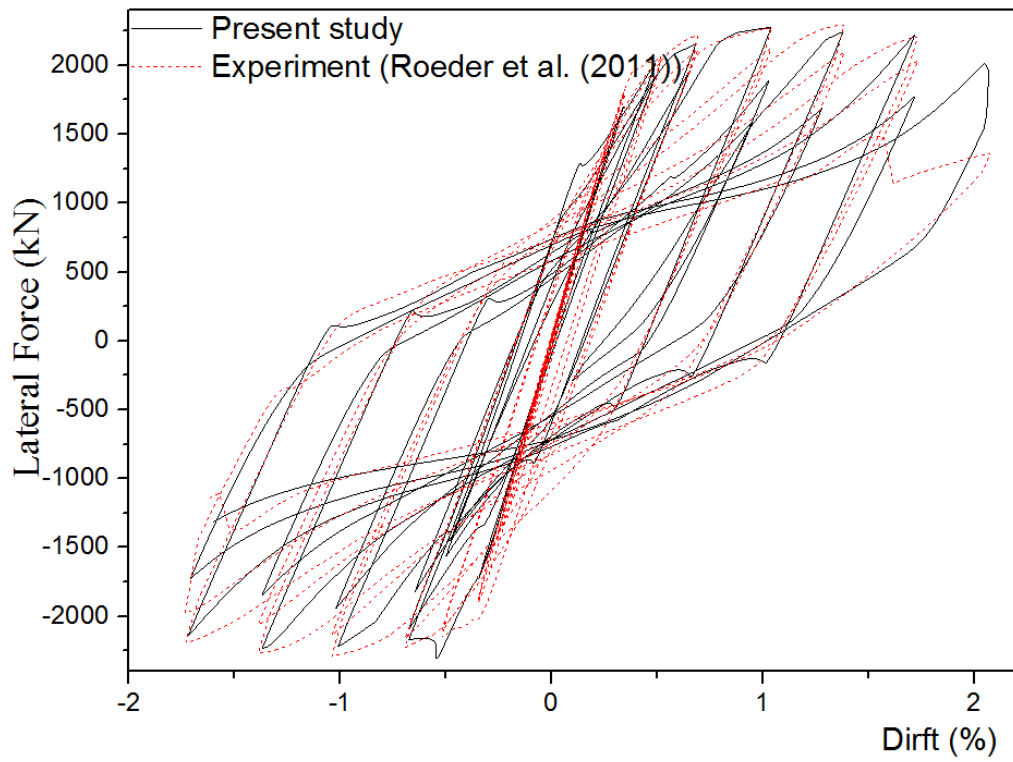
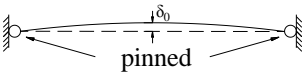
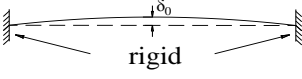
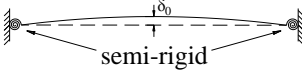
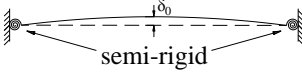


Fig. 7.18 Response of three-story one-bay frame

TABLES

Table 7-1 Four models for simulation of the single HSS brace

Model	End Condition	Initial Bowing δ_0	Residual Stress
M1		$L/1000$	Yes
M2		$L/1000$	Yes
M3		$L/1000$	Yes
M4		$L/1000$	No

Note: δ_0 is the magnitude of initial geometrical imperfection respectively; L is the length of the member.

CHAPTER 8. SUMMARY AND FUTURE WORK

In this chapter, the main findings of this research project will be summarized, and the future work is also presented.

8.1 Summary

In this thesis, a new flexibility-based beam-column element allowing for member imperfections, semi-rigid connections, rigid end zone and end offsets, and distributed plasticity is proposed for the second-order direct analysis of frame structures under static and dynamic loads. The work that incorporates member initial bowing into the flexibility-based element has not been done before. The plastic zone method in conjunction with the fiber section approach is adopted in the proposed flexibility-based element to conduct second-order inelastic analysis. The geometrical initial imperfection is formulated in the element stiffness matrix while the residual stress is considered by fiber section, and as a result, the inelastic behavior of steel structures can be well predicted in accordance with design codes. As the second-order direct analysis requires the consideration of material yielding and initial imperfections, this new element provides a practical solution for engineering applications with higher computational efficiency and better numerical convergence than the conventional methods. Meanwhile, the section constitutive model derived from the section yield function can replace the section integration using the fiber section approach to represent the relationships between the internal forces and deformations. This technique will significantly enhance the computational efficiency of

both static and dynamic nonlinear analysis considering material yielding. Generally speaking, the proposed method can predict the actual behaviors of frame structures using one element per member. Finally, the proposed method is applied to design of frame structures with noncompact and slender CFT members under static loads and special concentrically braced frames (SCBFs) subjected to dynamic loads.

The main findings and contributions of this study are summarized as follows:

- (1) The proposed flexibility-based beam-column element can consider member initial imperfections explicitly. Meanwhile, it inherits the advantages of flexibility-based elements, having high accuracy and being powerful in the inelastic analysis. The geometrical and material nonlinearities of frame structures under static and dynamic loads can be well considered. For geometrical nonlinearity, the $P-\delta$ effect is incorporated into the proposed method at the element level while the $P-\Delta$ effect is accounted for by corotational technology. In terms of material nonlinearity, the distributed plasticity method is adopted to capture the plastic behavior. The fiber section approach also makes it possible to directly consider the influence of residual stress. These features make the proposed element able to simulate one member by one element. Therefore, it significantly reduces the engineers' modeling workload as well as the computational time of static and dynamic nonlinear analysis.
- (2) A section constitutive model derived from the section yield function can replace the section integration using the fiber section approach to represent the relationships between the internal forces and deformations. This technique will further reduce computer time and resource with same accuracy as fiber section method and therefore it is ready for static and dynamic nonlinear analysis.

- (3) Two zero-length springs are attached at the ends of the proposed element to account for joint flexibility required in direct analysis if the joint is not ideally pinned or fully rigid. The coupling effect of axial force and bending moments, which has been ignored by other researchers, can be taken into consideration. This hybrid element is able to capture the structural behaviour of a member with semi-rigid connections under monotonic or cyclic loading. Thus, the proposed method is applicable for static or dynamic nonlinear analysis of frame structures allowing semi-rigid connections.
- (4) An innovative method in line with direct analysis and satisfying the provisions in AISC360 (2016) is proposed for the design of noncompact and slender CFT members. Using the effective stress-strain relationships of the steel tube and the concrete infill, the proposed element with geometrical imperfections can well predict the complex behaviors of noncompact and slender CFT members. This approach considers all factors affecting member behaviors in the analysis process in accordance with code requirements. Both the geometrical and material nonlinearities are reflected in the second-order direct analysis. The effective stress-strain relationships implicitly account for the complex behaviors of noncompact and slender CFT members, for examples, local plate buckling, concrete confinement, material yielding. Furthermore, the proposed element has high accuracy such that one CFT member can be modeled by one proposed element. This method can be applied to direct analysis of compact, noncompact and slender CFT member.
- (5) The proposed element is extended to consider the effects of the rigid end zone and end offsets at the element level to simplify the model. A practical and innovative analytical model is proposed for the performance-based seismic design of special

concentrically braced frames (SCBFs). The gusset plate at the end of brace in SCBFs is simulated by a semi-rigid connection with rigid end zone. The joint stiffness of the beam-to-column connections can also be simulated by the proposed model. To this end, the brace complex behaviors such as tensile yield, compressive buckling and post-buckling during second-order dynamic analysis can be accurately captured by one proposed element per brace. Using the fracture constitutive relations of steel material, the proposed model can capture the fracture behavior of braces under cyclic loading. This new solution provides accurate predictions with significant savings of computational time, and therefore it will be extremely helpful for PBSB by dynamic nonlinear analysis.

8.2 Future work

This study presents a high-performance flexibility-based beam-column element considering many practical features for daily design. It is highly recommended for use in direct analysis of frame structures subjected to static and dynamic loads. There are still many detailed works on applying the direct analysis method to performance-based seismic design. In the future, the following aspects are recommended so that the innovative second-order direct analysis can be extended to routine seismic design.

- (1) To adopt the yield surface, provided in design codes or generated by cross-sectional analysis software, in the distributed fiber hinge method;
- (2) To study the behavior of SCBFs by the proposed method with more experimental test results;
- (3) To introduce warping and shear deformation effects into the proposed element;

- (4) To study the critical imperfection mode of frame structures under dynamic loads;
- (5) To improve the computational efficiency by employing CPU + GPU heterogeneous computing techniques and cloud techniques;

REFERENCES

- Abdalla, K., and Stavroulakis, G. (1995). "A Backpropagation Neural Network Model for Semi - rigid Steel Connections." *Computer - Aided Civil and Infrastructure Engineering*, 10(2), 77-87.
- Ahmadizadeh, M., and Maalek, S. (2014). "An investigation of the effects of socket joint flexibility in space structures." *Journal of Constructional Steel Research*, 102, 72-81.
- AISC (2011). "Manual of steel construction load resistance factor design", 14th Edition, AISC, Chicago, USA.
- AISC341 (2016). "Seismic provisions for structural steel buildings", American Institute of Steel Construction, AISC, Inc., 130 EAST RANDOLPH STREET, SUITE 2000, Chicago, Illinois, 60601-6204.
- AISC360 (2010). "Specification for Structural Steel Buildings." American Institute of Steel Construction, AISC, Inc., *One East Wacker Driver, Suite 700, Chicago, Illinois 60601-1802.*
- AISC360 (2016). "Specification for Structural Steel Buildings." American Institute of Steel Construction, AISC, Inc., *130 EAST RANDOLPH, SUITE 2000, Chicago, Illinois 60601-6204.*
- Alemdar, B. N. (2001). "Distributed plasticity analysis of steel building structural systems." *PhD Thesis, Department of Civil and Environmental Engineering, Georgia Institute of Technology, Atlanta.*

- Alemdar, B. N., and White, D. W. (2005). "Displacement, flexibility, and mixed beam–column finite element formulations for distributed plasticity analysis." *Journal of structural engineering*, 131(12), 1811-1819.
- Aristizabal-Ochoa, J. D. (2000). "Second-order axial deflections of imperfect 3-D beam-column." *Journal of engineering mechanics*, 126(11), 1201-1208.
- Aristizabal-Ochoa, J. D. (2010). "Second-order slope–deflection equations for imperfect beam–column structures with semi-rigid connections." *Engineering Structures*, 32(8), 2440-2454.
- Asgarian, B., Alanjari, P., and Aghaeidoost, V. (2015). "Three-dimensional joint flexibility element for modeling of tubular offshore connections." *Journal of Marine Science and Technology*, 20(4), 629-639.
- Astroza, R., Ebrahimian, H., and Conte, J. P. (2014). "Material parameter identification in distributed plasticity FE models of frame-type structures using nonlinear stochastic filtering." *Journal of Engineering Mechanics*, 141(5), 04014149.
- Auricchio, F., and Taylor, R. (1999). "A return-map algorithm for general associative isotropic elasto-plastic materials in large deformation regimes." *International Journal of Plasticity*, 15(12), 1359-1378.
- Auricchio, F., and Taylor, R. L. (1994). "A generalized elastoplastic plate theory and its algorithmic implementation." *Int J Numer Meth Eng*, 37(15), 2583-2608.
- Auricchio, F., and Taylor, R. L. (1995). "Two material models for cyclic plasticity: nonlinear kinematic hardening and generalized plasticity." *International Journal of Plasticity*, 11(1), 65-98.

- Babazadeh, A., Burgueño, R., and Silva, P. F. (2016). "Evaluation of the critical plastic region length in slender reinforced concrete bridge columns." *Engineering Structures*, 125, 280-293.
- Barsan, G. M., and Chiorean, C. G. (1999). "Computer program for large deflection elasto-plastic analysis of semi-rigid steel frameworks." *Computers & Structures*, 72(6), 699-711.
- Botez, M. D., Bredean, L. A., and Ioani, A. M. (2014). "Plastic hinge vs. distributed plasticity in the progressive collapse analysis." *Acta Technica Napocensis: Civil Engineering & Architecture*, 57(1), 24-36.
- Chan, S. L. (1988). "Geometric and material non-linear analysis of beam-columns and frames using the minimum residual displacement method." John Wiley & Sons, Ltd, 2657-2669.
- Chan, S. L., and Chui, P. T. (2000). *Non-linear static and cyclic analysis of steel frames with semi-rigid connections*, Elsevier.
- Chan, S. L., and Gu, J. X. (2000). "Exact tangent stiffness for imperfect beam-column members." *J Struct Eng-Asce*, 126(9), 1094-1102.
- Chan, S. L., and Zhou, Z. H. (1994). "Pointwise equilibrating polynomial element for nonlinear analysis of frames." *Journal of Structural Engineering*, 120(6), 1703-1717.
- Chan, S. L., and Zhou, Z. H. (1995). "2Nd-Order Elastic Analysis of Frames Using Single Imperfect Element Per Member." *J Struct Eng-Asce*, 121(6), 939-945.

- Chen, W.-F., and Kishi, N. (1987). *Moment-rotation Relation of Top and Seat-angle Connections*.
- Chen, W. F., and Chan, S. L. (1995). "2nd-order inelastic analysis of steel frames using element with midspan and end springs." *Journal of Structural Engineering*, 121(3), 530-541.
- Chen, W. F., and Sohal, I. (1995). "Plastic Design and Second-Order Analysis of Steel Frames." *Springer-Verlag New York Inc*.
- Chiorean, C. G. (2017). "Second-order flexibility-based model for nonlinear inelastic analysis of 3D semi-rigid steel frameworks." *Engineering Structures*, 136, 547-579.
- Cho, S. H., and Chan, S. L. (2008). "Second-order analysis and design of angle trusses, Part II: Plastic analysis and design." *Engineering Structures*, 30(3), 626-631.
- COPHK (2011). "Code of Practice for the Structural Use of Steel 2011." *Buildings Department, Hong Kong SAR Government*.
- Csébfalvi, A. (2007). "Optimal design of frame structures with semi-rigid joints." *Periodica Polytechnica. Civil Engineering*, 51(1), 9.
- de_Souza, R. M. (2000). "Force-based finite element for large displacement inelastic analysis of frames." *PhD Thesis, Department of Civil and Environmental Engineering, University of California, Berkeley*.
- Denavit, M. D. (2012). *Characterization of behavior of steel-concrete composite members and frames with applications for design*, University of Illinois at Urbana-Champaign.

- Denavit, M. D., Hajjar, J. F., Perea, T., and Leon, R. T. (2015). "Stability analysis and design of composite structures." *Journal of Structural Engineering*, 142(3), 04015157.
- Dides, M. A., and De la Llera, J. C. (2005). "A comparative study of concentrated plasticity models in dynamic analysis of building structures." *Earthq Eng Struct D*, 34(8), 1005-1026.
- Ding, F.X., Zhang, T., Liu, X.M., Lu, Z.-H., Guo, Q., and Jiang, G.-s. (2017). "Behavior of steel-reinforced concrete-filled square steel tubular stub columns under axial loading." *Thin-Walled Structures*, 119, 737-748.
- Du, Y., Chen, Z., Wang, Y.-B., and Liew, J. R. (2017). "Ultimate resistance behavior of rectangular concrete-filled tubular beam-columns made of high-strength steel." *Journal of Constructional Steel Research*, 133, 418-433.
- Du, Z.-L., Liu, Y.-P., and Chan, S.-L. (2017). "A second-order flexibility-based beam-column element with member imperfection." *Engineering Structures*, 143, 410-426.
- Ekhande, S. G., Selvappalam, M., and Madugula, M. K. (1989). "Stability functions for three-dimensional beam-columns." *Journal of Structural Engineering*, 115(2), 467-479.
- El-Tawil, S., and Deierlein, G. G. (1998). "Stress-resultant plasticity for frame structures." *Journal of engineering mechanics*, 124(12), 1360-1370.
- El-Tawil, S., and Deierlein, G. G. (2001). "Nonlinear analysis of mixed steel-concrete frames. I: Element formulation." *J Struct Eng-Asce*, 127(6), 647-655.

- Eurocode3 (2005). "EN 1993-1-1: Design of steel structures - General rules and rules for buildings." *European Committee for Standardization*.
- Faella, C., Piluso, V., and Rizzano, G. (1997). "A new method to design extended end plate connections and semirigid braced frames." *Journal of Constructional Steel Research*, 41(1), 61-91.
- Fell, B. V., Kanvinde, A. M., Deierlein, G. G., and Myers, A. T. (2009). "Experimental Investigation of Inelastic Cyclic Buckling and Fracture of Steel Braces." *J Struct Eng-Asce*, 135(1), 19-32.
- FEMA-356 (2000). "Commentary for the Seismic Rehabilitation of Buildings." *Federal Emergency Management Agency, Washington, DC*.
- Ferreira, M., Providência, P., Gala, P., and Almeida, J. (2017). "Improved displacement based alternative to force based finite element for nonlinear analysis of framed structures." *Engineering Structures*, 135, 95-103.
- Filippou, F. C., Bertero, V. V., and Popov, E. P. (1983). "Effects of bond deterioration on hysteretic behavior of reinforced concrete joints."
- Fong, M., Chan, S. L., and Uy, B. (2011). "Advanced design for trusses of steel and concrete-filled tubular sections." *Engineering Structures*, 33(12), 3162-3171.
- Fong, M., Cho, S. H., and Chan, S. L. (2009). "Design of angle trusses by codes and second-order analysis with experimental verification." *Journal of Constructional Steel Research*, 65(12), 2140-2147.
- Frye, M. J., and Morris, G. A. (1975). "Analysis of flexibly connected steel frames." *Canadian journal of civil engineering*, 2(3), 280-291.

- Güneyisi, E. M., D'Aniello, M., Landolfo, R., and Mermerdaş, K. (2014). "Prediction of the flexural overstrength factor for steel beams using artificial neural network." *Steel and Composite Structures*, 17(3), 215-236.
- Goto, Y., and Chen, W. F. (1987). "Second-order elastic analysis for frame design." *Journal of Structural Engineering*, 113(7), 1501-1519.
- Gourley, B. C., Tort, C., Denavit, M. D., Schiller, P. H., and Hajjar, J. F. (2008). "A synopsis of studies of the monotonic and cyclic behavior of concrete-filled steel tube members, connections, and frames." Newmark Structural Engineering Laboratory. University of Illinois at Urbana-Champaign.
- Gunnarsson, I. R. (2004). "Numerical performance evaluation of braced frame systems." University of Washington.
- Haddad, M., and Tremblay, R. "Influence of connection design on the inelastic seismic response of HSS steel bracing members." *Proc., TUBULAR STRUCTURES-INTERNATIONAL SYMPOSIUM-*, 639.
- Hajjar, J., Gourley, B., Tort, C., Denavit, M., and Schiller, P. (2013). "Steel-concrete composite structural systems." *Dept. of Civil and Environmental Engineering, Northeastern Univ., Boston*.
- Hajjar, J. F., Molodan, A., and Schiller, P. H. (1998). "A distributed plasticity model for cyclic analysis of concrete-filled steel tube beam-columns and composite frames." *Engineering Structures*, 20(4-6), 398-412.

- Han, L.-H., Yao, G.-H., and Zhao, X.-L. (2005). "Tests and calculations for hollow structural steel (HSS) stub columns filled with self-consolidating concrete (SCC)." *Journal of Constructional Steel Research*, 61(9), 1241-1269.
- Han, S.W., Kim, W. T., and Foutch, D. A. (2007). "Seismic behavior of hss bracing members according to width–thickness ratio under symmetric cyclic loading." *Journal of Structural Engineering*, 133(2), 264-273.
- Harrison, H. (1965). "The Application of the Principles of Plastic Analysis of Three Dimensional Steel Structures." *University of Sydney*.
- He, Z., Liu, W., Wang, X., and Ye, A. (2016). "Optimal Force-Based Beam-Column Element Size for Reinforced-Concrete Piles in Bridges." *Journal of Bridge Engineering*, 21(11), 06016006.
- Hsiao, P. C. (2012). *Seismic performance evaluation of concentrically braced frames*, University of Washington.
- Hsiao, P.-C., Lehman, D. E., and Roeder, C. W. (2012). "Improved analytical model for special concentrically braced frames." *Journal of Constructional Steel Research*, 73, 80-94.
- Hsiao, P. C., Lehman, D. E., and Roeder, C. W. (2012). "Improved analytical model for special concentrically braced frames." *Journal of Constructional Steel Research*, 73, 80-94.
- Hsiao, P. C., Lehman, D. E., and Roeder, C. W. (2013). "A model to simulate special concentrically braced frames beyond brace fracture." *Earthq Eng Struct D*, 42(2), 183-200.

- Hu, F., Shi, G., and Shi, Y. (2017). "Experimental study on seismic behavior of high strength steel frames: Global response." *Engineering Structures*, 131, 163-179.
- Ihaddoudène, A., Saidani, M., and Jaspart, J. (2017). "Mechanical model for determining the critical load of plane frames with semi-rigid joints subjected to static loads." *Engineering Structures*, 145, 109-117.
- Institution, B. S. (2004). "Eurocode 4: Design of composite steel and concrete structures. part 1-1: General rules and rules for buildings." *BSI, London, BS EN 1994*.
- Iu, C., Bradford, M., and Chen, W. (2009). "Second-order inelastic analysis of composite framed structures based on the refined plastic hinge method." *Engineering Structures*, 31(3), 799-813.
- Izzuddin, B. A. (1996). "Quartic formulation for elastic beam-columns subject to thermal effects." *Journal of Engineering Mechanics*, 122(9), 861-871.
- Jafari, V., Vahdani, S. H., and Rahimian, M. (2010). "Derivation of the consistent flexibility matrix for geometrically nonlinear Timoshenko frame finite element." *Finite Elem Anal Des*, 46(12), 1077-1085.
- Javed, M. F., Sulong, N. R., Memon, S. A., Rehman, S. K. U., and Khan, N. B. (2017). "FE modelling of the flexural behaviour of square and rectangular steel tubes filled with normal and high strength concrete." *Thin-Walled Structures*, 119, 470-481.
- Jiang, A.-y., Chen, J., and Jin, W.-l. (2013). "Experimental investigation and design of thin-walled concrete-filled steel tubes subject to bending." *Thin-Walled Structures*, 63, 44-50.

- Kang, C.-H., Oh, Y.-S., and Moon, T.-S. (2001). "Strength of Axially Loaded Concrete-Filled Tubular Stub Column." *Journal of Korean Society of Steel Construction*, 13(3), 279-287.
- Karamanci, E., and Lignos, D. G. (2014). "Computational Approach for Collapse Assessment of Concentrically Braced Frames in Seismic Regions." *Journal of Structural Engineering*, 140(8).
- Kim, D. K. (2005). "A database for composite columns." Georgia Institute of Technology.
- Kim, S. E., Uang, C. M., Choi, S. H., and An, K. Y. (2006). "Practical advanced analysis of steel frames considering lateral-torsional buckling." *Thin-walled structures*, 44(7), 709-720.
- King, W. S., White, D. W., and Chen, W. F. (1992). "Second-order inelastic analysis methods for steel-frame design." *Journal of Structural Engineering*, 118(2), 408-428.
- Kishi, N., Chen, W., Matsuoka, K., and Nomachi, S. (1987). *Moment-rotation relation of top-and seat-angle with double web-angle connections*, School of Civil Engineering, Purdue University.
- Kostic, S. M., Filippou, F. C., and Deretic-Stojanovic, B. (2016). "Generalized plasticity model for inelastic RCFT column response." *Computers & Structures*, 168, 56-67.

- Kostic, S. M., Filippou, F. C., and Lee, C.-L. (2013). "An efficient beam-column element for inelastic 3D frame analysis." *Computational Methods in Earthquake Engineering*, Springer, 49-67.
- Krishnan, S. (2010). "Modified Elastofiber Element for Steel Slender Column and Brace Modeling." *J Struct Eng-Asce*, 136(11), 1350-1366.
- Lai, Z., and Varma, A. H. (2015). "Noncompact and slender circular CFT members: Experimental database, analysis, and design." *Journal of Constructional Steel Research*, 106, 220-233.
- Lai, Z., and Varma, A. H. (2016). "Effective stress-strain relationships for analysis of noncompact and slender filled composite (CFT) members." *Engineering Structures*, 124, 457-472.
- Lai, Z., Varma, A. H., and Griffis, L. G. (2015). "Analysis and design of noncompact and slender CFT beam-columns." *Journal of Structural Engineering*, 142(1), 04015097.
- Lai, Z., Varma, A. H., and Zhang, K. (2014). "Noncompact and slender rectangular CFT members: Experimental database, analysis, and design." *Journal of Constructional Steel Research*, 101, 455-468.
- Lam, D., Dai, X., Han, L.-H., Ren, Q.-X., and Li, W. (2012). "Behaviour of inclined, tapered and STS square CFST stub columns subjected to axial load." *Thin-Walled Structures*, 54, 94-105.

- Lee, C.-L., and Filippou, F. C. (2015). "Frame Element with Mixed Formulations for Composite and RC Members with Bond Slip. I: Theory and Fixed-End Rotation." *Journal of Structural Engineering*, 141(11), 04015039.
- Lee S, G. S. (1987). "Seismic behavior of hollow and concrete-filled square tubular bracing members." *Research Report UMCE 87-11, Department of Civil Engineering, University of Michigan, Ann Arbor, MI.*
- Lehman, D. E., Roeder, C. W., Herman, D., Johnson, S., and Kotulka, B. (2008). "Improved seismic performance of gusset plate connections." *J Struct Eng-Asce*, 134(6), 890-901.
- Liang, Q. Q. (2009). "Performance-based analysis of concrete-filled steel tubular beam–columns, Part I: Theory and algorithms." *Journal of Constructional Steel Research*, 65(2), 363-372.
- Liew, J. R., and Xiong, D. (2009). "Effect of preload on the axial capacity of concrete-filled composite columns." *Journal of Constructional Steel Research*, 65(3), 709-722.
- Liew, J. Y. R., White, D. W., and Chen, W. F. (1993). "Second-Order Refined Plastic-Hinge Analysis for Frame Design : Part 1 and 2." *J Struct Eng-Asce*, 119(11), 3196-3216.
- Lightfoot, E., and Le Messurier, A. (1974). "Elastic analysis of frameworks with elastic connections." *Journal of the Structural Division*, 100(Proc. Paper 10632).
- Liu, J., and Astaneh-Asl, A. (2004). "Moment–rotation parameters for composite shear tab connections." *Journal of Structural Engineering*, 130(9), 1371-1380.

- Liu, S.-W., Liu, Y.-P., and Chan, S.-L. (2014a). "Direct analysis by an arbitrarily-located-plastic-hinge element—part 1: planar analysis." *Journal of Constructional Steel Research*, 103, 303-315.
- Liu, S.-W., Liu, Y.-P., and Chan, S.-L. (2014b). "Direct analysis by an arbitrarily-located-plastic-hinge element—part 2: spatial analysis." *Journal of Constructional Steel Research*, 103, 316-326.
- Liu, S. W., Liu, Y. P., and Chan, S. L. (2010). "Pushover Analysis by One Element Per Member for Performance-Based Seismic Design." *Int J Struct Stab Dy*, 10(1), 111-126.
- Liu, S. W., Liu, Y. P., and Chan, S. L. (2012). "Advanced analysis of hybrid steel and concrete frames Part 2: Refined plastic hinge and advanced analysis." *Journal of Constructional Steel Research*, 70, 337-349.
- Lowes, L. N., Mitra, N., and Altoontash, A. (2003). "A beam-column joint model for simulating the earthquake response of reinforced concrete frames."
- Lubliner, J., Taylor, R., and Auricchio, F. (1993). "A new model of generalized plasticity and its numerical implementation." *International Journal of Solids and Structures*, 30(22), 3171-3184.
- Lumpkin, E. J., Hsiao, P.-C., Roeder, C. W., Lehman, D. E., Tsai, C.-Y., Wu, A.-C., Wei, C.-Y., and Tsai, K.-C. (2012). "Investigation of the seismic response of three-story special concentrically braced frames." *Journal of Constructional Steel Research*, 77, 131-144.

- Ma, K., and Richard Liew, J. (2004). "Nonlinear plastic hinge analysis of three-dimensional steel frames in fire." *Journal of Structural Engineering*, 130(7), 981-990.
- Mageirou, G. E., and Gantes, C. J. (2006). "Buckling strength of multi-story sway, non-sway and partially-sway frames with semi-rigid connections." *Journal of Constructional Steel Research*, 62(9), 893-905.
- McKenna, F., Fenves, G., Filippou, F., and Mazzoni, S. (2009). "Open system for earthquake engineering simulation (OpenSees), 2000." URL http://opensees.berkeley.edu/wiki/index.php/Main_Page.
- McKenna, F., Fenves, G., and Scott, M. (2000). "Open system for earthquake engineering simulation." *University of California, Berkeley, CA*.
- Nakahara, H., and Sakino, K. "Flexural behavior of concrete filled square steel tubular beam-columns." *Proc., 12th World Conference on Earthquake Engineering*.
- Neuenhofer, A., and Filippou, F. C. (1997). "Evaluation of nonlinear frame finite-element models." *J Struct Eng-Asce*, 123(7), 958-966.
- Neuenhofer, A., and Filippou, F. C. (1998). "Geometrically nonlinear flexibility-based frame finite element." *Journal of Structural Engineering*, 124(6), 704-711.
- NIDA (2018). "User's Manual, Nonlinear Integrated Design and Analysis." *NIDA 10.0 HTML Online Documentation*. (<http://www.nidacse.com>).
- Nilforoushan, R. (1973). *Seismic behavior of multistory K-braced frame structures*, University of Michigan, Department of Civil Engineering.

- Nishiyama, I. (2002). *Summary of research on concrete-filled structural steel tube column system carried out under the US-Japan cooperative research program on composite and hybrid structures*, Building Research Inst.
- Nukala, P. K. V. V., and White, D. W. (2004a). "A mixed finite element for three-dimensional nonlinear analysis of steel frames." *Comput Method Appl M*, 193(23-26), 2507-2545.
- Nukala, P. K. V. V., and White, D. W. (2004b). "Variationally consistent state determination algorithms for nonlinear mixed beam finite elements." *Comput Method Appl M*, 193(33-35), 3647-3666.
- Orbison, J. G., McGuire, W., and Abel, J. F. (1982). "Yield surface applications in nonlinear steel frame analysis." *Comput Method Appl M*, 33(1-3), 557-573.
- Palmer, K. D., Roeder, C. W., Lehman, D. E., Okazaki, T., and Shield, C. (2012). "Experimental performance of steel braced frames subjected to bidirectional loading." *Journal of Structural Engineering*, 139(8), 1274-1284.
- Pi, Y.-L., Bradford, M. A., and Uy, B. (2006). "Second order nonlinear inelastic analysis of composite steel-concrete members. I: Theory." *Journal of structural engineering*, 132(5), 751-761.
- Pi, Y., and Trahair, N. (1994). "Nonlinear inelastic analysis of steel beam-columns. I: Theory." *Journal of Structural Engineering*, 120(7), 2041-2061.
- Popovics, S. (1973). "A numerical approach to the complete stress-strain curve of concrete." *Cement and concrete research*, 3(5), 583-599.

- Prabha, P., Marimuthu, V., Saravanan, M., and Jayachandran, S. A. (2010). "Evaluation of connection flexibility in cold formed steel racks." *Journal of Constructional Steel Research*, 66(7), 863-872.
- Remacle, J. F., Henrotte, F., Carrier-Baudouin, T., Bechet, E., Marchandise, E., Geuzaine, C., and Mouton, T. (2013). "A frontal Delaunay quad mesh generator using the L-infinity norm." *Int J Numer Meth Eng*, 94(5), 494-512.
- Rezaiee-Pajand, M., and Gharaei-Moghaddam, N. (2015). "Analysis of 3D Timoshenko frames having geometrical and material nonlinearities." *Int J Mech Sci*, 94-95, 140-155.
- Roeder, C. W., Lumpkin, E. J., and Lehman, D. E. (2011). "A balanced design procedure for special concentrically braced frame connections." *Journal of Constructional Steel Research*, 67(11), 1760-1772.
- Romstad, K. M., and Subramanian, C. V. (1970). "Analysis of frames with partial connection rigidity." *Journal of the Structural Division*, 96(11), 2283-2300.
- Sagiroglu, M., and Aydin, A. C. (2015). "Design and analysis of non-linear space frames with semi-rigid connections." *Steel and Composite Structures*, 18(6), 1405-1421.
- Sakino, K., Nakahara, H., Morino, S., and Nishiyama, I. (2004). "Behavior of centrally loaded concrete-filled steel-tube short columns." *Journal of Structural Engineering*, 130(2), 180-188.

- Saritas, A., and Soydas, O. (2012). "Variational base and solution strategies for non-linear force-based beam finite elements." *International Journal of non-linear Mechanics*, 47(3), 54-64.
- Scott, M. H., and Fenves, G. L. (2006). "Plastic hinge integration methods for force-based beam-column elements." *Journal of Structural Engineering*, 132(2), 244-252.
- Smith-Pardo, J. P., and Aristizábal-Ochoa, J. D. (1999). "Buckling reversals of axially restrained imperfect beam-column." *Journal of engineering mechanics*, 125(4), 401-409.
- So, A. K. W., and Chan, S. L. (1991). "Buckling and geometrically nonlinear analysis of frames using one element/member." *Journal of Constructional Steel Research*, 20(4), 271-289.
- Soroushian, P., and Alawa, M. S. (1988). "Efficient formulation of physical theory brace models." *Journal of Structural Engineering*, 114(11), 2457-2473.
- Spacone, E., Ciampi, V., and Filippou, F. (1996). "Mixed formulation of nonlinear beam finite element." *Computers & Structures*, 58(1), 71-83.
- Standard, I. (1893). "Criteria for earthquake resistant design of structures." *Indian Standards Institution, New Delhi, IS*, 1975.
- Surovek-Maleck, A. E., and White, D. W. (2004). "Alternative approaches for elastic analysis and design of steel frames. I: Overview." *J Struct Eng-Asce*, 130(8), 1186-1196.

- Teh, L. H., and Clarke, M. J. (1999). "Plastic-zone analysis of 3D steel frames using beam elements." *J Struct Eng-Asce*, 125(11), 1328-1337.
- Tort, C., and Hajjar, J. F. (2010). "Mixed finite element for three-dimensional nonlinear dynamic analysis of rectangular concrete-filled steel tube beam-columns." *Journal of engineering mechanics*, 136(11), 1329-1339.
- Tremblay, R., Archambault, M.-H., and Filiatrault, A. (2003). "Seismic response of concentrically braced steel frames made with rectangular hollow bracing members." *Journal of Structural Engineering*, 129(12), 1626-1636.
- Truong, V.-H., Nguyen, P.-C., and Kim, S.-E. (2017). "An efficient method for optimizing space steel frames with semi-rigid joints using practical advanced analysis and the micro-genetic algorithm." *Journal of Constructional steel research*, 128, 416-427.
- Uriz, P. (2005). "Towards earthquake resistant design of concentrically braced steel structures." *PhD dissertation, Dept. of Civil and Environmental Engineering, University of California, Berkeley, CA.*
- Uriz, P., Filippou, F. C., and Mahin, S. A. (2008). "Model for cyclic inelastic buckling of steel braces." *Journal of structural engineering*, 134(4), 619-628.
- Uriz, P., and Mahin, S. A. (2008). "Towards earthquake resistant design of concentrically braced steel structures." *PEER 2008/08, Pacific Earthquake Engineering Research Center, University of California at Berkeley, Berkeley, CA.*

- Van Long, H., and Hung, N. D. (2008). "Second-order plastic-hinge analysis of 3-D steel frames including strain hardening effects." *Engineering Structures*, 30(12), 3505-3512.
- Vogel, U. (1985). "Calibrating Frames." *Stahlbau*, 54 (october), 295-311.
- Wheeler, A., and Bridge, R. (2006). "The behaviour of circular concrete-filled thin-walled steel tubes in flexure." *Composite Construction in Steel and Concrete V*, 412-423.
- Williams, F. (1964). "An approach to the non-linear behaviour of the members of a rigid jointed plane framework with finite deflections." *The Quarterly Journal of Mechanics and Applied Mathematics*, 17(4), 451-469.
- Yoo, J.-H., Roeder, C. W., and Lehman, D. E. (2008). "Analytical performance simulation of special concentrically braced frames." *Journal of Structural Engineering*, 134(6), 881-889.
- Yoo, J. H. (2006). *Analytical investigation on the seismic performance of special concentrically braced frames*, ProQuest.
- Yoo, J. H., Lehman, D. E., and Roeder, C. W. (2008). "Influence of connection design parameters on the seismic performance of braced frames." *Journal of Constructional Steel Research*, 64(6), 607-623.
- Yoshioka, K., Inai, E., Hukumoto, N., Kai, M., Murata, Y., Noguchi, T., Tanaka, Y., Tokinoya, H., and Mukai, A. (1995). "Compressive Tests on CFT Short Columns Part 1: Circular CFT Columns." *Proceedings of the Second Joint*

Technical Coordinating Committee (JTCC) on Composite and Hybrid Structures.

Yu, C., and Shanmugam, N. (1986). "Stability of frames with semirigid joints." *Computers & structures*, 23(5), 639-648.

Yu, Y., and Zhu, X. (2016). "Nonlinear dynamic collapse analysis of semi-rigid steel frames based on the finite particle method." *Engineering Structures*, 118, 383-393.

Zhao, X.-M., Wu, Y.-F., and Leung, A. (2012). "Analyses of plastic hinge regions in reinforced concrete beams under monotonic loading." *Engineering Structures*, 34, 466-482.

Zhou, Z. H., and Chan, S. L. (2004). "Elastoplastic and large deflection analysis of steel frames by one element per member. I: One hinge along member." *Journal of Structural Engineering*, 130(4), 538-544.

Ziemian, R. D., and McGuire, W. (2002). "MASTAN2." *1 June 2011, Online Documentation.* (<http://www.mastan2.com>).

Ziemian, R. D., and McGuire, W. (2002). "Modified tangent modulus approach, a contribution to plastic hinge analysis." *J Struct Eng-Asce*, 128(10), 1301-1307.

Ziemian, R. D., McGuire, W., and Deierlein, G. G. (1992). "Inelastic Limit States Design .1. Planar Frame Studies." *J Struct Eng-Asce*, 118(9), 2532-2549.